Vibrations non linéaires géométriques de structures minces
—
Modèles d'ordre réduit et transition vers le chaos.

Synthèse des activités scientifiques en vue de l'obtention du diplôme d'habilitation à diriger les recherches

présenté par
Cyril Touzé

le 30 Novembre 2009

devant le jury composé de :

M. Christophe Pierre	*Rapporteur*
M. Michel Potier-Ferry	*Rapporteur*
M. Jean Kergomard	*Rapporteur*
M. Claude-Henri Lamarque	*Examinateur*
M. Jean-Baptiste Leblond	*Examinateur*
M. Jean-Jacques Marigo	*Examinateur*

"Le savoir est une attitude, une passion. C'est même, au fond, une attitude illicite : comme le goût de l'alcool, de l'érotisme ou de la violence, le besoin de savoir entraîne la formation d'un caractère qui n'est plus en équilibre. Il est tout à fait faux de dire que le chercheur poursuive la vérité, c'est elle qui le poursuit. Il la subit."

"C'était un douteur. L'incertitude de sa science lui avait révélé l'incertitude de tout savoir. Il aurait aimé devenir une personnalité et devinait, à ses meilleures heures, que le paralysant désordre de toutes les choses qui relèvent, peuvent relever un jour, ou ne relèveront jamais d'une vérité, ne permettait plus que la vaine stérilité de la subjectivité pure".

Robert Musil, L'Homme sans qualités*, 1932.*
Traduction française P. Jacottet, 1956.

"Toute parole tend à fixer quelque chose qui semble désirer d'être fixé, et périr de l'être. On ne peut donc ni se taire, ni parler, sans se corriger perpétuellement."

Philippe Jacottet, L'obscurité*, 1961.*

Table des matières

Introduction

L'essentiel des travaux de recherche présentés ici trouvent leur origine dans le domaine de l'acoustique musicale et plus spécificiquement du sons émis et des vibrations des instruments de type cymbale et gong. Ces instruments, de la famille des percussions et que l'on classe parfois parmi les idiophones[1], sont de prime abord très simples, comparés à d'autres instruments de musique dont la facture présente une complexité apparente plus grande (systèmes de clefs des instruments à vent type flûtes, clarinettes et saxophones, table d'harmonie et système de mise sous tension du jeu de cordes du piano, ...). Cependant cette simplicité cache une complexité uniquement due à la dynamique des vibrations mises en jeu, et pour lesquelles le terme de non-linéarité géométrique joue un rôle crucial : le négliger reviendrait à ôter à ces instruments toute la brillance de leur timbre ainsi que les effets typiques qu'on leur connait : glissements de fréquences, explosion fréquentielle due à un enrichissement spectral quelques millisecondes après la frappe, etc. L'oreille étant très sensible aux qualités et à l'évolution temporelle du spectre (donnant la couleur et le timbre typique de chaque instrument), tous les instruments de musique ont une non-linéarité dans leur mode de fonctionnement permettant de faire varier le timbre en fonction des paramètres de jeu. Cette non-linéarité est bien souvent contenue dans le mécanisme d'excitation. Pour les cymbales et les gongs, c'est une non-linéarité distribuée, due aux grandes amplitudes de vibration, et donc intrinsèque à la dynamique vibratoire, qui est en jeu.

Ainsi du point de vue de la mécanique, modéliser et simuler des sons de cymbales et de gongs nécessite au préalable une étude des modèles de plaques et de coques minces, en régime non linéaire géométrique, *i.e.* pour des lois de comportement matérielles élastiques linéaires et des grands déplacements (typiquement pour les structures minces, on observe des phénomènes non linéaires lorsque l'amplitude de vibration est de l'ordre de grandeur de l'épaisseur h). C'est ainsi que, partant des cymbales et des gongs, je me suis intéressé aux modèles de plaques en non linéaire géométrique. Les hypothèses de von Kármán pour les modèles de plaques minces, où l'inertie longitudinale est négligée et les termes membranaires se retrouvent via une fonction d'Airy, ont été utilisées, puis étendues aux cas des coques minces, peu profondes, à géométrie de calotte sphérique afin de se rapprocher du cas des cymbales (pour les coques on parle alors de modèle de Donnell peu profond, ou modèle de Donnell-Mushtari-Vlasov, même si les hypothèses sont celles du modèle de von Kármán pour les plaques). Ce travail a été mené en collaboration avec Olivier Thomas, depuis nos thèses respectives [T1][156]. Ces modèles sont par ailleurs très utilisés en ingénierie et interaction fluide/structure, pour des problèmes de stabilité, de vibrations sous écoulement, de flambage, ce qui m'a amené à étendre le champ des investigations, et plus particulièrement de m'intéresser à la réduction de modèles, et de travailler sur des panneaux à double courbure et des coques circulaires cylindriques, avec les hypothèses de Donnell (coque peu profonde et inertie membranaire négligée), ou avec des modèles plus complexes ne négligeant pas l'inertie longitudinale (modèles de Donnell profond, modèles de Flügge-Lur'e-Byrne), en collaboration avec Marco Amabili. Enfin récemment, une collaboration avec Dominique Chapelle et le groupe MACS de l'INRIA m'a permis de m'intéresser aux cas des coques discrétisées par éléments finis, avec cinématique de Reissner-Mindlin [41], donnant ainsi une vue encore plus générale sur les modèles existants et leurs différents niveaux de traitements numériques.

[1] idiophone : instrument dont le matériau lui-même produit le son lors d'un impact, soit par un instrument extérieur (comme une baguette), soit par une autre partie de l'instrument lui-même. Les idiophones (appelés aussi autophones) se distinguent des instruments à cordes (cordophones), à membrane (membranophones) et à vent (aérophones).

Du point de vue phénoménologique, les cymbales et les gongs présentent une richesse de comportement qu'il a fallu analyser et comprendre. La clef a été donnée par une expérience où l'on excite harmoniquement une telle structure avec une force d'amplitude croissante. On voit alors apparaitre deux bifurcations très nettes, marquant trois régimes distincts, dont le dernier est chaotique et se caractérise au niveau perceptif par un son très proche de celui obtenu en mode de jeu normal, lorsque la cymbale ou le gong est frappé vigoureusement par une mailloche ou une baguette. Le régime chaotique présente une spectre de vibration large bande, et son étude m'a amené à m'intéresser à la turbulence d'ondes (ou turbulence faible). Contrairement à la turbulence pleinement développée où il n'y a pas de relation de fermeture sur la hiérarchie des équations des moments et cumulants, la théorie de la turbulence d'ondes donne des développements analytiques possédant une fermeture et prédit des spectres théoriques.

L'étude de la première bifurcation a quant à elle été menée à son terme, mettant en évidence, tant expérimentalement que théoriquement, la prépondérance des résonances internes pour expliquer les transferts d'énergie intermodaux que l'on observe. Un élément clef pour la compréhension et la simulation de ces régimes périodiques et quasi-périodiques a été le développement de modèles d'ordre réduit fiables qualitativement et quantitativement. Ceci a été mené en développant le concept de *mode non linéaire* en théorie des vibrations, toujours en non linéaire géométrique. Une grande partie de ce document est consacrée aux modes non linéaires, sur lesquels j'ai développé une méthode de calcul fondée sur la théorie des formes normales, dont l'exploitation a permis de montrer de nombreux résultats, en vibration libre (prédiction de la tendance de non-linéarité) et en vibrations forcées (développement de modèles d'ordre réduit fiables et performants pour des amplitudes modérées).

Ainsi l'acoustique musicale et le son des cymbales a mené mes recherches vers de nombreuses contrées dans lesquelles je ne pensais pas initialement me promener. La présentation retenue pour ce document fait la part belle à la mécanique vibratoire afin de mettre en exergue la généralité des problèmes étudiées, si bien que le son des cymbales et des gongs n'en est plus qu'un lointain écho que le lecteur avisé saura retrouver entre les lignes. La simulation et la synthèse sonore de sons de cymbales et de gongs étant néammoins toujours d'actualité pour des projets dans un futur proche, cela sera mentionné dans les perspectives.

Le premier chapitre du document donnera les hypothèses et équations principales des modèles étudiés : modèles de von Kármán et Donnell peu profond pour les plaques minces parfaites et imparfaites et les coques sphériques, modèles avec inertie de membrane pour les panneaux à double courbure et les coques circulaires cylindriques. Le second chapitre sera entièrement consacré aux modes normaux non linéaires. La méthode sera présentée et replacée dans la littérature, puis les résultats importants obtenus seront montrés. Le troisième chapitre sera consacré à la transition vers le chaos. Les relations de résonance interne et deux couplages forts typiques seront étudiés, théoriquement et expérimentalement. Enfin le régime chaotique sera étudié pour une plaque de très grandes dimensions pour laquelle le régime de turbulence d'ondes est bien établi.

Remerciements

Les résultats présentés dans ce mémoire sont bien évidemment le fruit de nombreuses collaborations, rencontres, travaux en commun avec différentes personnes, qui toutes, d'une manière ou d'une autre –ne serait-ce parfois que par une brève remarque– ont contribué à ma formation scientifique et à l'accomplissement des travaux présentés dans ce mémoire. Je tiens donc à remercier tout particulièrement Antoine Chaigne, qui, un jour de janvier 1997, me proposa un sujet de thèse sur les instruments de type cymbale et gong, en me précisant que l'étude serait grandement exploratoire. Sans cette première rencontre scientifique et ce sujet, il va sans dire que j'aurais très vraisemblablement fait radicalement autre chose que de la mécanique non linéaire. La deuxième coincidence extraordinaire fut le choix d'Olivier Thomas de commencer sa thèse, un an après le début de la mienne, sur la partie mécanique des vibrations de cymbales. Pendant quasiment 5 ans (période recouvrant nos thèses, puis le post-doc effectué par Olivier à l'UME de l'ENSTA après sa thèse), nous avons travaillé ensemble, lui mettant au clair les modèles

de von Kármán pour les plaques et les coques peu profondes, et faisant de nombreuses études expérimentales d'une précision d'orfèvre ; moi développant les techniques de traitement de signal, les analyses en systèmes dynamiques (échelles multiples, bifurcations) et les réductions de modèles pour traiter les équations et les comparer aux mesures. Pour notre plus grande satisfaction, nous continuons toujours à pouvoir travailler ensemble sur des sujets communs : c'est une chance inestimable. Je tiens à remercier aussi tout particulièrement les personnes avec qui j'ai eu la chance de travailler plus récemment, et qui m'ont toutes appris beaucoup de choses. Par ordre chronologique : Paul Manneville, Denis Matignon, Marco Amabili, Olivier Cadot, Arezki Boudaoud, Jean-François Mercier, Dominique Chapelle, Marina Vidrascu,Jacques Sainte-Marie et Stefan Bilbao. Je souhaite aussi mentionner les personnes avec qui j'ai eu de nombreuses discussions et qui, ne serait-ce que par une remarque pertinente, ont fait avancer ma reflexion un moment donné : Christophe Pierre, Claude Lamarque, Gérard Iooss, Pierre Coullet, Bruno Cochelin, Sergio Bellizzi, Gaetan Kerschen, Michel Ferré, Olivier Doaré, Ziad Moumni, Liviu Nicu, Joël Frelat, Patrick Joly et Francis Collino. Enfin pour conclure (en espérant n'avoir oublié personne), un grand merci à tous les étudiants qui ont travaillé avec moi : Cédric Camier, Gaël Favraud, Benoit Odille, Alexis Huberdeau, Jean-Baptiste Milien, Fabrice Orphelin, Pierre Lanchantin, Loris Longo Mucciante, Mathieu Fontaine, Kevin Arcas, Eric Luminais, Nicolas Quaegebeur, Kim Pham, Daniele Manca, Lionel Feugères, Bastien Mallaroni.

Résumé

Les travaux présentés dans ce mémoire concernent les vibrations non linéaires géométriques (grande amplitude) des milieux minces, et plus particulièrement les plaques et les coques. Le premier chapitre présente les modèles utilisés dans le document, en rappelant les hypothèses qui président à leur établissement. Les modèles de von Kármán pour les plaques minces, de Donnell-Mushtari-Vlasov pour les coques peu profondes, ainsi que de Donnell pour coques profondes (avec inertie de membrane), et de Flügge-Lur'e-Byrne sont présentés pour des plaques circulaires parfaites et imparfaites, des coques sphériques peu profondes, des coques circulaires cylindriques et des panneaux à double courbure. Le chapitre 2 est entièrement consacré à la théorie des *modes non linéaire* et à son application pour établir des modèles d'ordre réduit pour les vibrations de coques en non linéaire géométrique. La définition d'un *mode non linéaire* (MNL) comme variété invariante de l'espace des phases est rappelée, puis une méthode, fondée sur la théorie des formes normales, et permettant de calculer aisément les MNLs, est présentée. Son application au cas des vibrations libres montre qu'elle permet à moindre coût une prédiction juste de la tendance de non-linéarité (comportement raidissant/assouplissant). L'utilisation des MNLs comme base réduite montre son excellent comportement pour diminuer drastiquement le nombre de degrés de libertés (ddls) pour le cas des vibrations forcées, harmoniques et basse fréquence. Le chapitre 3 traite de la transition vers le chaos observée lorsqu'on augmente l'amplitude d'un forçage harmonique pour les structures minces. Le cas générique observé à partir de nombreuses expériences est d'abord rappelé, montrant deux bifurcations nettes menant d'un régime périodique à une régime quasi-périodique, puis chaotique. La première bifurcation est analysée théoriquement et expérimentalement pour les cas particuliers de deux résonances internes. Enfin le régime chaotique est étudié à l'aide du formalisme de la turbulence d'ondes.

Abstract

This dissertation is devoted to geometrically non-linear (large-amplitude) vibrations of thin structures, with a special emphasis to the case of plates and shells. The first chapter introduces the models used in the document, recalling the basic assumptions they rely on. Von Kármán model for thin plates, Donnell-Mushtari-Vlasov model for shallow shells, Donell's non-shallow theory with in-plane inertia, and Flügge-Lur'e-Byrne theory are presented for perfect and imperfect circular plates, shallow spherical shells, circular cylindrical shells and doubly-curved panels. Chapter 2 is entirely devoted to the application of Non-linear Normal Modes (NNMs) in vibration theory, with a special emphasis to their use as reduced-order models for geometrically non-linear thin structures. The defintion of a NNM as an invariant manifold in phase space is recalled. Then a methodology is presented, which is based on the normal form theory, and allows one to compute easily and efficiently all NNMs in a single operation. Reduced-order models based on NNM formalism are then derived for thin shells, showing their excellent behaviour in the case of low-frequency, forced harmonic vibrations. Chapter 3 is concerned with the transition to chaos, obtained as one forces harmonically a thin shells with an increasing amplitude. The generic case, which has been observed in numerous experiments with various shells, is recalled. Two bifurcations are obtained, leading from a periodic to a quasi-periodic then finally to a chaotic regime. The first bifurcation is analysed theoretically and experimentally, for the particular cases of two specific internal resonances. Finally, the chaotic vibration is studied in the framework of wave turbulence.

CHAPITRE 1

Plaques et coques minces

Dans ce chapitre sont introduits les modèles principaux de plaques et de coques minces en grands déplacements qui seront utilisés par la suite. Le cadre général est celui des vibrations non linéaires géométriques. On supposera donc que les déplacements sont grands, mais que le matériau reste élastique linéaire. La section 1 montre alors que, dans le cadre général de l'élasticité tridimensionnelle, les non-linéarités apparaissant dans les équations du mouvement sont des fonctions quadratiques et cubiques du déplacement.

Les sections suivantes donnent les équations pour les milieux minces bidimensionnels, non-courbés (plaques) et courbés (coques). Dans le cas des plaques, la théorie de von Kármán est utilisée. Pour les coques, le modèle de Donnell-Mushtari-Vlasov (équivalent aux hypothèses de von Kármán) est présenté. Enfin des cinématiques plus complexes, où l'inertie membranaire n'est pas négligée, sont introduits.

Pour chacun des modèles présentés, l'étape de discrétisation est exposée. Une méthode de Galerkin est utilisée, où la base de fonctions de discrétisation employée est généralement la base des fonctions propres de l'opérateur linéaire. Pour le cas des plaques imparfaites et des modèles avec inertie de membrane présentés section 4, il est plus simple d'utiliser des fonctions ad-hoc, ce qui entraine l'apparition de termes de couplage linéaire.

Les modèles rappelés ici sont classiques dans la littérature, et l'on peut se référer à [42, 43, 44, 48, 52, 69, 87, 94, 112, 148, 167] pour plus de détails. Pour ce document, nous nous sommes surtout inspirés des travaux suivant : [R2,R6,R12] et [8, 156, 157]. Afin de ne rappeler que les résultats essentiels, les notations usuelles et évidentes ne seront pas rappelées.

1. Non-linéarités géométriques

En notant $\underline{U}$ le déplacement tridimensionnel, le tenseur lagrangien des déformations de Green-Lagrange $\underline{\underline{e}}$ s'écrit : $\underline{\underline{e}} = \frac{1}{2}\left(\underline{\underline{\nabla}}\,\underline{U} + \underline{\underline{\nabla}}^t\underline{U} + \underline{\underline{\nabla}}^t\underline{U}.\underline{\underline{\nabla}}\,\underline{U}\right)$, il est quadratique en fonction du déplacement. En élasticité tridimensionnelle, la dynamique est donnée par : $\mathrm{div}\,(\underline{\underline{F}}\,.\,\underline{\underline{\pi}}) + \underline{f} = \rho\frac{\partial^2\underline{U}}{\partial t^2}$, où $\underline{\underline{F}} = \underline{\underline{1}} + \nabla\underline{U}$ est le tenseur gradient de transformation, $\underline{\underline{\pi}}$ est le second tenseur lagrangien des contraintes de Piola-Kirchhoff, et $\underline{f}$ représente les efforts volumiques externes. En supposant le matériau élastique linéaire, les contraintes sont reliées aux déformations par la relation linéaire $\underline{\underline{\pi}} = \underline{\underline{\underline{\underline{\Lambda}}}} : \underline{\underline{e}}$, si bien que $\underline{\underline{\pi}}$ contient, de la même manière que $\underline{\underline{e}}$, des termes linéaires et quadratiques en déplacement. Comme le gradient de transformation est linéaire en déplacement, l'équation de la dynamique montre bien que les non-linéarités apparaissant sont polynomiales, d'ordre deux et trois en déplacement.

2. Plaques minces parfaites et imparfaites

Dans cette section est rappelé le modèle de von Kármán pour les plaques minces. Dans tout ce qui suit le matériau est supposé élastique linéaire. De nombreuses hypothèses président à l'établissement du modèle, dont les plus notables sont la simplification opérée dans la relation déformation/déplacement, où seuls quelques termes sont retenus ; ainsi que l'omission de l'inertie de membrane, ce qui permet l'introduction d'une fonction d'Airy. Les résultats données par le modèle de von Kármán sont excellents pour les plaques minces [173], cependant lorsque l'épaisseur augmente, il convient de réintroduire

l'inertie membranaire, voire le cisaillement en adoptant une cinématique type Reissner-Mindlin, ce qui complexifie grandement les équations du modèle.

2.1. Modèle de von Kármán.

H1: Les hypothèses de Kirchhoff-Love sont supposées vérifiées : tout segment reste droit et perpendiculaire à la surface moyenne lors des déformations. Cela implique en particulier que le cisaillement est négligé. De plus les angles de rotation sont supposés petits et sont linéarisés, ce qui permet d'écrire le déplacement de tout point de la plaque en fonction des trois déplacements (u, v, w) de la surface moyenne.

H2: Le déplacement transverse w est de l'ordre de l'épaisseur h, les déplacements longitudinaux (u, v) sont d'un ordre inférieur.

H3: Dans la partie membranaire du tenseur de Green-Lagrange, notée $\underline{\underline{\tilde{e}}}$, seuls les termes non linéaires dépendant de w seront retenus. Cette hypothèse peut être vue comme une conséquence de la précédente. Elle est justifiée par des développements asymptotiques [43, 44, 112, 156].

H4: Le terme de contraintes $\underline{\underline{\pi}}_{zz}$ est négligé (hypothèse de contraintes planes). Les termes de contraintes de cisaillement $\underline{\tau} = (\underline{\underline{\pi}}_{xz},\ \underline{\underline{\pi}}_{yz})^t$ sont aussi négligés, sauf dans les équations d'équilibre en résultante, où l'effort tranchant $\underline{Q} = \int_{-h/2}^{h/2} \underline{\tau} \mathrm{d}z$ est relié aux moments de flexion $\underline{\underline{M}} = \int_{-h/2}^{h/2} z\underline{\underline{\tilde{\pi}}} \mathrm{d}z$ par la relation suivante (en l'absence de moments extérieurs appliqués) [8, 69, 156] : $\underline{Q} = \mathrm{div}\underline{\underline{M}}$.

H5: L'inertie de rotation est négligée.

H6: L'inertie membranaire est négligée. Si de plus il n'y a pas d'efforts extérieurs longitudinaux, l'équation d'équilibre des composantes membranaires s'écrit simplement : $\mathrm{div}\underline{\underline{N}} = \underline{0}$, avec $\underline{\underline{N}} = \int_{-h/2}^{h/2} \underline{\underline{\tilde{\pi}}} \mathrm{d}z$ le tenseur (bidimensionnel) des forces de membrane. On peut alors introduire une fonction d'Airy F définie par $\underline{\underline{N}} = \Delta F \underline{\underline{1}} - \underline{\underline{\nabla}}\,\underline{\nabla} F$ et vérifiant $\mathrm{div}\underline{\underline{N}} = \underline{0}$. Pour clore le système et obtenir une formulation en (w, F) uniquement, il faut introduire une condition de compatibilité (analogue des conditions de Beltrami) reliant F à w.

Finalement les équations dynamiques du modèle de von Kármán s'écrivent, en tenant compte d'un amortissement visqueux $\mu\dot{w}$ et d'un forçage externe $p(\underline{x}, t)$:

$$D\,\Delta\,\Delta\, w + \rho h \ddot{w} = L(w, F) - \mu\dot{w} + p(\underline{x}, t), \tag{1a}$$

$$\Delta\,\Delta\, F = -\frac{Eh}{2} L(w, w) \tag{1b}$$

où $D = Eh^3/12(1-\nu^2)$ est la rigidité en flexion et L un opérateur bilinéaire qui l'on peut écrire en coordonnées intrinsèques [156, 157] :

$$L(w, F) = \Delta\, F\, \Delta\, w - \underline{\underline{\nabla}}\,\underline{\nabla} F : \underline{\underline{\nabla}}\,\underline{\nabla} w, \tag{2}$$

2.2. Plaque circulaire à bord libre. L'article [R2] traite le cas spécifique des plaques circulaires à bord libre. Les modes propres $\Phi_p(r, \theta)$ de la plaque sont alors donnés par une combinaison de fonctions de Bessel pour la partie radiale et de fonctions sinus/cosinus pour la partie orthoradiale. Il est à noter que les modes se caractérisent par un nombre de diamètres nodaux k et un nombre de cercles nodaux n. les modes tels que $k = 0$ sont axisymétriques. Les modes pour $k \geq 1$ sont asymétriques et dégénérés à cause de la symétrie de révolution : à une fréquence propre correspond deux déformées modales, l'une en sinus, l'autre en cosinus.

Afin de se ramener à un ensemble d'équations aux dérivées ordinaires (EDOs), le déplacement est décomposé sur la base des modes propres : $w(r, \theta, t) = \sum X_p(t)\Phi_p(r, \theta)$, que l'on insère dans les équations (1) adimensionnées. Pour résoudre l'équation de compatibilité (1b) un développement modal de la fonction F est aussi introduit, le calcul montre que les modes associés sont ceux de la plaque à bord

encastré, notés Ψ_b. Tout calculs faits, la dynamique s'exprime finalement comme un problème temporel pour les amplitudes modales $X_p(t)$:

$$\ddot{X}_p(t) + \omega_p^2 \, X_p(t) = \varepsilon \left[\sum_{i,j,k=1}^{+\infty} h_{ijk}^p \, X_i(t) \, X_j(t) \, X_k(t) - 2\mu_p \, \dot{X}_p(t) + Q_p(t) \right], \tag{3}$$

où $\varepsilon = 12(1-\nu^2)$ quand le déplacement est adimensionné par l'épaisseur h. Un amortissement modal a été supposé, Q_p est la force modale, et les pulsations propres et les coefficients non linéaires sont donnés par les formules suivantes (en supposant les modes normés de telle sorte que $\iint_{(\mathcal{S})} \Phi_\alpha^2 \, dS = 1$) :

$$\omega_p^2 = \iint_{(\mathcal{S})} \Phi_p \;\; \Delta \, \Delta \, \Phi_p \; dS, \tag{4}$$

$$h_{ijk}^p = -\frac{1}{2} \sum_{b=1}^{+\infty} \frac{1}{\xi_b^4} \iint_{(\mathcal{S})} L(\Phi_i, \Phi_j) \Psi_b \; dS \iint_{(\mathcal{S})} \Phi_p L(\Phi_k, \Psi_b) \; dS \; . \tag{5}$$

Comme annoncé section 1, les non-linéarités sont polynomiales. Ici seul un terme cubique apparait dans les équations, conséquence de la parfaite planéité : une force transverse appliquée vers le haut ou vers le bas doit donner un déplacement opposé mais égal en valeur absolue [C6]. Cette symétrie est rompue pour les coques (ou dès que l'on introduit une imperfection géométrique) où apparaissent alors des termes quadratiques.

2.3. Imperfection géométrique. L'article [R16] et la thèse de Cédric Camier [37] considèrent le cas d'un défaut de forme (imperfection géométrique à état de précontrainte nulle, noté $w_0(r,\theta)$), pour une plaque à bord libre. Les équations (1) deviennent alors :

$$D\Delta\Delta w + \rho h \ddot{w} = L(w,F) + L(w_0,F) - c\dot{w} + p, \tag{6a}$$

$$\Delta\Delta F = -\frac{Eh}{2}[L(w,w) + 2L(w,w_0)]. \tag{6b}$$

En projettant ces EDPs adimensionnées sur la base des modes propres de la plaque parfaite, on obtient le système d'EDOs :

$$\ddot{X}_p + \omega_p^2 X_p = \varepsilon \Big[\sum_{i=1}^{N_w} \alpha_i^p X_i + \sum_{i,j=1}^{N_w} \beta_{ij}^p X_i X_j + \sum_{i,j,k=1}^{N_w} h_{ijk}^p X_i X_j X_k + 2\mu_p \dot{X}_p - Q_p \Big]. \tag{7}$$

Le coefficient cubique h_{ijk}^p intervenant dans cette équation est celui de la plaque parfaite (5). Les nouveaux coefficients de couplage linéaire α_i^p et quadratique β_{ij}^p qui apparaissent s'expriment analytiquement en fonction de h_{ijk}^p est des coefficients a_p de la projection de l'imperfection géométrique sur la base des Φ_p selon l'expression : $w_0(r,\theta) = \sum^{N_0} a_p \Phi_p(r,\theta)$, soit :

$$\alpha_i^p = \sum_{r=1}^{N_0} \sum_{s=1}^{N_0} 2h_{ris}^p a_r a_s, \tag{8a}$$

$$\beta_{ij}^p = \sum_{s=1}^{N_0} (h_{jis}^p + 2h_{sji}^p) a_s \tag{8b}$$

Ainsi, à partir des caractéristiques linéaires et non linéaires de la plaque parfaite, on peut calculer analytiquement les caractéristiques de n'importe quelle plaque imparfaite. La figure 1, tirée de [R16], montre le résultat d'un calcul de fréquences propres pour un défaut ayant la forme du premier mode axisymétrique de plaque parfaite, d'amplitude $w_{m(0,1)}$ croissante. Le calcul est comparé avec une solution par éléments finis concordante.

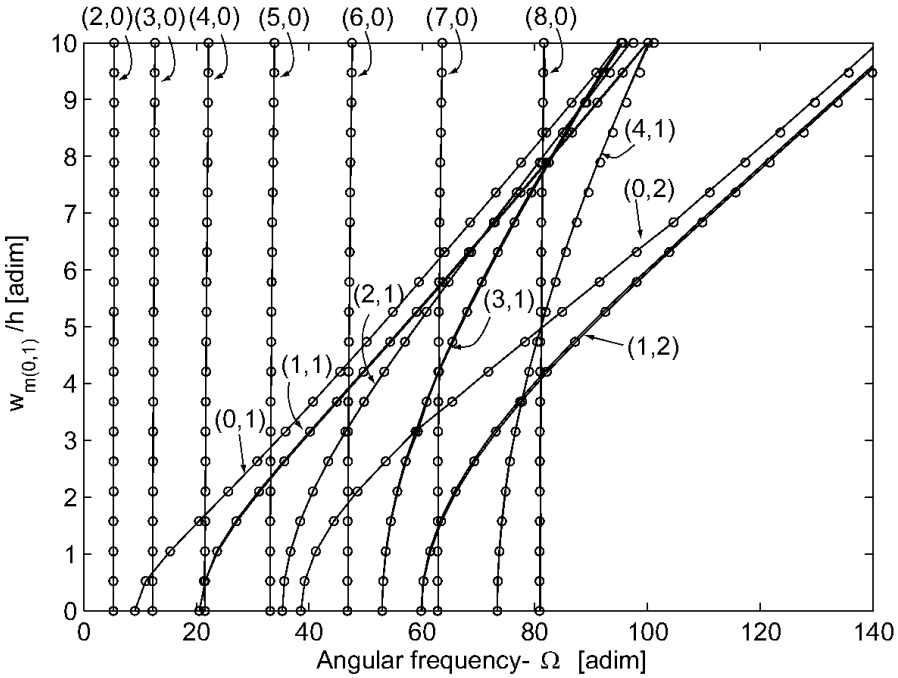

FIG. 1. Evolution des fréquences propres d'une plaque ayant une imperfection de la forme du mode (0,1), d'amplitude $w_{m(0,1)}$ croissante. Comparaison entre le modèle de plaque imparfaite (o) et un calcul par éléments finis (CASTEM, éléments DKT, trait plein).

3. Coques minces peu profondes

Pour les coques, les hypothèses (H1)-(H5) de la théorie de von Kármán peuvent être reconduites, on obtient alors le modèle de Donnell [8, 48]. Si de plus on rajoute l'hypothèse (H6), on obtient l'équivalent rigoureux du modèle de von Kármán, souvent appelé dans la littérature modèle de Donnell peu profond[1], valable tant que la courbure est faible, sinon l'inertie membranaire ne peut plus être négligée.

3.1. Coques sphériques. Cette section reprend des résultats de [R6] pour une coque sphérique peu profonde. En notant R le rayon de courbure de la coque, h son épaisseur et a son rayon, les hypothèses de von Kármán (ou le modèle de Donnell peu profond) mènent aux équations suivantes pour la dynamique :

$$D\,\Delta\,\Delta\,w + \frac{1}{R}\,\Delta\,F + \rho h\ddot{w} = L(w,F) - c\dot{w} + p(\underline{x},t), \tag{9a}$$

$$\Delta\,\Delta\,F - \frac{Eh}{R}\,\Delta\,w = -\frac{Eh}{2}L(w,w). \tag{9b}$$

On peut noter dans ces équations que le couplage entre les mouvements longitudinaux et de flexion a lieu ici dès le stade linéaire, contrairement aux plaques. Il est de plus remarquable que ces équations, généralement admises dans la littérature comme le modèle de coque sphérique [8, 56, 62, 64, 82, 171], sont en fait valables pour une géométrie non pas sphérique mais parabolique : ceci a été démontré dans [R16][37] en introduisant un défaut sphérique dans les équations (6), on se rend alors compte qu'il ne faut conserver que le premier terme du développement sphérique (terme parabolique) pour retrouver les équations (9).

Les articles [R6,R8] donnent les caractéristiques linéaires et non linéaires pour le cas d'un bord libre. Les modes propres $\Phi_p(r,\theta)$ s'écrivent à partir de fonctions de Bessel et de Kelvin [R6]. Le déplacement transverse est développé sur cette base, la fonction d'Airy F sur une combinaison des fonctions propres

[1] Donnell's non-linear shallow shell theory dans la littérature anglo-saxonne.

du problème de membrane à bord libre Φ_p et encastré Υ_j. Le problème linéaire associé à (9) ne dépend que d'un seul paramètre géométrique appelé rapport d'aspect, défini par $\kappa = \dfrac{a^4}{R^2\,h^2}$. La figure 2 montre l'évolution des fréquences propres lorsque l'on augmente la courbure.

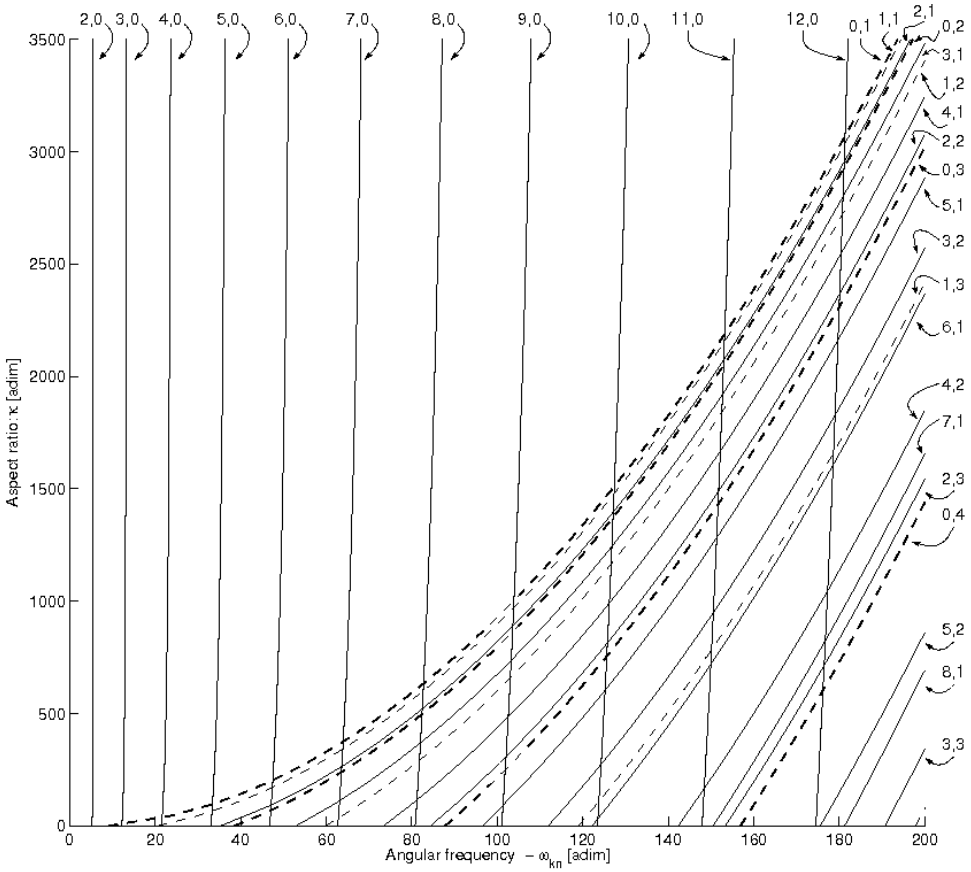

FIG. 2. Pulsations propres ω_{kn} (sans dimensions) pour une coque sphérique peu profonde de rapport d'aspect κ, et pour $\nu = 0.33$. Quand $\kappa = 0$, le rayon de courbure est infini, nous avons donc affaire à une plaque. Augmenter $\kappa = 0$ revient à augmenter la courbure de la coque.

Le problème adimensionné, sans amortissement ni forçage, projeté sur la base propre s'écrit au final :

$$\ddot{X}_p + \omega_p^2 X_p + \varepsilon_q \sum_{i=1}^{+\infty}\sum_{j=1}^{+\infty} \beta_{ij}^p X_i X_j + \varepsilon_c \sum_{i=1}^{+\infty}\sum_{j=1}^{+\infty}\sum_{k=1}^{+\infty} \Gamma_{ijk}^p X_i X_j X_k = 0, \tag{10}$$

où $\varepsilon_q = 12(1-\nu^2)\sqrt{\kappa}$ et $\varepsilon_c = 12(1-\nu^2)$ proviennent de l'adimensionnement. Les coefficients de couplage non linéaire s'écrivent :

$$\beta_{ij}^p = -\iint_{\mathcal{S}_\perp} \Phi_p L(\Phi_i, \Psi_j)\, dS - \frac{1}{2}\sum_{b=1}^{+\infty} \frac{1}{\xi_b^4} \iint_{\mathcal{S}_\perp} L(\Phi_i, \Phi_j)\Upsilon_b\, dS \iint_{\mathcal{S}_\perp} \Phi_p\, \Delta\, \Upsilon_b\, dS, \tag{11}$$

$$\Gamma_{ijk}^p = \frac{1}{2}\sum_{b=1}^{+\infty} \frac{1}{\xi_b^4} \iint_{\mathcal{S}_\perp} L(\Phi_i, \Phi_j)\Upsilon_b\, dS \iint_{\mathcal{S}_\perp} \Phi_p L(\Phi_k, \Upsilon_b)\, dS. \tag{12}$$

3.2. Coques circulaires cylindriques. Les hypothèses du modèle de Donnell pour les coques peu profondes (*i.e.* en négligeant l'inertie membranaire) peuvent être reprises pour traiter le cas des coques circulaires cylindriques, pourvu que l'on se limite à l'étude des modes tels que le nombre n d'ondes

circonférentielles (le nombre de lignes nodales est alors $2n$) soit tel que $1/n^2 \ll 1$, soit $n \geq 4$ ou 5 [8]. Le modèle de Donnell s'écrit alors, en coordonnée cylindrique :

$$D\,\Delta\,\Delta\,w + ch\dot{w} + \rho h\ddot{w} = f - p + \frac{1}{R}\frac{\partial^2 F}{\partial x^2} + \frac{1}{R^2}\left[\frac{\partial^2 F}{\partial \theta^2}\frac{\partial^2 w}{\partial x^2} - 2\frac{\partial^2 F}{\partial x \partial \theta}\frac{\partial^2 w}{\partial x \partial \theta} + \frac{\partial^2 F}{\partial x^2}\frac{\partial^2 w}{\partial \theta^2}\right], \quad \text{(13a)}$$

$$\frac{1}{Eh}\,\Delta\,\Delta\,F = -\frac{1}{R}\frac{\partial^2 w}{\partial x^2} + \left[\left(\frac{\partial^2 w}{R\partial x \partial \theta}\right)^2 - \frac{\partial^2 w}{\partial x^2}\frac{\partial^2 w}{R^2 \partial \theta^2}\right], \quad \text{(13b)}$$

où le déplacement transverse est pris positif lorsqu'il est dirigé vers le centre de la coque, f représente un effort extérieur (type forçage localisé) et p représente la pression due à l'interaction éventuelle fluide-structure lorsque la coque est remplie d'eau.

Ici nous reprenons la discrétisation proposée dans [6, 8, 10, 133], pour des conditions aux limites simplement supportées. C'est ce modèle qui sera utilisé au chapitre suivant, utilisant des résultats de [R9,R10]. Le déplacement w est développé sur la base des modes propres :

$$w(x,\theta,t) = \sum_{\substack{m=1\\k=1}}^{3} \left[A_{m,kn}(t)\cos(kn\theta) + B_{m,kn}(t)\sin(kn\theta)\right]\sin(\lambda_m x) + \sum_{m=1}^{4} A_{(2m-1),0}(t)\sin(\lambda_{(2m-1)}x), \quad \text{(14)}$$

où n est le nombre d'ondes circonférentielles, m le nombre de demi-longueur d'ondes longitudinales, $\lambda_m = m\pi/L$; $A_{m,n}(t)$ et $B_{m,n}(t)$ sont les coordonnées généralisées. Dans le cas d'une coque remplie d'eau, un modèle de fluide inviscide, incompressible et irrotationnel permet de donner une expression simple de la pression p en fonction des coordonnées modales, cf. [6]. Au final, si l'on renomme les coordonnées $\{A_{m,n}, B_{m,n}\}$ par X_n, on retrouve bien des équations d'oscillateurs non linéaires couplés avec termes quadratiques et cubiques, semblables aux équations (10). Les détails du calcul menant aux EDOs sont donnés dans [6, 10, 12], sans toutefois donner une formule analytique pour les coefficients non linéaires.

4. Modèles avec inertie de membrane

4.1. Cinématiques et Méthode Lagrangienne. Certaines des hypothèses les plus fortes des modèles de von Kármán et de Donnell-Mushtari-Vlasov peuvent être levées, ce qui prend particulièrement du sens lorsque l'on considère que l'épaisseur n'est plus complètement négligeable, ou que la courbure des coques devient trop grande. L'inertie de membrane peut ainsi être conservée dans les équations du mouvement, qui alors ne s'expriment plus en fonction de (w, F) mais des trois déplacements (u, v, w). L'article [173] montre que, pour le cas des plaques, l'inertie de membrane est absolument négligeable tant que l'épaisseur ne dépasse pas 1/20 des dimensions latérales.

Dans les cas des coques profondes il convient aussi de ne plus négliger l'inertie longitudinale. L'article [2] montre l'effet produit sur les fréquences propres, tandis que les réponses non linéaires sont montrées dans [5]. Enfin, la simplification opérée dans la relation déformation/déplacement (hypothèse H3 du modèle de von Kármán) peut aussi être revue afin d'introduire des cinématiques plus complexes. Divers modèles ont été proposé dans la littérature, parmi lesquels on peut citer ceux de Novozhilov, Sanders-Koiter, Flügge-Lur'e-Byrne...

Les sections suivantes exposent très brièvement les hypothèses du modèle de Flügge-Lur'e-Byrne et donnent la discrétisation utilisée pour le cas d'une coque circulaire cylindrique, ainsi que pour un panneau à double courbure : ces modèles ont été utilisés dans [R12] et seront repris au chapitre suivante.

4.2. Coque circulaire cylindrique. Dans le modèle de Flügge-Lur'e-Byrne, l'inertie membranaire est retenue. La cinématique est complexifiée par la prise en compte d'une dépendance linéaire en fonction de la coordonnée transverse z pour les déplacements longitudinaux u et v, la référence [8] en donne les détails.

Les équations sont ensuite obtenues par une méthode Lagrangienne [5, 8], pour une coque circulaire cylindrique aux bords simplement supportés. Comme les trois déplacements (u, v, w) sont conservées dans la formulation il est plus aisé d'utiliser une base de fonctions ad-hoc plutôt que la base modale pour discrétiser les équations. Ici les développements sont les suivants :

$$u(x,\theta,t) = \sum_{k=1}^{2} \left[u_{1,5k,c}(t)\cos(5k\theta) + u_{1,5k,s}(t)\sin(5k\theta)\right]\,\cos(\lambda_1 x) + \sum_{m=1}^{2} u_{2m-1,0}(t)\cos(\lambda_{2m-1}\,x)\;+\;\hat{u}, \tag{15a}$$

$$v(x,\theta,t) = \sum_{k=1}^{2} \left[v_{1,5k,c}(t)\sin(5k\theta) + v_{1,5k,s}(t)\cos(5k\theta)\right]\,\sin(\lambda_1 x) + \left[v_{3,10,c}(t)\sin(10\theta) + v_{3,10,s}(t)\cos(10\theta)\right]\,\sin(\lambda_3 x), \tag{15b}$$

$$w(x,\theta,t) = \left[w_{1,5,c}(t)\cos(5\theta) + w_{1,5,s}(t)\sin(5\theta)\right]\,\sin(\lambda_1 x) + \sum_{m=1}^{2} w_{2m-1,0}(t)\sin(\lambda_{2m-1}\,x), \tag{15c}$$

où $\lambda_m = \frac{m\pi}{a}$, et $\hat{u}$ et un terme non linéaire ajouté afin de satisfaire exactement la condition $N_x = 0$. C'est un modèle à 16 degrés de libertés (ddls), dont la convergence a été étudiée dans [5] pour le régime forcé au voisinage de la fréquence propre du mode (1,5).

Les équations discrétisées sont :

$$\ddot{q}_p + 2\zeta_p\omega_p\dot{q}_p + \sum_{i=1}^{P} z_i^p q_i + \sum_{i,j=1}^{P} z_{i,j}^p q_i q_j + \sum_{i,j,k=1}^{P} z_{i,j,k}^p q_i q_j q_k = f_p\cos(\omega t). \tag{16}$$

où $\mathbf{q} = [u_{m,n},\ v_{m,n},\ w_{m,n}]^T$ est le vecteur des coordonnées généralisées regroupant les inconnues introduites par (15). Un terme de couplage linéaire est présent dans les équations puisque la base modale n'a pas été utilisée pour la projection.

4.3. Panneau à double courbure. Un panneau à double courbure hyperbolique paraboloïde (les rayons de courbure principaux R_x et R_y étant tels que $R_x = -R_y$), utilisant la cinématique de Donnell pour coques profondes a été utilisé dans [R12]. Les conditions aux limites sont simplement supportées ; les fonctions de base utilisées pour la discrétisation sont :

$$\phi_{m,n}^{(u)}(x,y) = \cos(m\pi x/a)\sin(n\pi y/b), \tag{17a}$$

$$\phi_{m,n}^{(v)}(x,y) = \sin(m\pi x/a)\cos(n\pi y/b), \tag{17b}$$

$$\phi_{m,n}^{(w)}(x,y) = \sin(m\pi x/a)\sin(n\pi y/b). \tag{17c}$$

Deux termes non linéaires $\hat{u}$ et $\hat{v}$ sont ajoutées aux équations (17a) et (17b) afin que les conditions aux limites soient identiquement vérifiées [7]. Les équations du mouvement sont semblables à (16). Dans la suite du document, reprenant [R12], 22 fonctions de base sont retenues pour discrétiser le panneau et étudier ses vibrations forcées au voisinage du mode fondamental, à savoir : $\phi_{1,1}^{(w)}$, $\phi_{1,3}^{(w)}$, $\phi_{3,1}^{(w)}$, $\phi_{3,3}^{(w)}$, $\phi_{1,1}^{(u)}$, $\phi_{3,1}^{(u)}$, $\phi_{1,3}^{(u)}$, $\phi_{3,3}^{(u)}$, $\phi_{1,5}^{(u)}$, $\phi_{5,1}^{(u)}$, $\phi_{3,5}^{(u)}$, $\phi_{5,3}^{(u)}$, $\phi_{5,5}^{(u)}$, $\phi_{1,1}^{(v)}$, $\phi_{3,1}^{(v)}$, $\phi_{1,3}^{(v)}$, $\phi_{3,3}^{(v)}$, $\phi_{1,5}^{(v)}$, $\phi_{5,1}^{(v)}$, $\phi_{3,5}^{(v)}$, $\phi_{5,3}^{(v)}$, $\phi_{5,5}^{(v)}$.

CHAPITRE 2

Modes normaux non linéaires

1. Introduction : réduction de modèles

Une des difficultés principales auxquelles on est confronté en vibrations non linéaires réside dans le grand nombre de degrés de liberté (ddls) qu'il faut conserver dans les modèles afin de pouvoir fournir des prédictions correctes, tant qualitativement que quantitativement. Ceci est la conséquence directe du couplage non linéaire des coordonnées modales. Il en résulte une double difficulté. Premièrement l'analyse et la compréhension des dynamiques observées peut être obscurcie par la grande dimension de ces modèles, qui masque des phénomènes que l'on est capable de comprendre par comparaison avec des situations simples exhibées par des cas génériques que l'on trouve dans la théorie des bifurcations de codimension petite, ou l'analyse d'oscillateurs non linéaires canoniques (équation de Duffing, de Mathieu, de Van der Pol, ...). Deuxièmement les coûts de calcul numérique associés sont rapidement prohibitifs. La recherche de *modèles d'ordre réduit*, *comportant un petit nombre de degrés de liberté*, et ayant la capacité de produire des prédictions correctes est donc un enjeu majeur. Cette recherche peut être ramenée à celle d'une base optimale, capturant au mieux, dans l'espace des phases, les dynamiques du système étudié. Par cette définition, on sent d'ores et déjà que ces bases devront avoir une capacité *d'adaptation*, afin de rendre compte des éventuels changements de dynamiques via des bifurcations.

La littérature sur le sujet est extrêmement vaste et abondante, les méthodes proposées différant beaucoup selon les cas d'applications, les modèles numériques utilisés, le niveau de modélisation. En dynamique, la première idée consiste à utiliser la base des modes propres du problème linéarisé, ce qui donne déjà lieu à une réduction substantielle du nombre de degrés de liberté mis en jeu lorsque les EDP de départ sont discrétisées par des méthodes de type éléments finis. Cette méthode est très classique en vibrations linéaires, cf. par exemple [19, 109, 113, 130]. Cette base a de plus le bon goût de posséder des bonnes propriétés, en particulier elle découple les termes linéaires. Cependant, en incluant les non-linéarités géométriques, cela reste encore insuffisant à cause des termes de couplage non linéaire et la perte d'invariance des sous-espaces propres qui en résulte. D'autres méthodes tentent alors de remédier à cela en optimisant la variance entre une base orthogonale dont les directions sont les inconnues, et un nuage de points obtenus par une simulation directe ou par une expérience. C'est le principe de la méthode POD (pour Proper Orthogonal Decomposition[1]), qui est très largement utilisée dans tous les domaines de la physique, et dont l'article [91] propose une vue d'ensemble pour les applications relatives à la dynamique des structures.

Les avantages de la méthode POD sont nombreux, ce qui explique son succès[2]. Outre sa facilité d'implémentation, elle possède de plus une très grande souplesse de par sa capacité à s'ajuster au mieux aux données du problème. Mais cet avantage peut aussi être vu comme un double inconvénient. Premièrement car le modèle réduit s'applique parfaitement aux données utilisées, mais un changement de dynamique modifie le nuage de points, si bien qu'il faut alors recalculer une base POD. Deuxièmement, dans un contexte de modèle mathématique, on aimerait pouvoir se passer de la donnée d'une série chronologique d'observation afin de pouvoir être en mesure de calculer le modèle réduit : une stratégie

[1] Nous décidons ici de conserver l'acronyme anglais POD car le terme s'est popularisé sous cette forme aussi en français, cela étant peut-être aussi dû à un manque de traduction satisfaisante.

[2] Quantitativement la littérature sur les modèles réduits est très largement dominé (à plus de 75% au bas mot) par l'application de la POD et ses variantes.

n'utilisant que les propriétés intrinsèques des opérateurs apparaissant dans les EDPs de départ permettrait en effet d'effectuer une opération de moins.

Les *modes normaux non linéaires* (MNL) permettent de pallier un certain nombre de ces limitations. Comme nous le verrons par la suite c'est une méthode complètement non linéaire. La base optimale déduite est courbée dans l'espace des phases, et elle se calcule uniquement à partir des propriétés du spectre de l'opérateur linéaire des EDPs. Un bon point d'entrée pour ces méthodes non linéaires (issus généralement de la théorie des systèmes dynamiques : variétés invariantes et inertielles) est donné par les articles généraux [143, 155]. Ce chapitre est entièrement consacré aux MNL. En section 2, nous rappellerons les principales définitions tout en donnant les publications de références sur le sujet. Ensuite, une méthode fondée sur la théorie des formes normales sera décrite en détail en 3. Cette méthode a été exposée dans les articles [R4,R9], et a ensuite été exploitée pour montrer de nombreux résultats [R4,R5,R9,R10,R12,R13]. Tout d'abord nous montrons que la réduction à un mode non linéaire permet de prédire la bonne tendance de non-linéarité pour un ensemble d'oscillateurs, contrairement à la réduction à un mode linéaire qui peut conduire à des prédictions erronées. Des exemples de réduction de modèles sur des cas de coques et de panneaux à double courbure sont montrés section 5. Enfin la méthode POD est comparée aux réductions obtenues à l'aide des MNL sur le cas d'une coque circulaire cylindrique remplie d'eau en section 6.

2. Modes non linéaires : définitions

Les modes non linéaires sont ici introduits dans le cadre de la théorie des vibrations. Les équations de départ sur lesquelles on opère sont des oscillateurs couplés non linéairement, cas générique pour les grandes amplitudes de structures minces. La plupart des résultats utiles proviennent de la théorie des systèmes dynamiques [65, 75, 107, 164]. Ces résultats généraux sont ici particularisés pour tenir compte du fait que l'on traite des problèmes d'ordre deux en temps (des ensembles d'oscillateurs).

Les premiers travaux sur les MNL remontent à Rosenberg [145, 146] dans les années 1960. En utilisant des résultats de Lyapunov [105] qui montrent l'existence de familles d'orbites périodiques au voisinage des sous-espaces propres[3], il définit ainsi un mode non linéaire comme "une vibration à l'unison", décrite par une orbite périodique. Cette définition a été reprise entre autre par Manevitch et Mikhlin [106, 111], Rand [141] et Vakakis [93, 161, 162].

Au début des années 1990, la thématique connait un nouvel essor avec les travaux de S. Shaw et C. Pierre [35, 149, 150, 151]. En utilisant le formalisme des systèmes dynamiques et le théorème de réduction à la variété centrale, ils définissent un mode non linéaire comme une variété invariante de l'espace des phases, tangente à l'origine aux sous-espaces propres. Cette définition élargit le champ d'application de celle de Rosenberg, car elle permet, entre autre, de traiter les systèmes amortis.

Les deux définitions équivalentes rappelées ci-dessus montrent que le concept de MNL repose sur des théorèmes forts et bien connus, respectivement le théorème de Lyapunov [105] sur les orbites périodiques et celui de la variété centrale [21, 38, 65, 88, 137]. Étrangement, les théorèmes de Poincaré et Poincaré-Dulac [50, 138] ne sont pas utilisés. C'est le sens des travaux de Jézéquel et Lamarque [84], ainsi que de ceux que j'ai mené [R4,R9], de montrer que les MNL peuvent être définis dans le cadre de la théorie des formes normales, ce qui est complètement logique étant donné l'équivalence qui existe entre variété invariante et forme normale [54, 74]. In fine on obtient une troisième description dont on peut montrer les équivalences avec les autres formulations [R4].

[3] Les résultats de Lyapunov [105] sont pour les systèmes à n ddl et sans résonance interne. Ils ont été étendus par Weinstein et Moser au cas des resonances internes [115, 163].

3. Calcul asymptotique et formes normales

Le point de départ est un ensemble d'oscillateurs non linéaires couplés avec non-linéarités quadratiques et cubiques, conformément à ce que l'on a vu au chapitre 1. On suppose de plus que la partie linéaire a déjà été découplée, si tel n'est pas le cas il suffit de la diagonaliser et d'effectuer un changement de variables linéaires classique. La dynamique est donc décrite par :

$$\ddot{X}_p + \omega_p^2 X_p + 2\xi_p \omega_p \dot{X}_p + \sum_{i=1}^{N} \sum_{j \geq i}^{N} g_{ij}^p X_i X_j + \sum_{i=1}^{N} \sum_{j \geq i}^{N} \sum_{k \geq j}^{N} h_{ijk}^p X_i X_j X_k = 0, \tag{18}$$

Dans cette équation, X_p représente la $p^{\text{ème}}$ coordonnée modale. Un amortissement modal, de la forme $2\xi_p \omega_p \dot{X}_p$ a été ajouté. On considère ici un amortissement ad-hoc dont on suppose que les valeurs ont été finement accordées afin de représenter au mieux la structure étudiée[4].

Le calcul des modes non linéaires par développement asymptotique repose sur la théorie des formes normales, devenue standard en théorie des bifurcations, car elle permet de ramener les dynamiques au voisinage de points singuliers à leur forme la plus simple et donc de décrire les modèles génériques de bifurcation pour des codimensions croissantes, cf. par exemple [22, 36, 75, 107]. L'idée de Poincaré consistait à dire qu'un système non linéaire, aussi compliqué soit-il, peut en fait cacher une dynamique extrêmement simple, si bien que, par un changement de variables non linéaire, on devrait être en mesure d'éliminer tous les termes non linéaires qui obscurcissent la vue que l'on s'en fait. On aboutit ainsi à la définition des termes *résonnants* et *non-résonnants*. Les premiers, essentiels à la dynamique, ne peuvent être éliminés, tandis que les seconds peuvent l'être grâce à un changement de variables. Dans le meilleur des cas, s'il n'y a pas de relation de *résonances* entre les valeurs propres du problème linéarisé, on peut complètement éliminer les termes non linéaires (théorème de Poincaré) [138], si bien que le système dynamique original est en fait équivalent à un système linéaire. S'il y a des termes résonnants, alors ceux-ci ne sont pas éliminés. A la fin du changement de variables, on aboutit tout de même à une expression beaucoup plus simple du système dynamique, qui ne comprend plus que les termes résonnants, et qui est appelée *forme normale du système* (théorème de Poincaré-Dulac) [50].

Dans la suite de l'exposé nous nous plaçons en dimension finie. L'extension en dimension infinie nécessite quelques amendements techniques mais est possible, cf. [68, 76, 77]. Les relations de résonances entre les valeurs propres $\{\lambda_k\}_{k=1...N}$ de l'opérateur linéaire se définissent de la manière suivante :

$$\forall\ s = 1...N : \lambda_s = \sum_{i=1}^{N} m_i \lambda_i, \quad m_i \geq 0, \quad \sum m_i = p \geq 2, \tag{19}$$

où p est l'ordre de la résonance (relié au degré de non-linéarité), et N le nombre de valeurs propres du système.

Dans le cas des systèmes vibratoires conservatifs, les valeurs propres sont toutes imaginaires pures et complexes conjuguées : le spectre est de la forme $\{\pm i\omega_p\}_{p=1...N}$. Il en résulte qu'il existera *toujours* des termes résonnants, puisque l'on peut toujours écrire la relation triviale de résonance d'ordre 3 : $i\omega_p = i\omega_p - i\omega_p + i\omega_p$. Par conséquent il restera toujours des monômes résonnants dans la forme normale. Ceci est heureux car le terme résonnant relié à la relation précédente est le terme en X_p^3 dans la $p^{\text{ème}}$ équation d'oscillateur, *i.e.* le terme type "Duffing" qui rend les fréquences directement dépendante de l'amplitude. Par contre les résonances internes faisant intervenir plusieurs modes, du type $\omega_i \pm \omega_j = \omega_p$ (ordre deux), ou $\omega_i \pm \omega_j \pm \omega_k = \omega_p$ (ordre 3), dépendent des fréquences propres de la structure étudiée et donneront lieu, ou non, à des couplages forts entre modes que l'on reverra plus précisément au chapitre suivant.

[4] En particulier nous ne nous intéressons pas ici au problème d'une représentation correcte des termes d'amortissements dans les vibrations de structure incluant les phénomènes viscoélastiques, thermoélastiques, de couplage fluide-structure et de perte par les bords.

Le calcul des modes non linéaires développé dans les publications [R4,R9] suit rigoureusement la méthode utilisée pour démontrer les théorèmes de Poincaré et Poincaré-Dulac, à savoir une élimination itérative de tous les termes non-résonnants de (18) par récurrence sur les ordres successifs de non-linéarité. Cependant, à la différence de ce qui se fait dans les traités mathématiques où le cas des spectres imaginaires purs et complexes conjugués est traité [36, 54, 75], ainsi que ce qui avait été fait, pour les systèmes vibrants, par Jézéquel et Lamarque [84], ainsi que par Nayfeh [117], notre calcul conserve, au stade linéaire, des blocs matriciels de la forme :

$$\begin{pmatrix} 0 & 1 \\ -\omega_p^2 & 0 \end{pmatrix} \tag{20}$$

ce qui permet de rester pendant tout le calcul dans le domaine réel avec des équations d'oscillateurs. Cette différence technique nous est apparue comme un avantage, car on conserve un formalisme avec une assemblée d'oscillateurs non linéaires couplés qui s'interprète en continuité avec les approches usuelles de la mécanique vibratoire. De plus, ce formalisme permet une comparaison terme à terme avec les méthodes de calcul différentes (par variété invariante ou par développement en échelles multiples), ce qui rend plus aisée la démonstration de leur équivalence.

Ici nous présentons les résultats de [R9] prenant en compte le terme d'amortissement : ils généralisent les résultats de [R4] obtenus dans le cas conservatif. Les équations de départ (18) sont d'abord mises au premier ordre en utilisant la vitesse $Y_p = \dot{X}_p$ comme variable intermédiaire. On suppose ensuite qu'il n'existe pas de résonances internes entre les fréquences propres du système[5], ce qui nous permettra d'éliminer tous les monômes sauf ceux provenant des relations de résonance triviales. Il est à noter tout de même que s'il y a des relations de résonances internes, le calcul s'en accomode fort bien puisque les petits dénominateurs apparaissent : il suffit alors de conserver les monômes résonnants dans la dynamique normale. Le changement de variables, calculé jusqu'à l'ordre trois, s'écrit :

$$\begin{aligned} X_p =& R_p + \sum_{i=1}^{N}\sum_{j\geq i}^{N}(a_{ij}^p R_i R_j + b_{ij}^p S_i S_j) + \sum_{i=1}^{N}\sum_{j=1}^{N} c_{ij}^p R_i S_j \\ &+ \sum_{i=1}^{N}\sum_{j\geq i}^{N}\sum_{k\geq j}^{N}\left(r_{ijk}^p R_i R_j R_k + s_{ijk}^p S_i S_j S_k\right) + \sum_{i=1}^{N}\sum_{j=1}^{N}\sum_{k\geq j}^{N}\left(t_{ijk}^p S_i R_j R_k + u_{ijk}^p R_i S_j S_k\right), \end{aligned} \tag{21a}$$

$$\begin{aligned} Y_p =& S_p + \sum_{i=1}^{N}\sum_{j\geq i}^{N}(\alpha_{ij}^p R_i R_j + \beta_{ij}^p S_i S_j) + \sum_{i=1}^{N}\sum_{j=1}^{N} \gamma_{ij}^p R_i S_j \\ &+ \sum_{i=1}^{N}\sum_{j\geq i}^{N}\sum_{k\geq j}^{N}\left(\lambda_{ijk}^p R_i R_j R_k + \mu_{ijk}^p S_i S_j S_k\right) + \sum_{i=1}^{N}\sum_{j=1}^{N}\sum_{k\geq j}^{N}\left(\nu_{ijk}^p S_i R_j R_k + \zeta_{ijk}^p R_i S_j S_k\right) \end{aligned} \tag{21b}$$

Les coefficients introduits $\{a_{ij}^p, b_{ij}^p, c_{ij}^p, r_{ijk}^p, ..., \zeta_{ijk}^p\}$ sont calculés en une seule opération, à partir du spectre des valeurs propres et des coefficients de couplage initiaux du problème (18) : $\{g_{ij}^p, h_{ijk}^p\}$. Dans le cas conservatif, on obtient des expressions analytiques complètes [R4], dans le cas amortis les formules sont trop lourdes et les coefficients sont présentés comme solution de systèmes linéaires dans [R9]. La forme normale du système s'écrit alors : $\forall p = 1...N$:

[5]Dans le cas de systèmes faiblements dissipatifs, où l'amortissement est considéré comme une petite perturbation par rapport aux fréquences propres, on peut conserver la condition de résonance interne *sur les fréquences propres* et non sur les valeurs propres complexes $\lambda_p^{\pm} = -\xi_p\omega_p \pm i\omega_p\sqrt{1-\xi_p^2}$. On montre en effet (cf. annexes de [R9]) que si l'on fait des développements limités en puissance de l'amortissement $O(\xi)$, alors les petits dénominateurs sont ceux du cas conservatif avec une précision en $O(\xi^2)$. Par contre si le système est fortement amorti alors il faut revoir les relations de résonance et les écrire directement sur les valeurs propres complexes.

$$
\begin{aligned}
&\ddot{R}_p + \omega_p^2 R_p + 2\xi_p\omega_p\dot{R}_p + \left(h^p_{ppp} + A^p_{ppp}\right) R_p^3 + B^p_{ppp} R_p \dot{R}_p^2 + C^p_{ppp} R_p^2 \dot{R}_p \\
&\quad + R_p \Bigg[\sum_{j>p}^{N} \Big[(h^p_{pjj} + A^p_{pjj} + A^p_{jpj}) R_j^2 + B^p_{pjj} \dot{R}_j^2 + (C^p_{pjj} + C^p_{jpj}) R_j \dot{R}_j \Big] \\
&\qquad + \sum_{i<p} \Big[(h^p_{iip} + A^p_{iip} + A^p_{pii}) R_i^2 + B^p_{pii} \dot{R}_i^2 + (C^p_{pii} + C^p_{ipi}) R_i \dot{R}_i \Big] \Bigg] \\
&\quad + \dot{R}_p \Bigg[\sum_{j>p}^{N} \left(B^p_{jpj} R_j \dot{R}_j + C^p_{jjp} R_j^2 \right) + \sum_{i<p} \left(B^p_{iip} R_i \dot{R}_i + C^p_{iip} R_i^2 \right) \Bigg] \; = \; 0
\end{aligned}
\tag{22}
$$

Les coefficients $(A^p_{ijk},\ B^p_{ijk},\ C^p_{ijk})$ proviennent de l'élimination des termes quadratiques. Leurs expressions sont :

$$
A^p_{ijk} = \sum_{l\geq i}^{N} g^p_{il} a^l_{jk} + \sum_{l\leq i} g^p_{li} a^l_{jk}, \tag{23a}
$$

$$
B^p_{ijk} = \sum_{l\geq i}^{N} g^p_{il} b^l_{jk} + \sum_{l\leq i} g^p_{li} b^l_{jk}. \tag{23b}
$$

$$
C^p_{ijk} = \sum_{l\geq i}^{N} g^p_{il} c^l_{jk} + \sum_{l\leq i} g^p_{li} c^l_{jk}. \tag{23c}
$$

Ces développements appellent les commentaires suivants :

- Le changement de variable (21) est tangent à l'identité, ce qui permet de voir les modes non linéaires comme une continuation des sous-espaces propres linéaires.
- Dans les Eqs. (22), tous les termes non-résonnants, qui brisent l'invariance des sous-espaces propres linéaires, ont été eliminés. Retrouvant ainsi un découpage de l'espace des phases en variétés invariantes, on peut alors procéder à des troncatures propres. En particulier, comme il sera rappelé dans la section suivante, projeter la dynamique sur un seul MNL permet de prédire la tendance de non-linéarité du système, alors que la réduction à un mode linéaire peut donner des résultats erronés.
- Posé de cette manière, le passage en coordonnées *normales* se fait via un changement de variables : c'est le cadre adapté pour faire de l'analyse/synthèse modale non linéaire. On montre de plus que la dynamique sur les modes non linéaires n'est rien d'autre que la forme normale du système, ce qui peut aussi permettre d'écrire ex-nihilo des modèles phénoménologiques simples.
- Le développement asymptotique est limité, dans cette présentation, à l'ordre trois. C'est une limitation importante de la méthode, car le gain que l'on aura en réduction de modèle aux amplitudes modérées sera perdu pour des amplitudes très grandes. Le passage à l'ordre cinq permettrait de donner de meilleurs résultats pour des amplitudes plus grandes, cependant la complexité du changement de variable (le nombe de coefficients) augmentera fortement, il n'est alors pas certain que le gain en temps de calcul soit alors aussi important. Ce point sera rediscuté au vu des résultats, cf. section 5.
- Le cas où des résonances internes apparaissent dans le spectre linéaire ne pose pas de problèmes spécifiques : le coefficients devant annuler ces termes dans le changement de variables (21) est alors nul et les monômes résonnants associés restent dans la forme normale (22).
- Enfin il est à noter que la procédure itérative du calcul du développement asymptotique ne se prête pas à un calcul numérique.

3.1. Positionnement par rapport à la littérature. L'originalité principale de notre méthode par rapport à la littérature réside dans la forme réelle retenue tout au long du calcul, ce qui nous a permis, cf. [R4,C10-C11], de comparer terme à terme nos résultats avec ceux obtenus par la méthode de réduction à la variété centrale [35, 134, 150] et par la méthode des échelles multiples [99, 119, 121, 122, 125]. Ce travail de comparaison, déjà entamé par Nayfeh [118, 120], a été ainsi étendu. L'ajout de l'amortissement dans les calculs des MNLs est une extension originale, aucun résultat n'existant auparavant : soit l'ajout d'amortissement était mis au second ordre dans un développement en échelles multiples, ce qui revient à rajouter l'amortissement modal sur les équations de la forme normale (22) uniquement, sans tenir précisément compte de l'amortissement de toutes les autres variétés sur la dynamique normale [R9], soit il est considéré dans une procédure numérique qui ne donne pas lieu à une étude paramétrique de son influence [78, 81].

Ensuite l'application de notre méthode a donné de nombreux résultats qui sont détaillés dans la suite de ce chapitre. En se restreignant à un seul mode non linéaire, on montre déjà un résultat intéressant sur la tendance de non-linéarité. Ensuite l'utilisation des MNLs comme base réduite pour la dynamique basse fréquence des coques minces a montré d'excellents résultats, qui seront comparés avec la méthode POD.

4. Tendance de non-linéarité

La tendance de non-linéarité[6] est la dépendance de la fréquence des oscillations avec l'amplitude. Si la fréquence augmente avec l'amplitude, on a un système raidissant, sinon il est assouplissant[7]. Pour un oscillateur de Duffing, il existe des expressions analytiques qui permettent de prédire sa tendance de non-linéarité [123],[C6]. Cependant, pour un ensemble de N oscillateurs décrits par une équation type (18), il n'y a plus de solution analytique. Le recours à la simulation numérique étant assez coûteux pour faire cette prédiction, on trouve, dans de nombreuses publications des années 1970-1980, des calculs de type de non-linéarité où la dynamique est restreinte au mode considéré, cf. par exemple [64, 72, 171] pour des coques sphériques, [71] pour des plaques circulaires imparfaites. Nayfeh fut le premier à montrer que ces troncatures trop sévères pouvaient donner lieu à des prédictions erronées [124]. Depuis, des calculs corrects sont publiés, soit en utilisant un nombre de modes linéaires suffisant pour avoir atteint la convergence (cf. par exemple les travaux d'Amabili, Pellicano et Païdoussis sur les coques circulaires cylindriques [10, 13, 133] qui résolvent les résultats contradictoires obtenus auparavant [9, 11, 49, 55]), soit par des développements en échelles multiples qui *in fine* s'apparentent à un réduction sur les modes non linéaires (cf. section précédente) [17, 142].

Notre contribution sur ce sujet a été de démontrer que c'est la perte d'invariance des modes linéaires qui est responsable des erreurs de prédictions. En se plaçant sur le mode non linéaire associé, on a alors une méthode simple et rapide qui permet de prédire la bonne tendance de non-linéarité, sans faire appel à des simulations numériques coûteuses [R4]. Nous avons appliqué la méthode au cas des coques sphériques, afin de prédire le type de non-linéarité en fonction de la courbure [R8], ainsi que pour des plaques comportant une imperfection géométrique [R13]. Dans la prochaine section 4.1 nous montrons comment le formalisme de MNLs permet une prédiction rapide et correcte dans le cas général, avec ou sans amortissement [R4,R9]. Le cas d'un amortissement fort a permis de plus de montrer que celui-ci pouvait changer la tendance de non-linéarité [R9], résultat qui n'avait jamais été mis en évidence auparavant.

[6] on parle aussi du type de non-linéarité.

[7] Les termes anglais sont : hardening et softening-type non-linearity.

4.1. Cas général.

Cas conservatif

La tendance de non-linéarité pour un oscillateur non linéaire de Duffing avec termes quadratiques et cubiques :

$$\ddot{X}_p + \omega_p^2 X_p + g_{pp}^p X_p^2 + h_{ppp}^p X_p^3 = 0, \tag{24}$$

se définit via le coefficient $\tilde{\Gamma}_p$ qui gouverne la dépendance des oscillations non linéaires ω_{NL} en fonction de l'amplitude du mouvement a, via $\omega_{NL} = \omega_p(1 + \tilde{\Gamma}_p a^2)$. Pour l'équation (24), qui représente la troncature du système complet (18) au p$^{\text{ème}}$ sous-espace propre linéaire, le coefficient $\tilde{\Gamma}_p$ peut se calculer analytiquement par une méthode perturbative (cf par exemple [123]) :

$$\tilde{\Gamma}_p = \frac{1}{8\omega_p^2}\left(3h_{ppp}^p - \frac{10{g_{pp}^p}^2}{3\omega_p^2}\right). \tag{25}$$

En utilisant cette formule pour prédire les tendances de non-linéarités des modes de basse fréquence d'une structure mince, on peut aboutir à des résultats faux car, comme on l'a vu précédemment, se restreindre à un sous-espace propre linéaire, non-invariant, revient à simuler des trajectoires qui n'existent pas dans l'espace des phases complet. Ce faisant, on néglige tous les termes de couplage non linéaires entre modes propres, et qui peuvent avoir une importance considérable sur la tendance de non-linéarité. La bonne démarche consiste à regarder ce qui se passe dans le sous-espace invariant, en ne conservant qu'un seul mode non linéaire. La dynamique est alors gouvernée par :

$$\ddot{R}_p + \omega_p^2 R_p + (A_{ppp}^p + h_{ppp}^p)R_p^3 + B_{ppp}^p R_p {\dot{R}_p}^2 \;=\; 0\;, \tag{26}$$

où l'on voit apparaitre deux termes supplémentaires qui rendent compte de la présence de tous les autres oscillateurs. Un développement asymptotique au premier ordre sur (26) donne la tendance de non-linéarité sur le mode non linéaire, noté cette fois-ci Γ_p :

$$\Gamma_p = \frac{3(A_{ppp}^p + h_{ppp}^p) + \omega_p^2 B_{ppp}^p}{8\omega_p^2}. \tag{27}$$

En développant les termes A_{ppp}^p et B_{ppp}^p on peut faire apparaître explicitement que Γ_p contient des termes correctifs par rapport à $\tilde{\Gamma}_p$:

$$\Gamma_p = \tilde{\Gamma}_p - \frac{1}{8\omega_p^2}\left[\sum_{l\neq p}\frac{(8\omega_p^2 - 3\omega_l^2)}{\omega_l^2(4\omega_p^2 - \omega_l^2)}(g_{pl}^p + g_{lp}^p)g_{pp}^l\right] \tag{28}$$

Un exemple à deux ddl illustre ce résultat analytiquement et numériquement dans [R4].

Prise en compte de l'amortissement

Lorsqu'un terme d'amortissement modal est inséré dans les équations, comme cela a été fait à la section 3, la dynamique sur un mode non linéaire est alors gouvernée par l'équation suivante :

$$\ddot{R}_p + \omega_p^2 R_p + 2\xi_p\omega_p\dot{R}_p + \left(h_{ppp}^p + A_{ppp}^p\right)R_p^3 + B_{ppp}^p R_p\dot{R}_p^2 + C_{ppp}^p R_p^2\dot{R}_p = 0. \tag{29}$$

Le calcul de la tendance de non-linéarité donne le même résultat que (27), à la différence près que désormais les coefficients A_{ppp}^p et B_{ppp}^p dépendent de l'amortissement. A l'aide d'un cas simple à deux ddls, nous avons montré dans [R9] que l'amortissement avait une tendance général à rendre les comportements plus assouplissants. Dans certains cas, il peut même changer le comportement de raidissant à assouplissant. Cependant, ramené aux cas de structures minces (généralement peu amorties), on constate que les modifications apportées par la prise en compte de valeurs d'amortissements réalistes, restent faibles [R13].

4.2. Application aux coques sphériques. Cette section résume des résultats obtenus dans [R8]. On considère le modèle de coque sphérique peu profonde, de rayon a, d'épaisseur h et de rayon de courbure R, avec un bord libre, présenté section 3.1 du chapitre 1. Le formalisme présenté ci-dessus permet de mener une étude paramétrique complète afin de déterminer la tendance de non-linéarité lorsque l'on fait varier le rapport d'aspect $\kappa = \frac{a^4}{R^2 h^2}$. Lorsque $\kappa = 0$, le rayon de courbure R est infini : les équations se résument à celles d'une plaque et le comportement est raidissant pour tous les modes. Diminuant R, et donc augmentant κ, les modes peuvent alors passer d'un comportement raidissant à assouplissant. Le calcul est mené en utilisant la formule (27). La formule développée (28) montre en outre que :

- Les seules résonances susceptibles de modifier le type de non-linéarité sont des résonances 2:1, *i.e. lorsque la fréquence ω_p du mode étudié vaut le double d'une fréquence propre d'un autre mode l.*
- La formule fait intervenir tous les coefficients quadratiques g_{ij}^p qu'il faut a priori calculer, ce qui peut être couteux. La procédure est alors grandement accélérée en constatant que :
  (1) Seulement un petit nombre de coefficients g_{ij}^p sont non-nuls, car les modes p, i, et j impliqués doivent vérifier des relations de commensurabilité entre leurs nombres respectifs de diamètres nodaux (ces *règles de couplage* sont explicitées dans [R6]). Ceci réduit drastiquement le nombre de termes à retenir dans (28).
  (2) Les coefficients g_{ij}^p dépendent très peu de κ [R6]. On peut donc à moindre frais les considérer constant sur des sous-intervalles de calcul.

La figure 1 montre le résultat obtenu pour le mode (3,0). Pour $\kappa = 0$ on obtient bien une non-linéarité raidissante typique des plaques. Le comportement devient assouplissant pour $\kappa = 49.69$, où une résonance 2:1 entre le mode (0,1) et (3,0) a lieu. Ensuite le comportement est assouplissant et tend vers zéro (comportement neutre) pour les grandes valeurs de κ. Sur cette figure est aussi montré l'effet de la

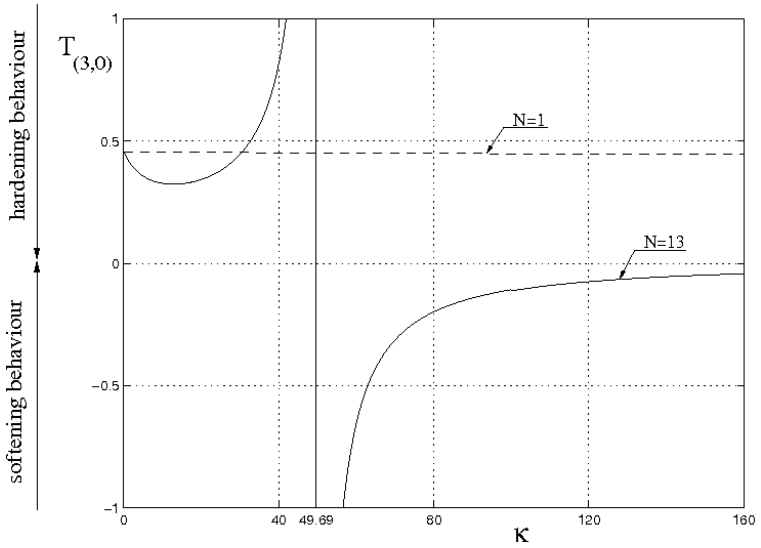

FIG. 1. Tendance de non-linéarité pour le mode (3,0) en fonction du rapport d'aspect κ pour une coque sphérique peu profonde. En pointillé : valeur prédite si l'on se restreint la dynamique au mode linéaire. Trait plein : valeur prédite en conservant 13 modes linéaires pour calculer le mode non linéaire.

troncature. La courbe en pointillé est obtenue en ne conservant qu'un mode linéaire dans la dynamique. La prise en compte des autres modes permet de révéler la courbure du sous-espace invariant et de donner la bonne tendance de non-linéarité. Ce résultat est générique de ceux obtenus pour les modes purement asymétriques, *i.e.* de la forme (k,0). Ceux-ci ayant des fréquences propres ne dépendant quasiment pas du rapport d'aspect κ (cf. [R6] et figure 2 du chapitre 1), on trouve que le comportement change de nature uniquement lorsque les résonances internes 2:1 ont lieu. Un comportement différent est obtenus pour les modes axisymétriques et mixtes, dont les fréquences propres dépendent drastiquement de κ. La

figure 2 montre le résultat obtenu pour le mode (0,2), où l'on constate que la tendance de non-linéarité diminue fortement dès les petites valeurs de κ pour changer de signe en $\kappa = 13.73$, sans rencontrer de résonance 2:1. Celles-ci arrivent par la suite et se traduisent par de petites zones où le comportement redevient raidissant. La convergence est aussi montrée sur la figure 2. Les règles de couplage évoquées précédemment montrent ici que seuls les modes axisymétriques peuvent avoir une influence sur le type de non-linéarité d'un mode axisymétrique.

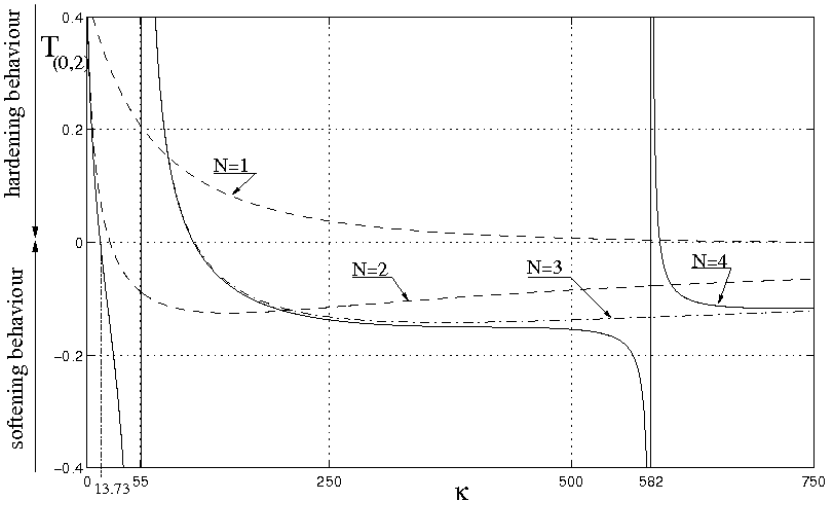

FIG. 2. Tendance de non-linéarité pour le mode (0,2) d'une coque sphérique en fonction de κ (trait plein). Les courbes en pointillées montrent la convergence de la solution lorsque l'on augmente le nombre de modes axisymétriques utilisés dans le calcul, respectivement : N=1, mode (0,2) uniquement ; N=2, modes (0,1) et (0,2) ; N=3, modes (0,1) à (0,3) ; N=4, modes (0,1) à (0,4). la solution convergée est calculée avec les 7 premiers modes axisymétriques, elle coincide avec celle obtenue pour N=4.

Effet de l'amortissement

La figure 3 montre l'effet de l'amortissement sur le type de non-linéarité du mode (0,1). Deux lois de variation de l'amortissement ont été considérées :

cas (i): $\forall\ p = 1 \ldots N,\ \ \xi_p = \xi\,/\,\omega_p$

cas (ii): $\forall\ p = 1 \ldots N,\ \ \xi_p = \xi$

Le cas (i) correspond à un amortissement modal indépendant de la fréquence, dont on augmente la valeur nominale ξ pour mesurer la variation de la tendance de non-linéarité. Le cas (ii) correspond à une variation de l'amortissement modal linéaire avec la fréquence. Dans les deux cas on observe qu'il faut arriver à des valeurs très grandes de l'amortissement pour observer des changements significatifs. Pour des structures métalliques, l'amortissement ξ est de l'ordre de 10^{-3}, au plus 10^{-2} : notre prédiction montre que l'effet de l'amortissement sur le type de non-linéarité ne peut se faire ressentir que pour des valeurs beaucoup plus importantes (0.1 voire 0.3 pour avoir quelquechose de significatif). Une particularité du cas (ii) est qu'il ne gomme pas la discontinuité qui existe à la résonance 2:1, ceci apparait effectivement dans les petits dénominateurs obtenus analytiquement [R9,R13]. Cependant cela ne devrait pas avoir de conséquences au niveau expérimental. En effet, en présence d'une résonance 2:1, les solutions sont toujours couplées si bien que la solution 1 ddl n'existe pas, et parler de tendance de non-linéarité n'a plus de sens dans un petit intervalle autour de cette résonance.

5. Réduction de modèles de coque

Dans cette section on montre comment on peut utiliser le formalisme des MNLs afin d'effectuer des modèles d'ordre réduit performants pour des vibrations forcées harmoniques de coques minces. La

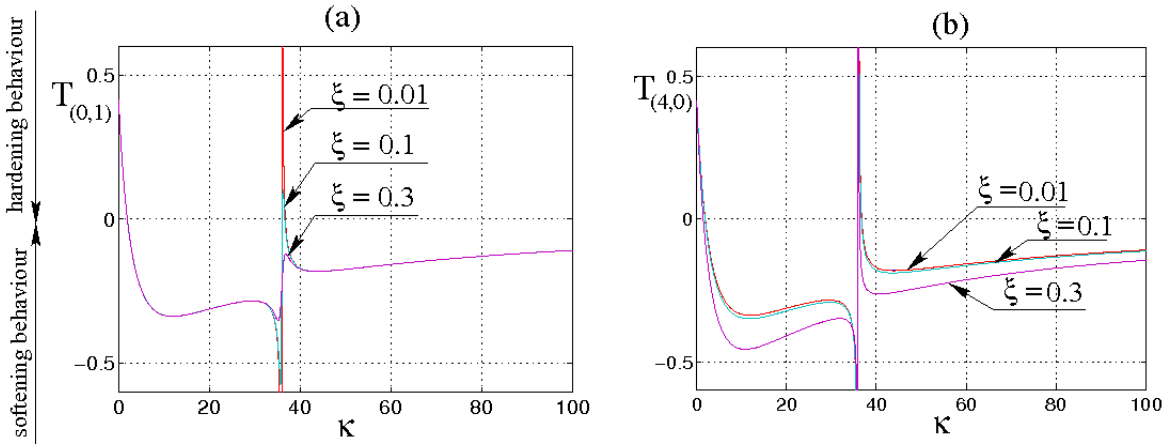

FIG. 3. Tendance de non-linéarité pour le mode (0,1) d'une coque sphérique en fonction du rapport d'aspect κ, et pour différentes valeurs de l'amortissement. (a) : amortissement correspondant au cas (i), avec les valeurs ξ = 0.01 (en rouge), 0.1 (cyan) et 0.3 (violet). (b) : amortissement correspondant au cas (ii), avec les mêmes valeurs de ξ.

présentation reprend des résultats montrés dans [R9] et [R12]. Le cas des poutres a été traité dans [R5] et n'est pas repris ici. Dans ce document, nous ne reprenons que les deux modèles présentés chapitre 1, à savoir le panneau hyperbolique paraboloide de la section 4.3, forcé au voisinage de son mode fondamental, et pour lequel un seul mode non linéaire permet de prédire la dynamique. Puis le cas de la coque circulaire cylindrique de la section 4.2, forcé au voisinage d'un mode asymétrique, caractérisé par une valeur propre dégénérée et l'occurrence de deux modes propres ayant la même fréquence (modes compagnons). Dans ce cas-là la dynamique forcée au voisinage d'un tel mode est plus complexe à cause de la résonance 1:1 entre les deux valeurs propres, si bien que le modèle minimal sera composé de deux MNLs.

Dans tout ce qui suit deux hypothèses fortes, relatives à la manière dont le modèle réduit est construit, viendront nuancer les résultats. Premièrement les MNLs sont calculés à l'aide d'un développement asymptotique d'ordre 3, si bien que l'on s'attend à des résultats qui peuvent se déteriorer aux très grandes amplitudes. Deuxièmement le terme de forçage n'est pas inclus dans le calcul des MNLs. Nous utilisons les variétés du problème non-forcé, indépendantes du temps, afin de réduire une dynamique dépendante du temps. L'ajout de ce terme de forçage dans la procédure même du calcul des MNLs est réalisable avec le formalisme des formes normales, comme démontré dans [53]. Cependant, son effet principal est de rendre la variété invariante dépendante du temps. Les calculs numériques montrés dans [78, 81], tenant compte de cet effet, montre en effet que les oscillations de la variété sont très petites.

5.1. Panneau à double courbure. La coque étudiée ici est un panneau hyperbolique paraboloide (panneau HP), déjà présenté en détail au chapitre précédent. Le panneau retenu pour les simulations numériques a les dimensions suivantes : $a = b = 0.1$ m, $R_x = -R_y = 1$ m, et épaisseur $h = 1$ mm ; les propriétés matérielles sont : module d'Young $E = 206.10^9$ Pa, masse volumique $\rho = 7800$ kg.m^{-3} et coefficient de Poisson $\nu = 0.3$. La réponse de la coque à un forçage harmonique au voisinage de la première fréquence propre ω_1 est calculée numériquement. La convergence de la solution a été étudiée pour une amplitude d'excitation de 4.37 N appliquée au centre de la coque [7]. Il a été montré que 22 fonctions de base étaient nécessaires pour obtenir une solution convergée. Les fonctions de base retenues sont : $\phi^{(w)}_{1,1}$, $\phi^{(w)}_{1,3}$, $\phi^{(w)}_{3,1}$, $\phi^{(w)}_{3,3}$, $\phi^{(u)}_{1,1}$, $\phi^{(u)}_{3,1}$, $\phi^{(u)}_{1,3}$, $\phi^{(u)}_{3,3}$, $\phi^{(u)}_{1,5}$, $\phi^{(u)}_{5,1}$, $\phi^{(u)}_{3,5}$, $\phi^{(u)}_{5,3}$, $\phi^{(u)}_{5,5}$, $\phi^{(v)}_{1,1}$, $\phi^{(v)}_{3,1}$, $\phi^{(v)}_{1,3}$, $\phi^{(v)}_{3,3}$, $\phi^{(v)}_{1,5}$, $\phi^{(v)}_{5,1}$, $\phi^{(v)}_{3,5}$, $\phi^{(v)}_{5,3}$, $\phi^{(v)}_{5,5}$.

La courbe de réponse en fréquence pour les six coordonnées principales est montrée figure 4. Elle est calculée numériquement par une méthode de continuation par pseudo-longueurs d'arc implémentée dans le logiciel AUTO [47]. Cette solution de référence à 22 degrés de liberté est comparée à deux

solutions réduites ne comportant qu'un seul ddl, obtenues respectivement en projetant la dynamique sur le premier mode linéaire (solution LNM) et sur le premier mode non linéaire (NNM sur la figure 4). La solution LNM reproduit le caractère raidissant de la solution de référence mais les erreurs commises sur les amplitudes sont beaucoup trop grandes pour qu'elle soit acceptable. A contrario, la réduction à un seul mode non linéaire donne un résultat très proche de la référence, avec une légère surestimation du caractère raidissant.

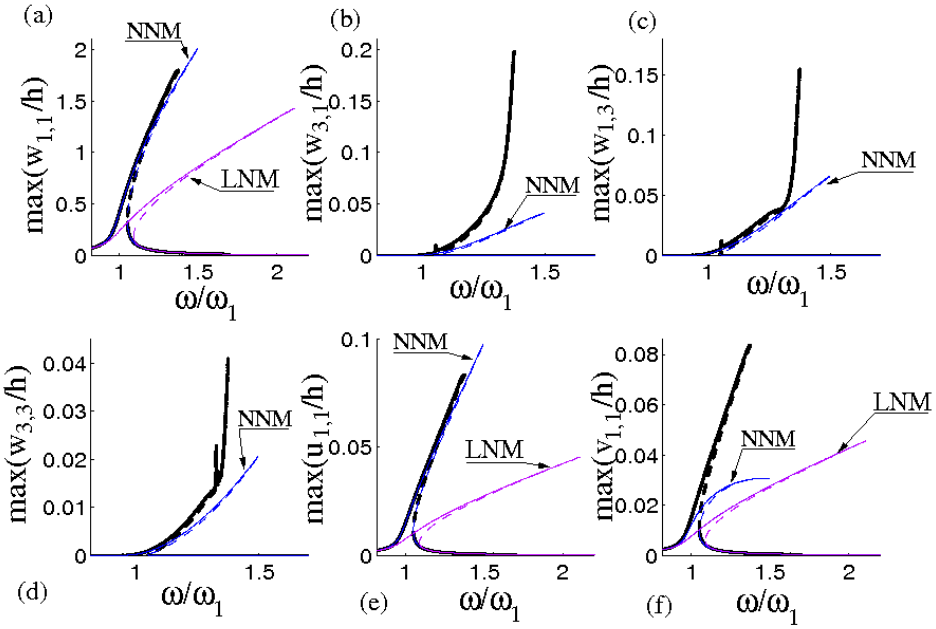

FIG. 4. Amplitudes maximales de la réponse des 6 coordonnées généralisées principales en fonction de la fréquence d'excitation, pour une amplitude de forçage de 4.37 N. Solution de référence (noir) ; Modèle réduit à un mode linéaire (LNM) et à un mode non linéaire (NNM). Coordonnées : (a) : $w_{1,1}$. (b) : $w_{3,1}$. (c) : $w_{1,3}$. (d) : $w_{3,3}$. (e) : $u_{1,1}$. (f) : $v_{1,1}$.

Il est à noter que l'énergie vibratoire est essentiellement concentré dans la coordonnée $w_{1,1}$, figure 4(a), les réponses des autres termes étant d'un ordre inférieur. Nous voyons cependant apparaitre un des points forts de la méthode MNL : grâce au changement de variables non linéaire, on obtient une réponse sur tous les modes et donc toutes les coordonnées généralisées, et pas uniquement sur le mode directement excité, alors qu'on ne simule qu'une seule équation d'oscillateur. Pour les autres coordonnées montrées sur la figure 4, $w_{3,1}$, $w_{1,3}$, $w_{3,3}$, $u_{1,1}$ et $v_{1,1}$, la solution MNL donne une bonne approximation de leurs valeurs, ce qui confirme que la courbure de la variété invariante est ici seule responsable, via les termes non-résonnants, des couplages faibles observés ici entre coordonnées généralisées. Pour le modèle réduit ne comportant qu'un seul mode linéaire, on ne retrouve de l'énergie que sur les 3 coordonnées $w_{1,1}$, $u_{1,1}$ et $v_{1,1}$, qui sont linéairement couplées afin de donner le premier sous-espace propre linéaire.

La figure 5 montre les réponses temporelles obtenues sur la branche du haut, pour une fréquence d'excitation $\omega = 1.3\omega_1$, permettant de mieux apprécier la qualité du modèle réduit sur un signal de vibration. Alors qu'un seul oscillateur est simulé, le changement de variables permet de recouvrer des formes d'ondes complexes et différentes, très proches de la simulation de référence. A contrario, on mesure mieux avec cette représentation que le modèle réduit à un MNL donne des résultats qui ne sont pas acceptables.

Les excellents résultats donnés par la réduction à un mode non linéaire proviennent du fait que la dynamique est finalement assez simple dans ce cas-là, l'essentiel de la complexité résidant dans la courbure de la variété invariante qui est captée par le mode non linéaire. On aurait pu penser qu'en

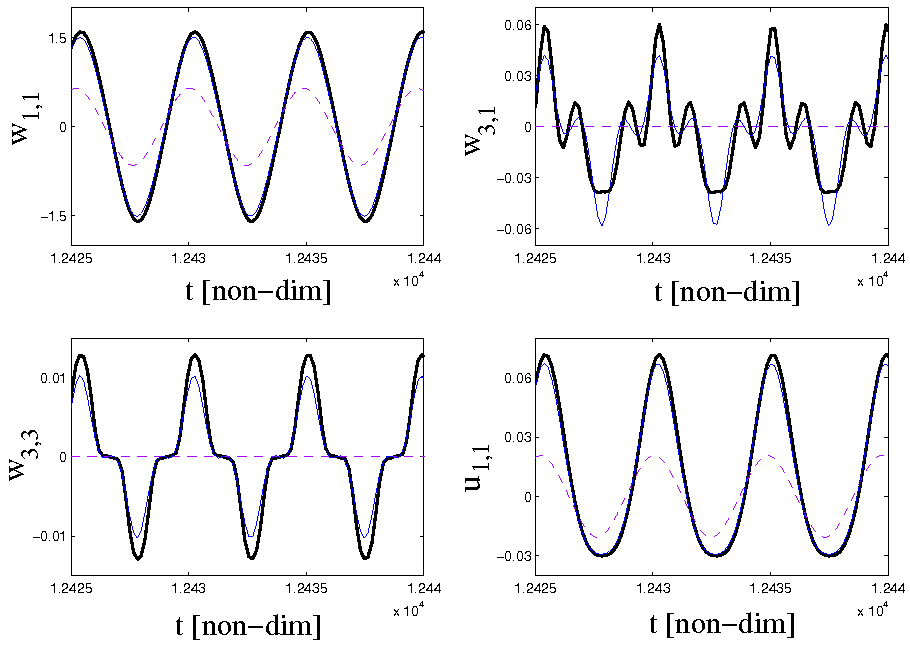

FIG. 5. Réponses temporelles de 4 coordonnées généralisées pour le panneau HP, pour une fréquence d'excitation $\omega = 1.3\omega_1$, d'amplitude $\tilde{f} = 4.37$ N. La solution de référence (22 ddls, courbe noire épaisse) est comparée à la réduction à un MNL (courbe bleue fine) et un mode linéaire (courbe pointillée magenta).

augmentant le nombre de modes linéaires on obtiendrait une convergence assez rapide, or ce n'est pas du tout le cas : l'étude de convergence en fonction du nombre de modes linéaires a été menée dans [R12] et montre qu'il faut 15 modes linéaires pour retrouver la solution de référence. On est donc dans un cas où la courbure de la variété est prononcée et relie un grand nombre de modes linéaires, si bien qu'une fois cette complexité géométrique calculée dans le changement de variables non linéaire, il ne reste plus qu'à simuler une dynamique simple à un seul ddl. Il est enfin à noter que dans ce cas de vibrations forcées harmoniques, augmenter le nombre de MNLs dans la troncature n'améliore pas le résultat car la solution de référence est essentiellement contenue dans la variété invariante. Ce qui a été observée ici numériquement : des coordonnées de MNLs ajoutées avaient une amplitude nulle et la solution n'était pas meilleure que celle obtenue avec un seul MNL. Ansi le modèle réduit proposé ici est bien le meilleur possible puisqu'il est directement convergé et très proche de la solution. Les différences que l'on observe sont dues uniquement aux deux approximations qui ont été faites pour calculer le modèle réduit, à savoir :

– le développement asymptotique tronqué à l'ordre trois.
– le calcul de variété invariante indépendante du temps.

Pour illustrer ce propos, on montre figure 6 les courbes de réponse en fréquence obtenues pour une valeur inférieure de l'amplitude du forçage ($\tilde{f} = 2.84$ N) et une valeur supérieure ($\tilde{f} = 6.62$ N). Comme attendu, les résultats sont quasiment parfaits pour 2.84 N, car les deux approximations mentionnées donnent ici lieu à des erreurs négligeables. Par contre, aux plus grandes amplitudes, la troncature au MNL calculé à l'ordre 3 donne de nouveau des résultats qui se détériorent. Ces tests numériques permettent d'évaluer la limite de validité du modèle réduit à des amplitudes de vibration de l'ordre de $1.5h$.

Les gains en temps de calcul ont été évalués en mesurant le temps nécessaire pour faire une courbe de réponse en fréquence avec le logiciel AUTO. Pour le modèle de référence (22ddls), il a fallu 2 heures pour parcourir la courbe montrée figure 4[8]. Pour le modèle réduit composé d'un seul NNM, il faut de l'ordre de

[8]Les temps de simulation ont été mesurés sur un processeur Pentium 4 cadencé à 2.4GHz (simulations réalisées au début de l'année 2007).

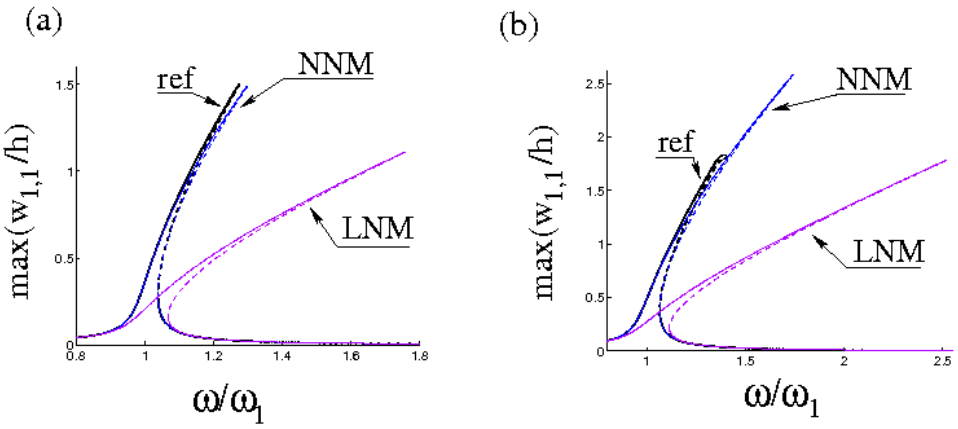

FIG. 6. Courbes de réponse en fréquence pour (a) : $\tilde{f}$ = 2.84 N, et (b) : $\tilde{f}$ = 6.62 N. La solution de référence (22 ddls, noire) est comparée aux modèles réduits composés d'un mode linéaire (LNM) et un mode non linéaire (NNM).

30 secondes pour parcourir la courbe de réponse en fréquence. A ce temps on doit ajouter le temps passé dans les changement de variables, 2 minutes aller/2 minutes retour, soit un temps total de simulation de 4 minutes 30 ; soit un temps de calcul divisé par 26. Dans [R12], 4 cas de coques différentes sont testés, montrant à chaque fois un gain en temps de calcul très appréciable, de l'ordre de 25. En conclusion sur cet exemple on peut dire que le modéle réduit MNL est le meilleur possible, puisque celui qui se situe au plus proche de la véritable solution, comme le montre le fait qu'ajouter des MNLs supplémentaires ne rapproche pas de la solution de référence. Pour corriger les erreurs d'amplitude obtenues à partir du forçage de 4.37 N, la seule solution est de lever les deux hypothèses utilisées ici pour fabriquer le modèle réduit. Cependant il est alors loin d'être acquis que les gains en temps de calcul seront aussi substantiels. Pousser le développement à l'ordre 5 augmenterait considérablement le temps passé dans les changements de variables non linéaires, qui prennent déjà la plus grande partie du temps de calcul pour les simulations présentées à l'ordre 3. Enfin les méthodes numériques existantes dans la littérature (ce qui serait évidemment la bonne solution pour ne plus avoir le problème du développement asymptotique) sont très coûteuses [80, 81, 135].

5.2. Coque circulaire cylindrique. Dans cette section nous reprenons la coque circulaire cylindrique, de longueur a, de rayon R, simplement supportée aux extrémités, avec cinématique de Flügge-Lur'e-Byrne, présentée en section 4.2. Les caractéristiques de la coque utilisée pour les simulations sont : $a = 520$ mm, $R = 149.4$ mm, $h = 0.519$ mm, $E = 1.98 \times 10^{11}$ Pa, $\rho = 7800$ kg.m^{-3}, $\nu = 0.3$; elle est forcée sinusoidalement au voisinage de la fréquence de résonance du mode $(m, n) = (1, 5)$. Celui-ci étant asymétrique, la valeur propre est double et il y a deux modes propres ayant la même fréquence. Ces modes compagnons sont notés $(1, 5, c)$ et $(1, 5, s)$ par la suite, le troisième indice faisant référence au fait que la coordonnée angulaire est soit en cosinus, soit en sinus. L'excitation est située sur un nœud du mode $(1, 5, s)$, qui ne se trouve donc pas directement excité par le forçage extérieur. Par contre, étant en résonance 1:1 avec la configuration $(1, 5, c)$, il se trouvera rapidement avoir de l'énergie par couplage non linéaire.

La solution de référence est composée de 16 degrés de liberté. Elle est comparée figure 7 à une solution composée de deux modes non linéaires, pour une amplitude de forçage de 2 N. Une comparaison avec un modèle réduit composé de modes linéaires n'a pas été possible ici : tous les modèles réduits testés avec N_{lin} modes inférieurs à 16 donnaient un comportement raidissant ; seule la troncature à 16 modes linéaires (*i.e.* ne présentant aucune réduction par rapport à la solution de référence) prédisait un comportement assouplissant. Le modèle réduit composé de deux MNLs est le modèle minimal que l'on puisse espérer à cause de la résonance 1:1, qui implique que des solutions couplées vont avoir lieu dans un sous-espace de dimension 5.

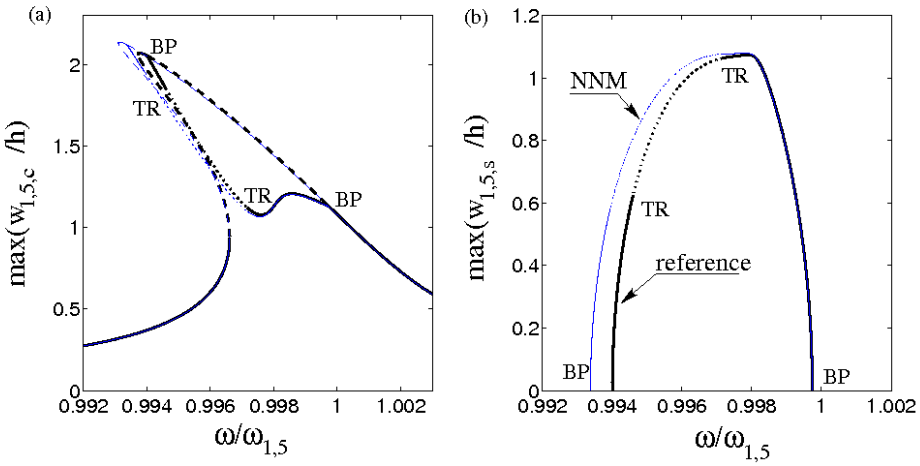

FIG. 7. Courbes de réponse en fréquences pour la coque circulaire cylindrique, en fonction de la fréquence d'excitation, pour une amplitude de 2 N. La solution de référence (trait épais noir) est comparée à un modèle réduit composé de 2 MNLs (trait fin bleu). (a) : Amplitude maximale du mode directement excité $w_{(1,5,c)}$. (b) : Amplitude maximale du mode compagnon $w_{(1,5,s)}$. BP : point de bifurcation fourche menant à la solution couplée. TR : Bifurcation Tore (Neimarck-Sacker) de la solution couplée menant au régime quasipériodique.

La solution de référence est composée de deux branches. La première est caractérisée par une participation nulle du mode $(1, 5, s)$: seul le mode directement excité est présent dans la réponse, qui est de nature assouplissante. Sur cette première branche se trouvent deux points de bifurcation fourche (BP sur la figure 7) desquels émane une seconde branche de solutions couplées où le mode $(1, 5, s)$ a une amplitude non-nulle. Sur cette seconde branche, deux autres points de bifurcation sont présents, où une bifurcation de Neimarck-Sacker (TR sur la figure 7) mène à un comportement quasipériodique dans la réponse.

Le modèle réduit composé de deux MNLs reproduit parfaitement ce diagramme de bifurcation, avec une très légère surestimation du caractère assouplissant. En augmentant l'amplitude du forçage, on a pu évaluer le modèle réduit comme étant fiable jusqu'à des amplitudes de vibration de l'ordre de 3 fois l'épaisseur. Le gain en temps de calcul est ici d'un facteur 32 [R12].

6. Comparaison avec la méthode POD

Dans cette section nous allons comparer la méthode de réduction par MNL à la méthode POD. Le modèle choisi pour effectuer cette comparaison est une coque circulaire cylindrique remplie d'eau, forcée harmoniquement au voisinage du mode $(1, 5)$. La cinématique est de Donnell avec l'hypothèse de coque peu profonde, si bien que l'inertie membranaire est négligée (modèle présenté au chapitre 1, section 3.2). Nous reprenons ici des résultats publiés dans [R10].

La méthode POD est extrêmement utilisée dans tous les domaines de la science pour sa rapidité et sa facilité d'implémentation, que ce soit en statistique [86, 95, 103] (où elle est plus couramment appelée méthode de Karhunen-Loève), en science atmosphérique [104] ou en analyse d'épisodes climatiques précis comme l'ENSO (El Nino Southern Oscillation) [25] et plus généralement en océanographie et météorologie (où la méthode est appelée EOF pour Empirical Orthogonal Functions), en Analyse de données et traitement du signal (où la méthode est équivalente à la PCA, pour Principal Component Analysis)[83], enfin dans les domaines biomédical [26] et biomécanique [136]. En mécanique, les premières applications ont eu lieu dans le domaine de la mécanique des fluides et plus particulièrement de

la turbulence pour l'extraction de structures cohérentes [29, 70]. Sont désormais traités avec cette méthode des cas d'interaction jet/tourbillon [108], d'écoulements derrière une cavité [131] ou encore de convection de Bénard-Marangoni [20]. De nombreuses extensions existent, en particulier le cas de la BOD (Biorthogonal Decomposition) où les variables temps et espaces sont simultanément traitées [73].

En dynamique des structures, la méthode POD fut beaucoup employée à partir de la fin des années 1990 [24, 57, 58, 61, 90, 96, 166]. L'article [91] propose une vue d'ensemble des travaux existants. La question importante du lien entre les modes POD et les modes linéaires a été traitée dans [57, 102], mettant en évidence que les modes POD convergent vers les modes linéaires lorsque le nombre d'observations tend vers l'infini. Par conséquent, l'utilisation des modes POD est parfois sans grand intérêt par rapport aux modes linéaires, comme montré dans [147]. Pour le cas des structures soumises à des forçages aléatoires, citons aussi [27, 59]. Pour ce qui est des modes POD utilisés véritablement comme base réduite, citons [15, 16, 63] pour le cas des coques circulaires cylindriques, [61] pour le cas des élastiques, enfin les articles [97, 100] et les références qui s'y trouvent sont un bon point d'entrée pour la méthode POD et d'autres méthodes de réduction de modèles pour les systèmes mécaniques Lagrangiens et discrétisés par éléments finis.

Avant même de montrer des résultats numériques de la comparaison entre la méthode POD et les MNLs, les remarques suivantes sont importantes afin de bien comprendre ce qui distingue les deux méthodes, et ce que l'on est en droit d'en attendre :

- La méthode POD est essentiellement linéaire, puisqu'il s'agit de trouver les hyperplans de l'espace des phases les plus proches des données que l'on fournit pour construire le modèle. Cela peut être vu comme un avantage puisque la construction de la base réduite est relativement simple (essentiellement il s'agit de résoudre un problème aux valeurs propres), mais aussi comme un inconvénient : si la structure de données présente un nuage de points courbés dans l'espace des phases, des hyperplans ne seront pas adaptés pour bien capturer l'information. La méthode MNL pallie ce problème en proposant des sous-variétés courbes de l'espace des phases : c'est une méthode essentiellement non linéaire.
- la méthode POD est globale au sens où elle décompose l'espace des phases complet à l'aide d'une base orthogonale adpatée. A contrario la construction des MNLs repose sur une théorie locale, valable uniquement au voisinage d'un point fixe.
- Les deux méthode diffèrent par la manière dont le modèle réduit est construit. Alors que la méthode POD a besoin d'une série temporelle de données afin de construire les axes POD, les caractéristiques du spectre de l'opérateur linéaire sont suffisant pour construire les MNLs. Ceci peut être vu comme un avantage dans le contexte de modèles prédictifs où l'on travaille sur des modèles mathématiques, et où l'on souhaite se passer d'une étape supplémentaire consistant à calculer une réponse du modèle de référence. Cependant, dans les cas expérimentaux ou dans des problèmatiques de contrôle où l'on n'a pas de modèles, cela constitue bien évidemment un avantage pour la méthode POD.

La première comparaison est montrée figure 8, pour une coque circulaire cylindrique remplie d'eau, forcée au voisinage de la fréquence propre du mode $(1, 5, c)$. La description détaillée des procédures utilisées pour le modèle POD sont décrites dans [15]. Les points notés b et c sur la courbe de référence ont été utilisés pour construire les bases réduites POD. Le point b se trouve juste avant la bifurcation de Neimarck-Sacker, la réponse y est périodique ; le point c se trouve juste après, la solution de référence est quasipériodique. Il est à noter que l'utilisation d'une série temporelle au point b n'a jamais donné de modèle POD satisfaisant [15]. La réponse quasipériodique au point c a permis quant à elle de fournir un modèle POD correct, à la condition de ne pas oublier la symétrie de révolution qui permet d'avoir des ondes progressives dans deux directions opposées [15], information qu'il faut rajouter a posteriori pour que le modèle réduit recouvre les symétries du problème original.

Les réponses en fréquence montrées figure 8, obtenues pour un forçage extérieur d'amplitude 3 N, sont coincidentes avec la solution de référence, les deux modèles réduits rendant bien compte du diagramme de bifurcation. Il est cependant à noter que seuls 2 MNLs sont utilisés, alors qu'il est nécessaire

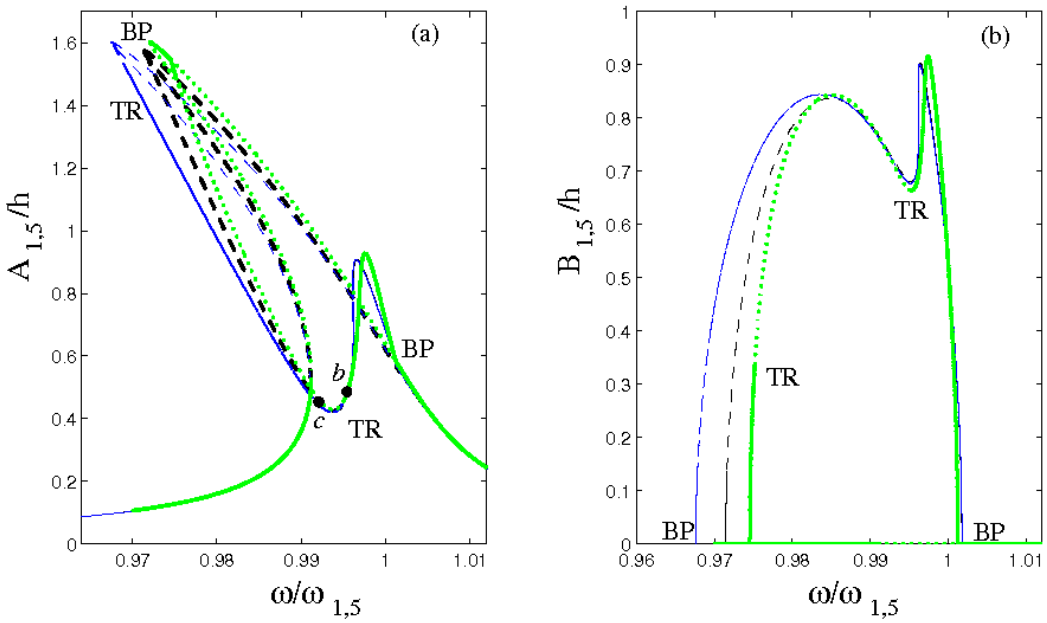

FIG. 8. Réponse en fréquence d'une coque circulaire cylindrique remplie d'eau au voisinage de la fréquence propre du mode $(1, 5, c)$. Solution de référence (16 ddls, courbe noire), réduction MNL (2 ddls, courbe bleue) et réduction POD (3 modes PODS, courbe verte). (a) : maximum du déplacement de la coordonnée modale $A_{1,5}$ du mode $(1, 5, c)$. (b) : coordonnée modale $B_{1,5}$ du mode $(1, 5, s)$.

d'avoir 3 modes POD pour retrouver le diagramme de bifucation correct. La solution ne contenant que deux modes POD manque systématiquement le point de bifurcation fourche si bien qu'il ne prédit jamais de solutions couplées.

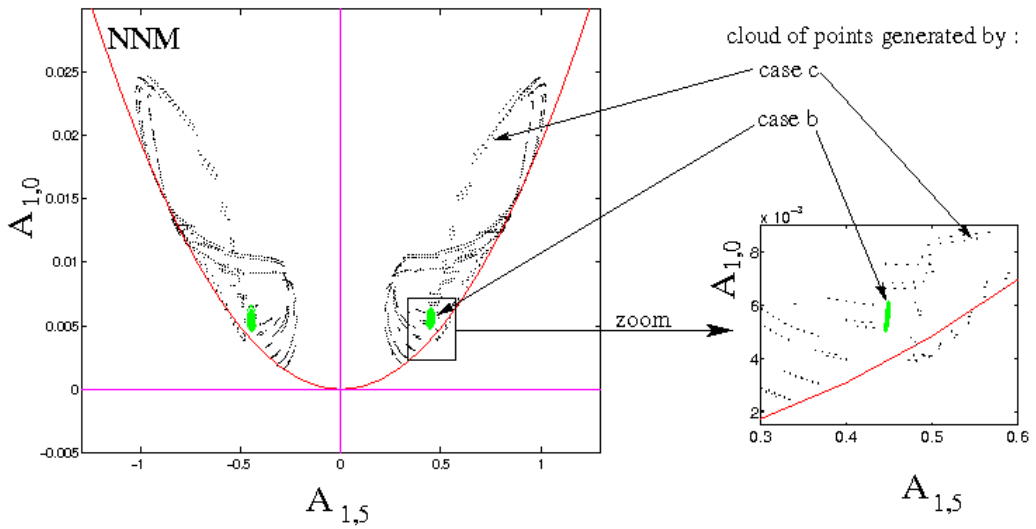

FIG. 9. Section de Poincaré, plan de coupe $(A_{(1,5)}, A_{(1,0)})$. Nuages de points : section avec les orbites périodiques et quasipériodiques calculées aux point b et c de la figure 8. Axes verticaux et horizontaux : axes POD. Courbe NNM : section de la variété invariante correspondant au mode non linéaire issu de $(1, 5, c)$.

Une interprétation géométrique permet de comprendre pourquoi ce troisième mode POD est nécessaire alors que seuls deux MNLs suffisent. La figure 9 montre une section de Poincaré dans l'espace des phases complet, qui est de dimension 33 (la solution de référence est à 16 ddls, soit 32 coordonnées généralisées puisqu'il compter une paire déplacement/vitesse par ddl, et il faut ajouter le terme de forçage pour rendre le système dynamique autonome). La section de Poincaré est effectuée dans le plan $(A_{(1,5)}, A_{(1,0)})$[9], pour mettre en exergue le rôle joué par le premier mode axisymétrique. Les nuages de points sont donnés par les solutions de référence aux point b et c. On comprend déjà mieux pourquoi la solution quasipériodique permet de trouver plus facilement les axes POD, car elle parcourt un sous-espace plus grand de l'espace des phases, ce gain d'information permettant d'avoir beaucoup plus de précisions sur le calcul des modes POD. Cet argument a déjà été employé dans [16, 89] afin de souligner que des réponses chaotiques sont a priori de bons candidats pour construire des bases POD.

Les axes droits de la figure 9 sont les hyperplans donnés par la méthode POD. Les deux premiers hyperplans donnés par la méthode POD sont respectivement très proches des modes linéaires $(1, 5, c)$ et $(1, 5, s)$ (celui-ci n'étant pas reporté sur la coupe). Le troisième hyperplan, contenant encore suffisamment d'énergie afin d'être indispensable, est quant à lui proche du mode linéaire axisymétrique $(1, 0)$ (axe vertical de la figure 9)[10]. Si l'on se restreint aux deux premiers modes POD, toute l'information contenue selon $A_{(1,0)}$ est oubliée, et le modèle n'est pas correct. Cette remarque est consistante avec les travaux d'Amabili *et al.* [10, 13, 14] soulignant l'importance des modes axisymétriques dans les troncatures de modèles de coques circulaires, ainsi que les résultats que nous avons obtenus sur les coques sphériques [R6,R8]. A contrario, les variétés MNLs passent exactement à proximité du nuage de points. Le couplage entre les modes asymétriques et axisymétriques est ainsi complètement inclus dans la géométrie de la variété, si bien que seuls les deux modes non linéaires qui sont les continuations des modes linéaires $(1, 5, c)$ et $(1, 5, s)$ sont nécessaires pour fournir le meilleur modèle réduit possible.

Des courbes de réponses en fréquences obtenues pour une amplitude de forçage plus grande (8 N) sont montrées dans [R10], où les mêmes modèles réduits sont comparés (deux MNLs et 3 PODs construits avec la réponse quasipériodique à 3 N). La méthode POD prédit des bonnes amplitudes, par contre les points de bifurcations sont significativement décalés par rapport à la solution de référence. Le modèle MNL donne quant à lui des points de bifurcation bien placés mais surestime le caractère assouplissant du mode excité. Ces limitations, une fois de plus, sont dues uniquement aux deux approximations faites pour calculer les MNLs : calcul asymptotique à l'ordre 3 et variétés indépendantes du temps pour un problème forcé.

Enfin des diagrammes de transition vers le chaos, obtenus par section stroboscopique de Poincaré sur une simulation à fréquence d'excitation fixe et amplitude du forçage croissant, sont montrés dans [R10]. Un modèle à 5 POD, dont la construction est détaillée dans [16] permet de capturer les première bifurcations, pour des amplitudes de forçage allant jusqu'à 600 N. A contrario, le modèle à 2 MNLs donne des solutions divergentes pour une amplitude de 240 N : les limites de validité du développement asymptotique étant atteintes. Ce sont là les conséquences de la nature locale et globale et modèles réduits, soulignée en introduction.

[9] Conformément aux notations du chapitre 1, section 3.2., la coordonnée généralisée du mode $(1, 5, c)$ est notée $A_{(1,5)}$, celle du mode $(1, 5, s)$, $B_{(1,5)}$.

[10] Les valeurs précises des positions des axes sont données dans [15] et [R10].

CHAPITRE 3

Transition vers le chaos

1. Observations expérimentales

Lorsque l'on excite une structure mince avec une force sinusoidale d'intensité croissante, on observe généralement deux bifurcations, menant d'un régime périodique à un régime chaotique, caractérisé par un spectre de vibration large bande. Ces expériences ont été à la base des analyses menées sur les instruments de percusion de type cymbales et gongs, lors de ma thèse [T1] et celle d'Olivier Thomas [156]. Ce qui nous guidait alors était que le son produit par une cymbale lors du régime forcé chaotique est très proche de celui obtenu en mode de jeu normal, lorsque l'on excite la cymbale par un coup de baguette. Ayant en main une expérience très contrôlée et parfaitement reproductible, où l'énergie n'est envoyée qu'à une seule fréquence et dont on contrôle précisément l'amplitude, le but était alors de retrouver les caractéristiques de la vibration libre à partir des analyses des expériences en forcé et de la description fine des transitions observées. Ceci nous a amené a étudier précisément chacune des bifurcations, ainsi que les régimes observés.

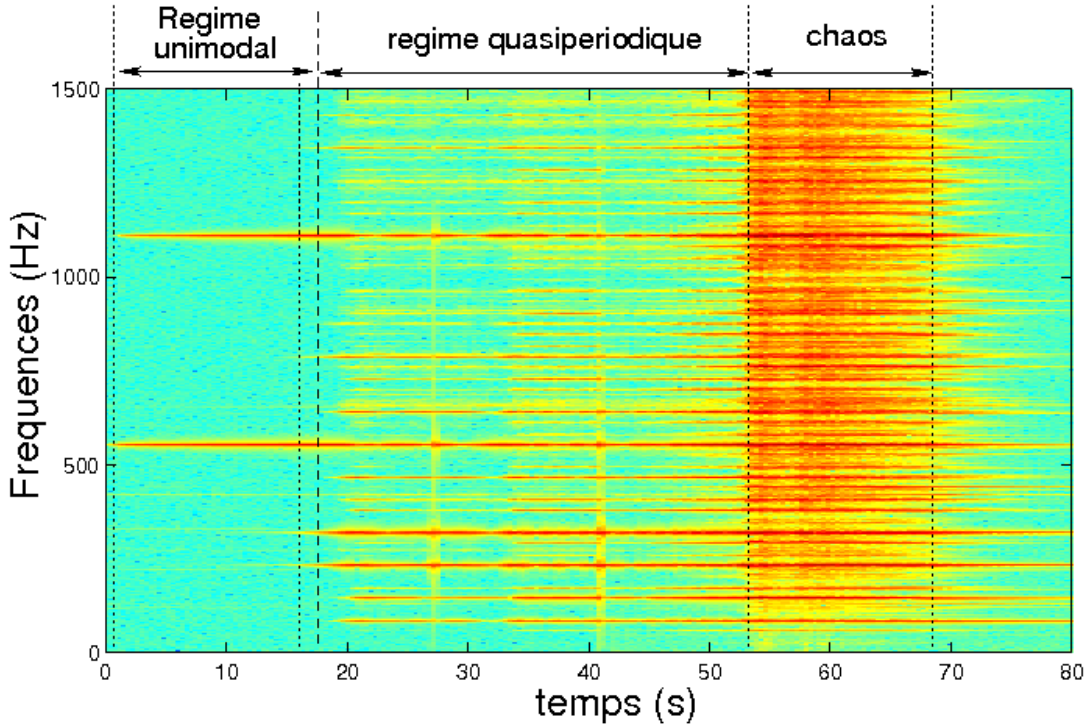

FIG. 1. Diagramme temps-fréquence d'une expérience de vibrations forcées sur un gong excité à 556 Hz avec une amplitude croissante au cours du temps. On distingue trois régimes distincts, séparés par des bifurcations.

La figure 1 montre le spectrogramme obtenu lors d'une expérience typique sur un gong, excité à F_{exc} =556 Hz. Le premier régime se caractérise par une vibration unimodale, faiblement non linéaire.

En effet, la fréquence d'excitation choisie est généralement celle d'un mode propre afin d'assurer la meilleure injection d'énergie au système pour lui faire atteindre des grandes amplitudes de vibration pour des valeurs de forces raisonnables. Avant la première bifurcation, seul le mode excité participe à la vibration, et le spectre montre la fréquence d'excitation ainsi que les premiers harmoniques, signe que la non-linéarité géométrique est déjà présente. La première bifurcation se caractérise par l'apparition de nombreux sous-harmoniques, le spectre restant formé de raies distinctes, signe d'un régime quasi-périodique. De nombreuses analyses effectuées sur différentes cymbales et gongs, nous ont montré que les sous-harmoniques apparaissant pouvaient toujours être reliés à des fréquences propres. De plus, des relations de commensurabilité, du type $f_i + f_j = F_{exc}$ sont vérifiées entre des couples de sous-harmoniques (f_i, f_j) apparaissant dans le spectre. Cette relation est une relation de résonance interne d'ordre 2, dont le cas général a été vu lors du chapitre précédent. Ainsi cette première bifurcation a pu être analysée comme un *couplage inter-modal par résonance interne* : les modes propres du système dont les fréquences propres vérifient ces relations de résonance interne sont susceptibles de s'échanger de l'énergie [R7]. Le couplage devient effectif à partir d'un certain niveau d'excitation, lorsque la vibration unimodale devient instable au profit de la solution couplée, stable. Enfin, pour des amplitudes de forçage encore plus grande, le régime quasi-périodique devient instable au profit d'un régime chaotique, où le spectre de vibration devient véritablement large bande. Les exposants de Lyapunov ont été calculés sur des séries temporelles de mesures, montrant effectivement la présence d'un exposant positif [R1].

L'analyse de la première bifurcation a été l'objet de plusieurs études dont nous reprendrons les résultats principaux à la section suivante. Le cas le plus simple de la résonance 1:1[1] est étudié théoriquement et expérimentalement dans le cas des plaques, puis le cas de la résonance 1:1:2 sera traité pour le cas des coques sphériques.

2. Couplages modaux et résonances internes

2.1. Résonance 1:1. Le cas de la résonance 1:1 a fait l'objet de nombreuses publications, depuis les études de Tobias sur des disques en rotation à la fin des années 1950 [159, 160, 165], qui donnaient les résultats essentiels, sans tenir compte de l'amortissement. La résonance 1:1 apparait aussi pour les géométries rectangulaires : pour les membranes [170], et pour les plaques excitées paramétriquement, où les études de Yang et Sethna [168, 169], et Chang et al. [40], donnent un tableau complet (bifurcations locales et globales). Revenant au cas des disques en rotation, Raman et Mote ont donné une version plus actuelles des résultats de Tobias, avec bifurcations globales et expériences [139, 140]. Pour le cas des plaques circulaires, les résultats de Sridhar et Nayfeh ont longtemps fait référence [67, 153, 154], jusqu'à ce qu'une erreur dans la condition de solvabilité soit corrigée simultanément et indépendamment par Yeo et Lee [172] et notre étude [R2]. Depuis 2002, de nouvelles contributions traitent encore le cas de la résonance 1:1, par exemple [3] pour les coques peu profondes.

Nos études [R2,R3] sur le sujet donnent une approche complète du problème, avec les versants théoriques et expérimentaux, l'étude des variations des paramètres sensibles (comme l'amortissement, les désaccords entre fréquences propres dus à des imperfections) sur les zones d'instabilité et les réponses couplées. La forme normale de la résonance 1:1, qui gouverne la dynamique sur la variété invariante, s'écrit :

$$\ddot{q_1} + \omega_1^2\, q_1 = \varepsilon \left[\Gamma_1\, q_1^3 + C_1\, q_1 q_2^2 - 2\mu\, \dot{q_1} + Q_1\, \cos\Omega t\right], \tag{30a}$$

$$\ddot{q_2} + \omega_2^2\, q_2 = \varepsilon \left[\Gamma_2\, q_2^3 + C_2\, q_2 q_1^2 - 2\mu\, \dot{q_2} + Q_2\, \cos\Omega t\right], \tag{30b}$$

où les fréquences propres ω_1 et ω_2 sont proches, et proches de la fréquence d'excitation Ω. On introduit les paramètres de désaccord σ_1 et σ_2 selon : $\omega_2 = \omega_1 + \varepsilon\sigma_1$, et $\Omega = \omega_1 + \varepsilon\sigma_2$. La solution est cherchée à l'aide de la méthode des échelles multiples [120, 123], c'est donc une solution perturbative au premier

[1] Une résonance 1:1 existe lorsque deux modes propres se trouvent avoir des fréquences propres égales. Pour les plaques et les coques circulaires, le cas est extrêmement fréquent puisque tous les modes asymétriques, étant dégénérés, présentent une telle résonance.

ordre que l'on va exhiber. Les amplitudes modales q_1 et q_2 sont développées selon :

$$q_1(t) = A_1(T_1)\exp(i\omega_1 T_0) \; + \; c.c. + O(\varepsilon), \tag{31a}$$

$$q_2(t) = A_2(T_1)\exp(i\omega_2 T_0) \; + \; c.c. + O(\varepsilon), \tag{31b}$$

où $T_0 = t$ est l'échelle de temps rapide et $T_1 = \varepsilon t$ l'échelle de temps lente, $A_1(T_1)$ et $A_2(T_1)$ sont les amplitudes complexes inconnues dont la dépendance en temps (modulation d'amplitude) est donnée par les conditions de solvabilité (la notation $c.c.$ indique "complexe conjugué"). Réécrivant les amplitudes complexes sous la forme $A_1(T_1) = a_1(T_1)\exp i(\sigma_2 T_1 - \gamma_1(T_1))$ et $A_2(T_1) = a_2(T_1)\exp i((\sigma_2 - \sigma_1)T_1 - \gamma_2(T_1))$, on aboutit à un système dynamique de dimension 4, à l'échelle de temps T_1, dont les solutions donnent l'évolution temporelle de la modulation d'amplitude. Le cas particulier où $Q_2 = 0$ a été plus particulièrement étudié afin de mettre en évidence le transfert d'énergie via les termes non linéaires. L'étude complète du système dynamique, des points fixes et de leur stabilité est menée en détail dans [R2]. En particulier, la zone d'instabilité pour la solution non-couplée (*i.e.* tel que $a_1 \neq 0$ et $a_2 = 0$) s'écrit analytiquement :

$$\sigma_2 = \sigma_1 - \frac{C_2 a_1^2}{\omega_2} \pm \sqrt{\frac{C_2^2 a_1^4}{4\omega_2^2} - \mu^2}. \tag{32}$$

A l'intérieur de cette zone, les solutions couplées peuvent exister. La figure 2 montre cette zone d'instabilité, ainsi que les solutions couplées qui se développent dès que la solution non-couplée entre dans la région.

L'étude expérimentale [R3] confirme toutes les caractéristiques des solutions trouvées théoriquement. En particulier la solution couplée fait apparaître une onde progressive sur la plaque qui a été observée. Le cas d'un forçage Q_2 non-nul a lui aussi été étudié, montrant l'existence d'une seconde branche de solutions couplées, dont les amplitudes sont similaires à celles montrées figure 2, mais en opposition de phase par rapport à la première branche. Cette solution nouvelle a elle aussi été observée en perturbant la vibration (en tapant sur la plaque) lorsque le régime couplé était obtenu : on passait ainsi d'une solution en phase à la seconde branche couplée en opposition de phase [R3].

2.2. Résonance 1:1:2. Une résonance 1:2 intervient lorsqu'une fréquence propre du système est égale au double d'une autre. Les premières études théoriques et expérimentales sur cette résonance ont été menées sur un système de 2 poutres élancées connectées en L et sur lesquelles une masse glissante permettait d'ajuster les fréquences propres pour les mettre en résonance 1:2 [66, 127]. Cette résonance se retrouve pour le cas des arches [158], des cables [28], des coques circulaires cylindriques [144], des coques à double courbure [4]. Le cas de la résonance 1:1:2 intervient lorsqu'un mode axisymétrique a une fréquence double d'une paire de modes asymétriques, déjà en résonance 1:1. Le cas parfait, où aucun désaccord entre les fréquences propres n'est considéré, a été étudié dans [126]. Notre étude théorique [R6] a montré l'importance de ces désaccords, mettant en évidence que le couplage ne peut se faire que vers l'une ou l'autre des deux configurations asymétriques, mais pas les deux simultanément.

Considérons le cas expérimental où le premier mode axisymétrique (0,1) d'une coque sphérique est excité par une force ponctuelle placée au centre de la coque. Ce mode, noté 3 pour la suite, a sa fréquence propre double d'une paire de modes asymétriques notés 1 et 2. La forme normale du système s'écrit :

$$\ddot{q_1} + \omega_1^2 q_1 = \varepsilon_q \left[\alpha_1 q_1 q_3 - 2\mu_1 \dot{q_1}\right], \tag{33a}$$

$$\ddot{q_2} + \omega_2^2 q_2 = \varepsilon_q \left[\alpha_2 q_2 q_3 - 2\mu_2 \dot{q_2}\right], \tag{33b}$$

$$\ddot{q_3} + \omega_3^2 q_3 = \varepsilon_q \left[\alpha_3 q_1^2 + \alpha_4 q_2^2 - 2\mu_3 \dot{q_3} + Q\cos\Omega t\right], \tag{33c}$$

où seuls les termes quadratiques ont été retenus, et où le forçage n'apparait pas sur les modes 1 et 2 puisqu'étant placé sur un point nodal. Les paramètres de désaccord suivants sont introduits : $\omega_2 = \omega_1 + \varepsilon_q\sigma_0$, $\omega_3 = 2\omega_1 + \varepsilon_q\sigma_1$, et $\Omega = \omega_3 + \varepsilon_q\sigma_2$. Une solution en échelles multiples est recherchée, pour laquelle toutes les branches de solution sont analytiques. L'analyse de stabilité fait apparaitre deux zones d'instabilité, correspondant chacune à un couplage entre le mode 3 et le mode 1 (solution C1), et un couplage entre le mode 3 et le mode 2 (solution C2). Au point d'intersection de ces 2 régions,

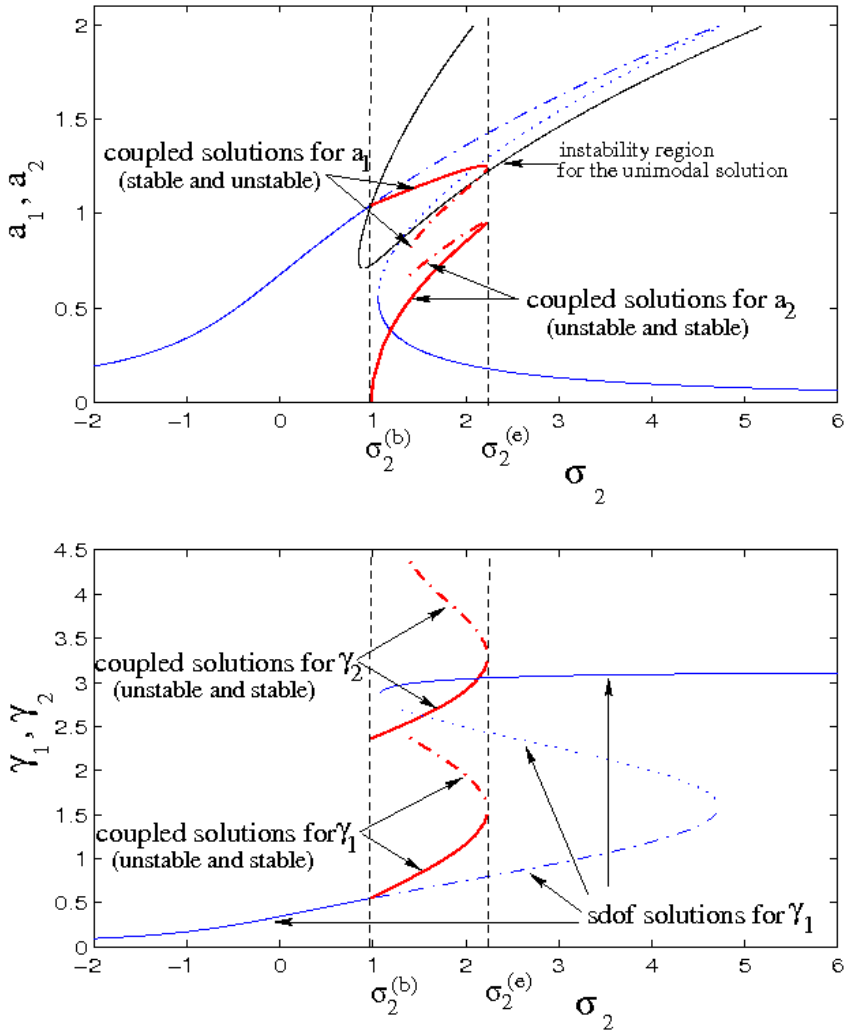

FIG. 2. Amplitudes (a_1, a_2) et phases (γ_1, γ_2) de la solution au premier ordre pour la résonance 1:1. La solution non-couplée (Duffing classique) en bleu, pénètre à l'intérieur de la région d'instabilité (en noir) pour $\sigma_2 = \sigma_2^{(b)}$. La solution couplée existe jusqu'à la valeur $\sigma_2^{(e)}$.

un échange de stabilité entre les deux solutions s'opère. Ainsi tant que les non-linéarités cubiques ne sont pas prises en compte, on ne peut observer un transfert d'énergie que vers l'une ou l'autre des deux configurations asymétriques, mais pas vers les deux simultanément.

L'article [R11] confirme expérimentalement toutes ces prédictions théoriques. La figure 3 montre le recalage entre les courbes théoriques et mesurées. Un très bon accord qualitatif est obtenu. Quantitativement, des différences subsistent, dues aux imperfections de la coque ainsi qu'à la non-prise en compte des termes cubiques dans le modèle (33). L'effet des termes cubiques a été étudié dans [C18], les imperfections dans [R16]. Enfin le cas de la résonance interne d'ordre trois $\omega_1 + 2\omega_2 = \omega_3$ a été étudiée dans [C8].

3. Turbulence d'ondes

Lorsque l'on continue d'augmenter l'amplitude du forçage après le régime quasipériodique, un régime chaotique s'établit. Celui-ci se caractérise auditivement par un son très riche et brillant, très similaire à celui rendu par une cymbale en mode de jeu usuel (excitation impulsionnelle). Le spectre

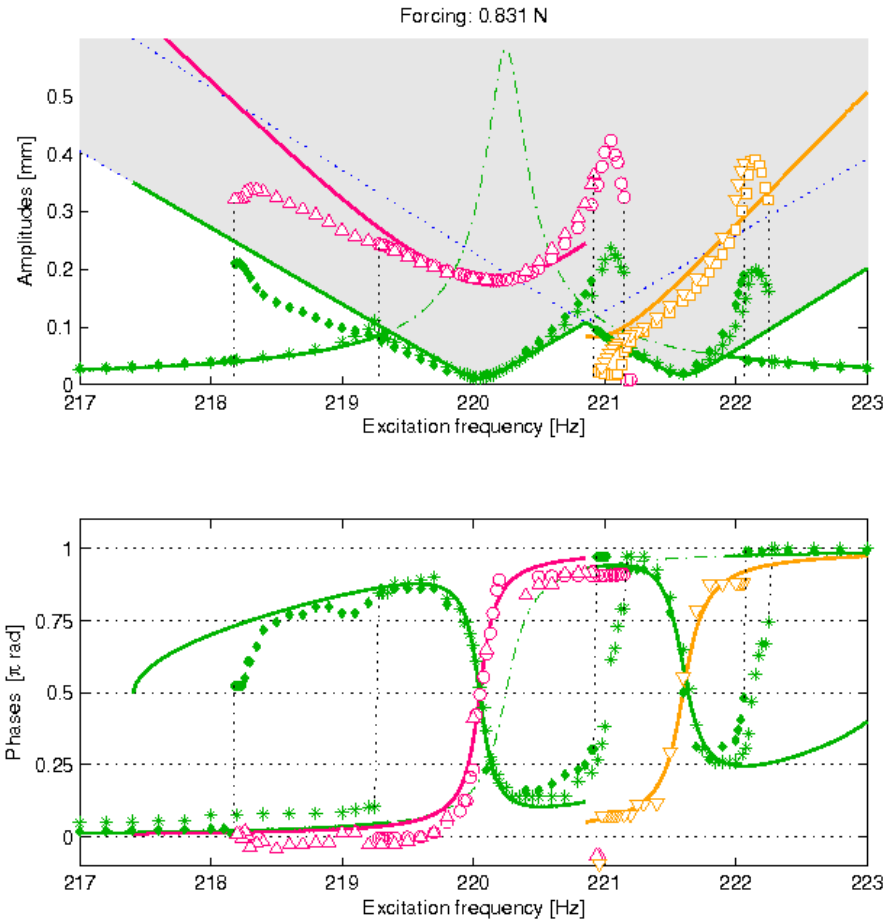

FIG. 3. Amplitudes et phases des coordonnées modales pour le système (33) présentant une relation de résonance 1:1:2. Comparaison théorie/expérience. Zone grisée : région d'instabilité de la solution non-couplée. Vert : mode 3 (directement excité), rouge et orange : modes compagnons 1 et 2.

vibratoire est alors large bande. En utilisant un espace des phases reconstruit à partir de séries temporelles mesurées, nous avons pu mettre en évidence la présence d'au moins un exposant de Lyapunov positif [R1]. Nos premières idées, au cours de ma thèse, ont consisté à tester, avec des méthodes de traitement de signaux chaotiques [1, 85], la dimension de l'attracteur reconstruit, afin de pouvoir dire si une dynamique à petit nombre de degrés de liberté était en jeu, ou non. La convergence de ces calculs de dimension étaient généralement difficile, et les séries temporelles vraisemblablement trop courtes pour pouvoir peupler les attracteurs avec une densité de points suffisante pour obtenir des résultats fiables. Les critères de résonance interne apparaissent eux plus sûrs pour estimer le nombre de modes impliqués dans la vibration. Cependant l'identification à partir de résultats expérimentaux reste possible (bien que difficile) dans le régime quasipériodique uniquement, et montre déjà un nombre assez grand de modes excités par échange d'énergie[2]. Un autre éclairage permettant de mieux décrire ce régime chaotique consiste alors à utiliser les résultats de la théorie de turbulence d'ondes (ou turbulence faible).

[2]Sur la figure 1 on dénombre déjà aisément 6 modes excités en dessous de la fréquence d'excitation, laissant à penser qu'il y a déjà au moins 7 modes (en ajoutant celui directement excité par le forçage) qui participent à la vibration, soit un espace des phases de dimension au moins 15.

La turbulence d'ondes est une théorie qui décrit les propriétés statistiques de systèmes dissipatifs hors équilibre. Elle repose sur 3 hypothèses fortes qui permettent de mener analytiquement les calculs et de se défaire du problème de la fermeture des équations[3]. Les hypothèses sont les suivantes :

- Le milieu est dispersif
- La non-linéarité est faible, ce que l'on peut traduire dans les EDPs du mouvement par la présence d'un coefficent ε devant les termes non linéaires. Ceci permet en outre de séparer clairement deux échelles de temps, une échelle de temps rapide linéaire et une échelle de temps lente non linéaire sur laquelle l'énergie se redistribue via les non-linéarités du système.
- Il existe une "fenêtre de transparence" ou "régime inertiel" où l'on peut considérer la dynamique Hamiltonienne.

La troisième hypothèse reprend la vision "classique" de la turbulence et permet de chercher des solutions avec un flux d'énergie des grandes échelles vers les petites échelles (cascade directe) ou l'inverse. L'énergie est supposée être injectée à basse fréquence, et la dissipation n'est censée jouer qu'aux petites échelles.

Les résultats forts de la turbulence d'ondes sont dus à Zakharov dans les années 1960 [174] : il fut le premier à montrer l'existence de solutions hors équilibre à l'équation cinétique qui résoud le problème de la fermeture. Les spectres tirés de ces solutions ont des propriétés similaires à ceux postulés par Kolmogorov pour la turbulence pleinement développée, et sont analytiques. Les articles récents [34, 46, 128], ainsi que les thèses [33, 45] donnent une vue d'ensemble sur le sujet.

La théorie fut appliquée au cas des plaques minces dans [51], montrant l'existence d'une cascade directe pour une plaque parfaite, et prédisant un spectre de puissance du déplacement de la forme $P_w(k) = C\frac{P^{1/3}}{[12(1-\nu^2)]^{1/6}}\frac{\ln^{1/3}(k_\star/k)}{\sqrt{E/\rho}\,k^4}$, où C est une constante et P le flux d'énergie par unité de masse. Omettant la dépendance logarithmique négligeable devant le terme en k^{-4} et traduisant ce spectre dans le domaine des fréquences temporelles, la prédiction théorique est donc d'un spectre de vitesse indépendant de la fréquence : $P_{\dot w}(f) = C' P^{1/3} f^0$.

Nous avons mené des expériences, dont les résultats sont reportés dans [R14,R15], sur une grande plaque mince, de dimensions latérales 1m×2m, d'épaisseur $h = 0.5$ mm, issue d'un réverbérateur à plaque et étudiée pour faire un modèle de réverbération artificielle dans la thèse de K. Arcas [18]. Cette plaque a été choisie pour sa grande densité modale. Elle est excitée par une force ponctuelle harmonique. Expérimentalement, le flux d'énergie P est proportionnel à la puissance injectée $I =< F\dot w(x_0) >$, où F est la force appliquée à la plaque et $\dot w(x_0)$ la vitesse au point x_0 où est appliquée la force. Les spectres de puissance de la vitesse mesurée en un point différent du forçage sont montrés figure 4(a), pour des valeurs croissantes de la puissance injectée I. On observe une première gamme de fréquence, analogue du régime inertiel, qui se développe au fur et à mesure que l'on augmente l'amplitude de la force, avec une dépendance en $P_{\dot w}(f) \sim f^{-\beta}$, $\beta = 0.5 \pm 0.2$; suivi d'une chute assez nette qui donnerait l'échelle dissipative. Ces spectres bruts peuvent être recalés sur une courbe universelle, figure 4(b), selon la formule : $P_v(f) = (I/I_0)^{1/2}\,\phi\,(f/f_c)\,, \quad f_c \propto f_i(I/I_0)^\alpha$, où ϕ est la fonction universelle et f_c une fréquence de coupure, que l'on trouve proportionelle à la puissance injectée à la puissance α, avec $\alpha = 0.33 \pm 0.01$, cf. figure 4(c).

En remplaçant la dépendance de f_c en fonction de I trouvée, et prenant pour la fonction ϕ la dépendance en $f^{-1/2}$ mesurée, on trouve au final un spectre expérimental de la forme $P_{\dot w}(f) \sim I^{0.66\pm0.07} f^{-0.5\pm0.2}$, ce qui est significativement différent de la prédiction théorique. Une mesure indépendante de la notre, effectuée par N. Mordant à l'ENS [114], confirme ces lois de puissance. Le spectre théorique prédit une dépendance en $P^{1/3}$ par rapport à la puissance injectée. C'est un résultat général de la turbulence d'ondes : pour une interaction à N ondes[4], la dépendance sera en $P^{1/(N-1)}$. Pour la plaque parfaite, la

[3] C'est ce problème de fermeture qui rend la turbulence hydrodynamique pleinement développée insoluble analytiquement [60].

[4] Une interaction à N ondes est possible si deux onditions sont remplies : il faut que la non-linéarité soit d'ordre au plus $N-1$, et on doit remplir la double condition de résonance définie par la variété résonante [128, 174].

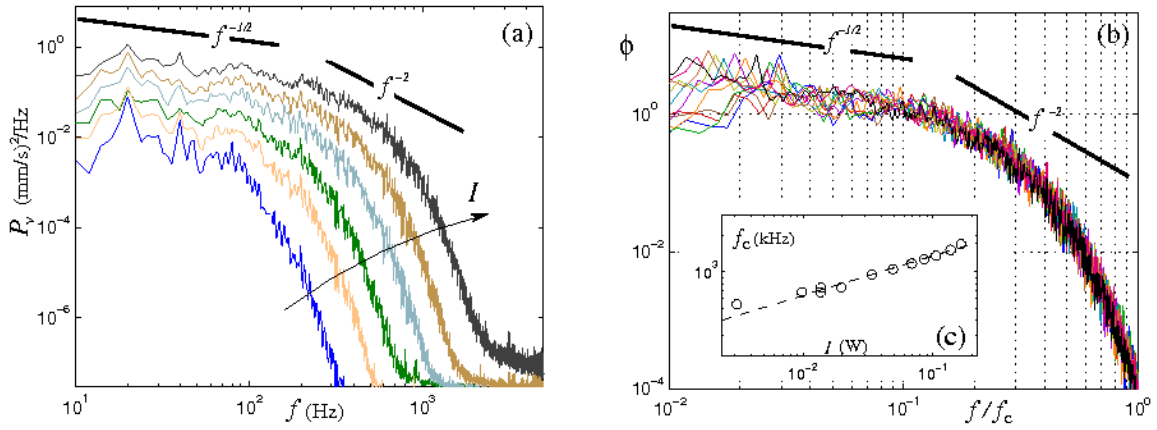

FIG. 4. Spectres de puissance de la vitesse. (a) : spectres bruts pour différentes valeurs de la puissance injectée I. (b) : spectres mis à l'échelle. (c) : Evolution de la fréquence de coupure avec la puissance injectée, mettant en évidence la loi $f_c \propto I^\alpha$, $\alpha = 0.33$.

non-linéarité d'ordre 3 implique une interaction à quatre ondes, ce qui explique la puissance $P^{1/3}$ prédite théoriquement. Expérimentalement, la plaque est imparfaite, et ces imperfections font apparaitre une forte non-linéarité quadratique [R16]. L'exposant $I^{0.66\pm0.07}$ que l'on mesure est d'ailleurs plus proche de $1/2$ que de $1/3$, ce qui laisse à penser que la non-linéarité quadratique joue une rôle important dans le régime de cascade.

Afin d'expliquer la différence observée entre spectre théorique et expérimental, on pourrait remettre en question l'hypothèse de faible non-linéarité et de séparation nette entre les échelles de temps linéaires et non linéaires. Il a été prouvé théoriquement que lorsque cette hypothèse ne tient plus, la dynamique se complexifie et ne peut plus être considérée comme une superposition d'ondes, faisant apparaitre un comportement intermittent tel que celui observé en turbulence pleinement développée [34, 128]. L'intermittence est caractérisée par les fonctions de densité de probabilités des incréments de vitesse $\Delta_\tau v = v(t+\tau) - v(t)$ et le comportement des fonctions de structures $S_p(\tau) = \langle |\Delta_\tau v|^p \rangle$. Nos mesures [R14] montrent qu'aucun comportement intermittent n'apparait. De plus, les mesures rapportées dans [114] montrent bien que les ondes persistent. L'hypothèse à remettre en question est donc plutôt celle de l'existence d'un régime inertiel où la dynamique peut être considérée comme Hamiltonienne.

Même si l'amortissement dans les plaques métalliques est très faible, il joue à toutes les fréquences. Une mesure fine de l'amortissement de la plaque sur la bande [0,20kHz] a été faite par K. Arcas pendant sa thèse [18]. Sur la bande de fréquence [30, 2000 Hz], un comportement très net de l'amortissement $\gamma_f(f) \sim f^{1/2}$ est observé [R14]. En considérant que la puissance injectée P est égale à la puissance dissipée entre 0 et la fréquence de coupure, on peut écrire : $P = \rho S h \int_0^{f_c} \gamma_f(f) P_{\dot{w}}(f) df$, ce qui donne, avec les quantitées mesurées : $P = \rho S h P^{2/3} f_c$, soit une fréquence de coupure se comportant en $f_c \sim P^{1/3}$, ce qui est conforme aux mesures. De nouvelles mesures sont en cours afin de faire varier l'amortissement dans la plaque pour conforter ce scénario. Il est aussi à noter que la présence d'une faible dissipation pour les systèmes hors-équilibre est au cœur des problèmes actuels [31]. Enfin des premières simulations numériques réalisées par C. Josserand[5] en tenant compte d'amortissement montrent aussi l'apparition de cette fréquence de coupure très nette.

[5] C. Josserand, présentation lors du workshop "Wave Turbulence", paris, IHP, Avril 2009.

Conclusions et perspectives

Les travaux présentés dans ce mémoire ont pour point commun les vibrations non linéaires géométriques (grandes amplitudes) de structures minces. Les travaux que nous avons menés ont exploré plus particulièrement deux points précis : la réduction de modèles, en utilisant le formalisme des modes non linéaires, et la transition vers les régimes de vibration chaotiques pour ces systèmes continus. Nous reprenons ici, de manière synthétique, les résultats qui nous semblent les plus marquants pour chacun des deux thèmes, ce qui donne l'occasion de donner les pistes de recherche qui sont envisagées pour les prochaines années.

Modes non linéaires et réduction de modèles

Nos études sur les modes non linéaires ont montré que la théorie des formes normales donne un formalisme simple permettant de calculer la dynamique dans l'espace des phases engendré par les variétés invariantes. Les troncatures sont donc de meilleures qualités, la compréhension que l'on a des résonances internes et des couplages aussi. Il permet en outre la prise en compte de l'amortissement de manière aisée. En ne conservant qu'un seul MNL dans la forme normale, on est à-même de prédire la tendance de non-linéarité pour un coût de calcul faible.

Les résultats obtenus en utilisant les MNLs en réduction de modèles de coques montrent que c'est la meilleure base réduite possible pour les systèmes excités harmoniquement en très basses fréquences. Les tests de convergence effectués sur plusieurs modèles [R9,R10,R12] montrent effectivement que les erreurs commises par notre méthode sont dues uniquement aux deux approximations faites lors du calcul des MNLs, à savoir le développement asymptotique tronqué à l'ordre trois, et la prise en compte de variétés indépendantes du temps pour un problème forcé. Les perspectives de travail sont les suivantes :

- À court terme, nous prévoyons de tester la robustesse des modèles réduits MNLs pour une excitation aléatoire dont on contrôle la largeur de bande. Partant d'une excitation à bande étroite centrée sur une fréquence propre, et en élargissant la largeur de bande (celle-ci incluant de plus en plus de modes), on obtiendrait ainsi un résultat quantitatif permettant de juger de leur qualité sur des excitations autres que monofréquentielles, et ce toujours pour des amplitudes d'excitations fortes qui impliquent des non-linéarités géométriques.

- Un travail complet de numérisation des procédures de calcul est envisagé à moyen terme, travail qui se décompose en deux volets distincts.
  (1) Le premier volet consiste à numériser la procédure de discrétisation des EDPs, l'idée étant d'utiliser la méthode des éléments finis avec des éléments de coques pour gagner en souplesse et en généralité. Ce travail a déjà été entamé, en collaboration avec le groupe MACS de l'INRIA, en utilisant des éléments de la famille MITC[6]. Les coefficients de couplage non linéaires quadratiques et cubiques sont exprimés à partir du travail des forces internes et calculés par intégrations sur les éléments. Pour la validation, ce calcul direct des coefficients est comparé aux résultats analytiques présentés au chapitre 1, ainsi qu'aux résultats données par une méthode qui consiste à imposer des déplacements statiques ayant la forme de combinaisons

[6]MITC signifie Mixed Interpolation of Tensorial Components, ces éléments sont particulièrement désignés pour empêcher le phénomène de verrouillage numérique pour les coques minces [41].

linéaires de modes propres bien choisis. À partir de la force résultante, donnée par le calcul élément fini, on peut remonter aux coefficients selon une méthode proposée dans [110, 116]. Ce travail, déjà bien entamé, devrait donner ses premiers résultats en 2010.

(2) Le second volet consiste à adopter une procédure numérique pour le calcul des variétés invariantes afin de pallier aux limitations en amplitude montrée dans ce document. Il est déjà acquis que la méthode des formes normales ne pourra pas continuer à être utilisée : la procédure de calcul en elle-même (reposant sur une récurrence qui élimine à chaque ordre les termes non-résonnants) ne se prête pas à une numérisation. L'idée sera alors de reprendre la formulation en termes de variétés invariantes : celle-ci donnant une EDP qui décrit la géométrie de la variété dans l'espace des phases, on pourra appliquer des techniques numériques de résolution d'EDP à ce problème. Une première réflexion a déjà été entamée sur le sujet. Plutot que de résoudre cette EDP avec une méthode de type Galerkin, comme proposé dans [80, 81, 135], il est possible de voir l'EDP comme un problème en temps dont l'amplitude joue le rôle du temps. Des stratégies plus classiques de résolution peuvent donc être mises en œuvre, pour des amplitudes croissantes. L'étude récente [129] propose d'ailleurs des idées semblables, et met en évidence les problèmes de convergence et de stabilité numériques associés à ce problème et qui le rendent difficile et coûteux numériquement. Par contre une stratégie numérique par continuation d'orbites périodiques, comme proposé dans [23, 92, 132, 152] n'est a priori pas envisagée.

– À long terme, il est envisagé d'étendre les investigations au cas des non-linéarités matérielles. Des travaux existent déjà sur le cas des non-linéarités non-régulières et les problèmes de contact [79, 101], l'extension à des non-linéarités matérielles type comportement élasto-plastique ou pseudo-élastique pour les matériaux à mémoire de forme (MMF) sera donc prochainement mise à l'étude. Pour le comportement élasto-plastique, une modélisation simplifiée telle que présentée dans [39] sera un bon point de départ. Pour les MMF, une collaboration avec le groupe Matériaux et Structures (MS) de l'UME, qui possède une grande expérience expérimentale et théorique sur ce sujet sera entamée. Là aussi, des modèles simples d'oscillateurs pseudo-élastiques tels que présentés dans [30, 98] seront un bon point de départ.

Transition vers le chaos

Les perspectives de travail sur cette partie portent essentiellement sur la seconde bifurcation et le régime chaotique. La plus grande difficulté de ces dernières années a été d'ordre numérique, afin de trouver des intégrateurs temporels stables pour simuler la seconde bifurcation. Ce problème est résolu depuis peu par deux méthodes différentes :

– Pour les systèmes d'oscillateurs provenant de la discrétisation modale telle que présentée dans le chapitre 1, la méthode des BDF (Backward Differentiation method) est stable au passage de la seconde bifurcation. Des simulations sont donc en cours afin de regarder précisément comment l'énergie se répartit quand survient le régime chaotique : a-t-on de nouveaux couplages par résonance interne qui sont excités, ou bien une bifurcation globale et un chaos à grand nombre de degrés de liberté est-elle présente ? Les premières simulations, ainsi que les études expérimentales sur la turbulence d'ondes, montrent que c'est la deuxième solution qui semble intervenir.
– Une collaboration avec Stefan Bilbao (Université d'Edimbourgh) a été entamée, afin d'utiliser un code qu'il a développé par différences finies, et schéma en temps conservatif en temps [32]. Les premières simulations montrent un très bon comportement du code, qui retrouve les spectres théoriques de turbulence d'onde. Une comparaison avec la méthode modale sera menée sur le cas d'une plaque rectangulaire, afin de mettre en évidence les avantages et limites de chacune des deux méthodes, en regard de la simulation de ces régimes chaotiques, ainsi que de la synthèse sonore.

A l'aide de ces deux outils numériques, plusieurs points seront aussi prochainement mis à l'étude pour aller le plus loin possible dans les analyses et terminer le travail entamé lors de ma thèse de doctorat avec l'obtention de sons de synthèse réalistes.

– L'ajout d'une imperfection géométrique dans le code par différences finies. L'idée est de voir l'effet des termes quadratiques sur les spectres du régime turbulent, étant donné que ceux-ci ne sont pas pris en compte dans [51] et semblent avoir un rôle prépondéranrt expérimentalement [R14].
– La prise en compte d'un amortissement réaliste. Ce point sera aussi rapidement mis à l'étude, pour deux raisons particulières. Tout d'abord en lien avec la turbulence d'ondes, où l'on a vu l'importance de l'amortissement sur la fréquence de coupure. Une confirmation numérique, ainsi que des comparaisons expérimentales où la valeur de la dissipation est contrôlée en approchant une plaque poreuse à proximité de la plaque vibrante, sont en cours. Deuxièmement pour la synthèse sonore, où l'on connait l'importance cruciale de l'amortissement.

Publications

Revues internationales avec comité de lecture.

[R16] C. Camier, **C. Touzé** and O. Thomas : Non-linear vibrations of imperfect free-edge circular plates and shells, Eur. J. Mechanics, A/solids, vol. 28, pp. 500-515, 2009.
[R15] O. Cadot, A. Boudaoud and **C. Touzé** : Statistics of power injection in a plate set into chaotic vibration, Eur. Phys. J. B, vol. 66, pp. 399-407, 2008.
[R14] A. Boudaoud, O. Cadot, B. Odille and **C. Touzé** : Observation of wave turbulence in vibrating plates, Physical Review Letters, **100**, 234504, 2008.
[R13] **C. Touzé**, C. Camier, G. Favraud and O. Thomas : Effect of imperfections and damping on the type of non-linearity of circular plates and shallow spherical shells, Mathematical Problems in Engineering, vol. 2008, Article ID 678307, 19 pages, doi :10.1155/2008/678307, 2008.
[R12] **C. Touzé**, M. Amabili and O. Thomas : Reduced-order models for large-amplitude vibrations of shells including in-plane inertia, Computer Methods in Applied Mechanics and Engineering, **197**(21-24), 2030-2045, 2008.
[R11] O.Thomas, **C. Touzé** and E. Luminais : Non-linear vibrations of free-edge thin spherical shells : experiments on a 1:1:2 internal resonance, Nonlinear Dynamics, **49**(1-2), 259-284, 2007.
[R10] M. Amabili and **C. Touzé** : Reduced-order models for non-linear vibrations of fluid-filled circular cylindrical shells : comparison of POD and asymptotic non-linear normal modes methods, Journal of Fluids and Structures, **23**(6), 885-903, 2007.
[R9] **C. Touzé** and M. Amabili : Non-linear normal modes for damped geometrically non-linear systems : application to reduced-order modeling of harmonically forced structures, Journal of Sound and Vibration, **298**(4-5), 958-981, 2006.
[R8] **C. Touzé** and O.Thomas : Non-linear behaviour of free-edge shallow spherical shells : Effect of the geometry, International Journal of non-linear Mechanics, **41**(5), 678-692, 2006.
[R7] A. Chaigne, **C. Touzé** and O. Thomas : Nonlinear vibrations and chaos in gongs and cymbals, Acoustical Science and Technology, Acoust. Soc. of Japan, **26**(5), 403-409, 2005.
[R6] O. Thomas, **C. Touzé** and A. Chaigne : Non-linear vibrations of free-edge thin spherical shells : modal interaction rules and 1:1:2 internal resonance, Int. J. of Solids and Structures, **42**(11-12), 3339-3373, 2005.
[R5] **C. Touzé**, O.Thomas and A. Huberdeau : Asymptotic non-linear normal modes for large-amplitude vibrations of continuous structures, Computers and Structures, **82**(31-32), 2671-2682,2004.
[R4] **C. Touzé**, O.Thomas and A. Chaigne : Hardening/softening behaviour in non-linear oscillations of structural systems using non-linear normal modes, Journal of Sound and Vibration, **273**(1-2), 77-101, 2004.
[R3] O.Thomas, **C. Touzé** and A. Chaigne : Asymmetric non-linear forced vibrations of free-edge circular plates, part II : experiments, Journal of Sound and Vibration, **265**(5), 1075-1101, 2003.
[R2] **C. Touzé**, O.Thomas and A. Chaigne : Asymmetric non-linear forced vibrations of free-edge circular plates, part I : theory, Journal of Sound and Vibration, **258**(4), 649-676, 2002.
[R1] **C. Touzé** and A. Chaigne : Lyapunov exponents from experimental time series. Application to cymbal vibrations, Acta Acustica, **86**(3), 557-567, 2000.

Articles de conférence.

[C26] C. Touzé, C. Camier and O. Thomas : Type of non-linearity of damped imperfect plates using non-linear normal modes, ENOC-2008, European Non-linear Dynamics conference, Saint-Petersbourg, Russia, July 2008.
[C25] O. Thomas, L. Nicu, C. Ayela and C. Touzé : Buckling and non-linear vibrations of a MEMS biosensor, ENOC-2008, European Non-linear Dynamics conference, Saint-Petersbourg, Russia, July 2008.
[C24] C. Camier, C. Touzé et O. Thomas : Effet des imperfections géométriques sur les vibrations non linéaires de plaques circulaires minces, 18ème Congrès Français de Mécanique, Grenoble, Aout 2007.
[C23] C. Touzé, M. Amabili, O. Thomas and C. Camier : Reduction of geometrically non-linear models of shell vibrations including in-plane inertia, Proc. EUROMECH Colloquium No. 483, FEUP, Porto, Portugal, July 2007.
[C22] O. Thomas, L. Nicu, C. Ayela and C. Touzé : Buckling and non-linear vibrations of a piezoelectric stratified plate – Application to a MEMS biosensor, Proc. EUROMECH Colloquium No. 483, FEUP, Porto, Portugal, July 2007.
[C21] O. Thomas, L. Nicu, C. Ayela et C. Touzé : Flambage et vibrations non linéaires d'une plaque stratifiée piézoélectrique.

Application à un biocapteur MEMS. Proc. of 8ème colloque national en calcul de structures, Giens, Mai 2007.
[C20] M. Amabili, C. Touzé and O. Thomas : Comparison of Galerkin, POD and Non-linear normal modes models for nonlinear vibrations of circular cylindrical shells, ASME IMECE 2006, International Mech. Engin. Congress and Exposition, Chicago, Illinois USA, November 2006.
[C19] C. Touzé, M. Amabili and O. Thomas : reduced-order models for damped geometrically non-linear vibrations of thin shells via real normal form, Second International Conference on Non-Linear Normal Modes and Localization, Samos, June 2006.
[C18] O. Thomas and C. Touzé : Large-amplitude forced vibrations of thin shallow spherical shells : reduced-order models at resonance and mode coupling, Second International Conference on Non-Linear Normal Modes and Localization, Samos, June 2006.
[C17] C. Touzé and O. Thomas : Type of non-linearity of shallow spherical shells using non-linear normal modes, Fifth Euromech Non-linear Dynamics Conference (ENOC 2005), Eindhoven, August 2005.
[C16] O. Thomas, E. Luminais and C. Touzé : Non-linear modal interactions in free-edge thin spherical shells : measurements of a 1:1:2 internal resonance, Third MIT Conference on computational fluid and solid mechanics, Boston, June 2005.
[C15] O. Thomas, C. Touzé et E. Luminais : Modèles réduits de structures minces en vibrations non linéaires, Proc. of colloque national en calcul de structures, Giens, Mai 2005.
[C14] C. Touzé and O. Thomas : Reduced-order modeling for a cantilever beam subjected to harmonic forcing, Proc. of EUROMECH 457 : "Nonlinear modes of vibrating systems", Fréjus, June 7-9, 2004.
[C13] A. Chaigne, C. Touzé and O. Thomas : Mechanical models of musical instruments and sound synthesis : the case of gongs and cymbals, Proc. of ISMA 2004, Nara, Japon, April 2004.
[C12] C. Touzé et O. Thomas : Modes normaux non linéaires de systèmes continus, 16eme congrès français de Mécanique, Nice, septembre 2003.
[C11] C. Touzé, O. Thomas and A. Chaigne : Non-linear oscillations of continuous systems with quadratic and cubic non-linearities using non-linear normal modes, Second MIT Conference on computational fluid and solid mechanics, Boston, June 2003.
[C10] C. Touzé and O. Thomas : Determination of non-linear normal modes for conservative systems, Ninth ICSV, Orlando, July 2002.
[C9] A. Chaigne, M. Fontaine, O. Thomas, M. Ferré and C. Touzé : Vibrations of shallow spherical shells and gongs : a comparative study, Forum Acusticum, Séville, 2002.
[C8] C. Touzé, P. Lanchantin, A. Chaigne et O. Thomas : Transferts d'énergie par couplage modal : étude d'un cas particulier, Actes du sixième congrès français d'Acoustique, papier No. 269, pp. 558-563, Lille, Avril 2002.(Conférence invitée)
[C7] O. Thomas, C. Touzé et A. Chaigne : Sur la vibration à un mode asymétrique des plaques circulaires en grands déplacements, Actes du congrès français de Mécanique, Nancy, septembre 2001.
[C6] O. Thomas, C. Touzé and A. Chaigne : Non-linear behaviour of gongs through the dynamics of simple rods systems, Proceedings of the ISMA, Perugia (Italie), september 2001.
[C5] A. Chaigne, C. Touzé and O.Thomas : Non-linear axisymmetric vibrations of gongs, Proceedings of the ISMA, Perugia (Italie), september 2001.
[C4] C. Touzé, F. Orphelin and A. Chaigne : Application of prediction methods to non-linear percussion instruments, Proceedings of ICSV7, July 2000.
[C3] O. Thomas, C. Touzé and A. Chaigne : Non-linear resonances in large-deflection vibrations of free-edge circular plates, Proceedings of ICSV7, July 2000.
[C2] C. Touzé et D. Matignon : Techniques d'ordre supérieur pour l'élimination d'exposants de Lyapunov fallacieux, Rencontres du non linéaire, IHP, Editions Paris Onze, pp. 87-92, Mars 2000.
[C1] C. Touzé, A. Chaigne, T. Rossing and S. Schedin : Analysis of cymbal vibrations using non-linear signal processing tools, Proceedings of the ISMA, pp. 377-382, 1998.

Publication interne / Thèse.

C. Touzé : Intégration temporelle numérique pour les systèmes dynamiques, rapport interne ENSTA, janvier 2009.

C. Touzé et O. Doaré : Dynamique des sytèmes mécaniques : ondes et vibrations, polycopié de cours de l'ENSTA, cours MS204, deuxième année du cycle ingénieur, ENSTA, 2006.

C. Touzé : A normal form approach for non-linear normal modes, Publications du LMA, numéro 156, (ISSN : 1159-0947, ISBN : 2-909669-20-3), Marseille, Janvier 2003.

[T1] C. Touzé : Analyse et modélisation de signaux vibratoires et acoustiques chaotiques. Application aux instruments de percussion non linéaires. Thèse de doctorat de l'Université paris VI, novembre 2000.

Bibliographie

[1] H. D. I Abarbanel : *Analysis Of Observed Chaotic Data*. Kluwer Academic, New-York, 1997.

[2] A. Abe, Y. Kobayashi et G. Yamada : Non-linear vibration characteristics of clamped laminated shallow shells. *Journal of Sound and Vibration*, 234:405–426, 2000.

[3] A. Abe, Y. Kobayashi et G. Yamada : Nonlinear dynamic behaviors of clamped laminated shallow shells with one-to-one internal resonance. *Journal of Sound and Vibration*, 304(3-5):957–968, 2007.

[4] K. A. Alhazza : *Nonlinear vibrations of doubly curved cross-ply shallow shells*. Thèse de doctorat, Virginia polytechnic institute and state university, 2002.

[5] M. Amabili : A comparison of shell theories for large-amplitude vibrations of circular cylindrical shells : Lagrangian approach. *Journal of Sound and Vibration*, 264:1091–1125, 2003.

[6] M. Amabili : Theory and experiments for large-amplitude vibrations of empty and fluid-filled circular cylindrical shell with imperfections. *Journal of Sound and Vibration*, 262(4):921–975, 2003.

[7] M. Amabili : Non-linear vibrations of doubly-curved shallow shells. *International Journal of Non-linear Mechanics*, 40(5):683–710, 2005.

[8] M. Amabili : *Nonlinear vibrations and stability of shells and plates*. Cambridge University Press, 2008.

[9] M. Amabili et M. P. Païdoussis : Review of studies on geometrically nonlinear vibrations and dynamics of circular cylindrical shells and panels, with and without fluid-structure interaction. *ASME Applied Mechanical Review*, 56(4):349–381, 2003.

[10] M. Amabili, F. Pellicano et M. P. Païdoussis : Non-linear vibrations of simply supported, circular cylindrical shells, coupled to quiescent fluid. *Journal of Fluids and Structures*, 12:883–918, 1998.

[11] M. Amabili, F. Pellicano et M. P. Païdoussis : Further comments on nonlinear vibrations of shells. *Journal of Fluids and Structures*, 13(1):159–160, 1999.

[12] M. Amabili, F. Pellicano et M. P. Païdoussis : Non-linear dynamics and stability of circular cylindrical shells containing flowing fluid, part I : stability. *Journal of Sound and Vibration*, 225(4):655–699, 1999.

[13] M. Amabili, F. Pellicano et M. P. Païdoussis : Non-linear dynamics and stability of circular cylindrical shells containing flowing fluid, part II : large-amplitude vibrations without flow. *Journal of Sound and Vibration*, 228(5):1103–1124, 1999.

[14] M. Amabili, F. Pellicano et M. P. Païdoussis : Non-linear dynamics and stability of circular cylindrical shells containing flowing fluid, part III : truncation effect without flow and experiments. *Journal of Sound and Vibration*, 237(4):617–640, 2000.

[15] M. Amabili, A. Sarkar et M. P. Païdoussis : Reduced-order models for nonlinear vibrations of cylindrical shells via the proper orthogonal decomposition method. *Journal of Fluids and Structures*, 18(2):227–250, 2003.

[16] M. Amabili, A. Sarkar et M. P. Païdoussis : Chaotic vibrations of circular cylindrical shells : Galerkin versus reduced-order models via the proper orthogonal decomposition method. *Journal of Sound and Vibration*, 290(3-5):736–762, 2006.

[17] H. N. Arafat et A. H. Nayfeh : Non-linear responses of suspended cables to primary resonance excitation. *Journal of Sound and Vibration*, 266:325–354, 2003.

[18] K. Arcas : *Etude et simulation d'un réverbérateur à plaque*. Thèse de doctorat, Ecole doctorale de l'Ecole Polytechnique, 2009.

[19] J. H. Argyris et H. P. Mlejnek : *Dynamics of Structures*. North-Holland, Amsterdam, 1991.

[20] N.M. Arifin, N.S.M. Noorani et A. Kiliçman : Modelling of Marangoni convection using proper orthogonal decomposition. *Nonlinear Dynamics*, 48:331–337, 2007.

[21] V.I. Arnold : *Geometrical methods in the theory of ordinary differential equations*. Springer, Berlin, 1977.

[22] V.I. Arnold : *Chapitres supplémentaires de la théorie des équations différentielles ordinaires*. Mir-Librairie du Globe, Paris, 1980.

[23] R. Arquier, S. Bellizzi, R. Bouc et B. Cochelin : Two methods for the computation of nonlinear modes of vibrating systems at large amplitudes. *Computers and Structures*, 84(24-25):1565–1576, 2006.

[24] M.F.A Azeez et A.F. Vakakis : Proper orthogonal decomposition of a class of vibro-impact oscillations. *Journal of Sound and Vibration*, 240:859–889, 2001.

[25] A.G. Barnston et C.F. Ropelewski : Prediction of ENSO episodes using canonical correlation analysis. *Journal of climate*, 5:1316–1345, 1992.

[26] P.V. Bayly, E.E. Johnson, P.D. Wolf, W.M. Smith et R.E. Ideker : Predicting patterns of epicardial potentials during ventricular fibrillation. *IEEE Transactions on Biomedical Engineering*, 42:898–907, 1995.
[27] S. Bellizzi et R. Sampaio : POMs analysis of randomly vibrating systems obtained from Karhunen-Loève expansion. *Journal of Sound and Vibration*, 297(3-5):774–793, 2006.
[28] F. Benedettini, G. Rega et R. Alaggio : Non-linear oscillations of a four-degree-of-freedom model of a suspended cable under multiple internal resonance conditions. *Journal of Sound and Vibration*, 182(5):775–798, 1995.
[29] G. Berkooz, P. Holmes et J.L. Lumley : The proper orthogonal decomposition in the analysis of turbulent flows. *Annual review of Fluid Mechanics*, 25:539–575, 1993.
[30] D. Bernardini et F. Vestroni : Non-isothermal oscillationsof pseudo-elastic devices. *International Journal of Non-linear Mechanics*, 38:1297–1313, 2003.
[31] E. Bertin et O. Dauchot : Far-from-equilibirum state in a weakly dissipative model. *Phys. Rev. Lett.*, 102:160601, 2009.
[32] S. Bilbao : A family of conservative finite difference schemes for the dynamical von Kármán plate equations. *Numerical Methods for Partial Differential Equations*, 24(1):193–216, 2007.
[33] L. Biven : *Structure functions, cumulants and breakdown criteria for weak turbulence*. Thèse de doctorat, University of Warwick, Mathematics Institute, 2002.
[34] L. Biven, S. Nazarenko et A.C. Newell : Breakdown of wave turbulence and the onset of intermittency. *Physics Letters A*, 280:28–32, 2001.
[35] N. Boivin, C. Pierre et S. Shaw : Non-linear normal modes, invariance, and modal dynamics approximations of non-linear systems. *Nonlinear Dynamics*, 8:315–346, 1995.
[36] A. D. Brjuno : Analytical form of differential equations. *Transactions of Moscow Mathematical Society*, 25:131–288, 1971.
[37] C. Camier : *Modélisation et étude numérique des vibrations non-linéaires de plaques circulaires minces imparfaites : application aux cymbales*. Thèse de doctorat, Ecole doctorale de l'Ecole Polytechnique, 2009.
[38] J. Carr : *Applications of centre manifold theory*. Springer-Verlag, New-York, 1981.
[39] N. Challamel et G. Gilles : Stability and dynamics of a harmonically excited elastic-perfectly plastic oscillator. *Journal of Sound and Vibration*, 301(3-5):608–634, 2007.
[40] S.I. Chang, A.K. Bajaj et C.M. Krousgrill : Non-linear vibrations and chaos in harmonically excited rectangular plates with one-to-one internal resonance. *Non-linear Dynamics*, 4:433–460, 1993.
[41] D. Chapelle et K.-J. Bathe : *The finite Element analysis of shells - Fundamentals*. Springer, Berlin, 2003.
[42] C.Y. Chia : *Nonlinear analysis of plates*. McGraw Hill, New-York, 1980.
[43] H-N Chu et G. Herrmann : Influence of large amplitudes on free flexural vibrations of rectangular elastic plates. *Journal of Applied Mechanics*, 23:532–540, 1956.
[44] P.G. Ciarlet : A justification of the von Kármán equations. *Arch. Rat. Mech. analysis*, 73:349–389, 1980.
[45] C. Connaughton : *New directions in Wave Turbulence*. Thèse de doctorat, University of Warwick, Mathematics Institute, 2002.
[46] C. Connaughton, S. Nazarenko et A. C. Newell : Dimensional analysis and weak turbulence. *Physica D*, 184:86–97, 2003.
[47] E.J. Doedel, R. Paffenroth, A.R. Champneys, T.F. Fairgrieve, Y.A. Kuznetsov, B.E. Oldeman, B. Sandstede et X. Wang : Auto 2000 : Continuation and bifurcation software for ordinary differential equations. Rapport technique, Concordia University, 2002.
[48] L. H. Donnell : A new theory for the buckling of thin cylinders under axial compression and bending. *Transactions of the American Society of Mechanical Engineers*, 56:795–806, 1934.
[49] E. H. Dowell : Comments on the nonlinear vibrations of cylindrical shells. *Journal of Fluids and Structures*, 12(8):1087–1089, 1998.
[50] H. Dulac : Solutions d'un système d'équations différentielles dans le voisinage de valeurs singulières. *Bulletin de la Société Mathématique de France*, 40:324–383, 1912.
[51] G. Düring, C. Josserand et S. Rica : Weak turbulence for a vibrating plate : Can one hear a kolmogorov spectrum ? *Phys. Rev. Lett.*, 97:025503, 2006.
[52] G. J. Efstathiades : A new approach to the large-deflection vibrations of imperfect circular disks using galerkin's procedure. *Journal of Sound and Vibration*, 16(2):231–253, 1971.
[53] C. Elphick, G. Iooss et E. Tirapegui : Normal form reduction for time-periodically driven differential equations. *Physics Letters A*, 120(9):459–463, 1987.
[54] C. Elphick, E. Tirapegui, M.E. Brachet, P. Coullet et G. Iooss : A simple global characterization for normal forms of singular vector fields. *Physica D*, 29:95–127, 1987.
[55] D. A. Evensen : Nonlinear vibrations of cylindrical shells – logical rationale. *Journal of Fluids and Structures*, 13(1): 161–164, 1999.
[56] H.A. Evensen et R.M. Ewan-Iwanowsky : Dynamic response and stability of shallow spherical shells subject to time-dependent loading. *AIAA Journal*, 5(5):969–976, 1967.
[57] B.F. Feeny : On the proper orthogonal modes of continuous vibration systems. *ASME Journal of Vibration and Acoustics*, 124(1):157–160, 2002.
[58] B.F. Feeny et R. Kappagantu : On the physical interpretation of proper orthogonal modes in vibrations. *Journal of Sound and Vibration*, 211(4):607–616, 1997.

[59] B.F. Feeny et Y. Liang : Interpreting proper orthogonal modes of randomly excited vibration systems. *Journal of Sound and Vibration*, 265:953–966, 2003.
[60] U. Frisch : *Turbulence*. Cambridge Univers. Press, 1995.
[61] I. Georgiou : Advanced proper orthogonal decomposition tools : Using reduced order models to identify normal modes of vibration and slow invariant manifolds in the dynamics of planar nonlinear rods. *Nonlinear Dynamics*, 41(1-3):69–110, 2005.
[62] P. B. Gonçalves : Axisymmetric vibrations of imperfect shallow spherical caps under pressure loading. *Journal of Sound and Vibration*, 174(2):249–260, 1994.
[63] P.B. Gonçalves, F.M.A. Silva et Z.J.G.N. Del Prado : Low-dimensional models for the nonlinear vibration analysis of cylindrical shells based on a perturbation procedure and proper orthogonal decomposition. *Journal of Sound and Vibration*, 315:641–663, 2008.
[64] P. L. Grossman, B. Koplik et Y-Y. Yu : Nonlinear vibrations of shallow spherical shells. *ASME Journal of Applied Mechanics*, 39E:451–458, 1969.
[65] J. Guckenheimer et P. Holmes : *Nonlinear oscillations, dynamical systems and bifurcations of vector fields*. Springer-Verlag, New-York, 1983.
[66] A. G. Haddow, A. D. S. Barr et D.T. Mook : Theoretical and experimental study of modal interaction in a two-degree-of-freedom structure. *Journal of Sound and Vibration*, 97:451–473, 1984.
[67] J. Hadian et A.H. Nayfeh : Modal interaction in circular plates. *Journal of Sound and Vibration*, 142:279–292, 1990.
[68] M. Haragus et G. Iooss : *Local bifurcations, center manifolds, and normal forms in infinite dimensional systems*. EDP Science, 2009.
[69] G. Herrmann : Influence of large amplitudes on flexural vibrations of elastic plates. Rapport technique, No. 3578, National Advisory Committee for Aeronautics (NACA), 1955.
[70] P. Holmes, J.L. Lumley et G. Berkooz : *Coherent structures, dynamical systems and symmetry*. Cambridge University Press, 1996.
[71] D. Hui : Large-amplitude axisymmetric vibrations of geometrically imperfect circular plates. *Journal of Sound and Vibration*, 2(91):239–246, 1983.
[72] D. Hui : Large-amplitude vibrations of geometrically imperfect shallow spherical shells with structural damping. *AIAA Journal*, 21(12):1736–1741, 1983.
[73] P. Hémon et F. Santi : Applications of biorthogonal decompositions in fluid-structure interactions. *Journal of Fluids and Structures*, 17:1123–1143, 2003.
[74] G. Iooss : Global characterization of the normal form for a vector field near a closed orbit. *Journal of Differential Equations*, 76:47–76, 1988.
[75] G. Iooss et M. Adelmeyer : *Topics in bifurcation theory*. World scientific, New-York, 1998. second edition.
[76] G. Iooss et E. Lombardi : Polynomial normal forms with exponentially small remainder for analytic vector fields. *Journal of Differential Equations*, 212:1–61, 2005.
[77] G. Iooss et E. Lombardi : Approximate invariant manifolds up to exponentially small terms. *Journal of Differential Equations*, to appear, 2009.
[78] D. Jiang : *Nonlinear modal analysis based on invariant manifolds. Application to rotating blade systems*. Thèse de doctorat, University of Michigan, 2004.
[79] D. Jiang, C. Pierre et S. Shaw : Large-amplitude non-linear normal modes of piecewise linear systems. *Journal of Sound and Vibration*, 272(3-5):869–891, 2004.
[80] D. Jiang, C. Pierre et S. Shaw : The construction of non-linear normal modes for systems with internal resonance. *International Journal of Non-linear Mechanics*, 40(5):729–746, 2005.
[81] D. Jiang, C. Pierre et S. Shaw : Nonlinear normal modes for vibratory systems under harmonic excitation. *Journal of Sound and Vibration*, 288(4-5):791–812, 2005.
[82] M. W. Johnson et E. Reissner : On transverse vibrations of shallow spherical shells. *Quarterly Applied Mathematics*, 15(4):367–380, 1956.
[83] I.T. Jolliffe : *Principal Component Analysis*. Springer, 2002. second edition.
[84] L. Jézéquel et C. H. Lamarque : Analysis of non-linear dynamical systems by the normal form theory. *Journal of Sound and Vibration*, 149(3):429–459, 1991.
[85] H. Kantz et T. Schreiber : *Nonlinear Time Series Analysis*. Cambridge university press, Cambridge, 1997.
[86] K. Karhunen : Uber lineare methoden in der wahrscheinlichtkeitsrechnung. *Annals of Academic Science Fennicae, Series AI Mathematics and Physics*, 37:3–79, 1946.
[87] Th.von Kármán : Festigkeitsprobleme im maschinenbau. *Encyklopädie der Mathematischen Wissenschaften*, 4(4):311–385, 1910.
[88] A. Kelley : The stable, center-stable, center, center-unstable and unstable manifolds. *Journal of Differential Equations*, 3:546–570, 1967.
[89] G. Kerschen, B.F. Feeny et J.C. Golinval : On the exploitation of chaos to build reduced-order models. *Computer Methods in Applied Mechanics and Engineering*, 192:1785–1795, 2003.
[90] G. Kerschen et J.C. Golinval : Physical interpretation of the proper orthogonal modes using the singular value decomposition. *Journal of Sound and Vibration*, 249(5):849–865, 2002.

[91] G. Kerschen, J.C. Golinval, A.F. Vakakis et L.A. Bergman : The method of proper orthogonal decomposition for dynamical characterization and order reduction of mechanical systems : an overview. *Nonlinear Dynamics*, 41:147–169, 2005.
[92] G. Kerschen, M. Peeters, J.C. Golinval et A.F. Vakakis : Non-linear normal modes, part I : a useful framework for the structural dynamicist. *Mechanical Systems and Signal Processing*, 23(1):170–194, 2009.
[93] M.E. King et A.F. Vakakis : Energy-based formulation for computing nonlinear normal modes in undamped continuous systems. *Journal of Vibration and Acoustics*, 116:332–340, 1994.
[94] W. T. Koiter : On the nonlinear theory of thin elastic shells. part I, II and III. *In Proc. Koninklijke Nederlandse Akademie van Wetenshappen*, volume B69, pages 1–54, 1965.
[95] D. Kosambi : Statistics in function space. *Journal of Indian Mathematical Society*, 7:76–88, 1943.
[96] E. Kreuzer et O. Kust : Analysis of long torsional strings by proper orthogonal decomposition. *Archive of Applied Mechanics*, 67(1-2):68–80, 1996.
[97] P. Krysl, S. Lall et J.E. Marsden : Dimensional model reduction in non-linear finite element dynamics of solids and structures. *International Journal for numerical methods in engineering*, 51:479–504, 2001.
[98] W. Lacarbonara, D. Bernardini et F. Vestroni : Nonlinear thermomechanical oscillations of shape-memory devices. *International Journal of Solids and Structures*, 41(5-6):1209–1234, 2004.
[99] W. Lacarbonara, G. Rega et A. H. Nayfeh : Resonant nonlinear normal modes. part I : analytical treatment for structural one-dimensional systems. *International Journal of Non-linear Mechanics*, 38(6):851–872, 2003.
[100] S. Lall, P. Krysl et J.E. Marsden : Structure-preserving model reduction for mechanical systems. *Physica D*, 184:304–318, 2003.
[101] D. Laxalde et F. Thouverez : Complex non-linear modal analysis for mechanical systems : Application to turbomachinery bladings with friction interface. *Journal of Sound and Vibration*, 322(4-5):1009–1025, 2009.
[102] Z.W. Lin, K.H. Lee, P. Lu, S.P. Lim et Y.C. Liang : The relationship between eigenfunctions of karhunen-loève decomposition and the modes of distributed parameter vibration system. *Journal of Sound and Vibration*, 256(4):791–799, 2002.
[103] M. Loeve : Fonctions aléatoires du second ordre. *In* P. Lévy, éditeur : *Processus stochastiques et mouvement brownien*, Paris, 1948.
[104] E.N. Lorenz : Empirical orthogonal functions and statistical weather prediction. Rapport technique, Statistical Forecast Project Report 1, Department of Meteorology, MIT, 1956.
[105] A.M. Lyapunov : Problème général de la stabilité du mouvement. *Annales de la faculté des sciences de Toulouse*, Série 2,9:203–474, 1907.
[106] L.I. Manevitch et Yu.V. Mikhlin : On periodic solutions close to rectilinear normal vibration modes. *J. Appl. Math. Mech. (PMM)*, 36(6):1051–1058, 1972.
[107] P. Manneville : *Instabilités, chaos et turbulence*. Editions de l'Excole Polytechnique, Palaiseau, 2004.
[108] S. Maurel, J. Borée et J.L. Lumley : Extended proper orthogonal decomposition : application to jet/vortex interaction. *Flow, Turbulence and Combustion*, 67:125–136, 2001.
[109] L. Meirovitch : *Computational Methods in Structural Dynamics*. Sijthoff and Noordhoff, The Netherlands, 1980.
[110] M. Mignolet et C. Soize : Stochastic reduced-order models for uncertain geometrically nonlinear dynamical systems. *Computer Methods in AppL. Mech. Engrg.*, 197:3951–3963, 2008.
[111] Yu.V. Mikhlin : Normal vibrations of a general class of conservative oscillators. *Non-linear Dynamics*, 11:1–15, 1996.
[112] O. Millet, A. Hamdouni et A. Cimetière : Justification du modèle bidimensionnel non-linéaire de plaque par développement asymptotique des équations d'équilibre. *C. R. Académie des Sciences IIb*, 324:349–354, 1997.
[113] H. J.-P. Morand et R. Ohayon : *Fluid structure interaction*. J. Wiley & sons, 1995.
[114] N. Mordant : Are there waves in elastic wave turbulence ? *Phys. Rev. Lett.*, 100:234505, 2008.
[115] J.K. Moser : Periodic orbits near an equilibrium and a theorem. *Communications in Pure and Applied Mathematics*, 29:727–747, 1976.
[116] A.A. Muravyov et S.A. Rizzi : Determination of nonlinear stiffness with application to random vibration of geometrically nonlinear structures. *Computers and Structures*, 81:1513–1523, 2003.
[117] A. H. Nayfeh : *Method of Normal Forms*. John Wiley & sons, New-York, 1993.
[118] A. H. Nayfeh : On direct methods for constructing nonlinear normal modes of continuous systems. *Journal of Vibration and Control*, 1:389–430, 1995.
[119] A. H. Nayfeh : Reduced-order models of weakly non-linear spatially continuous systems. *Nonlinear Dynamics*, 16:105–125, 1998.
[120] A. H. Nayfeh : *Nonlinear interactions : analytical, computational and experimental methods*. Wiley series in nonlinear science, New-York, 2000.
[121] A. H. Nayfeh, C. Chin et S. A. Nayfeh : On nonlinear normal modes of systems with internal resonance. *Trans. ASME/Journal of Vibration and Acoustics*, 118:340–345, 1996.
[122] A. H. Nayfeh et W. Lacarbonara : On the discretization of distributed-parameter systems with quadratic and cubic non-linearities. *Nonlinear Dynamics*, 13:203–220, 1997.
[123] A. H. Nayfeh et D. T. Mook : *Nonlinear oscillations*. John Wiley & sons, New-York, 1979.
[124] A. H. Nayfeh, J. F. Nayfeh et D. T. Mook : On methods for continuous systems with quadratic and cubic nonlinearities. *Nonlinear Dynamics*, 3:145–162, 1992.

[125] A. H. Nayfeh et S. A. Nayfeh : On nonlinear normal modes of continuous systems. *Trans. ASME/Journal of Vibration and Acoustics*, 116:129–136, 1994.
[126] A. H. Nayfeh et R. A. Raouf : Non-linear oscillations of circular cylindrical shells. *International Journal of Solids Structures*, 23(12):1625–1638, 1987.
[127] A. H. Nayfeh et L. D. Zavodney : Experimental observation of amplitude and phase-modulated responses of two internally coupled oscillators to a harmonic excitation. *ASME Journal of Applied Mechanics*, 55:706–710, 1988.
[128] A.C. Newell, S. Nazarenko et L. Biven : Wave turbulence and intermittency. *Physica D*, 152-153:520–550, 2001.
[129] D. Noreland, S. Bellizzi, C. Vergez et R. Bouc : Nonlinear modes of clarinet-like musical instruments. *Journal of Sound and Vibration*, 324(3-5):983–1002, 2009.
[130] R. Ohayon et C. Soize : *Structural Acoustics and Vibration*. Academic Press, London, 1998.
[131] L. Pastur, F. Lusseyran, Y. Fraigneau et B. Podvin : Determining the spectral signature of spatial coherent structures in an open cavity flow. *Physical review E*, 72:065301, 2005.
[132] M. Peeters, R. Viguié, G. Sérandour, G. Kerschen et J.C. Golinval : Non-linear normal modes, part II : toward a practical computation using numerical continuation techniques. *Mechanical Systems and Signal Processing*, 23(1):195–216, 2009.
[133] F. Pellicano, M. Amabili et M. P. Païdoussis : Effect of the geometry on the non-linear vibration of circular cylindrical shells. *International Journal of Non-linear Mechanics*, 37:1181–1198, 2002.
[134] E. Pesheck : *Reduced-order modeling of nonlinear structural systems using nonlinear normal modes and invariant manifolds*. Thèse de doctorat, University of Michigan, 2000.
[135] E. Pesheck, C. Pierre et S. Shaw : A new Galerkin-based approach for accurate non-linear normal modes through invariant manifolds. *Journal of Sound and Vibration*, 249(5):971–993, 2002.
[136] K. Pham : Réduction de modèle pour la simulation cardiaque. Rapport technique, INRIA/MACS, 2007. Stage de Master TACS.
[137] V. Pliss : Principal reduction in the theory of stability of motion. *Izv. Akad. Nauk. SSSR Math. Ser.*, 28:1297–1324, 1964. (in Russian).
[138] H. Poincaré : *Les méthodes nouvelles de la mécanique céleste*. Gauthiers-Villars, Paris, 1892.
[139] A. Raman et C. D. Mote Jr. : Effects of imperfection on the non-linear oscillations of circular plates spinning near critical speed. *International Journal of Non-linear Mechanics*, 36:261–289, 2001.
[140] A. Raman et C. D. Mote Jr. : Experimental studies on the non-linear oscillations of imperfect circular disks spinning near critical speed. *International Journal of Non-linear Mechanics*, 36:291–305, 2001.
[141] R.H. Rand : A direct method for non-linear normal modes. *International Journal of Non-linear Mechanics*, 9:363–368, 1974.
[142] G. Rega, W. Lacarbonara et A. H. Nayfeh : Reduction methods for nonlinear vibrations of spatially continuous systems with initial curvature. *Solid Mechanics and its applications*, 77:235–246, 2000.
[143] G. Rega et H. Troger : Dimension reduction of dynamical systems : Methods, models, applications. *Nonlinear Dynamics*, 41:1–15, 2005.
[144] F. A. Mc Robie, A. A. Popov et J. M. T. Thompson : Auto-parametric resonance in cylindrical shells using geometric averaging. *Journal of Sound and Vibration*, 227(1):65–84, 1999.
[145] R. M. Rosenberg : The normal modes of nonlinear n-degree-of-freedom systems. *Journal of Applied Mechanics*, 29:7–14, 1962.
[146] R. M. Rosenberg : On non-linear vibrations of systems with many degrees of freedom. *Advances in Applied Mechanics*, 9:155–242, 1966.
[147] R. Sampaio et C. Soize : Remarks on the efficiency of POD for model reduction in non-linear dynamics of continuous elastic systems. *International Journal for numerical methods in Engineering*, 72(1):22–45, 2007.
[148] J.L.Jr. Sanders : Nonlinear theories for thin shells. *Quarterly of Applied Mechanics*, 21:21–36, 1963.
[149] S. W. Shaw et C. Pierre : Non-linear normal modes and invariant manifolds. *Journal of Sound and Vibration*, 150(1):170–173, 1991.
[150] S. W. Shaw et C. Pierre : Normal modes for non-linear vibratory systems. *Journal of Sound and Vibration*, 164(1):85–124, 1993.
[151] S. W. Shaw et C. Pierre : Normal modes of vibration for non-linear continuous systems. *Journal of Sound and Vibration*, 169(3):85–124, 1994.
[152] J.C. Slater : A numerical method for determining nonlinear normal modes. *Nonlinear Dynamics*, 10(1):19–30, 1996.
[153] S. Sridhar, D. T. Mook et A. H. Nayfeh : Non-linear resonances in the forced responses of plates, part I : symmetric responses of circular plates. *Journal of Sound and Vibration*, 41(3):359–373, 1975.
[154] S. Sridhar, D. T. Mook et A. H. Nayfeh : Non-linear resonances in the forced responses of plates, part II : asymmetric responses of circular plates. *Journal of Sound and Vibration*, 59(2):159–170, 1978.
[155] A. Steindl et H. Troger : Methods for dimension reduction and their applications in nonlinear dynamics. *International Journal of Solids and Structures*, 38:2131–2147, 2001.
[156] O. Thomas : *Analyse et modélisation de vibrations non-linéaires de milieux minces élastiques. Application aux instruments de percussion*. Thèse de doctorat, Université Pierre et Marie Curie, Paris VI, 2001.
[157] O. Thomas et S. Bilbao : Geometrically nonlinear flexural vibrations of plates : In-plane boundary conditions and some symmetry properties. *Journal of Sound and Vibration*, 315(3):569–590, 2008.

[158] W. M. Tien, N. S. Namachchivaya et A. K. Bajaj : Non-linear dynamics of a shallow arch under periodic excitation, I : 1 :2 internal resonance. *International Journal of Non-linear Mechanics*, 29(3):349–366, 1994.
[159] S. A. Tobias : Free undamped non-linear vibrations of imperfect circular disks. *Proc. of the Instn. of Mech. Eng.*, 171:691–700, 1957.
[160] S. A. Tobias et R. N. Arnold : The influence of dynamical imperfection on the vibration of rotating disks. *Proc. of the Instn. of Mech. Eng.*, 171:669–690, 1957.
[161] A. F. Vakakis, L. I. Manevitch, Y. V. Mikhlin, V. N. Philipchuck et A. A. Zevin : *Normal modes and localization in non-linear systems*. Wiley, New-York, 1996.
[162] A.F. Vakakis : Non-linear normal modes (nnms) and their application in vibration theory : an overview. *Mechanical Systems and Signal Processing*, 11(1):3–22, 1997.
[163] A. Weinstein : Normal modes for nonlinear hamiltonian systems. *Inv. Math.*, 20:47–57, 1973.
[164] S. Wiggins : *Introduction to applied nonlinear dynamical systems and chaos*. Springer-Verlag, New-York, 2003. Second edition.
[165] C.J.H Williams et S.A. Tobias : Forced undamped non-linear vibrations of imperfect circular disks. *Journal of Mechanical Engineering science*, 5:325–335, 1963.
[166] C.G. Wu, Y.C. Liang, W.Z. Lin, H.P. Lee et S.P. Lim : A note on equivalence of proper orthogonal decomposition methods. *Journal of Sound and Vibration*, 265:1103–1110, 2003.
[167] N. Yamaki : *Elastic stability of circular cylindrical shells*. North-Holland, Amsterdam, 1984.
[168] X.L. Yang et P.R. Sethna : Local and global bifurcations in parametrically excited vibrations of nearly square plates. *International journal of Non-linear Mechanics*, 26(2):199–220, 1991.
[169] X.L. Yang et P.R. Sethna : Non-linear phenomena in forced vibrations of a nearly square plate -antisymmetric case. *Journal of Sound and Vibration*, 155(3):413–441, 1992.
[170] K. Yasuda et T. Asano : Nonlinear foced oscillations of a rectangular membrane with degenerated modes. *Bulletin of JSME*, 29(255):3090–3095, 1986.
[171] K. Yasuda et G. Kushida : Nonlinear forced oscillations of a shallow spherical shell. *Bull. JSME*, 27(232):2233–2240, 1984.
[172] M. H. Yeo et W. K. Lee : Corrected solvability conditions for non-linear asymmetric vibrations of a circular plate. *Journal of Sound and Vibration*, 257(4):653–665, 2002.
[173] Z. Yosibash et R.M. Kirby : Dynamic response of various von kármán non-linear plate models and their 3-d counterparts. *International Journal of Solids and Structures*, 42:2517–2531, 2005.
[174] V. E. Zakharov, V. S. Lvov et G. Falkovisch : *Kolmogorov Spectra of Turbulence I : Wave Turbulence*. Springer Verlag, Berlin, 1992.

Annexe 1 : Asymmetric non-linear forced vibrations of free-edge circular plates, part I : theory

Cette annexe donne le texte complet de l'article :

C. Touzé, O. Thomas et A. Chaigne : Asymmetric non-linear forced vibrations of free-edge circular plates, part I : theory, Journal of Sound and Vibration, **258**(4), pp. 649-676, 2002.

Journal of Sound and Vibration (2002) **258**(4), 649–676
doi:10.1006/jsvi.2002.5143, available online at http://www.idealibrary.com on IDEAL®

ASYMMETRIC NON-LINEAR FORCED VIBRATIONS OF FREE-EDGE CIRCULAR PLATES. PART 1: THEORY

C. Touzé, O. Thomas† and A. Chaigne

ENSTA - UME, Chemin de la Hunière, 91761 *Palaiseau Cedex, France, and ENST, Département TSI,* 46 *rue Barrault,* 75634 *Paris Cedex* 13*, France.*
E-mails: *touze@ensta.fr*, *othomas@ensta.fr*, *chaigne@ensta.fr*

(*Received* 4 *June* 2001, *and in final form* 23 *January* 2002)

In this article, a detailed study of the forced asymmetric non-linear vibrations of circular plates with a free edge is presented. The dynamic analogue of the von Kàrmàn equations is used to establish the governing equations. The plate displacement at a given point is expanded on the linear natural modes. The forcing is harmonic, with a frequency close to the natural frequency ω_{kn} of one asymmetric mode of the plate. Thus, the vibration is governed by the two degenerated modes corresponding to ω_{kn}, which are one-to-one internally resonant. An approximate analytical solution, using the method of multiple scales, is presented. Attention is focused on the case where one configuration which is not directly excited by the load gets energy through non-linear coupling with the other configuration. Slight imperfections of the plate are taken into account. Experimental validations are presented in the second part of this paper.

1. INTRODUCTION

Circular plates can exhibit large flexural vibrations, of the order of the plate thickness. In this case, a linear model is not sufficient to predict the behaviour of the plate, since typical phenomena such as jump phenomenon, hysteresis or internal resonance are often encountered [1]. In this paper, the dynamic analogue of the von Kàrmàn equations is used to include geometrical non-linearities in the local vibration equations, taking into account the stretching of the mid-plane of the plate.

Attention is focused here on the flexural vibration of circular thin plates, with a free edge, subjected to harmonic excitation. The displacement of a given point of the plate is expanded on the natural modes, which are derived from the linear part of the governing equations. These modes can be either axisymmetric, exhibiting no nodal diameters and hence being independant of the angular co-ordinate θ; or asymmetric, with at least one nodal diameter. For each frequency associated with an asymmetric mode shape there are two corresponding independent modes [2]. Following Tobias and Arnold [3], these two degenerated modes are called the two *preferential configurations*. If the plate is perfect, the shapes of the two configurations have the same dependence on the radial co-ordinate, and differ only by the position of their nodal diameters, the ones of the first being located on the maxima of amplitude of the second. In the case of a real plate, owing to inevitable small imperfections, it has been shown both theoretically and experimentally that such

† Present address: ENSTA – UMA.

0022-460X/02/$35.00

modes have slightly different modal frequencies and that one configuration is moderately rotated with respect to the other, so that the perfect spatial symmetry is broken [3, 4].

The axisymmetric vibrations of circular plates have been studied exhaustively in the past; see, for example references [5, 6] for one-mode vibration of a plate with various boundary conditions (clamped and simply supported) and without damping, references [7, 8] for multi-mode responses involving internal resonances between axisymmetric modes in the case of a clamped circular plate with model damping, and references [1, 9] for general considerations and a survey of the existing literature.

Incidentally, only a few studies have considered the asymmetric case. This is particularly astonishing since for any circular plate, axisymmetric modes are few compared to the number of asymmetric ones. Hence, asymmetric modes are likely to play a preponderant role in the vibrations of plates. The main contribution to the subject is due to Tobias, Arnold and Williams who were the first to consider the non-linear coupling between the two preferential configurations of an asymmetric mode shape [3, 10, 11]. They have shown, in particular, that beating travelling waves may appear due to this coupling. This study was conducted on rotating discs clamped at their centre, with a free edge, and the damping was neglected. A recent contribution by Raman and Mote considers the same case of a spinning disc, both theoretically and experimentally [12, 13]. Dugdale proposed a succinct theoretical work, including damping [14]. Efstathiades brought a major contribution to the subject, since he has taken into account the possible imperfections of the plate in the derivation of the governing equations. He used the von Kàrmàn equations and the Galerkin procedure [4]. Sridhar *et al.* presented a systematic analysis of the forced response of a clamped circular plate, including damping. They came to the conclusion that a travelling wave component is possible only if an internal resonance exists between modes of frequency well apart from the excitation frequency [15]. Asymmetric linear vibrations of circular plates of linearly varying thickness have also been considered recently in references [16, 17]. Finally, recent development in computer simulations leads to numerical studies, which generally use a finite element method combined with the harmonic balance method, see for example references [18, 19].

The main purpose of this paper is to present a complete and self-contained analysis of the response of circular thin plates with a free edge and free centre subjected to harmonic excitation, when the excitation frequency is close to one natural frequency. In this paper, only the one-to-one internal resonances between the two preferential configurations of an asymmetric mode are considered. To take into account large deflections, of order of the plate thickness, the non-linear plate model used here is the dynamic analogue of the von Kàrmàn equations [20, 21].

This work has been motivated by the fact that only scattered contributions on the subject are available in the literature. Bringing them together, and developing some points that were sometimes overlooked by previous authors allows one to present a detailed analysis in a uniform manner. The solution for the deflection of the plate is expanded into the linear natural modes. The governing partial differential equations lead to a set of second order differential equations, in a similar way to Sridhar *et al.* reference [15]. The problem is then reduced to the case of a one-mode vibration. The case of an asymmetric mode is studied in detail, with damping and imperfections of the plate taken into account, hence extending the results of Tobias *et al.*, and those presented in references [22, 23]. The temporal part of the deflection is solved by the multiple scales method. A detailed study of the dynamical system arising from this technique is presented, which complements the results of Tobias *et al.* It is shown, in particular, how the coupling between preferential configurations can give rise to a travelling wave component in the response. An exhaustive

set of experiments will be described in a companion paper, whose aim is to confirm all the present developments.

2. PROBLEM FORMULATION

In what follows, a thin plate of diameter $2a$ and thickness h, made of a homogeneous isotropic material of density ρ, Poisson ratio v and Young's modulus E, is considered. The only non-zero external loads are normal to the surface of the plate, and represented by a pressure denoted $p(r, \theta, t)$.

2.1. LOCAL EQUATIONS

The following non-linear local equations governing the motion of the plate are used:

$$D\Delta\Delta w + \rho h\ddot{w} = L(w, F) - \mu\dot{w} + p(r, \theta, t), \tag{1a}$$

$$\Delta\Delta F = -\frac{Eh}{2} L(w, w), \tag{1b}$$

where

$$L(w, F) = w_{,rr}\left(\frac{F_{,r}}{r} + \frac{F_{,\theta\theta}}{r^2}\right) + F_{,rr}\left(\frac{w_{,r}}{r} + \frac{w_{,\theta\theta}}{r^2}\right) - 2\left(\frac{w_{,r\theta}}{r} - \frac{w_{,\theta}}{r^2}\right)\left(\frac{F_{,r\theta}}{r} - \frac{F_{,\theta}}{r^2}\right), \tag{2}$$

w is the vertical displacement at a given point of co-ordinates (r, θ) of the middle surface of the plate, $D = Eh^3/12(1 - v^2)$ is the flexural rigidity, μ is a damping coefficient; $\ddot{w}$ and $w_{,r\theta}$ denote the second partial derivatives with respect to time and spatial co-ordinates, respectively, and

$$\Delta(\bullet) = (\bullet)_{,rr} + \frac{1}{r}(\bullet)_{,r} + \frac{1}{r^2}(\bullet)_{,\theta\theta} \tag{3}$$

is the Laplacian. The force function F is defined by

$$N_r = \frac{1}{r}F_{,r} + \frac{1}{r^2}F_{,\theta\theta}, \qquad N_\theta = F_{,rr}, \qquad N_{r\theta} = N_{\theta r} = \frac{1}{r^2}F_{,\theta} - \frac{1}{r}F_{,r\theta}, \tag{4}$$

where $N_{\alpha\beta}$, $\alpha, \beta \in \{r, \theta\}$ are the membrane forces per unit length in polar co-ordinates, related to the components of the second Piola–Kirchhoff stress tensor $\pi_{\alpha\beta}$ [24, 25]:

$$[N_r, N_{r\theta}, N_\theta] = \int_{-h/2}^{h/2} [\pi_r, \pi_{r\theta}, \pi_\theta]\, \mathrm{d}z. \tag{5}$$

Equations (1a, b) are known as the dynamic analogues of the von-Kàrmàn equations, where damping and forcing have been added. The underlying assumptions are the following. Firstly, the plate is assumed to be thin, i.e., $h/a \ll 1$. Secondly, the Kirchhoff–Love hypotheses are assumed to be satisfied. Thirdly, only the non-linear terms of lowest order are kept in the expression of the strains as functions of the displacement. Finally, the in-plane and rotatory inertia terms are neglected [4, 15, 20, 26].

Equation (1b) follows from the compatibility equation, and shows the non-linear coupling between the transverse displacement w and the stretching of the mid-plane of the plate, resulting in a non-zero function F.

2.2. BOUNDARY CONDITIONS

In the case of a free edge, the external load vanishes at the edge of the plate. The boundary conditions written in cylindrical co-ordinates are, for any point at the edge [26],

$$N_r = N_{r\theta} = 0, \tag{6a, b}$$

$$M_r = 0, \quad \frac{1}{r} M_{r\theta,\theta} + Q_r = 0, \tag{6c, d}$$

where M_r and $M_{r\theta}$ are the bending and twisting moments and Q_r is the transverse shear force. Their definitions in terms of the Piola–Kirchhoff stress tensor are

$$[M_r, M_{r\theta}] = \int_{-h/2}^{h/2} [\pi_r, \pi_{r\theta}] z \, \mathrm{d}z, \quad Q_r = \int_{-h/2}^{h/2} \pi_{zr} \, \mathrm{d}z \tag{7a, b}$$

and they are related to the deflection w by the relations

$$M_r = -D\left(w_{,rr} + \frac{\nu}{r} w_{,r} + \frac{\nu}{r^2} w_{,\theta\theta}\right), \tag{8a}$$

$$M_{r\theta} = -D(1-\nu)\left(\frac{w_{,r\theta}}{r} - \frac{w_{,\theta}}{r^2}\right), \tag{8b}$$

$$Q_r = -D(\Delta w)_{,r}. \tag{8c}$$

Combining now equations (6a–d) with equations (4) and (8a, c), one obtains the boundary conditions in terms of w and F, for all θ and t:

$$F_{,r} + \frac{1}{a} F_{,\theta\theta} = 0, \quad F_{,r\theta} - \frac{1}{a} F_{,\theta} = 0, \quad \text{at } r = a, \tag{9a}$$

$$w_{,rr} + \frac{\nu}{a} w_{,r} + \frac{\nu}{a^2} w_{,\theta\theta} = 0, \quad \text{at } r = a, \tag{9b}$$

$$w_{,rrr} + \frac{1}{a} w_{,rr} - \frac{1}{a^2} w_{,r} + \frac{2-\nu}{a^2} w_{,r\theta\theta} - \frac{3-\nu}{a^3} w_{,\theta\theta} = 0, \quad \text{at } r = a. \tag{9c}$$

2.3. DIMENSIONLESS FORM OF THE EQUATIONS

It is convenient to rewrite the previous equations in terms of dimensionless variables of order $O(1)$. They are denoted by overbars, and defined as follows:

$$r = a\bar{r}, \quad t = a^2\sqrt{\rho h/D}\bar{t}, \quad w = (h^2/a)\bar{w}, \quad F = (Eh^5/a^2)\bar{F}, \tag{10}$$

$$\mu = [2Eh^5/a^4]\sqrt{\rho h/D}\bar{\mu}, \quad p = (Eh^7/a^7)\bar{p}. \tag{11}$$

Substituting these variables into equations (1a, b) and dropping for simplicity the overbars in the result, we find for all r, θ and t,

$$\Delta\Delta w + \ddot{w} = \varepsilon[L(w, F) - 2\mu\dot{w} + p], \tag{12a}$$

$$\Delta\Delta F = -\tfrac{1}{2} L(w, w), \tag{12b}$$

where $\varepsilon = 12(1-\nu^2)h^2/a^2$. The boundary conditions take the same form as in equations (9a–c), with $a = 1$. In addition, the solution must be bounded for $r = 0$.

One can notice that the von Kàrmàn equations, whose assumptions are summarized in section 2.1, are valid if the magnitude of displacement w is of the order of magnitude of the

plate thickness h. It would then have been apparently logical to choose $\bar{w} = w/h$ as a dimensionless variable for w. However, in this case, the parameter ε would have been equal to $12(1-\nu^2)a^2/h^2$, which is large compared to 1 when $h/a \ll 1$, and thus the non-linear terms in equation (12a) would have been of larger order than the linear terms. To derive the analytical perturbation solution of section 6, the non-linear terms of equation (12a) must be of lower order than the linear terms. If $\bar{w} = w/(h^2/a)$, then $\varepsilon = 12(1-\nu^2)h^2/a^2$ is small compared to 1. As already mentioned by Nayfeh *et al.* [7, 15], the present theory offers corrections to the linear small deflection theory and enables one to predict the typical non-linear phenomena presented in section 6. This approach is mathematically valid for displacement w of order h^2/a. In experimental situations, it allows a fair interpretation of observed data up to displacements of the order of the thickness h.

3. MODAL EXPANSION

The displacement w is written as the product of a function of the space co-ordinates and a function of time. Assuming that the non-linear nature of w is contained in the temporal part of the solution, it is expanded as follows:

$$w(r,\theta,t) = \sum_{p=1}^{+\infty} \Phi_p(r,\theta) q_p(t), \tag{13}$$

where the q_p are unknown functions of time and Φ_p are the linear natural modes of the plate with a *free edge*, corresponding to the eigenfunctions of the linear part of the problem defined by equations (12a) and (9b, c) (see section A.1).

Substituting equation (13) into equation (12b) leads to

$$\Delta\Delta F = \sum_{p=1}^{+\infty} \sum_{q=1}^{+\infty} E_{pq}(r,\theta) q_p(t) q_q(t) \tag{14}$$

with

$$E_{pq} = -\tfrac{1}{2} L(\Phi_p, \Phi_q). \tag{15}$$

Following the same method, an expansion of $F(r,\theta,t)$ is assumed to have the form

$$F(r,\theta,t) = \sum_{s=1}^{+\infty} \Psi_s(r,\theta)\eta_s(t), \tag{16}$$

so that

$$\Delta\Delta F = \sum_{s=1}^{+\infty} [\Delta\Delta\Psi_s(r,\theta)]\eta_s(t), \tag{17}$$

where the η_s are unknown functions of time and the Ψ_s are chosen so that the following equation is fulfilled, for all r and θ:

$$\Delta\Delta\Psi(r,\theta) = \xi^4 \Psi(r,\theta), \tag{18}$$

where ξ is an unknown real number. Boundary conditions (9a), rewritten in terms of Ψ through equation (16), give, for all θ,

$$\Psi(r=1,\theta) = 0, \quad \Psi_{,r}(r=1,\theta) = 0. \tag{19}$$

It turns out that the Ψ_s, solutions of equation (18), exhibit the same spatial dependence as the natural modes of a circular plate with *clamped edge* (section A.2).

By substituting equation (16) into equation (14), multiplying the result by Ψ_b $(b > 1)$, integrating on the surface $(\mathscr{S})$ of the plate and using the orthogonality properties of the eigenmodes, one obtains

$$\eta_b(t) = \sum_{p=1}^{+\infty} \sum_{q=1}^{+\infty} G_{pqb}\, q_p(t) q_q(t) \tag{20}$$

with

$$G_{pqb} = \frac{\int\int_{(\mathscr{S})} E_{pq} \Psi_b \,\mathrm{d}S}{\xi_b^4 \int\int_{(\mathscr{S})} \Psi_u^2 \,\mathrm{d}S} = -\frac{1}{2} \frac{\int\int_{(\mathscr{S})} L(\Phi_p, \Phi_q) \Psi_b \,\mathrm{d}S}{\xi_b^4 \int\int_{(\mathscr{S})} \Psi_u^2 \,\mathrm{d}S}, \tag{21}$$

so that

$$F(r, \theta, t) = \sum_{b=1}^{+\infty} \left(\sum_{p=1}^{+\infty} \sum_{q=1}^{+\infty} G_{pgb} q_p(t) q_q(t) \right) \Psi_b(r, \theta). \tag{22}$$

As is predictable from equation (12b), which shows that F is of order w^2, one can observe that F is a function of the q_p squared only, which corresponds to the order of the non-linear terms. This explains why F and, therefore, the stretching of the mid-plane are neglected in the linear theory.

Substituting equation (22) into equation (12a), multiplying the result by Φ_α $(\alpha > 1)$, integrating on the surface $(\mathscr{S})$ of the plate and using the orthogonality properties of the eigenmodes leads to

$$\ddot{q}_\alpha(t) + \omega_\alpha^2 q_\alpha(t) = \varepsilon \left[\sum_{p=1}^{+\infty} \sum_{q=1}^{+\infty} \sum_{u=1}^{+\infty} \Gamma_{pq\alpha u}\, q_p(t) q_q(t) q_u(t) - 2\mu_\alpha \dot{q}_\alpha(t) + \tilde{Q}_\alpha(t) \right], \tag{23}$$

where μ_α denotes the dimensionless modal damping of the αth mode. The dimensionless pulsation ω_α, the coefficients $\Gamma_{pq\alpha u}$ and the forcing $\tilde{Q}_\alpha(t)$ are defined as follows:

$$\omega_\alpha^2 = \frac{\int\int_{(\mathscr{S})} \Phi_\alpha \Delta\Delta \Phi_\alpha \,\mathrm{d}S}{\int\int_{(\mathscr{S})} \Phi_\alpha^2 \,\mathrm{d}S}, \quad \tilde{Q}_\alpha(t) = \frac{\int\int_{(\mathscr{S})} p \Phi_\alpha \,\mathrm{d}S}{\int\int_{(\mathscr{S})} \Phi_\alpha^2 \,\mathrm{d}S}, \tag{24}$$

$$\Gamma_{pq\alpha u} = -\frac{1}{2} \sum_{b=1}^{+\infty} \frac{\int\int_{(\mathscr{S})} L(\Phi_p, \Phi_q) \Psi_b \,\mathrm{d}S \int\int_{(\mathscr{S})} \Phi_\alpha L(\Phi_u, \Psi_b) \,\mathrm{d}S}{\xi_b^4 \int\int_{(\mathscr{S})} \Phi_\alpha^2 \,\mathrm{d}S \int\int_{\mathscr{S}} \Psi_b^2 \,\mathrm{d}S}. \tag{25}$$

The two partial-differential equations (12a, b) have been substituted by the above set of coupled non-linear differential equations (23), whose unknowns are the functions $q_\alpha(t)$. One can notice that the mathematical derivations have been kept general. The infinity of modes is *a priori* supposed to take part in the vibration, the αth differential equation in q_α of set (23) governing the contribution of the αth mode.

4. ONE-MODE VIBRATION

In this section, the external pressure $p(r, \theta, t)$ is assumed to be equal to zero everywhere, except on a localized surface S_{dr}, where the pressure is harmonic with frequency Ω. The area of S_{dr} is assumed to be negligible with respect to the area $\mathscr{S}$ of the plate. The corresponding forcing terms are then $\tilde{Q}_\alpha(t) = Q_\alpha \cos \Omega t$, where the value of Q_α depends on the mode shape Φ_α.

The deflection of the plate is governed by the modes which are directly excited by the load near their resonance, and by the modes indirectly excited through an internal

resonance. The other modes, possibly excited in the transient part of the vibration, decay with time because of the damping. Their magnitudes in the steady state are neglected in the present study. If not, the linear normal modes Φ_p mix with each other in order to give *non-linear modes*, whose shapes depend on the vibration amplitude. These effects have been considered both in experimental and theoretical viewpoints, see for example the papers of Shaw and Pierre [27] and references therein, Nayfeh and Nayfeh [28] or Benamar *et al.* [29]. This approach has not been followed in this article for the two following reasons. First, form an experimental viewpoint, it is shown in reference [29] that the differences between linear and non-linear mode shapes become significant only when the deflection amplitude is larger than the thickness of the plate, which is not the case considered here. Second, as shown in reference [28], corrections due to non-linear modes appear as second order in a perturbation scheme such as the multiple scales method used here. As only a first order multiple scales development is considered in this study, non-linear modes are not taken into account. To summarize, only the modes with natural frequencies close to Ω are assumed to have significant responses in the steady state. As a consequence, set (23) reduces to the equations governing the response of the excited modes only.

If Ω is close to the natural frequency ω_{0n} of one particular axisymmetric mode, say Φ_{0n}, set (23) reduces to only one equation. The mode shape of Φ_{0n} has no nodal radii, n nodal circles, and depends only on the radial co-ordinate r (Figure 1), so that $\Phi_{0n} = R_{0n}(r)$, with R_{0n} defined in section A.1. Thus, the problem is written as

$$w(r, t) = R_{0n}(r)q(t), \tag{26a}$$

$$\ddot{q}(t) + \omega_{0n}^2 q(t) = \varepsilon[\Gamma q(t)^3 - 2\mu_{0n}\dot{q}(t) + Q\cos\Omega t]. \tag{26b}$$

The mathematical expression of the coefficient Γ in equation (26b) is specified in section B.1. Numerical values of Γ for different axisymmetric modes are listed in Table 1. This case of axisymmetric vibration has already been exhaustively studied, and the interested reader can refer to references [6, 7, 22].

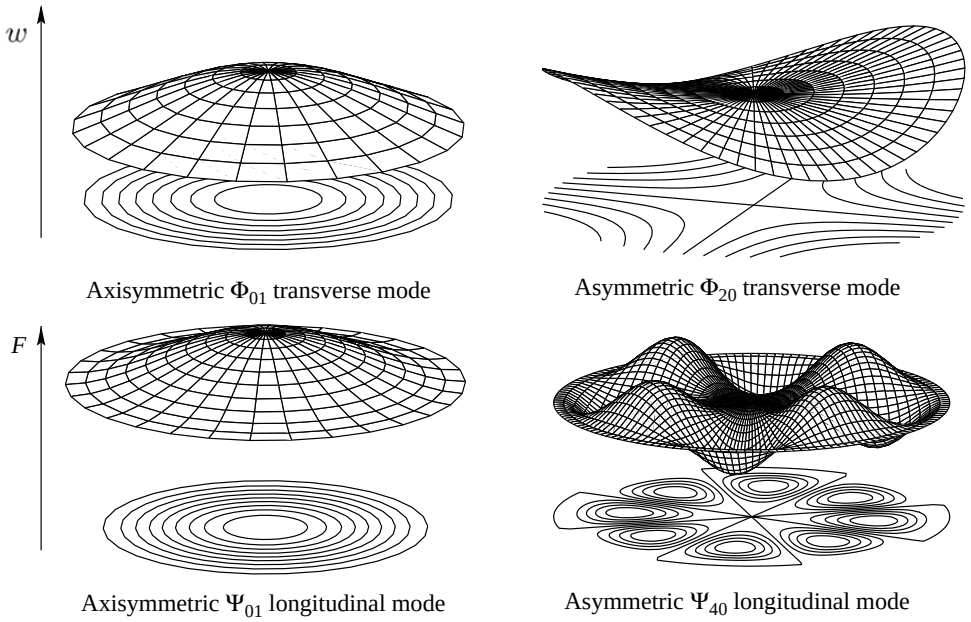

Figure 1. Mode shapes of typical transverse (w) and longitudinal (F) modes.

TABLE 1

ω_{kn} and Γ for a few modes. The calculations have been made with $\nu = 0{\cdot}38$

Mode $(k,n)^{\dagger}$	ω_{kn}	Γ (axisym.)	Γ (asym.)	Number of terms‡
2·0	5·093	—	−1·898	3
0·1	9·175	−8·575	—	4
3·0	11·90	—	−17·03	4
1·1	20·58	—	−31·83	5
4·0	20·97	—	−70·72	8
2·1	35·21	—	−70·01	9
0·2	38·61	−164·4	—	4
0·3	87·92	−1078·0	—	6

† k: Number of nodal radii; n: number of nodal circles.

‡ Number of modes Ψ_b taken into account in the numerical calculus corresponding to equation (25), to obtain a four significant digit precision.

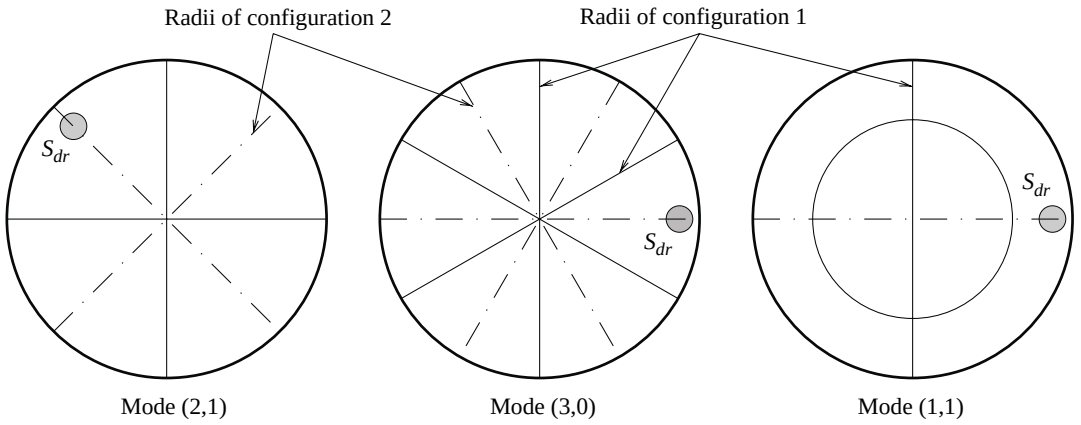

Figure 2. Position of nodal radii of both configurations for various asymmetric modes, in the case of a *perfect* plate. Position of the surface S_{dr} of the forcing located on a nodal radius of configuration 2.

If Ω is close to the natural frequency ω_{kn} of one particular asymmetric mode, the two preferential configurations $\Phi_1 = \Phi_{kn1} = R_{kn}\cos k\theta$ and $\Phi_2 = \Phi_{kn2} = R_{kn}\sin k\theta$, which are independent and orthogonal, are likely to take part in the vibration. They display k nodal radii, n nodal circles and exhibit the same dependence on r. Examples of mode shapes are shown in Figure 1. Expressions of R_{kn} are given in section A.1. Set (23) then reduces to two equations only.

If S_{dr} is assumed to be centred on a nodal radius of configuration 2, Φ_2, only configuration 1 is directly excited by the external pressure (see Figure 2). Thus, the direct load Q_2 of configuration Φ_2 is zero, and the problem becomes

$$w(r,\theta,t) = R_{kn}(r)[q_1(t)\cos k\theta + q_2(t)\sin k\theta], \tag{27a}$$

$$\ddot{q}_1 + \omega_{kn}^2 q_1 = \varepsilon[\Gamma(q_1^3 + q_1 q_2^2) - 2\mu_{kn}\dot{q}_1 + Q_1\cos\Omega t], \tag{27b}$$

$$\ddot{q}_2 + \omega_{kn}^2 q_2 = \varepsilon[\Gamma(q_2^3 + q_1^2 q_2) - 2\mu_{kn}\dot{q}_2]. \tag{27c}$$

One can notice that the coefficients of the non-linear terms found in equations (27b, c) are equal, and that the coefficients of q_2^3 and $q_1^2 q_2$ in equation (27b), and the ones of q_1^3 and $q_1 q_2^2$ in equation (27c) are equal to zero. This is a consequence of the particular dependence

of Φ_1 and Φ_2 on cosine and sine, and also because the two configurations are situated symmetrically with respect to each other. These results have already been pointed out by Efstathiades [4], and the corresponding mathematical development are given in section B.2. It is probably a general result for all natural modes of a axisymmetric structure, where the dependence in θ is decoupled from the other spatial co-ordinates. Some values of ω_{kn} and Γ have been computed numerically, and given in Table 1.

Equations (27b, c) show that the deflection of the plate is governed by two modes, Φ_1 and Φ_2. Because they share similar mode shapes and natural frequencies, one usually says that the plate is subjected to a *one-mode vibration*.

Equation (22) is convenient for deducing the in-plane vibration of the plate. For this purpose, one has to calculate the values of the coefficients G_{pqb}, with Φ_p and Φ_q taken among the two preferential configurations Φ_1 and Φ_2 with k nodal radii. It can be deduced from section B.2 that the only non-zero G_{pqb} are the ones corresponding to the longitudinal mode Ψ_b which are either axisymmetric, or have twice as many nodal radii ($l = 2k$). It means that the vibration of w on the mode Φ_1 (or Φ_2) leads, via non-linear coupling, to a stretching of the mid-plane based on all its axisymmetric modes ($l = 0$) and all its asymmetric modes of $l = 2k$ nodal radii. Figure 1 shows the transverse mode Φ_{20} and two associated longitudinal modes Ψ_{01} and Ψ_{40}. In addition, it can be derived from equation (22) that the mid-plane is subjected to an oscillatory stretching of pulsation 2Ω, which is two times faster than w.

5. THE CASE OF A SLIGHTLY IMPERFECT PLATE

In usual experimental conditions, an *a priori* perfect plate often presents slightly different natural frequencies, and exhibits a small angular shift of the nodal radii compared to the exact symmetric case [3, 4]. Thus, in the following mathematical developments, a distinction is made between the two natural frequencies, which will be now denoted by ω_1 and ω_2, with $\omega_1 \simeq \omega_2$. The angular shifts of the mode shapes of the two configurations are introduced with the help of two angles, ϕ_1 and ϕ_2 (Figure 3), so that

$$\Phi_1^*(r, \theta) = R_{kn}(r) \cos(k\theta + \phi_1), \tag{28a}$$

$$\Phi_2^*(r, \theta) = R_{kn}(r) \sin(k\theta + \phi_2). \tag{28b}$$

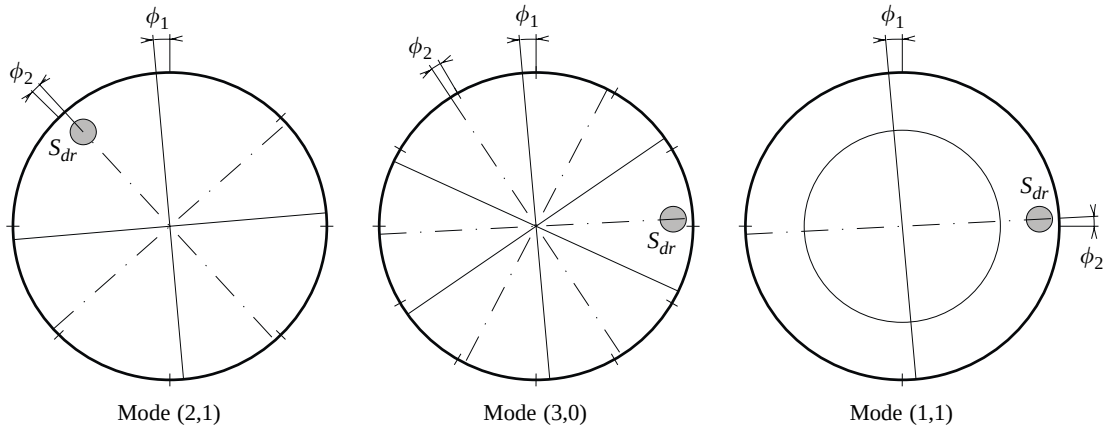

Figure 3. Angular shifts of nodal radii of both configurations for various asymmetric modes, in the case of a *real* plate.

The displacement w then becomes

$$w(r,\theta,t) = R_{kn}(r)[q_1^*(t)\cos(k\theta+\phi_1) + q_2^*(t)\sin(k\theta+\phi_2)] \tag{29a}$$

$$= R_{kn}(r)[q_1(t)\cos(k\theta) + q_2(t)\sin(k\theta)] \tag{29b}$$

with

$$\begin{pmatrix} q_1 \\ q_2 \end{pmatrix} = \begin{pmatrix} \cos\phi_1 & \sin\phi_2 \\ -\sin\phi_1 & \cos\phi_2 \end{pmatrix} \begin{pmatrix} q_1^* \\ q_2^* \end{pmatrix}. \tag{30}$$

It is obvious from the above mathematical derivations that set (27b, c), with two different angular frequencies ω_1 and ω_2, is sufficient to predict the behaviour of a plate with small imperfections. With q_1 and q_2 given by equations (27b, c), one has to invert equation (30) to obtain q_1^* and q_2^*. These variables are replaced in equation (29a) in order to obtain the displacement w. Values of ω_1, ω_2, ϕ_1 and ϕ_2 can be measured on a real plate in experimental conditions.

One can note that the model presented in this paper provides corrections for the perfect plate theory. It is not valid, in particular, if the plate shows large imperfections. This can be the case if holes of significant area compared to the area of the plate are present, or if the boundary conditions are far from being axisymmetric, or if some masses, not negligible compared to the mass of the plate, are added. In those cases, a valid analytical expression of the modes would not be separated in terms of spatial co-ordinates (such as $\Phi(r,\theta) = R(r)f(\theta)$). In particular, the nodal curves would not be perfect circles and radii as in the ideal case.

Finally, in experimental situations, it has been found very difficult to completely cancel the forcing of configuration 2. Therefore, in the following section, a term Q_2, small compared to Q_1, will be added in set (27b, c) for the sake of generality.

6. ANALYTICAL PERTURBATIVE SOLUTION

This section is devoted to the analysis of the set of coupled Duffing equations derived from equation (27). As this temporal part may occur in many different physical systems once the projection onto the normal modes basis have been carried out, the analysis brought in this section will be provided for variable coefficients. The problem under study is written as

$$\ddot{q}_1 + \omega_1^2 q_1 = \varepsilon[\Gamma_1 q_1^3 + C_1 q_1 q_2^2 - 2\mu\dot{q}_1 + Q_1\cos\Omega t], \tag{31a}$$

$$\ddot{q}_2 + \omega_2^2 q_2 = \varepsilon[\Gamma_2 q_2^3 + C_2 q_2 q_1^2 - 2\mu\dot{q}_2 + Q_2\cos\Omega t], \tag{31b}$$

where $\omega_1 \simeq \omega_2 \simeq \Omega$.

Most results will be presented for equal coefficients ($\Gamma_1 = \Gamma_2 = C_1 = C_2$), corresponding to the case of a circular plate with slight imperfections, but some interesting phenomena will be exhibited for other values of the coefficients.

System (31) has already been studied in the past by many different investigators. A study of equation (31) for a subharmonic forced excitation ($\Omega \simeq 3\omega_1$), and for the specific case of a perfect circular plate without internal detuning ($\omega_1 = \omega_2$), is given in reference [30]. The major contributions have been brought in the study of the vibrations of rectangular plates, where *degenerated modes* are observed, i.e., two modes having different mode shapes but identical natural frequencies. Yasuda and Asano [31] and Chang *et al.* [32] performed a thorough analysis of the different behaviours exhibited by a system of form (31). The first authors were primarily interested in the case of an equivalent forcing

on the two modes ($Q_1 \simeq Q_2$). Chang *et al.* conducted an exhaustive study of the bifurcations. Lewandowski studied in reference [33] the effects of internal resonance on backbone curves with a two harmonics solution. This leads to backbone curves with loops, additional branches and bifurcation points. One-to-one resonances were also studied with parametric excitation, see reference [34] for the case of a nearly square plate with parametric in-plane excitation, or reference [35] for a review of the literature.

The aim of this section is to provide an extension of some of these previously mentioned results. The effect of important physical parameters such as damping, or the internal detuning between the two modal frequencies ω_1 and ω_2, will be systematically investigated. System (31) will be analytically solved by using the method of multiple scales [1]. Existence conditions for fixed points as well as their stability will be studied. Special emphasis will be put on the loss of stability of single-degree-of-freedom solution for the case of a coupled solution. Diagrams will be drawn, which show under which conditions this energy transfer is effective. The case of a softening non-linearity is presented. Experimental validations will be presented in the second part of this paper.

6.1. MULTIPLE-SCALES SOLUTION

System (31) is solved by the method of multiple scales [1]. To the first order:

$$\begin{aligned} q_1(t) &= q_{11}(T_0, T_1) + \varepsilon q_{12}(T_0, T_1) + O(\varepsilon^2), \\ q_2(t) &= q_{21}(T_0, T_1) + \varepsilon q_{22}(T_0, T_1) + O(\varepsilon^2), \end{aligned} \tag{32}$$

where $T_j = \varepsilon^j t$. Substituting these expressions into equation (31), equating coefficients of like powers of ε and using $D_j = \partial/\partial T_j$, one obtains

order ε^0:

$$\begin{aligned} D_0^2 q_{11} + \omega_1^2 q_{11} &= 0, \\ D_0^2 q_{21} + \omega_2^2 q_{21} &= 0, \end{aligned} \tag{33}$$

order ε^1:

$$\begin{aligned} D_0^2 q_{12} + \omega_1^2 q_{12} &= -2D_0 D_1 q_{11} + \Gamma_1 q_{11}^3 + C_1 q_{11} q_{21}^2 - 2\mu D_0 q_{11} + Q_1 \cos \Omega t, \\ D_0^2 q_{22} + \omega_2^2 q_{22} &= -2D_0 D_1 q_{21} + \Gamma_2 q_{21}^3 + C_2 q_{21} q_{11}^2 - 2\mu D_0 q_{21} + Q_2 \cos \Omega t. \end{aligned} \tag{34}$$

The solutions of equation (33) can be written in the form

$$\begin{aligned} q_{11}(t) &= A_1(T_1) \exp(\mathrm{i}\omega_1 T_0) + c.c., \\ q_{21}(t) &= A_2(T_1) \exp(\mathrm{i}\omega_2 T_0) + c.c., \end{aligned} \tag{35}$$

where *c.c.* stands for complex conjugate. A_1 and A_2 are unknown functions of T_1; their dependence with time will be exhibited when solving the solvability conditions. For this purpose, one introduces the two following detuning parameters:

$$\omega_2 = \omega_1 + \varepsilon\sigma_1, \quad \Omega = \omega_1 + \varepsilon\sigma_2. \tag{36}$$

σ_1 gives a measure of the internal detuning between the two modal configurations. In a completely perfect case, $\omega_1 = \omega_2$, thus $\sigma_1 = 0$. σ_2 measures the detuning between the excitation frequency and the natural frequency of configuration (1). Substituting equations (35) into equation (34), and setting all the resonant terms to zero to avoid secular terms in

the solution gives the solvability conditions

$$-2i\omega_1(A_1' + \mu A_1) + 3\Gamma_1 A_1^2 \bar{A}_1 + C_1 A_2(2A_1\bar{A}_2 + \bar{A}_1 A_2 e^{2i\sigma_1 T_1}) + \frac{Q_1}{2} e^{i\sigma_2 T_1} = 0,$$
$$-2i\omega_2(A_2' + \mu A_2) + 3\Gamma_2 A_2^2 \bar{A}_2 + C_2 A_1(2A_2\bar{A}_1 + \bar{A}_2 A_1 e^{-2i\sigma_1 T_1}) + \frac{Q_2}{2} e^{i(\sigma_2-\sigma_1)T_1} = 0, \quad (37)$$

where $(\,)'$ stands now for the derivation with respect to T_1.

Equations (37) are solved in introducing the polar forms

$$A_1(T_1) = a_1(T_1)\exp(i\theta_1(T_1)),$$
$$A_2(T_1) = a_2(T_1)\exp(i\theta_2(T_1)), \quad (38)$$

where the amplitudes a_i and the phases θ_i are now real functions of T_1. Substituting equation (38) into equation (37), identifying real and imaginary parts, one obtains a dynamical system which governs the evolution of amplitudes and phases of the response. This system can be transformed into an autonomous one when defining

$$\gamma_1 = \sigma_2 T_1 - \theta_1, \qquad \gamma_2 = (\sigma_2 - \sigma_1)T_1 - \theta_2. \quad (39)$$

One finally obtains

$$a_1' = -\mu a_1 - \frac{C_1 a_1 a_2^2}{2\omega_1}\sin 2(\gamma_2 - \gamma_1) + \frac{Q_1}{4\omega_1}\sin\gamma_1, \quad (40a)$$

$$a_1\gamma_1' = \sigma_2 a_1 + \frac{3\Gamma_1}{2\omega_1}a_1^3 + \frac{C_1 a_1 a_2^2}{2\omega_1}(2 + \cos 2(\gamma_2 - \gamma_1)) + \frac{Q_1}{4\omega_1}\cos\gamma_1, \quad (40b)$$

$$a_2' = -\mu a_2 + \frac{C_2 a_2 a_1^2}{2\omega_2}\sin 2(\gamma_2 - \gamma_1) + \frac{Q_2}{4\omega_2}\sin\gamma_2, \quad (40c)$$

$$a_2\gamma_2' = (\sigma_2 - \sigma_1)a_2 + \frac{3\Gamma_2}{2\omega_2}a_2^3 + \frac{C_2 a_2 a_1^2}{2\omega_2}(2 + \cos 2(\gamma_2 - \gamma_1)) + \frac{Q_2}{4\omega_2}\cos\gamma_2. \quad (40d)$$

In the more general case, Q_1 and Q_2 are not equal to zero. Thus a_1 and a_2 are always excited and different from zero. This situation makes it necessary to study the complete four-dimensional system (40) without any simplification, which makes the analytical derivations unsolvable due to the complexity of the involved expressions. The case $Q_2 = 0$ will be studied in detail below. This allows one to simplify some expressions by letting $a_2 = 0$, and to show when the coupling between the two configurations becomes effective. In an experimental context, it is very difficult to ensure that $Q_2 = 0$. The case of a residual excitation on configuration (2) will be taken into account in a companion paper.

Dynamical system (40) exhibits a number of different possible behaviours. For example, limit cycles and chaotic behaviour were found in numerical simulations of equation (40), for specific values of the coefficients [32, 36]. A complete study of the bifurcation set will not be conducted in this paper. We have been more interested in the situation where an initially non-excited configuration can get energy through non-linear coupling. This phenomenon seems physically more interesting since it shows how energy is transferred between modal configurations. Moreover, all experiments conducted in our laboratory on circular plates, as well as previous experiments carried out on cymbals and gongs [36, 37], showed that an internal resonance is excited before one can observe chaotic behaviour predicted by equations (40). The interested reader can get a meticulous study of the bifurcations exhibited by equations (40) in reference [32].

6.2. FIXED POINTS

In this section, general fixed-point equations will be established when $Q_2 = 0$. All solution curves will be drawn in the space (σ_2, a_1, a_2), although some figures will show the two projections on the planes (σ_2, a_1) and (σ_2, a_2) on the same plot. As long as $a_2 = 0$ (i.e., as the energy transfer has not been realized), only configuration (1) is involved in the vibration: this solution will be referred to as the single-degree-of-freedom (s.d.o.f) solution. When both a_1 and a_2 are different from zero, the solution curves will be called the coupled solutions.

General fixed-point equations with $a_1 \neq 0$ are written as

$$\mu a_1 + \frac{C_1 a_1 a_2^2}{2\omega_1} \sin 2(\gamma_2 - \gamma_1) = \frac{Q_1}{4\omega_1} \sin \gamma_1, \tag{41a}$$

$$\sigma_2 + \frac{3\Gamma_1}{2\omega_1} a_1^2 + \frac{C_1 a_2^2}{2\omega_1} (2 + \cos 2(\gamma_2 - \gamma_1)) + \frac{Q_1}{4\omega_1 a_1} \cos \gamma_1 = 0, \tag{41b}$$

$$\mu a_2 = \frac{C_2 a_2 a_1^2}{2\omega_2} \sin 2(\gamma_2 - \gamma_1), \tag{41c}$$

$$\sigma_2 - \sigma_1 + \frac{3\Gamma_2}{2\omega_2} a_2^2 + \frac{C_2 a_1^2}{2\omega_2} (2 + \cos 2(\gamma_2 - \gamma_1)) = 0. \tag{41d}$$

Equation (41c) shows explicitly that the possible energy transfer is managed by C_2. Setting $C_2 = 0$ in equation (41c) shows that the only fixed point for a_2 is zero. When $C_2 \neq 0$, a solution with $a_2 \neq 0$ is possible only if the following equality is fulfilled:

$$\sin 2(\gamma_2 - \gamma_1) = \frac{2\omega_2 \mu}{C_2 a_1^2}. \tag{42}$$

Equation (42) gives an existence condition for coupled solutions:

$$a_1^2 \geqslant \frac{2\omega_2 \mu}{|C_2|}. \tag{43}$$

This condition is only valid for coupled solutions, since in the plane $(a_2 = 0)$, equation (41c) gives no information.

A second existence condition for general fixed points can be derived from equation (41d). As the absolute value of the cosine function must be less than one, the following condition must be fulfilled:

$$\left| 1 + \frac{\omega_2}{C_2 a_1^2} (\sigma_2 - \sigma_1) + \frac{3\Gamma_2 a_2^2}{2 C_2 a_1^2} \right| \leqslant \frac{1}{2}. \tag{44}$$

The limiting values of inequality (44) define two paraboloids $\mathscr{P}_1$ and $\mathscr{P}_2$ in the space (σ_2, a_1, a_2). Branches of solution can develop only inside the region defined by the two paraboloids. Condition (43) shows that coupled solutions can exist only if the amplitude a_1 is greater than a threshold value. These two conditions define a region $(\mathscr{D})$ where fixed points can exist. This region $(\mathscr{D})$ is represented in Figure 4.

The resonance curve of the s.d.o.f. solution is also shown in Figure 4, where one can see that fixed points for the s.d.o.f. solution can exist outside $(\mathscr{D})$. This is only a calculation artefact due to the use of the polar form (equation (38)). In fact, dynamical system (40) does not accept fixed points outside region $(\mathscr{D})$. However, in the plane $(a_2 = 0)$, dynamical system (37) accepts the usual fixed points of the s.d.o.f. solution (namely, the resonance curve plotted in Figure 4). This is due to the fact that in polar form, setting $a_2 = 0$ lets γ_2

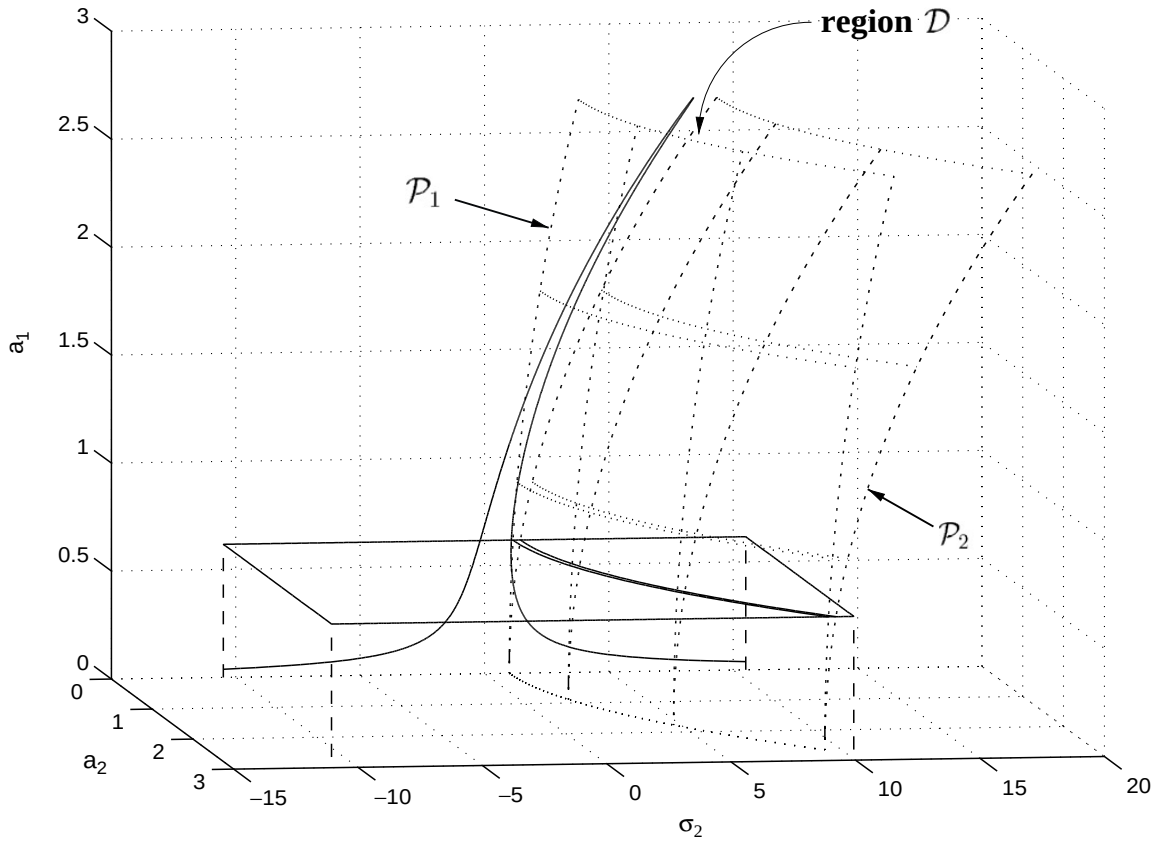

Figure 4. Definition of region ($\mathscr{D}$) in space (σ_2, a_1, a_2) where fixed points of dynamical system (40) can exist. The parameters for this figure have been set to the following values: $\Gamma_i = C_i = -5$, $\mu = 0{\cdot}15$, $\omega_1 = 2\pi$, $\sigma_1 = 1$. The value of the forcing Q_1 is set to 10. The threshold value defined by equation (43) is represented by the horizontal plane.

be undefined. One can find the usual s.d.o.f. solution branches in the plane $(a_2 = 0)$ by using Cartesian co-ordinates to solve equation (37).

Eliminating the angles in equation (41) gives the general relations for the fixed points in the space (σ_2, a_1, a_2):

$$\left[\sigma_2 - \sigma_1 + \frac{3\Gamma_2}{2\omega_2}a_2^2 + \frac{C_2 a_1^2}{\omega_2}\right]^2 + \mu^2 = \frac{C_2^2 a_1^4}{4\omega_2^2}, \tag{45a}$$

$$\frac{Q_1^2}{16\omega_1^2} = \mu^2 a_1^2\left[1 + \frac{C_1\omega_2 a_2^2}{C_2\omega_1 a_1^2}\right]^2 + \left[\frac{3\Gamma_1}{2\omega_1}a_1^3 - \frac{3\Gamma_2 C_1}{2C_2\omega_1}\frac{a_2^4}{a_1} + \sigma_2 a_1 + (\sigma_1 - \sigma_2)\frac{\omega_2 C_1 a_2^2}{\omega_1 C_2 a_1}\right]^2. \tag{45b}$$

Setting $a_2 = 0$ in equation (45b) gives the usual relation for the fixed points of the s.d.o.f. solution. The coupled solutions are solution of equation (45). The stability of the different solution branches will now be investigated. Analytically, we will restrict ourselves to the stability analysis in the plane $(a_2 = 0)$. General stability of coupled solutions will be determined numerically.

6.3. STABILITY ANALYSIS

In this section, we will show that the s.d.o.f. solution loses stability through pitchfork bifurcation. First, the location where coupled solution can start to develop from the plane

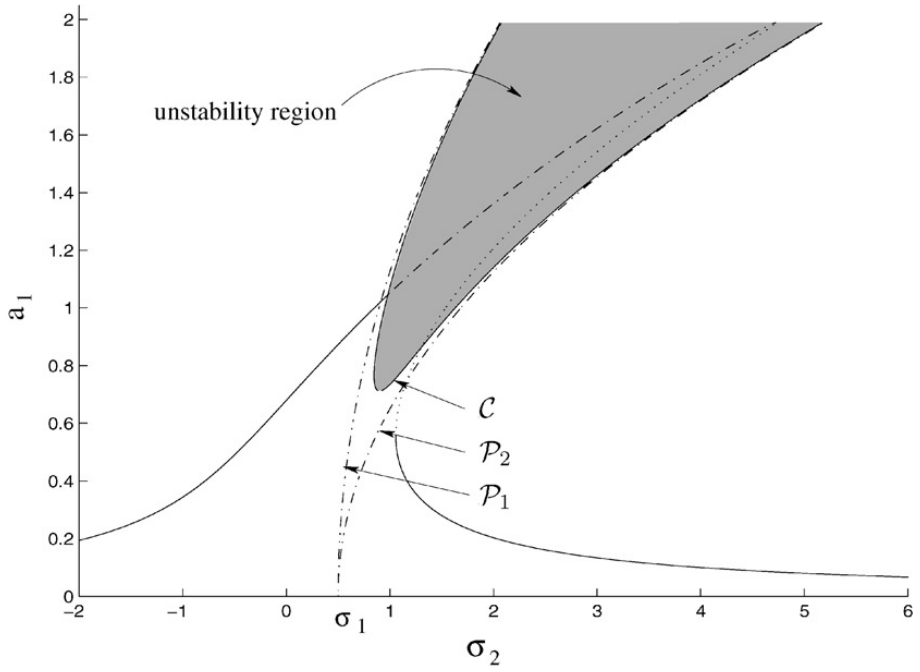

Figure 5. Definition of the unstability region in plane ($a_2 = 0$). The dashed lines represent the trace of $\mathscr{P}_1$ and $\mathscr{P}_2$ on plane ($a_2 = 0$). The curve $\mathscr{C}$ is the line where coupled-mode solution can arise. When $\mu = 0$, the two regions are identical. The s.d.o.f resonance curve is shown with the following convention: dotted line for unstable state with respect to configuration (1), dash–dotted line for unstable states due to coupling with configuration (2). The following parameters values have been used: $\Gamma_1 = \Gamma_2 = C_1 = C_2 = -5$, $\omega_1 = 2\pi$, $\mu = 0{\cdot}2$, $\sigma_1 = 0\text{cot}5$, $Q_1 = 10$ and $\varepsilon = 0{\cdot}1$.

($a_2 = 0$) are found by setting $a_2 = 0$ in equation (45a). This gives the two branches

$$\sigma_2 = \sigma_1 - \frac{C_2 a_1^2}{\omega_2} \pm \sqrt{\frac{C_2^2 a_1^4}{4\omega_2^2} - \mu^2}. \tag{46}$$

The curve $\mathscr{C}$, which connects the two branches defined by equation (46), is delimiting a region inside which coupled-mode solutions can arise. We will show next that the s.d.o.f. solution in this region is unstable with respect to perturbation in the a_2 direction. Hence this domain will be called the *unstability region*. One can notice that the minimum value of $\mathscr{C}$ is obtained for $a_1^2 = 2\omega_2\mu/|C_2|$, which is fully consistent with condition (43). Setting $\mu = 0$ in equation (46) gives the two relationships that define the trace of the two paraboloids $\mathscr{P}_1$ and $\mathscr{P}_2$ in the plane ($a_2 = 0$), as can be seen in Figure 5. Hence, the effect of the damping is to make a distinction between region ($\mathscr{D}$) where fixed points for equation (40) exist, and the unstability region. This demonstration will be finalized by conducting a linear stability analysis in the plane ($a_2 = 0$).

The Jacobian matrix $\mathscr{J}$ of equation (40) with $a_2 = 0$ is written as

$$\mathscr{J} = \begin{pmatrix} -\mu & -\sigma_2 a_1 - \dfrac{3\Gamma_1}{2\omega_1} a_1^3 & 0 & 0 \\ \dfrac{\sigma_2}{a_1} + \dfrac{9\Gamma_1}{2\omega_1} a_1 & -\mu & 0 & 0 \\ 0 & 0 & -\mu + \dfrac{C_2 a_1^2}{2\omega_2} \sin 2(\gamma_2 - \gamma_1) & 0 \\ \dfrac{2(\sigma_1 - \sigma_2)}{a_1} & \dfrac{C_2 a_1^2}{\omega_2} \sin 2(\gamma_2 - \gamma_1) & 0 & -\dfrac{C_2 a_1^2}{\omega_2} \sin 2(\gamma_2 - \gamma_1) \end{pmatrix} \tag{47}.$$

One can see that the upper-left square block (two-dimensional) of the Jacobian matrix is only related to the stability of the s.d.o.f. solution. This part is exactly the same as that calculated for a single Duffing equation, and it governs the stability of the different solution branches for the s.d.o.f. case. The lower-right part of $\mathscr{J}$ governs the stability of the s.d.o.f. solution with respect to disturbances due to the second resonant oscillator. The eigenvalues associated to this block are

$$\lambda_1 = -\mu + \frac{C_2 a_1^2}{2\omega_2} \sin 2(\gamma_2 - \gamma_1),$$
$$\lambda_2 = -\frac{C_2 a_1^2}{\omega_2} \sin 2(\gamma_2 - \gamma_1). \tag{48}$$

One can see that if the oscillators are undamped, the eigenvalues have opposite signs, and thus the s.d.o.f. solution is unstable. In a conservative case, the situation is the following: curve $\mathscr{C}$ is identical to $\mathscr{P}_1$ and $\mathscr{P}_2$, thus as soon as the s.d.o.f. resonance curve comes into region $(\mathscr{D})$, it becomes unstable with respect to perturbations due to the coupling with the second oscillator. When damping is considered, $\mathscr{C}$ and $\mathscr{P}_1 \cup \mathscr{P}_2$ are not identical anymore. As long as the resonance curve does not cross $\mathscr{C}$, it remains stable, as it can be seen on the eigenvalues, where the occurrence of μ lets a portion of phase space where the two eigenvalues are still negative. Finally, one can study under which condition one of the eigenvalues vanishes by forming the product $\lambda_1\lambda_2$. Eliminating the angles in favour of the other parameters and setting $\lambda_1\lambda_2 = 0$ yields equation (46). Thus curve $\mathscr{C}$ is not only the place where coupled solutions can arise, but also the location where the s.d.o.f solution loses its stability through pitchfork bifurcation.

6.4. GENERALIZED STABILITY CURVE

A generalized stability curve is presented in Figure 6 in the space (σ_2, a_1, a_2). It can be seen that as soon as the s.d.o.f solution crosses the unstability region, the stable solution

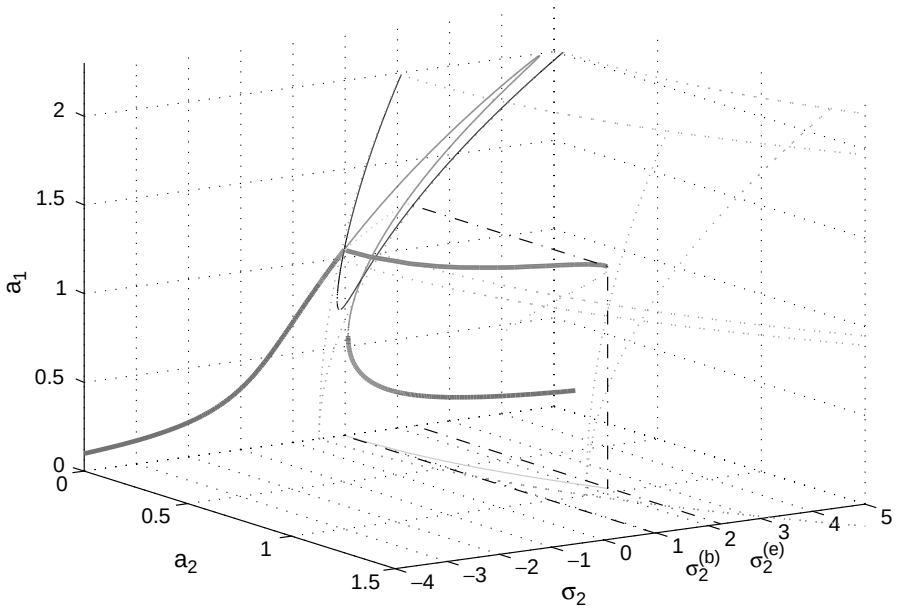

Figure 6. Generalized stability curve for $\Gamma_1 = \Gamma_2 = C_1 = C_2 = -5$, $\omega_1 = 2\pi$, $\sigma_1 = 0{\cdot}5$, $\varepsilon = 0{\cdot}1$, $\mu = 0{\cdot}2$ and $Q_1 = 10$ ($Q_2 = 0$). All the solution branches remain inside region $\mathscr{D}$. Stable solutions are represented with bold lines. The coupled-mode branches develop between $\sigma_2^{(b)}$ and $\sigma_2^{(e)}$. All the other branches are unstable.

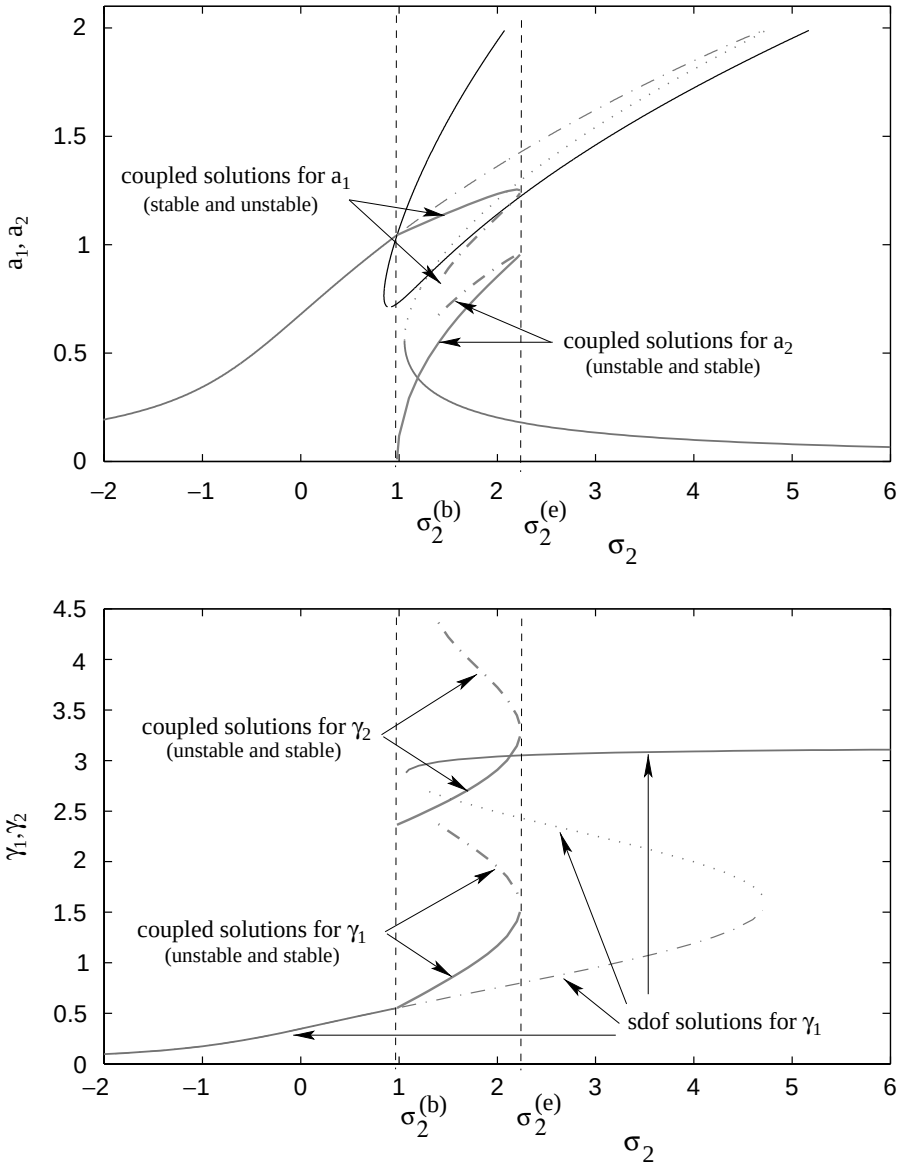

Figure 7. Generalized stability curve for $\Gamma_1 = \Gamma_2 = C_1 = C_2 = -5$, $\omega_1 = 2\pi$, $\sigma_1 = 0{\cdot}5$, $\varepsilon = 0{\cdot}1$, $\mu = 0{\cdot}2$ and $Q_1 = 10$ ($Q_2 = 0$).

becomes the coupled one, which then gets out of the plane ($a_2 = 0$). The stability of the two branches of coupled solutions was numerically investigated using the software *dstool* [38].

The coupled-mode solution arises at $\sigma_2^{(b)}$, which is the value of the detuning for the beginning of the unstability region, and disappears at $\sigma_2^{(e)}$, a value that cannot be determined analytically.

The projections on the two planes ($a_2 = 0$) and ($a_1 = 0$) are represented on Figure 7, where the values of the angles γ_1 and γ_2 have also been reported. The typical behaviour of the phase for the s.d.o.f solution is clearly visible for γ_1. The unstability due to the presence of the second resonant oscillator is shown as the dash–dotted line. Coupled-mode solutions develop between $\sigma_2^{(b)}$ and $\sigma_2^{(e)}$. They exhibit a phase difference which is nearly equal to $\pi/2$. This behaviour is expressed in equation (42). When damping is absent, and for the case considered here, the phases of the two configurations are shifted by exactly $\pi/2$. In fact, when $\mu = 0$, coupled-mode solutions develop when the s.d.o.f solution crosses

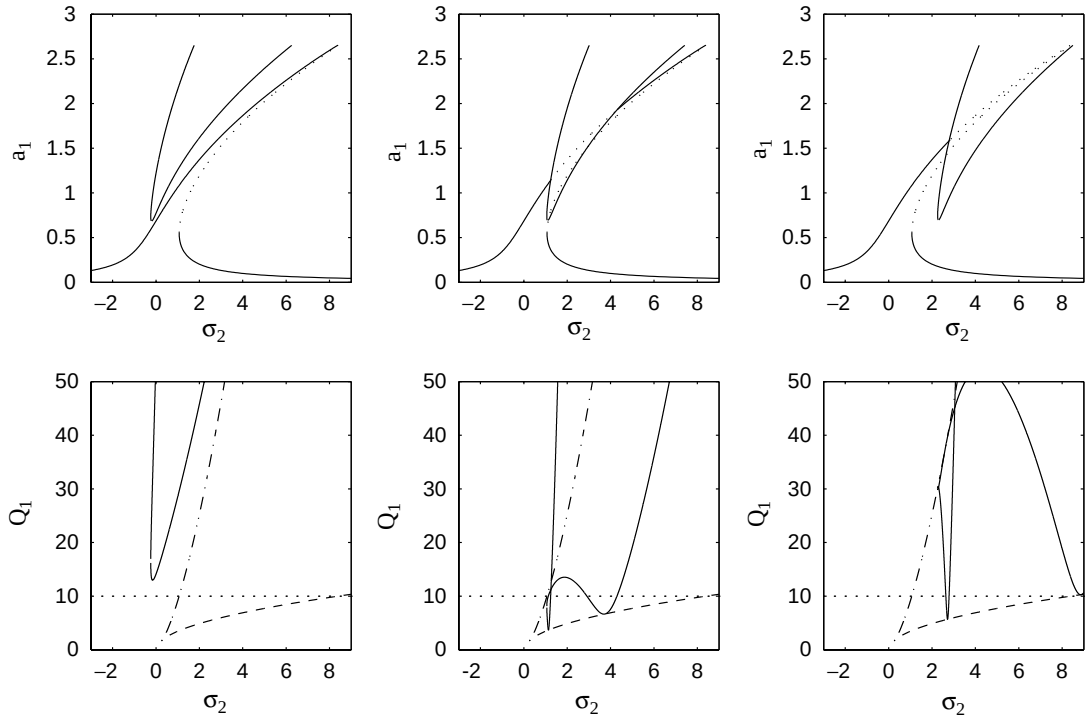

Figure 8. Resonance curves with the unstability region (first row) and pitchfork bifurcation curves (solid lines) as well as saddle-node bifurcation curves (dash–dotted lines) in the plane (σ_2, Q_1), for three different values of the internal detuning. From left to right: $\sigma_1 = -0{\cdot}5, 0{\cdot}8$ and 2. In the first row, the amplitude of the excitation is fixed at $Q_1 = 10$.

$\mathscr{P}_1$. On this paraboloid, we have $\cos 2(\gamma_2 - \gamma_1) = -1$. According to equation (42), coupled-mode solutions stay on $\mathscr{P}_1$ and thus $\gamma_2 - \gamma_1 = \pi/2$. When $\mu \neq 0$, this is not true anymore, and the phases differ from $\pi/2$ in inverse proportion with a_1^2.

6.5. EFFECT OF THE INTERNAL DETUNING σ_1, DAMPING μ AND FORCING Q_1

The place where pitchfork and saddle-node bifurcations occur for the s.d.o.f solution can be represented in the parameter space (σ_2, Q_1). The pitchfork bifurcations are given by the intersection of equation (46) with the s.d.o.f resonance curve defined by

$$a_1^2\left(\mu^2 + \left(\sigma_2 + \frac{3\Gamma_1}{2\omega_1}a_1^2\right)^2\right) = \frac{Q_1^2}{16\omega_1^2}. \tag{49}$$

The saddle-node bifurcations (corresponding to the vertical tangent in the s.d.o.f resonance curve) are found by differentiating equation (49) and letting $\partial\sigma_2/\partial a_1 = 0$. This gives the relationships

$$a_{1(SN)}^2 = \frac{2\omega_1}{9\Gamma_1}\left[-2\sigma_2 \pm \sqrt{\sigma_2^2 - 3\mu^2}\right], \tag{50}$$

where (SN) stands for saddle node. These curves are represented in the second row of Figure 8 for different values of the internal detuning σ_1, and for $\Gamma_1 = -5$, $C_2 = -4$, $\omega_1 = 2\pi$ and $\mu = 0{\cdot}15$. The corresponding resonance curves for $Q_1 = 10$ are shown in the first row. From left to right, we have, successively: $\sigma_1 = -0{\cdot}5$, $0{\cdot}8$ and 2. One can see that the unstability region depends only on three parameters: the internal detuning σ_1, the coupling coefficient C_2 and the damping μ.

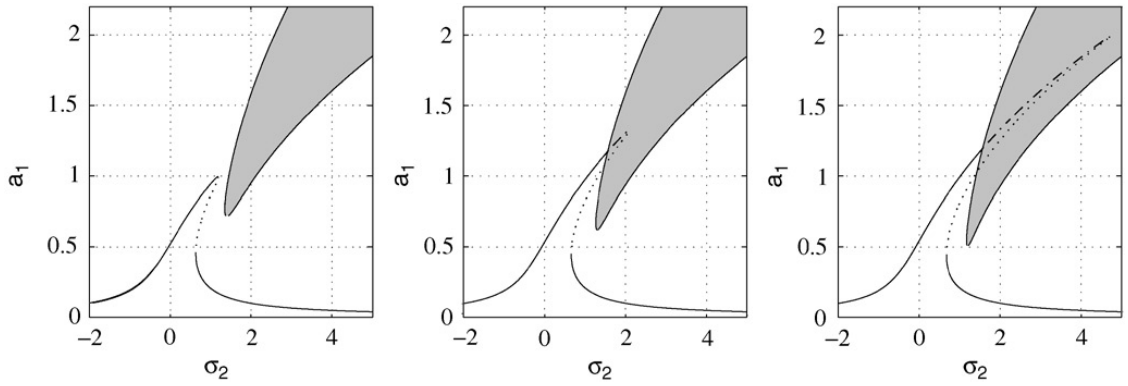

Figure 9. Effect of the damping on both the s.d.o.f resonance curve and the unstability region. $Q_1 = 5$, $\Gamma_1 = C_2 = -5$, $\omega_1 = 2\pi$, $\sigma_1 = 1$. From left to right: $\mu = 0{\cdot}2, 0{\cdot}15$ and $0{\cdot}\ 1$.

The effect of the amplitude of the forcing Q_1 can be easily seen in Figure 8. As the unstability region does not depend on Q_1, the pitchfork bifurcation curves give the limiting value for which the energy transfer from the excited oscillator to the second one is possible. For $\sigma_1 = -0{\cdot}5$, for example, a magnitude of $Q_1 = 10$ is not sufficient for obtaining coupled solutions. The critical value is given by the minimum of the pitchfork curve, corresponding to $Q_1 = 12{\cdot}9$. It should be pointed out that increasing the value of $|\sigma_1|$ leads to consider larger forcing amplitudes to make the coupling effective. This is particularly pronounced when σ_1 is negative in the hardening case, and it will be illustrated in the next paper.

The damping coefficient μ acts both on the s.d.o.f resonance curve and on the unstability region, which is not the case for Q_1. Increasing μ tends to raise the minimum value of the unstability region (this can be seen on condition (43)) and to lower the maximum value of the s.d.o.f resonance curve. Increasing the damping is more dramatic than just decreasing the forcing Q_1 for coupled-mode solutions to develop (see Figure 9).

6.6. STUDY OF UNCOMMON CASES

The aim of this section is to show that dynamical system (40) can exhibit a number of different possible solutions when varying the coefficients. As already mentioned, a complete study of the bifurcations of the coupled solutions will not be conducted here, the reader is referred to reference [32] for global bifurcation sets in the case of rectangular plates. The goal here is to investigate the stability of the s.d.o.f solution. For this purpose, we will examine some generalized stability curves in two different cases.

First, the case of a softening non-linearity will be exhibited. This case can be encountered when studying the rolling motion of a ship (see reference [1] for example), or the non-linear vibrations of circular cylindrical shells [39].

A generalized stability curve is shown in Figure 10 where the damping and the internal detuning have been chosen so that the crossing of the s.d.o.f solution with the unstability region is narrow. This example shows that a narrow intersection is sufficient for a coupled solution to develop, and that a stable s.d.o.f solution and a stable coupled solution can coexist for a wide range of the detuning parameter σ_2. This feature is of course not specific to the softening case. General behaviour reported for the hardening case can be transposed to the softening case.

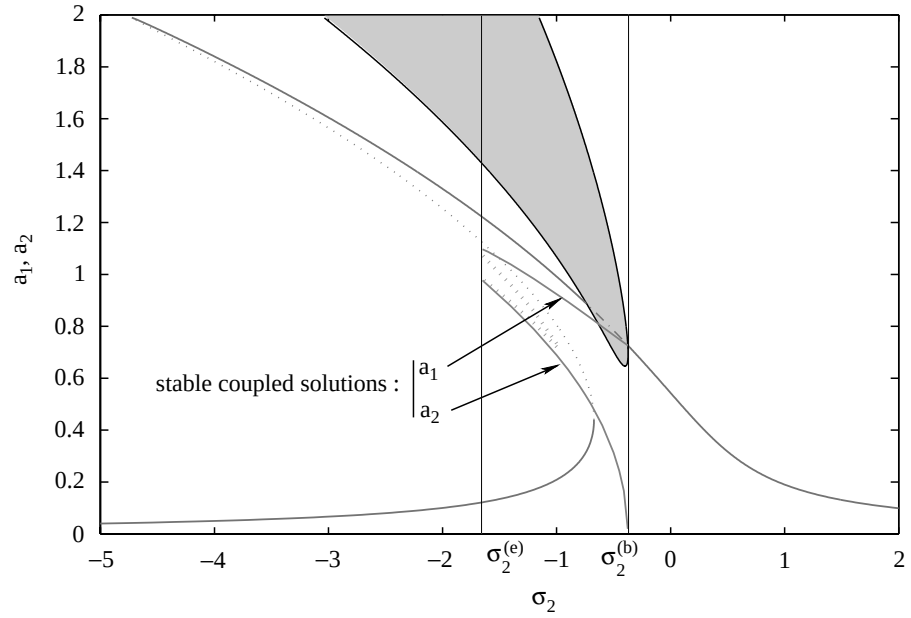

Figure 10. Generalized stability curve in the softening case: $\Gamma_1 = \Gamma_2 = 5$, $C_1 = C_2 = 3$, $\omega_1 = 2\pi$, $\sigma_1 = -0{\cdot}2$, $\mu = 0{\cdot}1$ and $Q_1 = 5$. For the sake of clarity, only a limited number of unstable coupled solutions have been reported.

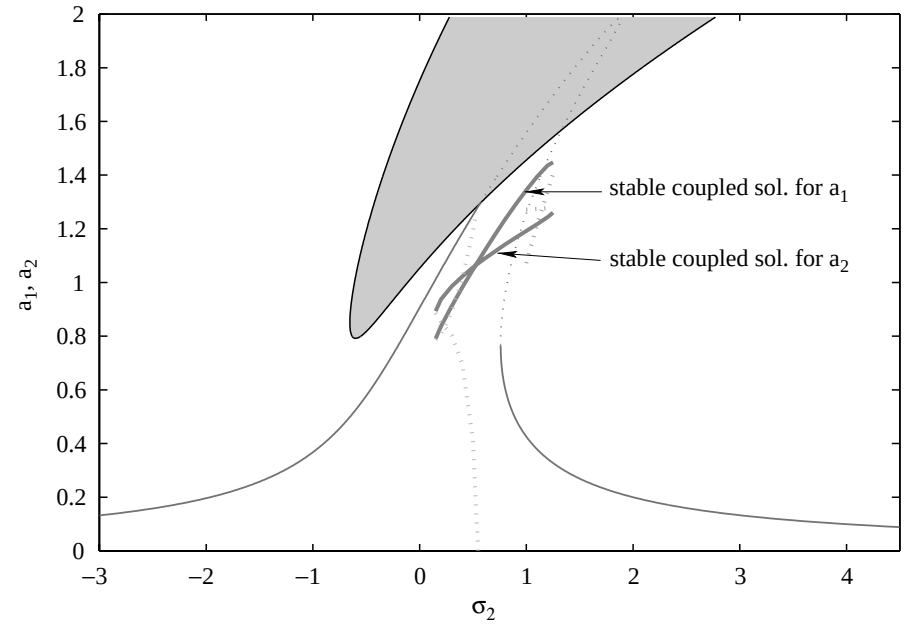

Figure 11. Generalized stability curve for the following values of the parameters: $\Gamma_1 = C_1 = -2$, $\Gamma_2 = C_2 = -4$, $\omega_1 = 2\pi$, $\sigma_1 = -1$, $\mu = 0{\cdot}2$ and $Q_1 = 10$. Two unstable coupled branches are found, which are represented by dashed lines. The first one arises from the intersection with the unstability region. The second one collapses with the stable coupled solution for $\sigma_2 = 1{\cdot}25$.

Finally, a case where an unusual jump phenomenon can occur is exhibited in Figure 11. As mentioned earlier, the stability of the coupled solutions has not been analytically studied due to the complexity of the algebraic manipulations involved. The particularity of the case exhibited here is the unstability of the coupled solution which arises from the

intersection of the s.d.o.f resonance curve with the unstability region. The coupled-mode stable solutions are not connected to the plane ($a_2 = 0$), as usually seen. This feature has been observed when the s.d.o.f solution crosses the unstability region by the second condition defined by equation (46). In this case, the value of $\cos 2(\gamma_2 - \gamma_1)$ is near $+1$, and not -1.

A jump phenomenon occurs when increasing the frequency of the forcing at the external border of the unstability region: a_1 jumps from its s.d.o.f value to the lower stable coupled solution. Meanwhile, a_2 jumps from zero to its coupled value. This could be experimentally observed when linking together two non-linear cubic oscillators with parameters values that share the same properties as the one exhibited here.

7. SOLUTION FOR THE DEFLECTION

Following equations (32), (35), (38) and (27a), to the first approximation, a solution for the steady state deflection w can be written in the form:

$$w(r, \theta) = R_{kn}(r)[2a_1 \cos(\Omega t - \gamma_1) \cos k\theta + 2a_2 \cos(\Omega t - \gamma_2) \sin k\theta]. \tag{51}$$

w results from the superposition of the two preferential configurations, sometimes denoted as two stationary waves. With the help of little algebra, the deflection w can be rewritten in the form

$$w(r, \theta) = R_{kn}(r)[2a_3(\theta) \cos(\Omega t - \varepsilon k\theta - \gamma_3(\theta))], \tag{52}$$

where a_3 and γ_3 are constant when $\gamma_2 - \gamma_1 = \varepsilon\pi/2$, $a_1 = a_2$ and $\varepsilon = \pm 1$. Thus, the deflection can be viewed as a shape $R_{kn}(r) \cos k\theta$ progressing round the disc at speed Ω/k, sometimes called a travelling wave. It travels clockwise or anticlockwise, depending on the sign of ε. If $a_1 \neq a_2$ and $\gamma_2 - \gamma_1 \neq \varepsilon\pi/2$, a_3 and γ_3 are slowly varying functions of $k\theta$, and a travelling wave is still obtained, with its amplitude and speed slightly beating around their average value [3]. Section 6 shows that travelling waves can be obtained in the range of the coupled solutions, which has been verified during experiments.

8. CONCLUSION

An exhaustive study of the one-mode asymmetric non-linear forced vibrations of free-edge circular plates has been presented in this paper, bringing together scattered contributions on the subject and revisiting a number of points which were overlooked by previous authors.

This research was initiated by the study of non-linear percussion instruments, a family in which one can find cymbals and gongs [36, 37]. Non-linear effects are of prime importance for the sound generation in those instruments where the vibration amplitudes are sometimes larger than the thickness. In the context of developing a physical model that would account for the non-linear phenomena exhibited by those instruments, the first step of the modelling procedure (limitation to the one-mode vibration case) is exposed here. As the energy transfer and the selection of modes in multi-mode responses are both governed by eigenfrequency relationships, irrespective of the mode shape (as predicted by normal form theory, for example reference [40], or as observed in experiments [36, 37]), it has been necessary to develop first a complete study of the one-mode asymmetric case.

To remain close to the case of percussion instruments, original developments have been performed in this study for the modal expansion with *free-edge* boundary conditions.

Special efforts have been put in the computation of the non-linear coefficients derived from the projection onto the normal modes basis.

The temporal part has been exhaustively studied, precising the results of Tobias *et al.* by systematically considering the effect of damping. Exhaustive analysis of the effect of all the coefficients has been done, as well as the study of uncommon cases which are usually not found in the literature. An unusual jump phenomenon has hence been predicted. Finally, the solution for the deflection has been written, showing that travelling waves are generic when coupled-mode solutions arise. All these results generalize the case considered by Chang, Bajaj and Krousgrill who worked on one-to-one internal resonance for rectangular plates for which $C_1 = C_2$ with particular attention paid to the bifurcation sets and the onset of chaotic behaviour.

The second part of the present paper will be concerned with experimental validations. Experimental resonance curves will be compared to theoretical ones. The case of a residual forcing on configuration (2) will be depicted. This will lead to the occurrence and the observation of a new solution branch which was not studied here. Finally, the approximations considered in the above-presented theory will be systematically discussed.

ACKNOWLEDGMENTS

The authors would like to thank the developers of the code *dstool* from the Center for Applied Mathematics at Cornell University. This software has been of great help in the study of the dynamics. The first author would like to thank Paul Manneville for showing him the wild nature encountered in dynamical system theory, as well as Pierre Lanchantin for his last-minute vigilance.

REFERENCES

1. A. H. Nayfeh and D. T. Mook 1979 *Nonlinear Oscillations*. New York: John Wiley and Sons.
2. L. Meirovitch 1967 *Analytical Methods in Vibrations*. New York: MacMillan Publishing Co.
3. S. A. Tobias and R. N. Arnold 1957 *Proceedings of the Institution of Mechanical Engineers* **171**, 669–690. The influence of dynamical imperfection on the vibration of rotating disks.
4. G. J. Efstathiades 1971 *Journal of Sound and Vibration* **16**, 231–253. A new approach to the large-deflection vibrations of imperfect circular disks using Galerkin's procedure.
5. N. Yamaki 1961 *Zeitschrift für Angewandte Mathematik und Mechanik* **41**, 501–510. Influence of large amplitudes on flexural vibrations of elastic plates.
6. G. C. Kung and Y. H. Pao 1972 *Journal of Applied Mechanics* **39**, 1050–1054. Nonlinear flexural vibration of a clamped circular plate.
7. S. Sridhar, D. T. Mook and A. H. Nayfeh 1975 *Journal of Sound and Vibration* **41**, 359–373. Nonlinear resonances in the forced responses of plates. Part I: symmetric responses of circular plates.
8. J. Hadian and A. H. Nayfeh 1990 *Journal of Sound and Vibration* **142**, 279–292. Modal interaction in circular plates.
9. M. Sathyamoorthy 1996 *Applied Mechanical Review Part* 2 **49**, S55–S62. Nonlinear vibrations of plates: an update of recent research.
10. S. A. Tobias 1957 *Proceedings of the Institution of Mechanical Engineers* **171**, 691–701. Free undamped non-linear vibrations of imperfect circular disks.
11. C. J. H. Williams and S. A. Tobias 1963 *Journal of Mechanical Engineering Science* **5**, 325–335. Forced undamped non-linear vibrations of imperfect circular discs.
12. A. Raman and C. D. Mote Jr 2001 *International Journal of Non-linear Mechanics* **36**, 261–289. Effects of imperfection on the non-linear oscillations of circular plates spinning near critical speed.

13. A. Raman and C. D. Mote Jr 2001 *International Journal of Non-linear Mechanics* **36**, 291–305. Experimental studies on the non-linear oscillations of imperfect circular disks spinning near critical speed.
14. D. S. Dugdale 1979 *International Journal of Engineering Science* **17**, 745–756. Non-linear vibration of a centrally clamped rotating disc.
15. S. Sridhar, D. T. Mook and A. H. Nayfeh 1978 *Journal of Sound and Vibration* **59**, 159–170. Nonlinear resonances in the forced responses of plates. Part II: asymmetric responses of circular plates.
16. U. S. Gupta and A. H. Ansari 1998 *Journal of Sound and Vibration* **215**, 231–250. Asymmetric vibrations and elastic stability of polar orthotropic circular plates of linearly varying profile.
17. U. S. Gupta and N. Goyal 1999 *Journal of Sound and Vibration* **220**, 641–657. Forced asymmetric response of linearly tapered circular plates.
18. P. Ribeiro and M. Petyt 2000 *International Journal of Non-linear Mechanics* **35**, 263–278. Non-linear free vibration of isotropic plates with internal resonance.
19. P. Ribeiro and M. Petyt 1999 *Journal of Sound and Vibration* **226**, 955–983, 985–1010. Geometrical non-linear, steady-state, forced, periodic vibration of plates, part I and II.
20. G. Herrmann 1955 *NACA Technical Report 3578*. Influence of large amplitudes on flexural vibrations of elastic plates.
21. O. Millet, A. Hhamdouni and A. Ccimetiére 2001 *International Journal of Non-linear Mechanics* **35**. A classification of thin plate models by asymptotic expansion of non-linear three-dimensional equilibrium equations.
22. O. Thomas, C. Touzé and A. Chaigne 2000 *Proceedings of the 7th International Congress on Sound and Vibration*, *Garmisch-Partenkirchen*. Non-linear resonances in large-deflection vibrations of free-edge circular plates.
23. O. Thomas, C. Touzé and A. Chaigne 2001 *Actes du Congrès Francais de Mécanique*, *Nancy*. Sur la vibration à un mode asymétrique des plaques circulaires en grands déplacements.
24. M. Géradin and D. Rixen 1996 *Théorie des Vibrations*. Paris: Masson; second edition.
25. G. A. Holzapfel 2000 *Nonlinear Solid Mechanics*. New York: John Wiley and Sons.
26. C. Y. Chia 1980 *Nonlinear Analysis of Plates.* New York: McGraw-Hill.
27. S. W. Shaw and C. Pierre 1994 *Journal of Sound and Vibration* **169**, 319–347. Normal modes of vibration for non-linear continuous systems.
28. A. H. Nayfeh and S. A. Nayfeh 1994 *Transactions of the American Society of Mechanical Engineers Journal of Vibration and Acoustics* **116**, 129–136. On nonlinear modes of continuous systems.
29. R. Benamar, M. M. K. Bennouna and R. G. White 1991 *Journal of Sound and Vibration* **164**, 295–316. The effects of large vibration amplitudes on the mode shapes and natural frequencies of thin elastic structures. Part II: fully clamped rectangular isotropic plates.
30. T. A. Nayfeh and A. F. Vakakis 1994 *International Journal of Non-linear Mechanics* **29**, 233–245. Subharmonic travelling waves in a geometrically non-linear circular plate.
31. K. Yasuda and T. Asano 1986 *Bulletin of JSME* **29**, 3090–3095. Nonlinear forced oscillations of a rectangular membrane with degenerated modes.
32. S. I. Chang, A. K. Bajaj and C. M. Krousgrill 1993 *Nonlinear Dynamics* **4**, 433–460. Non-linear vibrations and chaos in harmonically excited rectangular plates with one-to-one internal resonance.
33. R. Lewandowski 1996 *Meccanica* **31**, 323–346. On beams membranes and plates vibration backbone curves in cases of internal resonance.
34. X. L. Yang and P. R. Sethna 1991 *International Journal of Non-linear Mechanics* **26**, 199–220. Local and global bifurcations in parametrically excited vibrations of nearly square plates.
35. A. H. Nayfeh and B. Balachandran 1989 *Applied Mechanical Review Part* 2 **42**, S175–S201. Modal interactions in dynamical and structural systems.
36. C. Touzé 2000 *Ph.D. Thesis*, *Université Pierre et Marie Curie*, *Paris VI.* Analyse et modélisation de signaux vibratoires et acoustiques chaotiques. Application aux intruments de percussion non-linéaires.
37. C. Touzé and A. Chaigne 2000 *Acta Acustica* **86**, 557–567. Lyapunov exponents from experimental time series: application to cymbal vibrations.
38. J. Guckenheimer, M. R. Myers, F. J. Wicklin and P. A. Worfolk 1995 *Technical Report*, *Center for Applied Mathematics*, *Cornell University*, *Ithaca*, *NY* 14853, *U.S.A.* DsTool: a dynamical system toolkit with an interactive graphical interface.

39. M. Amabili, F. Pellicano and A. F. Vakakis 2000 *Journal of Vibration and Acoustics* **122**, 346–354. Nonlinear vibrations and multiple resonances of fluid-filled circular shells. Part 1: equations of motion and numerical results.
40. P. Manneville 1990 *Dissipative Structures and Weak Turbulence*. New York: Academic Press.
41. A. Leissa 1993 *Vibration of Plates*. New York: Acoustical Society of America.

APPENDIX A: EXPRESSION OF THE MODE SHAPES

A.1. FREE EDGE (MODES Φ_α)

Following from the linear part of equation (12a), and boundary conditions (9b, c), the spatial part of the solution w satisfies, for all θ and t,

$$(\Delta\Delta - \zeta^4)\Phi = 0, \tag{A.1a}$$

$$\Phi_{,rr} + \nu\Phi_{,r} + \nu\Phi_{,\theta\theta} = 0 \quad \text{at } r = 1, \tag{A.1b}$$

$$\Phi_{,rrr} + \Phi_{,rr} - \Phi_{,r} + (2-\nu)\Phi_{,r\theta\theta} - (3-\nu)\Phi_{,\theta\theta} = 0 \quad \text{at } r = 1, \tag{A.1c}$$

$$\Phi(r=0) \text{ is bounded} \tag{A.1d}$$

with $\zeta^4 = \omega^2$. The solutions of the previous set are separated in r and θ, and are written as

$$\Phi_{0n}(r,\theta) = R_{0n}(r) \quad \text{for } k = 0, \tag{A.2a}$$

$$\left.\begin{matrix}\Phi_{kn1}(r,\theta)\\ \Phi_{kn2}(r,\theta)\end{matrix}\right| = R_{kn}(r)\left|\begin{matrix}\cos k\theta\\ \sin k\theta\end{matrix}\right. \quad \text{for } k > 0 \tag{A.2b}$$

with

$$R_{kn}(r) = \kappa_{kn}\left[\mathrm{J}_k(\zeta_{kn}r) - \frac{\tilde{\mathbf{J}}_k(\zeta_{kn})}{\tilde{\mathbf{I}}_k(\zeta_{kn})}\mathrm{I}_k(\zeta_{kn}r)\right], \tag{A.3}$$

where J_k is the Bessel functions of order k of the first kind, $\mathrm{I}_k(x) = \mathrm{J}_k(\mathrm{i}x)$ with $\mathrm{i} = \sqrt{-1}$, and $\tilde{\mathbf{J}}_k$ and $\tilde{\mathbf{I}}_k$ are defined as follows:

$$\tilde{\mathbf{J}}_k(x) = x^2\mathrm{J}_{k-2}(x) + x(\nu - 2k + 1)\mathrm{J}_{k-1}(x) + k(k+1)(1-\nu)\mathrm{J}_k(x), \tag{A.4a}$$

$$\tilde{\mathbf{I}}_k(x) = x^2\mathrm{I}_{k-2}(x) + x(\nu - 2k + 1)\mathrm{I}_{k-1}(x) + k(k+1)(1-\nu)\mathrm{I}_k(x). \tag{A.4b}$$

κ_{kn}, a constant, is chosen so that

$$\int\int_{(\mathscr{S})} \Phi_{kn}^2 \,\mathrm{d}S = 1. \tag{A.5}$$

ζ_{kn} is the $\tilde{n}$th solution of the following equation:

$$\begin{aligned}&\tilde{\mathbf{I}}_k(\zeta)[\zeta^3\mathrm{J}_{k-3}(\zeta) + \zeta^2(4-3k)\mathrm{J}_{k-2}(\zeta)\\ &+ \zeta k(k(1+\nu)-2)\mathrm{J}_{k-1}(\zeta) + k^2(1-\nu)(1+k)\mathrm{J}_k(\zeta)]\\ &- \tilde{\mathbf{J}}_k(\zeta)[\zeta^3\mathrm{I}_{k-3}(\zeta) + \zeta^2(4-3k)\mathrm{I}_{k-2}(\zeta)\\ &+ \zeta k(k(1+\nu)-2)\mathrm{I}_{k-1}(\zeta) + k^2(1-\nu)(1+k)\mathrm{I}_k(\zeta)] = 0.\end{aligned} \tag{A.6}$$

k is found to be the number of nodal radii. Because of the free-edge boundary conditions, the edge of the plate is not a nodal circle, and mode Φ_{10} is a rigid-body mode. So, the number n of nodal circles is not equal to $\tilde{n}$. In fact, for $k = 1$, $n = \tilde{n}$ and for $k \neq 1$, $n = \tilde{n} - 1$ [41]. Computed values of the ζ_{kn} can be found in reference [15] and their squared values ($\omega_{kn} = \zeta_{kn}^2$) are given in Table 1.

A.2. CLAMPED EDGE (MODES Ψ_s)

Combining equation (18) and boundary conditions (19), the spatial part of F satisfies, for all θ and t,

$$(\Delta\Delta - \xi^4)\Psi = 0, \qquad \Psi = 0, \quad \text{at } r = 1, \tag{A.7a, b}$$

$$\Psi_{,r} = 0, \quad \text{at } r = 1, \qquad \Psi(r = 0) \text{ is finite.} \tag{A.7c, d}$$

The solutions of the previous set are separated in r and θ:

$$\Psi_{0m}(r, \theta) = S_{0m}(r) \quad \text{for } l = 0, \tag{A.8a}$$

$$\left.\begin{matrix}\Psi_{lm1}(r, \theta) \\ \Psi_{lm2}(r, \theta)\end{matrix}\right| = S_{lm}(r) \left|\begin{matrix}\cos l\theta \\ \sin l\theta\end{matrix}\right. \quad \text{for } l > 0 \tag{A.8b}$$

with

$$S_{lm}(r) = \lambda_{lm}\left[\mathrm{J}_l(\xi_{lm}r) - \frac{\mathrm{J}_l(\xi_{lm})}{\mathrm{I}_l(\xi_{lm})}\mathrm{I}_l(\xi_{lm}r)\right], \tag{A.9}$$

where the ξ_{lm} is the mth solution of the following equation:

$$\mathrm{J}_{l-1}(\xi)\mathrm{I}_l(\xi) - \mathrm{I}_{l-1}(\xi)\mathrm{J}_l(\xi) = 0. \tag{A.10}$$

Computed values of the ξ_{lm} can be found in reference [41]. λ_{lm}, a constant, is chosen so that

$$\int\int_{(\mathscr{S})} \Psi_{lm}^2 \, \mathrm{d}S = 1. \tag{A.11}$$

l and m correspond to the numbers of nodal radii and circles, respectively.

We can remark that if $k \geqslant 1$ (or $l \geqslant 1$), each ζ_{kn} (or ξ_{lm}) is associated to the two degenerated modes of equation (A.2) (or equation (A.8)), one in cosine, the other in sine [2].

APPENDIX B: CALCULATION OF COEFFICIENTS Γ

B.1. THE CASE OF AN AXISYMMETRIC MODE Φ

In this section, all transverse modes Φ found in equation (25) equal Φ_{0n}. Taking equations (A.5) and (A.11), and definition (2) of the functional L into account, the only coefficient Γ obtained from equation (23) is

$$\Gamma = -\frac{1}{2}\sum_{l,m} \xi_{lm}^{-4}[\mathscr{I}_1(lm)\mathscr{J}_1(lm) + \mathscr{I}_2(lm)\mathscr{J}_2(lm)] \tag{B.1}$$

with

$$\begin{aligned}
\left.\begin{matrix}\mathscr{I}_1(lm) \\ \mathscr{I}_2(lm)\end{matrix}\right| &= \int\int_{(\mathscr{S})} L(\Phi_{0n}, \Phi_{0n}) \left|\begin{matrix}\Psi_{lm1} \\ \Psi_{lm2}\end{matrix}\right| \mathrm{d}S \\
&= \int_0^1 L(R_{0n}, R_{0n}) S_{lm} r \, \mathrm{d}r \int_0^{2\pi} \left|\begin{matrix}\cos l\theta \\ \sin l\theta\end{matrix}\right| \mathrm{d}\theta, \\
\left.\begin{matrix}\mathscr{J}_1(lm) \\ \mathscr{J}_2(lm)\end{matrix}\right| &= \int\int_{(\mathscr{S})} \Phi_{0n} L\left(\Phi_{0n}, \left|\begin{matrix}\Psi_{lm1} \\ \Psi_{lm2}\end{matrix}\right|\right) \mathrm{d}S \\
&= \int_0^1 R_{0n} L(R_{0n}, S_{lm}) r \, \mathrm{d}r \int_0^{2\pi} \left|\begin{matrix}\cos l\theta \\ \sin l\theta\end{matrix}\right| \mathrm{d}\theta.
\end{aligned} \tag{B.2}$$

Therefore, because of the value of the integrals of sine and cosine from 0 to 2π in the above equations, the only non-zero $\mathscr{I}_\alpha$ and $\mathscr{J}_\alpha$ are

$$\mathscr{I}_1(0m) = 4\pi \int_0^1 R''_{0n}(r) R'_{0n}(r) S_{0m}(r)\,\mathrm{d}r, \tag{B.3a}$$

$$\mathscr{J}_1(0m) = 2\pi \int_0^1 R_{0n}(r)[R''_{0n}(r) S'_{0m}(r) + R'_{0n}(r) S''_{0m}]\,\mathrm{d}r, \tag{B.3b}$$

where $R'(r)$ denotes the derivative with respect to r of function R of r. As a consequence, one can note that the only longitudinal (Ψ) modes involved are the axisymmetric ones. This result confirms the hypothesis of axisymmetric vibration used in reference [7].

As a conclusion, the coefficient Γ can be calculated using the following sum over all axisymmetric modes Ψ_{0m}:

$$\Gamma = -\frac{1}{2} \sum_{m=1}^{+\infty} \xi_{0m}^{-4} \mathscr{I}_1(0m) \mathscr{J}_1(0m), \tag{B.4}$$

where the values of $\mathscr{I}_1$ and $\mathscr{J}_1$ are given by equations (B.3a, b). Computed values of Γ for the first three modes Φ_{0n} can be found in Table 1.

B.2. THE CASE OF AN ASYMMETRIC MODE Φ

In this section, the transverse modes Φ of equation (25) can equal either $\Phi_1 = \Phi_{kn1}$ or $\Phi_2 = \Phi_{kn2}$, which are the two preferential modes. We then need to determine the following 16 coefficients:

$$\Gamma_{\alpha\beta\tilde{\alpha}\tilde{\beta}} = -\frac{1}{2} \sum_{l,m,\gamma} \xi_{lm}^{-4} \mathscr{I}_{\alpha\beta\gamma}(lm) \mathscr{J}_{\tilde{\alpha}\tilde{\beta}\gamma}(lm), \quad \alpha, \beta, \tilde{\alpha}, \tilde{\beta}, \gamma \in \{1, 2\}^5, \tag{B.5}$$

where (A.5) and (A.11) have been used and

$$\mathscr{I}_{\alpha\beta\gamma}(lm) = \int\int_{(\mathscr{S})} L(\Phi_{kn\alpha}, \Phi_{kn\beta}) \Psi_{lm\gamma}\,\mathrm{d}S = -2\,\mathrm{I}_1(kn, lm) \Pi^{(1)}_{\alpha\beta\gamma} + 2\mathrm{I}_2(kn, lm) \Pi^{(2)}_{\alpha\beta\gamma},$$

$$\mathscr{J}_{\tilde{\alpha}\tilde{\beta}\gamma}(lm) = \int\int_{(\mathscr{S})} \Phi_{kn\tilde{\alpha}} L(\Phi_{kn\tilde{\beta}}, \Psi_{lm\gamma})\,\mathrm{d}S = -2\,\mathrm{J}_1(kn, lm)\, \Pi^{(3)}_{\tilde{\alpha}\tilde{\beta}\gamma} + \mathrm{J}_2(kn, lm) \Pi^{(2)}_{\tilde{\alpha}\tilde{\beta}\gamma}$$

with

$$\mathrm{I}_1(kn, lm) = \int_0^1 \left[\frac{R'^2_{kn}}{r^2} - 2\frac{R_{kn} R'_{kn}}{r^3} + \frac{R^2_{kn}}{r^4}\right] S_{lm}\,\mathrm{d}r, \tag{B.6}$$

$$\mathrm{I}_2(kn, lm) = \int_0^1 R''_{kn} \left[R'_{kn} - k^2 \frac{R_{kn}}{r}\right] S_{lm}\,\mathrm{d}r, \tag{B.7}$$

$$\mathrm{J}_1(kn, lm) = \int_0^1 klR_{kn} \left[\frac{R'_{kn} S'_{lm}}{r} + \frac{R'_{kn} S_{lm} + R_{kn} S'_{lm}}{r^2} + \frac{R_{kn} S_{lm}}{r^3}\right] \mathrm{d}r, \tag{B.8}$$

$$\mathrm{J}_2(kn, lm) = \int_0^1 R_{kn} \left[R''_{kn} \left(S'_{lm} - l^2 \frac{S_{lm}}{r}\right) + S''_{lm} \left(R'_{kn} - k^2 \frac{R_{kn}}{r}\right)\right] \mathrm{d}r. \tag{B.9}$$

The $R_{kn}(r)$ and $S_{lm}(r)$ in the above equations are defined by equations (A.3) and (A.9). The factors $\Pi^{(i)}_{\alpha\beta\gamma}(k,l)$ are the following integrals:

$$\Pi^{(1)}_{\alpha\beta\gamma}(k,l) = \int_0^{2\pi} \begin{vmatrix} -\sin k\theta \\ \cos k\theta \end{vmatrix} \begin{vmatrix} -\sin k\theta \\ \cos k\theta \end{vmatrix} \begin{vmatrix} \cos l\theta \\ \sin l\theta \end{vmatrix} \mathrm{d}\theta,$$

$$\Pi^{(2)}_{\alpha\beta\gamma}(k,l) = \int_0^{2\pi} \begin{vmatrix} \cos k\theta \\ \sin k\theta \end{vmatrix} \begin{vmatrix} \cos k\theta \\ \sin k\theta \end{vmatrix} \begin{vmatrix} \cos l\theta \\ \sin l\theta \end{vmatrix} \mathrm{d}\theta,$$

$$\Pi^{(3)}_{\alpha\beta\gamma}(k,l) = \int_0^{2\pi} \begin{vmatrix} \cos k\theta \\ \sin k\theta \end{vmatrix} \begin{vmatrix} -\sin k\theta \\ \cos k\theta \end{vmatrix} \begin{vmatrix} -\sin l\theta \\ \cos k\theta \end{vmatrix} \mathrm{d}\theta.$$

The above notations mean that all $\Pi_{\alpha\beta\gamma}$ are obtained by making the product of three functions sine and/or cosine, each one being taken in a column of the above matrices, the values of α, β and γ determining the line ($\alpha = 2$ corresponds to the term 21, of the second line of the first column, $\gamma = 1$ to the term 13...).

One can show that the only non-zero values of the $\Pi_{\alpha\beta\gamma}$ are obtained for $l = 2k$ or 0, which means that only the Ψ_{0m} and $\Psi_{(2k)m}$ are involved in the sum of equation (B.5).

Table B.1 summarizes the values of the factors $\mathscr{I}_{\alpha\beta\gamma}$ and $\mathscr{J}_{\alpha\beta\gamma}$ as a function, on the one hand of α, β, γ and on the other hand of the value of l compared to k. First, one can see that the products $\mathscr{I}_{\alpha\alpha\gamma}\mathscr{J}_{\alpha\beta\gamma}$ and $\mathscr{I}_{\alpha\beta\gamma}\mathscr{J}_{\alpha\alpha\gamma}$ with $\alpha \neq \beta$ and for all l are always zero. This implies that

$$\Gamma_{1112} = \Gamma_{1121} = \Gamma_{2212} = \Gamma_{2221} = \Gamma_{1211} = \Gamma_{2111} = \Gamma_{1222} = \Gamma_{2122} = 0. \tag{B.10}$$

Moreover, the non-zero Γ follows

$$\Gamma_{1111} = \Gamma_{2222} = \Gamma_0 + \Gamma^{\bigstar}, \quad \Gamma_{1122} = \Gamma_{2211} = \Gamma_0 - \Gamma^{\bigstar}, \tag{B.11}$$

$$\Gamma_{1212} = \Gamma_{2121} = \Gamma_{1221} = \Gamma_{2112} = \Gamma^{\bigstar} \tag{B.12}$$

with

$$\Gamma_0 = -\pi^2 \sum_{m=1}^{+\infty} \xi_{0m}^{-4} (\mathrm{I}_{20} - k^2 \mathrm{I}_{10}) \mathrm{J}_{20}, \tag{B.13}$$

TABLE B.1

Coefficients $\mathscr{I}_{\alpha\beta\gamma}$ and $\mathscr{J}_{\alpha\beta\gamma}$

	Mode Ψ_{lm1} in cosine ($\gamma = 1$)		Mode Ψ_{lm2} in sine ($\gamma = 2$)	
$\alpha = \beta$	$l \notin \{0, 2k\}$	$\mathscr{I}_{111} = \mathscr{I}_{221} = 0$ $\mathscr{J}_{111} = \mathscr{J}_{221} = 0$	$\forall l$	$\mathscr{I}_{112} = \mathscr{I}_{222} = 0$ $\mathscr{J}_{112} = \mathscr{J}_{222} = 0$
	$l = 0$	$\mathscr{I}_{111} = \mathscr{I}_{221} = -2\pi k^2 \mathrm{I}_1 + 2\pi \mathrm{I}_2$ $\mathscr{J}_{111} = \mathscr{J}_{221} = \pi \mathrm{J}_2$		
	$l = 2k$	$\mathscr{I}_{111} = -\mathscr{I}_{221} = \pi k^2 \mathrm{I}_1 + \pi \mathrm{I}_2 \frac{\pi}{2}$ $\mathscr{J}_{111} = -\mathscr{J}_{221} = -2\pi k^2 \mathrm{J}_1 + \frac{\pi}{2}\mathrm{J}_2$		
$\alpha \neq \beta$	$\forall l$	$\mathscr{I}_{121} = \mathscr{I}_{211} = 0$ $\mathscr{J}_{121} = \mathscr{J}_{211} = 0$	$l \neq 2k$	$\mathscr{I}_{122} = \mathscr{I}_{122} = 0$ $\mathscr{J}_{122} = \mathscr{J}_{212} = 0$
			$l = 2k$	$\mathscr{I}_{122} = \mathscr{I}_{212} = \pi k^2 \mathrm{I}_1 + \pi \mathrm{I}_2 \frac{\pi}{2}$ $\mathscr{J}_{122} = \mathscr{I}_{122} = -2\pi k^2 \mathrm{J}_1 + \frac{\pi}{2}\mathrm{J}_2$

$$\Gamma^{\bigstar} = -\frac{\pi^2}{2}\sum_{m=1}^{+\infty} \xi_{(2k)m}^{-4}(k^2 \mathrm{I}_1^{\bigstar} + \mathrm{I}_2^{\bigstar})\left(\frac{\mathrm{J}_2^{\bigstar}}{2} - 2k^2 \mathrm{J}_1^{\bigstar}\right), \tag{B.14}$$

$$\mathrm{I}_{i0} = \mathrm{I}_i(kn, 0m), \quad \mathrm{J}_{i0} = \mathrm{J}_i(kn, 0m), \tag{B.15}$$

$$\mathrm{I}_i^{\bigstar} = \mathrm{I}_i(kn, (2k)m), \quad \mathrm{J}_i^{\bigstar} = \mathrm{J}_i(kn, (2k)m). \tag{B.16}$$

Γ_0 ($\Gamma^{\bigstar}$) results from the sum over the axisymmetric longitudinal modes Ψ_{0m} (the asymmetric longitudinal modes with $l = 2k$ nodal radii).

To obtain equations (27b, c), one has first to determine the non-linear terms resulting from set (23). They are listed below:

$$\text{equation in } q_1\text{:} \quad \Gamma_{11}q_1^3 + \Gamma_{12}q_2^3 + C_{11}q_1q_2^2 + C_{12}q_1^2q_2, \tag{B.17}$$

$$\text{equation in } q_2\text{:} \quad \Gamma_{21}q_1^3 + \Gamma_{22}q_2^3 + C_{21}q_1q_2^2 + C_{22}q_1^2q_2, \tag{B.18}$$

where

$$\Gamma_{11} = \Gamma_{1111}, \quad \Gamma_{22} = \Gamma_{2222}, \quad \Gamma_{12} = \Gamma_{2212}, \quad \Gamma_{21} = \Gamma_{1121}, \tag{B.19}$$

$$C_{11} = \Gamma_{1212} + \Gamma_{2112} + \Gamma_{2211}, \quad C_{22} = \Gamma_{2121} + \Gamma_{1221} + \Gamma_{1122}, \tag{B.20}$$

$$C_{12} = \Gamma_{1211} + \Gamma_{2111} + \Gamma_{1112}, \quad C_{21} = \Gamma_{1222} + \Gamma_{2122} + \Gamma_{2221}. \tag{B.21}$$

Then, with equations (B.10–B.12), one finally obtains

$$\Gamma_{12} = \Gamma_{21} = C_{12} = C_{21} = 0, \tag{B.22}$$

$$\Gamma_{11} = \Gamma_{22} = C_{11} = C_{22} = \Gamma_0 + \Gamma^{\bigstar} = \Gamma. \tag{B.23}$$

APPENDIX C: NOMENCLATURE

a	radius of the plate
h	thickness of the plate
ρ	density of the plate
v	the Poisson ratio
E	Young's modulus
$p(r, \theta, t)$	external load applied to the plate
$w(r, \theta, t)$	vertical displacement
F	force function
$N_{\alpha\beta}$	membrane force per unit length, $(\alpha, \beta) \in r, \theta$
$\pi_{\alpha\beta}$	components of the second Piola–Kirchhoff stress tensor
$M_r, M_{r\theta}$	bending and twisting moments
Q_r	transverse shear force
Φ_p	pth linear natural mode for the plate with free edge
Ψ_p	pth linear natural mode for the plate with clamped edge
μ_p	dimensionless modal damping of the pth mode
ω_p	dimensionless angular frequency of the pth mode
σ_1	internal detuning between the two preferential configurations
σ_2	detuning between the excitation pulsation and the pulsation of the first configuration

Annexe 2 : Non-linear vibrations of free-edge thin spherical shells : modal interaction rules and 1 :1 :2 internal resonance

Cette annexe donne le texte complet de l'article :

O. Thomas, C. Touzé et A. Chaigne : Non-linear vibrations of free-edge thin spherical shells : modal interaction rules and 1 :1 :2 internal resonance, International Journal of Solids and Structures, **42**(11-12), pp 3339-3373, 2005.

Available online at www.sciencedirect.com
SCIENCE DIRECT®
International Journal of Solids and Structures 42 (2005) 3339–3373
INTERNATIONAL JOURNAL OF SOLIDS and STRUCTURES
www.elsevier.com/locate/ijsolstr

Non-linear vibrations of free-edge thin spherical shells: modal interaction rules and 1:1:2 internal resonance ☆

Oliver Thomas [a,*], C. Touzé [b], A. Chaigne [b]

[a] *Structural Mechanics and Coupled Systems Laboratory, CNAM, 2 rue Conté, 75003 Paris, France*
[b] *ENSTA-UME, Chemin de la Hunière, 91761 Palaiseau Cedex, France*

Received 23 June 2004; received in revised form 25 October 2004
Available online 15 December 2004

Abstract

This paper is devoted to the derivation and the analysis of vibrations of shallow spherical shell subjected to large amplitude transverse displacement. The analog for thin shallow shells of von Kármán's theory for large deflection of plates is used. The validity range of the approximations is assessed by comparing the analytical modal analysis with a numerical solution. The specific case of a free edge is considered. The governing partial differential equations are expanded onto the natural modes of vibration of the shell. The problem is replaced by an infinite set of coupled second-order differential equations with quadratic and cubic non-linear terms. Analytical expressions of the non-linear coefficients are derived and a number of them are found to vanish, as a consequence of the symmetry of revolution of the structure. Then, for all the possible internal resonances, a number of rules are deduced, thus predicting the activation of the energy exchanges between the involved modes. Finally, a specific mode coupling due to a 1:1:2 internal resonance between two companion modes and an axisymmetric mode is studied.

Keywords: Shallow spherical shells; Geometrical non-linearities; Internal resonances, Non-linear vibrations

1. Introduction

Structures with a thin geometry, like beams, arches, plates and shells, can exhibit large amplitude flexural vibrations, whose magnitude is comparable to the order of their thickness. In those cases, typical non-linear

☆ This work was performed during a post-doctoral stay of the first author at ENSTA-UME.

* Corresponding author. Tel.: +33 0158 80 85 80; fax: +33 0140 27 27 16.
E-mail address: olivier.thomas@cnam.fr (O. Thomas).

0020-7683/$ - see front matter © 2004 Elsevier Ltd. All rights reserved.
doi:10.1016/j.ijsolstr.2004.10.028

behaviors can be observed, such as jump phenomena and energy exchanges between modal configurations and a linear prediction model is not sufficient (Nayfeh and Mook, 1979). In this paper, von Kármán non-linear dynamic equations are used in the special case of a shallow spherical cap in order to predict and simulate the observed phenomena.

In the literature devoted to geometrically non-linear (finite-amplitude) vibrations of shells, the largest part of the studies is concerned with circular cylindrical shells. The interested reader can refer to the exhaustive review proposed by (Amabili et al., 1998). For the case of spherical caps, most of the studies including geometrical non-linearities deal with axisymmetric deflections of perfectly symmetric structures. Moreover, the focus is generally put on dynamic buckling and snap-through behavior, whereas vibratory responses are seldom treated. Some works dealing with non-linear vibration of shells are briefly reviewed here and the interested reader can refer for a thorough bibliography to reviews of the literature by Leissa (1993b), Qatu (2002), Moussaoui and Benamar (2002) as well as the recent paper by Amabili and Païdoussis (2003). Evensen and Evan-Iwanowsky (1967) proposed a very complete work, analytical and experimental, and investigate buckling as well as non-linear vibrations of a clamped-edge spherical cap with the harmonic balance method. Gonçalves (1994) addressed the same problem, with geometrical imperfections, and used a Galerkin method with the analytical expressions of the mode shapes to solve the problem. Ye (1997) used a numerical Runge–Kutta method to solve the same problem. However, those studies are restricted to vibrations involving only one axisymmetric mode. A detailed study is proposed by Yasuda and Kushida (1984) who investigated the multi-mode axisymmetric response of a clamped spherical cap. The special case of a 1:2 internal resonance between two axisymmetric modes was addressed both theoretically and experimentally. Grossman et al. (1969) investigated the free oscillations axisymmetric frequencies dependence with the deflection amplitude, as a function of both the curvature of the shell and the boundary conditions. All those studies are restricted to axisymmetric vibrations. However, even if the excitation pattern is rotationally symmetric, a complete realistic study has to include asymmetric vibrations, since non-linear coupling between any modal configuration is likely to appear. Hui (1983) addressed one-mode asymmetric vibrations of a complete spherical shell with geometric imperfections and structural damping. To the knowledge of the authors, no analytical studies on non-linear multi-mode asymmetric vibrations of spherical shells have been published and the present work aims at filling this gap.

Spherical caps can be considered as a reference problem, mainly because their vibrations display important non-linear behaviors that are commonly observed in large deflection vibrations of thin structures. Firstly, as a consequence of the multiplicity of two of eigenfrequencies associated to asymmetric modes—a common feature of structures with an axisymmetric geometry (see e.g. Morand and Ohayon, 1995, Chapter 1)—1:1 internal resonances between companion modes are numerous and give rise to a variety of complex vibratory patterns, including traveling waves (see e.g. Tobias and Arnold, 1957; Raman and Mote, 2001; Touzé et al., 2002). Secondly, the curvature of the structure adds quadratic non-linearities in the oscillators that govern the dynamics of the system, whereas only cubic terms are present in the case of transversely symmetric structures such as rods and plates (Thomas et al., 2001). Thirdly, the spectral content of spherical shells depends on one geometrical parameter related to the curvature. Particular algebraic relations between natural frequencies can then be obtained for specific values of the curvature. As a consequence, numerous internal resonances that are related to both quadratic and cubic non-linear terms are likely to be observed on spherical shells. An example addressed in the present work is the 1:1:2 internal resonance between an axisymmetric mode and two companion modes.

The main goal of this paper is to present a exhaustive method for analysis and prediction of the large amplitude vibratory response of spherical shells, from the governing equations to their resolution. It extends a study on non-linear vibrations of circular plates (Touzé et al., 2002) to the case a curved shallow geometry. The non-linear behavior and the possible energy transfers between modal configurations related to the perfect axisymmetric geometry of the structure are especially addressed, extending results of the

literature. The free-edge boundary conditions have been chosen mainly because they are the easiest to realize experimentally. However, the results of the present study can be extended to any type of boundary conditions, provided they are in accordance with the rotational symmetry of the problem.

The non-linear partial differential equations (PDE) that govern the oscillations of the shell are expanded onto its eigenmodes. The main underlying assumptions of the model, as well as the hypothesis of shallowness, are discussed. Complete analytical expressions of the eigenmodes of the associated linear problem are derived and compared to a numerical solution. After expansion of the PDE onto the eigenmodes, a set of coupled second-order ordinary differential equations with quadratic and cubic non-linearities is obtained. The coefficients of the non-linear terms are calculated in the case of a perfect axisymmetric geometry and the coupling rules for the modal interactions are deduced. Possible truncation of the infinite dimensional problem are evaluated. Finally, the particular case of a 1:1:2 internal resonance is precisely investigated by a perturbation method, in the case of a harmonic forced excitation. The effect of slight imperfections of the structure is simulated by introducing slight differences in the companion modes frequencies. Experimental validations of the theoretical results will be presented in a forthcoming paper.

2. Formulation of the problem

2.1. Local equations

A spherical shell of thickness h, radius of curvature R and outer diameter $2a$, made of a homogeneous isotropic material of density ρ, Poisson's ratio ν and Young's modulus E, is considered. The geometry is specified in Fig. 1.

The equations of motions for shallow shells subjected to large deflections and moderate rotations, with small strain so that Hooke's law is verified, were derived by various authors in the case of particular geometries: Donnell (1934) and Evensen and Fulton (1965) for cylinders, Marguerre (1938), Leissa and Kadi (1971) and Alhazza (2002) for curved panels, Mushtari and Galimov (1961) and Koiter (1965) in the general case. A recent work presents a justification of these equations by an asymptotic method (Hamdouni and Millet, 2003). These equations have taken several names in the past: Donnell's equations, Marguerre's

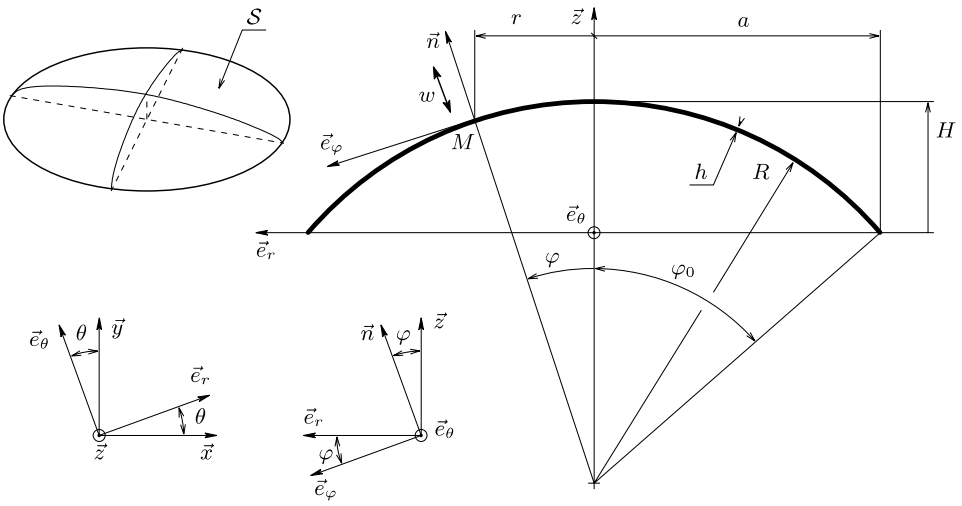

Fig. 1. Geometry of the shell: three-dimensional sketch and cross section.

equations, Koiter's equations or von Kármán's equations. They correspond to a generalization to the case of a curved geometry of von Kármán's model for large-deflection vibrations of plates (see e.g. Chu and Herrmann, 1956).

The main hypotheses are the following (see e.g. Koiter, 1965; Soedel, 1981):

- the shell is thin: $h/a \ll 1$ and $h/R \ll 1$;
- the shell is shallow: $a/R \ll 1$;
- the transverse normal stress are neglected with respect to the other stresses;
- Kirchhoff–Love hypotheses are used: the shear-strains are neglected and the normals to the undeformed mid-surface remain straight and normal and suffer no extension during the deformation;
- rotations of normals to the mid-surface are moderate, so that their sine and cosine are linearized (moderate rotations hypothesis);
- only the non-linear terms of the lowest order are kept in the strain expressions;
- the material is linear elastic, homogeneous and isotropic;
- in-plane and rotatory inertia are neglected;
- there is no membrane external forcing, which enables the use of an Airy stress function F.

With these assumptions fulfilled, one obtains the equations of motion in terms of the transverse displacement w along the normal to the mid-surface and the Airy stress function F, for all time t

$$D\Delta\Delta w + \frac{1}{R}\Delta F + \rho h\ddot{w} = L(w,F) - c\dot{w} + p, \tag{1a}$$

$$\Delta\Delta F - \frac{Eh}{R}\Delta w = -\frac{Eh}{2}L(w,w), \tag{1b}$$

where $D = Eh^3/12(1-\nu^2)$ is the flexural rigidity, c is a damping coefficient, p represents the external normal pressure, $\ddot{w}$ is the second partial derivative of w with respect to time, Δ is the Laplacian and L is a bilinear quadratic operator. With the assumption that the shell is shallow, angle φ defined in Fig. 1 is small and we get

$$\sin\varphi \simeq \varphi, \quad r = R\sin\varphi \simeq R\varphi. \tag{2}$$

Hence, the position of any point of the middle surface of the shell can be measured by its polar coordinates (r,θ), $r \in [0;a]$ and $\theta \in [0;2\pi]$ and the operators Δ and L of Eqs. (1a) and (1b) can be written

$$\Delta(\cdot) = (\cdot)_{,rr} + \frac{1}{r}(\cdot)_{,r} + \frac{1}{r^2}(\cdot)_{,\theta\theta} \tag{3}$$

and

$$L(w,F) = w_{,rr}\left(\frac{F_{,r}}{r} + \frac{F_{,\theta\theta}}{r^2}\right) + F_{,rr}\left(\frac{w_{,r}}{r} + \frac{w_{,\theta\theta}}{r^2}\right) - 2\left(\frac{w_{,r\theta}}{r} - \frac{w_{,\theta}}{r^2}\right)\left(\frac{F_{,r\theta}}{r} - \frac{F_{,\theta}}{r^2}\right), \tag{4}$$

where $(\cdot)_{,\alpha\beta} = \partial^2(\cdot)/\partial\alpha\partial\beta$. Expressions of F as a function of membrane stresses can be found in Touzé et al. (2002). Quadratic operator L defined by Eq. (4) has the same expression as in von Kármán's equations for circular plates (Efstathiades, 1971). A proof of Eqs. (1a) and (1b) can be obtained after writing the doubly curved panel equations formulated in Leissa and Kadi (1971) in polar coordinates.

The shallowness assumptions of Eq. (2) are valid as long as $\sin\varphi_0 \simeq \varphi_0$ (φ_0 is defined on Fig. 1). The corresponding shell geometries and limiting values of φ_0 are summarized in Fig. 2.

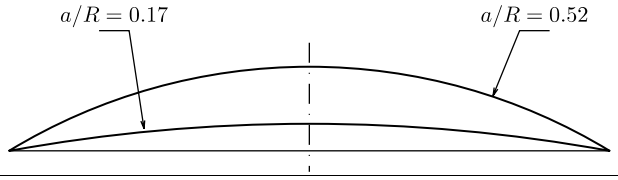

$\varphi_0/(\varphi_0^3/6) > 10$	$\varphi_0 > 31.4°$	$a/R < 0.52$	$H/a < 0.28$
$\varphi_0/(\varphi_0^3/6) > 100$	$\varphi_0 > 9.92°$	$a/R < 0.172$	$H/a < 0.087$

Fig. 2. Shell geometry so that Eqs. (2) are fulfilled, with $\sin\varphi_0 = a/R$. Parameters are defined on Fig. 1.

2.2. Free-edge boundary conditions

Boundary conditions are similar to those of a free-edge circular plate (Touzé et al., 2002) which yields for all t and θ

$$F \quad \text{and} \quad w \text{ are bounded at } r = 0, \tag{5a}$$

$$F_{,r} + \frac{1}{a}F_{,\theta\theta} = 0, \quad F_{,r\theta} - \frac{1}{a}F_{,\theta} = 0, \quad \text{at } r = a, \tag{5b}$$

$$w_{,rr} + \frac{\nu}{a}w_{,r} + \frac{\nu}{a^2}w_{,\theta\theta} = 0, \quad \text{at } r = a, \tag{5c}$$

$$w_{,rrr} + \frac{1}{a}w_{,rr} - \frac{1}{a^2}w_{,r} + \frac{2-\nu}{a^2}w_{,r\theta\theta} - \frac{3-\nu}{a^3}w_{,\theta\theta} = 0, \quad \text{at } r = a. \tag{5d}$$

The above equations stems from the vanishing of the external load at the edge: Eqs. (5b) are related to the membrane forces, Eq. (5c) to the bending moment and Eq. (5d) to the twisting moment and transverse shear force.

2.3. Dimensional analysis

Equations of motion (1a) and (1b) group different terms. On the one hand, terms ΔF in Eq. (1a) and Δw in Eq. (1b) are responsible for a *linear* coupling between transverse motion and membrane stretching, stemming from the curved geometry of the shell. On the other hand, terms $L(\cdot,\cdot)$ in both equations produce a *non-linear* coupling. Those two effects are independent from each other, since operator L is independent of curvature R. If R tends to infinity, one obtains von Kármán's equations (Efstathiades, 1971) for geometrically non-linear plates and if $L(\cdot,\cdot)$ vanishes, linear Donnell–Mushtari–Vlasov's model (Soedel, 1981) for shallow shells is obtained.

As the longitudinal inertia is neglected, F is slaved to transverse displacement w. Eq. (1b) shows that F contains both a linear and a quadratic term in w. By substituting F in Eq. (1a), one can show that curvature and non-linear coupling create together a *linear*, a *quadratic* and a *cubic* term in the equation that governs w, the first two terms arising from curvature. In order to balance their magnitude, dimensionless quantities (denoted by overbars) are introduced

$$w = w_0\bar{w}, \quad F = F_0\bar{F}, \quad r = a\bar{r}, \quad t = T_0\bar{t}, \quad \text{with } T_0 = a^2\sqrt{\frac{\rho h}{D}}. \tag{6}$$

w_0 and F_0 will be specified next. Substituting these variables in Eqs. (1a) and (1b) and omitting for clarity damping and forcing terms, one obtains for Eq. (1a)

$$\overline{\Delta\Delta w} + \ddot{\bar{w}} = -\chi\{\bar{w}\} + \frac{1}{2}\varepsilon_q\{\bar{w}^2\} - \varepsilon_c\{\bar{w}^3\}, \tag{7}$$

where $\{\bar{w}^n\}$ denotes a dimensionless term proportional to $\bar{w}^n$ supposed to be O(1). The order of magnitude of the different terms in Eq. (7) are specified by the following dimensionless factors:

$$\text{linear term } \{\bar{w}\}: \quad \chi = \frac{Eha^4}{DR^2} = 12(1-\nu^2)\frac{a^4}{R^2h^2}, \tag{8a}$$

$$\text{quadratic term } \{\bar{w}^2\}: \quad \varepsilon_q = \frac{Eha^2}{DR}w_0 = 12(1-\nu^2)\frac{a^2}{Rh^2}w_0, \tag{8b}$$

$$\text{cubic term } \{\bar{w}^3\}: \quad \varepsilon_c = \frac{Eh}{D}w_0^2 = 12(1-\nu^2)\frac{w_0^2}{h^2}. \tag{8c}$$

From these developments it appears naturally that curvature adds a linear term, which depends on the geometry of the shell only (parameter χ): it corresponds to the increase of transverse rigidity of the structure brought by the linear coupling between transverse motion and mid-plane stretching. It will be shown that χ brings a correction to the shell eigenfrequencies compared to those of the corresponding plate (Section 3.1).

Non-linear terms have the order of magnitude of ε_q and ε_c, which depends on the scaling w_0 of transverse displacement. As

$$\varepsilon_c = \varepsilon_q^2/\chi, \tag{9}$$

we find that cubic terms are of one order of magnitude smaller than that of quadratic terms. It is the usual scaling chosen for those terms when a perturbation method is used to solve the problem, so that these terms appear successively in the perturbative scheme (Nayfeh and Mook, 1979). We can also remark that the coefficient of cubic terms ε_c is independent of curvature R and that it is equal to the value it has in the case of a plate.

As a consequence, the balance between the magnitudes of the different terms is governed by the order of magnitude of transverse displacement w_0 only. Table 1 summarizes values obtained for ε_q and ε_c, for various choices of w_0 as compared to h. If the deflection is of the same order as the thickness (say $w_0 = h$), ε_q and ε_c are greater than 1, no small parameter appears in Eq. (7) and non-linear terms are of a larger order than linear terms. If the deflection is chosen one order smaller than h (i.e. $w_0 = h^2/a$), cubic terms only are small compared to the linear ones. This is the usual scaling chosen in the case of plate (Sridhar et al., 1978; Touzé et al., 2002). When curvature is non-negligible, one has to choose deflection two orders smaller than

Table 1
Analytical values and order of magnitude of ε_q and ε_c for various choice of transverse displacement scaling w_0 and shell geometries ($a/R = 0$ corresponds to a plate)

a/R	h/a	χ	$w_0 = h$		$w_0 = h^2/a$		$w_0 = h^3/a^2$	
			ε_q	ε_c	ε_q	ε_c	ε_q	ε_c
			$\frac{12(1-\nu^2)a^2}{Rh}$	$12(1-\nu^2)$	$\frac{12(1-\nu^2)a}{R}$	$\frac{12(1-\nu^2)h^2}{a^2}$	$\frac{12(1-\nu^2)h}{R}$	$\frac{12(1-\nu^2)h^4}{a^4}$
0	0.01	0	0	10	0	10^{-3}	0	10^{-7}
0	0.1	0	0	10	0	10^{-1}	0	10^{-3}
0.01	0.01	10	10	10	10^{-1}	10^{-3}	10^{-3}	10^{-7}
0.01	0.1	0.1	1	10	10^{-1}	10^{-1}	10^{-2}	10^{-3}
0.1	0.01	1000	10^2	10	1	10^{-3}	10^{-2}	10^{-7}
0.1	0.1	10	10	10	1	10^{-1}	10^{-1}	10^{-3}

χ, ε_q and ε_c are defined by Eqs. (8a)–(8c).

thickness ($w_0 = h^3/a^2$) to obtain both quadratic and cubic terms smaller than the linear ones. This is the solution adopted here since a perturbation method will be used in Section 5 to solve Eqs. (1a) and (1b). The above developments about scaling of the deflection w_0 show that non-linear phenomena become significant in curved structures for deflections of an order of magnitude between h^3/a^2 and h^2/a, smaller than in the case of plates.

The scaling F_0 of the stress function is chosen so that dimensionless variable F is O(1) when $\overline{\Delta\Delta F} \simeq -1/2\overline{L(w,w)}$ in Eq. (1b). This solution is suitable for any R, especially if R tends to infinity (the case of a plate). The following dimensionless variables are then defined:

$$r = a\bar{r}, \quad t = a^2\sqrt{\rho h/D}\bar{t}, \quad w = h^3/a^2\bar{w}, \quad F = Eh^7/a^4\bar{F}, \tag{10a}$$

$$c = [2Eh^4/Ra^2]\sqrt{\rho h/D}\bar{\mu}, \quad p = Eh^7/Ra^6\bar{p}. \tag{10b}$$

Substituting the above definitions in equations of motion (1a) and (1b) and dropping the overbars in the results, one obtains

$$\Delta\Delta w + \varepsilon_q \Delta F + \ddot{w} = \varepsilon_c L(w,F) + \varepsilon_q[-2\mu\dot{w} + p], \tag{11a}$$

$$\Delta\Delta F - \frac{a^4}{Rh^3}\Delta w = -\frac{1}{2}L(w,w), \tag{11b}$$

where $\varepsilon_q = 12(1-\nu^2)h/R$ and $\varepsilon_c = 12(1-\nu^2)h^4/a^4$. Boundary conditions (5a)–(5d), take the same form, with $a = 1$. Forcing and damping terms are scaled to the order of quadratic terms since only those nonlinear terms will be retained in the study of Section 5.

3. Modal analysis of the linear problem

3.1. Eigenfrequencies and mode shapes

An analytical expression of the natural frequencies of vibration of spherical shells with free-edge, axisymmetric as well as asymmetric, was proposed by Johnson and Reissner (1956). The main steps of the derivation of the expressions of the natural frequencies and mode shapes can be found in Appendix A and only some remarks are considered here.

The eigenmodes of the problem are the solutions of

$$\Delta\Delta\Phi + \chi\Delta\Psi - \omega^2\Phi = 0, \tag{12a}$$

$$\Delta\Delta\Psi = \Delta\Phi. \tag{12b}$$

They depend on one geometrical parameter only, the curvature parameter χ, that includes the joint influence of R, a and h. Transverse and membrane mode shapes $\Phi_{kn}(r,\theta)$ and $\Psi_{kn}(r,\theta)$ have k nodal diameters and n nodal circles. Associated dimensionless angular frequencies ω_{kn} are related to their dimensioned counterpart f_{kn} (in Hz) by the formula

$$f_{kn} = \frac{1}{2\pi a^2}\sqrt{\frac{D}{\rho h}}\omega_{kn} = \frac{h}{2\pi a^2}\sqrt{\frac{E}{12\rho(1-\nu^2)}}\omega_{kn}. \tag{13}$$

As membrane inertia is neglected, membrane motion is slaved to transverse motion. There are no membrane natural frequencies and each eigenfrequency ω_{kn} is associated to $\Phi_{kn}(r,\theta)$ and $\Psi_{kn}(r,\theta)$ (Kalnins, 1964).

The modes with at least one nodal diameter ($k \geqslant 1$) are called asymmetric modes. Each associated eigenfrequency has a multiplicity of two and the two corresponding independent modes are called *companion* or *preferential configurations*. The deformed shape of the first deduces from the other by a rotation of $\pi/2k$ around the symmetry axis.

3.2. Dependence on curvature

Fig. 3 shows the evolutions of several eigenfrequencies ω_{kn} with curvature parameter χ and suggests to classify the modes in two families.

- The first family groups all asymmetric modes $(k,0)$ with k nodal diameters ($k \geqslant 2$ since mode $(1,0)$ is a solid-body mode) and no nodal circles. These modes can be called *purely asymmetric*, and their natural frequencies only slightly depend on the curvature (Fig. 3). Their deformed shape is shown in Fig. 4 and their dependence on χ is shown on Fig. 5. Their transverse deformed shapes Φ only slightly depend on the curvature and on the contrary, membrane deformed shapes Ψ show a significant dependence on curvature.
- The second family groups axisymmetric modes $(0,n)$ with n nodal circles and asymmetric modes with at least one nodal circle (thus called *mixed* modes), since their frequencies increase with curvature and are always sorted in the same order (Fig. 3). Their deformed shape is shown in Fig. 6. For $k \in \{0,1\}$ the deformed shape do not depends on curvature (see Eq. (A.14) in Appendix A). For $k \geqslant 2$, the dependence is almost not visible (see Fig. 7), for both transverse and membrane modes.

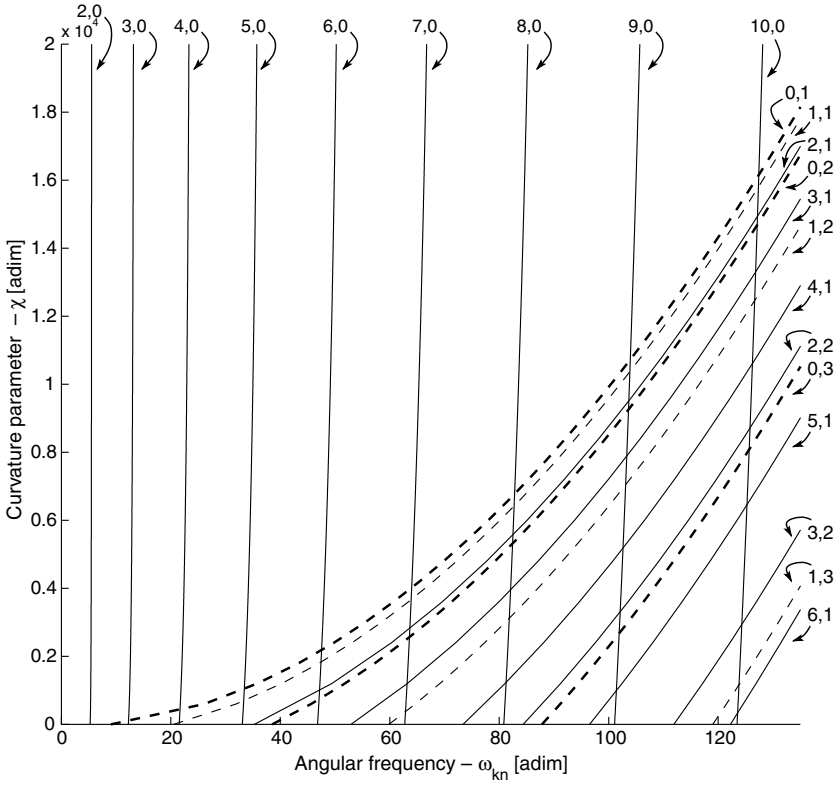

Fig. 3. Dimensionless natural frequencies ω_{kn} of the shell as a function of curvature parameter χ. (k,n) denotes the number of nodal diameters and circles, respectively.

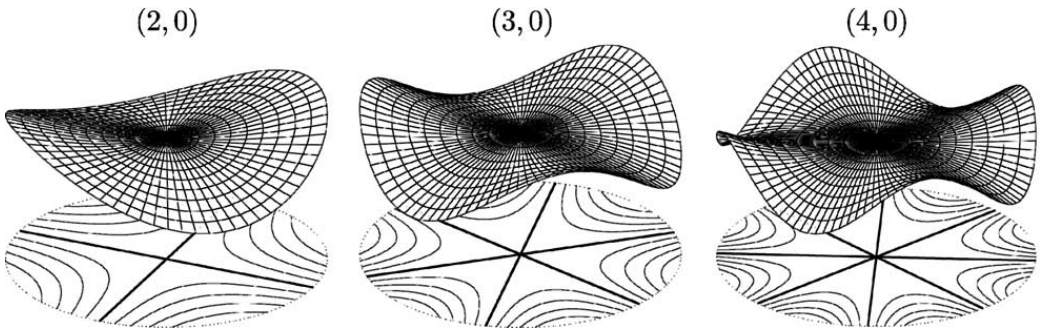

Fig. 4. First three asymmetric mode shapes $\Phi_{kn}(r,\theta)$ with no nodal circles, classified in ascending order of their frequencies.

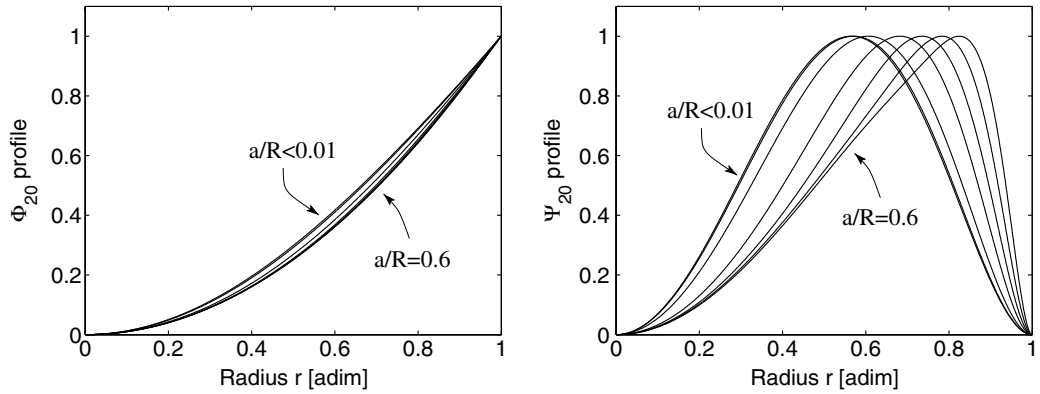

Fig. 5. Profiles of theoretical asymmetric $(2,0)$ mode shape, for several values of a/R between 0 and 0.6: (left) transverse mode and (right) membrane mode.

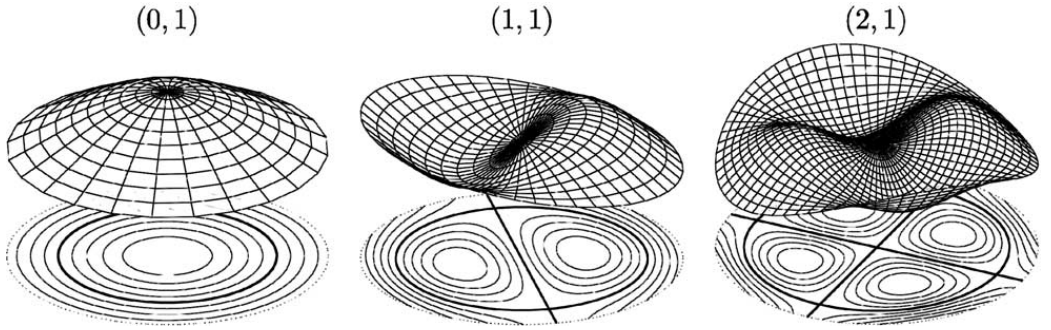

Fig. 6. First three axisymmetric and asymmetric mode shapes $\Phi_{kn}(r,\theta)$ with at least one nodal circle, classified in ascending order of their frequencies.

This analysis of the linear properties of the shell have importance even if one is interested in analyzing the non-linear vibratory regimes. The values of the natural frequencies governs the possible internal resonances relationships between modes and thus the possible modal interactions. This will be addressed in Section 4.2. The spatial dependence of the mode shapes are directly related to the values of the

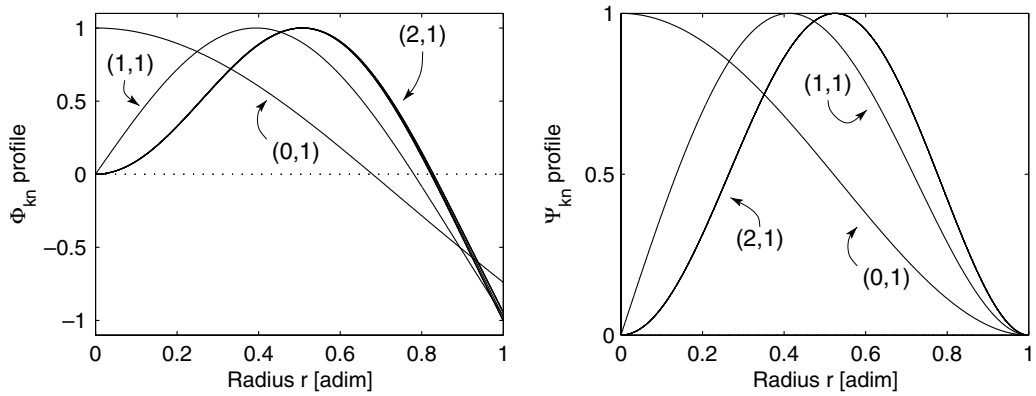

Fig. 7. Profiles of theoretical axisymmetric $(0,1)$ and asymmetric $(1,1)$ and $(2,1)$ mode shapes, for $a/R \in [0,0.6]$: (left) transverse mode and (right) membrane mode.

coefficients of the non-linear terms that governs the exchanges of energy between modes. This will be addressed in Sections 4.3 and 4.4

3.3. Comparison with a numerical solution

In order to precise the validity range of the assumptions of shallowness of Eq. (2), theoretical results of Section 3.1 are compared to a numerical modal analysis, using the finite elements code CASTEM 2000 (Verpeaux et al., 1988) with DKT elements. Fig. 8 shows that the shallow theory predicts the natural frequencies with an error less than 1%, provided that $a/R < 0.3$. This result is in agreement with Table 2. A similar result has been established by Kalnins (1964) who compared the analytical natural frequencies stemming from (12a) and (12b) written in spherical coordinates—the so called non-shallow shell theory—to those of the shallow theory, derived by Johnson and Reissner (1956) and used in the present study.

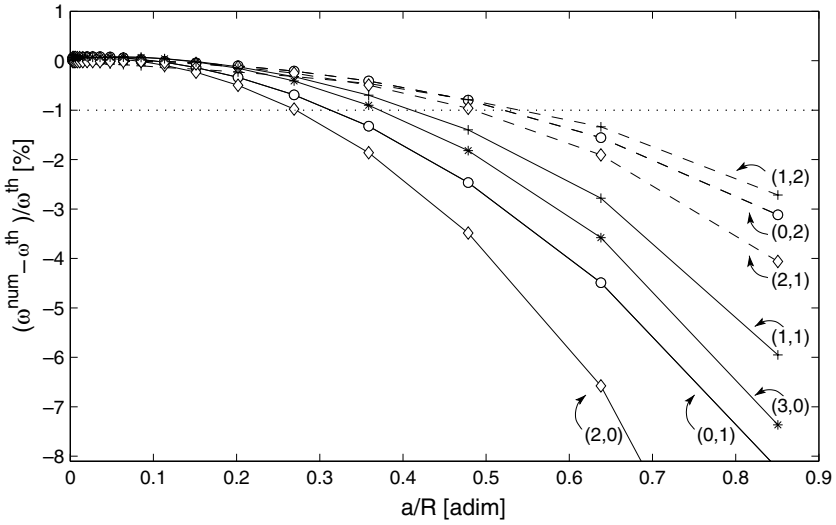

Fig. 8. Ratio of analytical ω^{th} and numerical ω^{num} solutions for the eigenfrequencies of the shell, in percent, as a function of a/R. Geometry of the simulated shell is defined by $a = 300\,\text{mm}$ and $h = 1\,\text{mm}$ and several values of R.

Table 2
Conditions on the number of nodal diameters and the expression in sine and cosine of the modes (both conditions must be fulfilled simultaneously) that lead to non-zero coefficients β^s_{pq} and Γ^s_{pqu}

$\beta^s_{pq} \neq 0$ $\Downarrow$ $k_s \in \{k_p + k_q, \mid k_p - k_q \mid\}$			$\Gamma^s_{pqu} \neq 0$ $\Downarrow$ $\{k_p + k_q, \mid k_p - k_q \mid\} \cap \{k_s + k_u, \mid k_s - k_u \mid\} \neq \emptyset$			
Φ_s	Φ_p	Φ_q	Φ_p	Φ_q	Φ_s	Φ_u
cos	cos	cos	cos	cos	cos	cos
	sin	sin	cos	cos	sin	sin
sin	cos	sin	sin	sin	cos	cos
	sin	cos	sin	sin	sin	sin
			cos	sin	cos	sin
			cos	sin	sin	cos
			sin	cos	sin	cos
			sin	cos	cos	sin

In order to study vibrations of shells with large curvature, it is possible to use in the following: (i) the eigenmodes calculated with a theoretical modal analysis in spherical coordinates (Kalnins, 1964), or (ii) to use numerical eigenmodes, calculated for example with the finite element method (see e.g. Lobitz et al., 1977, in the case of irregular plates). These tasks are beyond the scope of this article.

4. Modal expansion

4.1. Analytical expressions of the coupling coefficients

The aim of this section is to find a solution to the governing non-linear partial differential equations (11a) and (11b). The transverse deflection is expanded on the eigenmodes of the associated linear problem. The solution is sought as

$$w(r,\theta,t) = \sum_{p=1}^{+\infty} \Phi_p(r,\theta) q_p(t). \tag{14}$$

The $\{q_p\}_{p\in\mathbb{N}^*}$ are unknown functions of time—the modal coordinates—and Φ_p is the pth mode shape of the shell with free edge, whose analytical expression is given in Appendix A.

First, Eq. (11b) is solved by considering that

$$F = F_1 + F_2 \quad \text{with } \Delta\Delta F_1 = \frac{a^4}{Rh^3}\Delta w, \tag{15a}$$

$$\Delta\Delta F_2 = -\frac{1}{2} L(w,w). \tag{15b}$$

Eq. (15a) has already been solved for computing the linear modes in Section 3.1. Eq. (15b) shows the same form as for a circular plate ($\chi = 0$). It can be solved by using functions $\Upsilon_b(r,\theta)$ that exhibit the same spatial dependence as the transverse mode shapes of a clamped circular plate (Touzé et al., 2002). Their expression, along with the values of zeros ξ_b, can be found in Appendix B. Finally, the stress function is written

$$F(r,\theta,t) = F_1 + F_2 = \frac{a^4}{Rh^3} \sum_{b=1}^{+\infty} \Psi_b(r,\theta) q_b(t) + \sum_{b=1}^{+\infty} \Upsilon_b(r,\theta) \left(\sum_{p=1}^{+\infty} \sum_{q=1}^{+\infty} G^b_{pq} q_p(t) q_q(t) \right) \tag{16}$$

with

$$G^b_{pq} = -\frac{1}{2\xi_b^4}\iint_{\mathscr{S}_\perp} L(\Phi_p,\Phi_q)\Upsilon_b \mathrm{d}S \quad \text{and} \quad \iint_{\mathscr{S}_\perp} \Upsilon_b^2 \mathrm{d}S = 1, \tag{17}$$

where $\mathscr{S}_\perp$ is the projected surface $\mathscr{S}$ of the shell, i.e. the domain defined by $(r,\theta) \in [0 \quad 1] \times [0\ 2\pi]$.

This solution can now be substituted into (11a). Using Eq. (12a), multiplying by Φ_s, integrating over $\mathscr{S}_\perp$ and using the orthogonality properties of the modes leads to, for all $s \geqslant 1$

$$\begin{aligned}\ddot{q}_s(t) + \omega_s^2 q_s(t) = \varepsilon_{\mathrm{q}}\left[-\sum_{p=1}^{+\infty}\sum_{q=1}^{+\infty}\beta^s_{pq}q_p(t)q_{\mathrm{q}}(t) - 2\mu_s\dot{q}_s(t) + \tilde{Q}_s(t)\right] \\ - \varepsilon_{\mathrm{c}}\sum_{p=1}^{+\infty}\sum_{q=1}^{+\infty}\sum_{r=1}^{+\infty}\Gamma^s_{pqr}q_p(t)q_{\mathrm{q}}(t)q_r(t),\end{aligned} \tag{18}$$

where modal damping μ_s, depending on mode Φ_s, has been considered. Expressions of $\tilde{Q}_s(t)$, β^s_{pq} and Γ^s_{pqr} are

$$\tilde{Q}_s(t) = \iint_{\mathscr{S}_\perp} \Phi_s(r,\theta)p(r,\theta,t)\mathrm{d}S, \tag{19}$$

$$\beta^s_{pq} = -\iint_{\mathscr{S}_\perp} \Phi_s L(\Phi_p,\Psi_q)\mathrm{d}S - \frac{1}{2}\sum_{b=1}^{+\infty}\frac{1}{\xi_b^4}\iint_{\mathscr{S}_\perp} L(\Phi_p,\Phi_q)\Upsilon_b \mathrm{d}S \iint_{\mathscr{S}_\perp} \Phi_s \Delta\Upsilon_b \,\mathrm{d}S, \tag{20}$$

$$\Gamma^s_{pqu} = \frac{1}{2}\sum_{b=1}^{+\infty}\frac{1}{\xi_b^4}\iint_{\mathscr{S}_\perp} L(\Phi_p,\Phi_q)\Upsilon_b \,\mathrm{d}S \iint_{\mathscr{S}_\perp} \Phi_s L(\Phi_u,\Upsilon_b)\mathrm{d}S, \tag{21}$$

with, for all $p \geqslant 1$

$$\iint_{\mathscr{S}_\perp} \Phi_p^2 \mathrm{d}S = 1. \tag{22}$$

4.2. Reduced-order model

The initial problem described by the set of coupled partial differential equations (11a) and (11b) has been replaced by the *equivalent* discretized problem of the set (18) of non-linear coupled differential equations together with Eq. (14). At this stage, various approaches—analytical, numerical or a combination of both—can be used to solve the problem. In each cases, one has to truncate the set (18) to a finite number of oscillators. This operation has to be carefully performed, since a too crude truncation lead to predict erroneous results for the trend of non-linearity (see e.g. Nayfeh et al., 1992; Amabili et al., 1999; Touzé et al., 2004). The non-linear normal modes and the normal form theory offers a theoretical framework that allows to properly truncate the set (18) (see e.g. Touzé et al., 2004; Touzé and Thomas, 2004). In particular, it is shown that all the non-linear modes involved in internal resonances must be retained in the analysis. In our problem with quadratic and cubic non-linear terms, internal resonances are defined by the possible following relations between the natural frequencies of the shell:

$$\text{quadratic}: \quad \omega_p \simeq 2\omega_q \quad \text{or} \quad \omega_p \simeq \omega_{\mathrm{q}} \pm \omega_k, \tag{23a}$$

$$\text{cubic}: \quad \omega_p \simeq 3\omega_q \quad \text{or} \quad \omega_p \simeq 2\omega_q \pm \omega_k \quad \text{or} \quad \omega_p \simeq \omega_{\mathrm{q}} \pm \omega_k \pm \omega_m. \tag{23b}$$

4.3. Coupling rules

For a perfect axisymmetric structure, mode shapes with k nodal diameter are written in terms of $\cos k\theta$ and $\sin k\theta$. As coefficients β^s_{pq} and Γ^s_{pqu} involve integrations of products of those functions (see Eqs. (20) and (21)), a number of them vanish. The goal of the present section is to exhibit some rules that determine which coefficients vanish and consequently which modal interactions are possible. The mathematical derivations can be found in Appendix C.

Conditions for β^s_{pq} and Γ^s_{pqu} to be non-zero are summarized in Table 2. They depend on (i) the number of nodal diameters k_s, k_p, k_q and k_u of the modes Φ_s, Φ_p, Φ_q and Φ_u involved in the calculation of β^s_{pq} and Γ^s_{pqu} and (ii) the angular dependence in $\cos k\theta$ or $\sin k\theta$ of each of Φ_s, Φ_p, Φ_q and Φ_u. The number n of nodal circles has no influence.

Among those coefficients, some of them are involved in *resonant* non-linear terms. Those terms are called resonant because they can be viewed as forcing terms that excite a particular mode close to its resonance, when internal resonances relations between the natural frequencies exist. They are thus responsible for strong coupling—and thus large energy exchanges—between modal configurations. They cannot be removed by the computation of the normal form and thus govern the dynamics of the system (Guckenheimer and Holmes, 1983). As some coefficients vanish, the corresponding resonant terms are canceled and certain energy exchanges are impossible, even if relations of the form of Eqs. (23a) and (23b) are fulfilled. The end of this section exhibits a few rules that enable to predict the possible modal interactions.

In order to determinate if a particular modal interaction is possible, one has (i) to check if any of Eqs. (23a) and (23b) is fulfilled and (ii) to check if the associated resonant terms are non zero, using the following rules that hold on the number of nodal diameters of the involved modes. The rules holding on the nature in sine or cosine of companion modes are secondary because they cannot be responsible of cancellation of *all* resonant terms in a particular internal resonance. They are thus not addressed here.

The first rule stands that *all axisymmetric modes can be involved in modal interactions with one another, by both order-two* (Eq. (23a)) *and order three* (Eq. (23b)) *internal resonances*. Studies on modal interactions between axisymmetric modes were proposed by Sridhar et al. (1975) for circular plates and by Yasuda and Kushida (1984) in the case of spherical shells. The other rules, specifically related to particular internal resonances involving asymmetric modes, are given below. One should keep in mind that two asymmetric modes with natural frequencies such that $\omega_2 > \omega_1$ can have their numbers of nodal diameters such that $k_2 < k_1$: this situation exists if the numbers of nodal circles are such that $n_2 > n_1$ (see e.g. Fig. 3).

4.3.1. Order-two internal resonances

The coupling rules are summarized in Tables 3 and 4. Each table specifies the internal resonance considered (first line), the involved modes (second line), the resonant terms (third line) and the general conditions

Table 3
Rules determining if modal interaction between modes Φ_1 and Φ_2 is possible, when internal resonance $\omega_2 = 2\omega_1$ is fulfilled

$\omega_2 = 2\omega_1$		
Modes	Φ_1 (ω_1, k_1)	Φ_2 (ω_2, k_2)
Resonant terms	$q_1 q_2$	q_1^2
Rules	$k_1 \in \{k_1 + k_2, \lvert k_1 - k_2 \rvert\} \neq \emptyset$	$k_2 \in \{2k_2, 0\} \neq \emptyset$
Nature of involved modes		Modal interaction
Both modes axisymmetric: $k_1 = k_2 = 0$		Possible
Only mode Φ_1 asymmetric: $k_1 \neq 0$, $k_2 = 0$		Possible $\forall k_1$
Only mode Φ_2 asymmetric: $k_1 = 0$, $k_2 \neq 0$		Impossible
Both modes asymmetric: $k_1 \neq 0$, $k_2 \neq 0$		Possible if $k_2 = 2k_1$

k_p is the number of nodal diameters of mode Φ_p, and q_p is the time evolution of mode Φ_p in set (18).

Table 4
Rules determining if modal interaction between modes Φ_1, Φ_2 and Φ_3 is possible, when internal resonance $\omega_3 = \omega_1 + \omega_2$ is fulfilled

$\omega_3 = \omega_1 + \omega_2$			
Modes	$\Phi_1(\omega_1, k_1)$	$\Phi_2\ (\omega_2, k_2)$	$\Phi_3(\omega_3, k_3)$
Res. terms	$q_2 q_3$	$q_1 q_3$	$q_1 q_2$
Rule	for all three res. terms: $k_1 \in \{k_2 + k_3, \lvert k_2 - k_3 \rvert\} \neq \emptyset$		

Nature of involved modes	Modal interaction
All three modes axisymmetric: $k_1 = k_2 = k_3 = 0$	Possible
Only one of them is axymmetric	Impossible
Only one of them is axymmetric: e.g. $k_1 = 0$, $k_2 \neq 0$, $k_3 \neq 0$	Possible if $k_2 = k_3$
All three modes asymmetric: $k_1 \neq 0$, $k_2 \neq 0$, $k_3 \neq 0$	Possible if $\begin{cases} k_1 = k_2 + k_3 \\ k_2 = k_1 + k_3 \\ k_3 = k_1 + k_2 \end{cases}$

k_p is the number of nodal diameters of mode Φ_p, and q_p is the time evolution of mode Φ_p in set (18).

on the numbers of nodal diameters that lead to non-zero resonant terms and thus to a possible energy exchange between the involved modes (fourth line). Then, the particular cases of involved axisymmetric modes and/or asymmetric modes are considered (remaining lines).

These order-two internal resonances are specific to shells with a non-zero curvature, since plates show only order-three internal resonances. Section 5 of this paper is related to the case of Table 3.

4.3.2. Order-three internal resonances

The coupling rules are summarized in Tables 5–7, in a similar manner as for the previous case of order-two internal resonances. Some cubic non-linear terms are always resonant, even if no cubic internal resonance (Eq. (23b)) is fulfilled. An example is a term $q_i q_j^2$, which is resonant in the ith oscillator (of natural frequency ω_i) for any value of the natural frequency ω_j of mode Φ_j, since $\omega_i = \omega_i + \omega_j - \omega_j$. It can be proved (Sridhar et al., 1975; Lacarbonara et al., 2003) that those terms do not lead to large energy exchanges if they are the only ones present in the equations. Thus, only resonant terms specifically related to the cubic internal resonances of Eq. (23b) are considered in Tables 5–7.

These order-three internal resonances are common to any shell; in particular, they are the only internal resonances involved in vibrations of plates (when $\chi = 0$). However, they are of significant importance for shells with small curvature only, since cubic non-linear terms become negligible with respect to quadratic terms for large curvatures ($\varepsilon_c \ll \varepsilon_q$ if R is small compared to a, see Table 1). The case of Table 5 has been recently addressed by Lee et al. (2003) and cases of Tables 6 and 7 extend earlier results of Sridhar et al., 1978), corrected by Yeo and Lee (2002), in the case of circular plates.

Table 5
Rules determining if modal interaction between modes Φ_1 and Φ_2 is possible, when internal resonance $\omega_2 = 3\omega_1$ is fulfilled

$\omega_2 = 3\omega_1$		
Modes	$\Phi_1(\omega_1, k_1)$	$\Phi_2(\omega_2, k_2)$
Resonant terms	$q_1^2 q_2$	q_1^3
Rule	for both res. terms: $\{2k_1, 0\} \cap \{k_1 + k_2, \lvert k_1 - k_2 \rvert\} \neq \emptyset$	

Nature of involved modes	Modal interaction
Both modes axisymmetric: $k_1 = k_2 = 0$	Possible
Only one of them asymmetric	Impossible
Both modes asymmetric: $k_1 \neq 0$, $k_2 \neq 0$	Possible if $\begin{cases} k_2 = k_1 \\ k_2 = 3k_1 \end{cases}$

k_p is the number of nodal diameters of mode Φ_p, and q_p is the time evolution of mode Φ_p in set (18).

Table 6
Rules determining if modal interaction between modes Φ_1, Φ_2 and Φ_3 is possible, when internal resonance $\omega_3 = \omega_1 + 2\omega_2$ is fulfilled

$\omega_3 = \omega_1 + 2\omega_2$		
Modes	Φ_1 (ω_1, k_1) Φ_2 (ω_2, k_2)	Φ_3 (ω_3, k_3)
Res. terms	$q_2^2 q_3$	$q_1 q_2^2$
Rule	for all three res. terms: $\begin{cases} \{k_1 + k_2, \mid k_1 - k_2 \mid\} \cap \{k_2 + k_3, \mid k_2 - k_3 \mid\} \neq \emptyset \\ \{2k_2, 0\} \cap \{k_1 + k_3, \mid k_1 - k_3 \mid\} \neq \emptyset \end{cases}$	

Nature of involved modes	Modal interaction
All three modes axisymmetric: $k_1 = k_2 = k_3 = 0$	Possible
Only mode Φ_1 asymmetric: $k_1 \neq 0$, $k_2 = k_3 = 0$	Impossible
Only mode Φ_2 asymmetric: $k_2 \neq 0$, $k_1 = k_3 = 0$	Possible $\forall k_2$
Only mode Φ_3 asymmetric: $k_3 \neq 0$, $k_1 = k_2 = 0$	Impossible
Only mode Φ_1 axisymmetric: $k_1 = 0$, $k_2 \neq 0$, $k_3 \neq 0$	Possible if $k_3 = 2k_2$
Only mode Φ_2 axisymmetric: $k_2 = 0$, $k_1 \neq 0$, $k_3 \neq 0$	Possible if $k_1 = k_3$
Only mode Φ_3 axisymmetric: $k_3 = 0$, $k_1 \neq 0$, $k_2 \neq 0$	Possible if $k_1 = 2k_2$
All three modes asymmetric: $k_1 \neq 0$, $k_2 \neq 0$, $k_3 \neq 0$	Possible if $\begin{cases} k_1 = k_3 \ \forall k_2 \\ k_1 + k_3 = 2k_2 \\ k_1 = 2k_2 + k_3 \\ k_3 = k_2 + k_1 \end{cases}$

k_p is the number of nodal diameters of mode Φ_p, and q_p is the time evolution of mode Φ_p in set (18).

Table 7
Rules determining if modal interaction between modes Φ_1, Φ_2, Φ_3 and Φ_4 is possible, when internal resonance $\omega_4 = \omega_1 + \omega_2 + \omega_3$ is fulfilled

$\omega_4 = \omega_1 + \omega_2 + \omega_3$				
Modes	$\Phi_1(\omega_1, k_1)$	$\Phi_2(\omega_2, k_2)$	$\Phi_3(\omega_3, k_3)$	$\Phi_4(\omega_4, k_4)$
Res. terms	$q_2 q_3 q_4$	$q_1 q_3 q_4$	$q_1 q_2 q_4$	$q_1 q_2 q_3$
Rule	for all four res. terms: $\{k_1 + k_2, \mid k_1 - k_2 \mid\} \cap \{k_3 + k_4, \mid k_3 - k_4 \mid\} \neq \emptyset$			

Nature of involved modes	Modal interaction
All three modes axisymmetric: $k_1 = k_2 = k_3 = 0$	Possible
Only one of them asymmetric	Impossible
Only two asym.: e.g. $k_1 \neq 0$, $k_2 \neq 0$, $k_3 = k_4 = 0$	Possible if $k_1 = k_2$
Only one axisym.: $k_p = 0$, $k_q \neq 0$ ($q \neq p$)	Possible if $\begin{cases} k_1 = k_2 + k_3 \\ k_2 = k_1 + k_3 \\ k_3 = k_1 + k_2 \end{cases}$
All asym.: $k_1 \neq 0$, $k_2 \neq 0$, $k_3 \neq 0$, $k_4 \neq 0$	Possible if $\begin{cases} k_1 + k_2 = k_3 + k_4 \\ k_1 + k_3 = k_2 + k_4 \\ k_1 + k_4 = k_2 + k_3 \\ k_1 = k_2 + k_3 + k_4 \\ k_2 = k_1 + k_3 + k_4 \\ k_3 = k_1 + k_2 + k_4 \\ k_4 = k_1 + k_2 + k_3 \end{cases}$

k_p is the number of nodal diameters of mode Φ_p, and q_p is the time evolution of mode Φ_p in set (18).

4.4. Influence of curvature

Some numerical values of coefficients are now exhibited to evaluate the dependence of coefficients β^s_{pq} and Γ^s_{pqu} on the curvature of the shell. They were computed numerically using Eqs. (20) and (21) with the analytical expressions of the mode shapes of Appendix A and B.

Table 8
Numerical values of coefficients of quadratic resonant terms in the case of the 1:1:2 internal resonance between two companion asymmetric mode $(k,0)$ and the first axisymmetric mode $(0,1)$, as functions of curvature parameter χ and for $\nu = 0.33$

Mode (k,n)	Coef. of res. terms	Curvature parameter χ			
		10^{-9}	100	1000	10000
(2,0)	$\alpha_1 = \alpha_2$	1.9555	1.9562	1.9555	1.9453
	$\alpha_3 = \alpha_4$	0.9778	0.9782	0.9778	0.9727
(3,0)	$\alpha_1 = \alpha_2$	5.7070	5.7086	5.7122	5.6783
	$\alpha_3 = \alpha_4$	2.8535	2.8543	2.8562	2.8393
(4,0)	$\alpha_1 = \alpha_2$	11.201	11.203	11.212	11.166
	$\alpha_3 = \alpha_4$	5.6006	5.6016	5.6059	5.5833
(5,0)	$\alpha_1 = \alpha_2$	18.414	18.416	18.427	18.389
	$\alpha_3 = \alpha_4$	9.2072	9.2081	9.2137	9.1952
(6,0)	$\alpha_1 = \alpha_2$	27.333	27.335	27.346	27.328
	$\alpha_3 = \alpha_4$	13.667	13.668	13.674	13.665
(7,0)	$\alpha_1 = \alpha_2$	37.952	37.953	37.964	37.967
	$\alpha_3 = \alpha_4$	18.977	18.977	18.983	18.985

The $\{\alpha_i\}_{i=1\ldots4}$ are defined by Eqs. (25a)–(25c); $\alpha_1 = -\beta^1_{13} - \beta^1_{31} = \alpha_2 = -\beta^1_{23} - \beta^1_{32}$ and $\alpha_3 = -\beta^3_{11} = \alpha_4 = -\beta^3_{22}$. Twelve modes Υ_b have been retained in Eq. (20), in order to obtain a 5-digit precision.

Table 8 shows several values of quadratic coefficients α_i of resonant terms in the case of the 1:1:2 internal resonance treated in Section 5 (The coefficients are defined by Eqs. (25a)–(25c)). Fig. 9 presents the evolution of the relative value of coefficients α_i, that is the ratio of α_i to its value for $\chi = 10^{-9}$. One can observe that these quadratic coefficients depend only slightly on the curvature parameter χ. Moreover, the relative evolution with respect to χ of coefficient $\alpha_1 = \alpha_2$ is identical to that of $\alpha_3 = \alpha_4$, for a given value of the number k of nodal diameters of the companion modes. This is a consequence of the fact that for a given value of k, the $\{\alpha_i\}_{i=1,\ldots,4}$ all depend on the same modal shapes (Φ_{k0} and Φ_{01}).

Table 9 shows the only cubic coefficient that is involved in a single axisymmetric mode vibration. It does not depends on χ. The same table and Fig. 10 shows coefficient of the 1:1 internal resonance between two companion purely asymmetric modes with k nodal diameters (and no nodal circles). They depend very

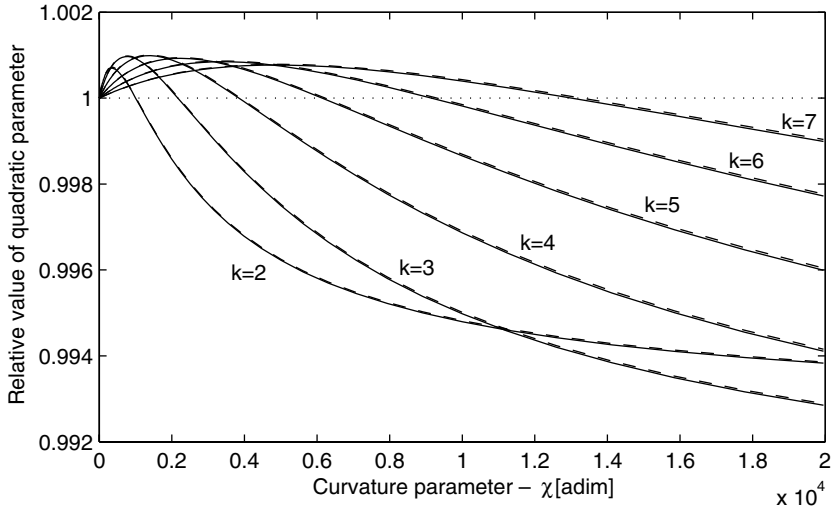

Fig. 9. Evolution of coefficients of quadratic resonant terms of Table 8 with respect to curvature parameter χ, for $k \in \{2,\ldots 7\}$: (—) ratio of $\alpha_1 = \alpha_2$ to their value for $\chi = 10^{-9}$ and (–) ratio of $\alpha_3 = \alpha_4$ to their value for $\chi = 10^{-9}$.

Table 9
Numerical values of coefficients of cubic resonant term in the case of a single axisymmetric mode $(0,n)$ or in the case of the 1:1 internal resonance between two companion asymmetric mode $(k,0)$, with respect to curvature parameter χ and for $\nu = 0.33$

Mode (k,n)	10^{-9}	Curvature parameter χ		
		100	1000	10,000
(0,1)		8.5287		
(0,2)		163.77		
(0,3)		1076.6		
(2,0)	1.8966	1.8985	1.9053	1.9093
(3,0)	16.984	17.304	17.987	18.121
(4,0)	70.001	70.203	71.724	77.034
(5,0)	202.83	203.32	207.26	226.33
(6,0)	476.77	477.68	485.36	531.57
(7,0)	975.31	976.78	989.45	1078.1

Twelve modes Υ_b have been retained in Eq. (21), in order to obtain a five-digit precision.

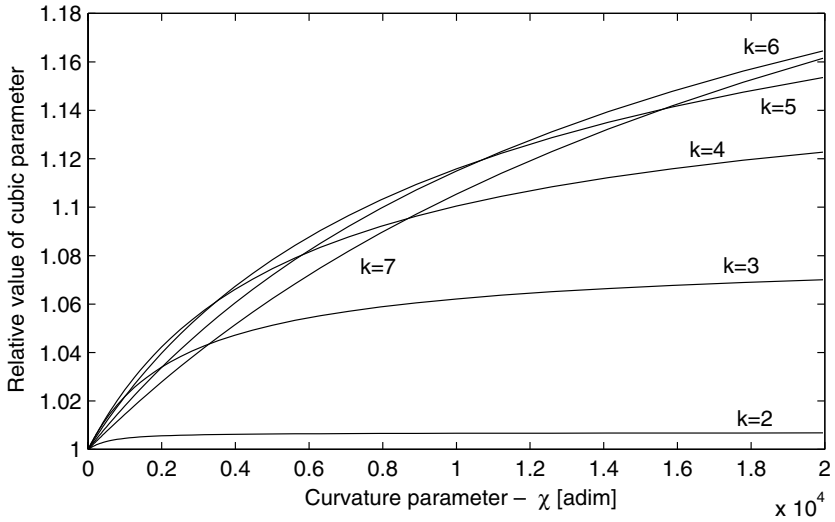

Fig. 10. Evolution of coefficients of cubic resonant terms of Table 9, related to purely asymmetric modes with k nodal diameters, with respect to curvature parameter χ. The ratio between the coefficient to its value for $\chi = 10^{-9}$ is plotted, for $k \in \{2,\ldots 7\}$.

slightly on the curvature parameter χ. The numerical values of this latter case are in agreement with those computed in Touzé et al. (2002) for a circular plate.

One can conclude that coefficients are almost constant as a function of χ. It is a consequence of the fact that the shell mode shapes slightly depend on curvature, as shown in Section 3.1. Thus, the dependence of the dynamics of the shell upon its geometry is mainly governed by the value of ε_q (Eq. (8b)), since ε_c is a constant with respect to the curvature (Eq. (8c)).

5. Application: the case of a one-to-one-to-two internal resonance

This section is devoted to the analysis of a system exhibiting a one-to-one-to-two (1:1:2) internal resonance, corresponding to the interaction between two companion asymmetric mode with an axisymmetric mode, whose natural frequency is nearly equal to twice that of the asymmetric ones. This specific internal

resonance is studied here because it has been observed on a real shell at the laboratory, with energy transfer between the first (0,1) axisymmetric mode and the sixth (6,0) asymmetric. Fig. 11 shows the vibration pattern measured with a scanning laser vibrometer, when the structure is excited at its center by means of a sinusoidal forcing. The vibrations patterns resulting from two excitation conditions—related to two frequencies of excitations close to the natural frequency of the (0,1) mode—are shown on Fig. 11, with and without coupling with one of the companion asymmetric (6,0) modes. Precise measurements and model fitting will be reported in a forthcoming paper.

Two-to-one internal resonance occurs in many different physical systems and has been already studied by a number of investigators (see e.g. Nayfeh and Balachandran, 1989; Nayfeh, 2000, and references therein, for a quick survey including references on spring pendulum, ships, surface waves in closed basins, etc.). For mechanical systems displaying geometrical non-linearities, this specific resonance has been studied both theoretically and experimentally for a structure composed of two slender beams and two dense masses, which were adjusted so that the first two natural frequencies were in the ratio 1:2 (Haddow et al., 1984; Nayfeh and Zavodney, 1988). The two-dof dynamical system has also been studied by Miles (1984), Yamamoto and Yasuda (1977), and the particular phenomenon of saturation was exhibited. As structures with curvature display quadratic non-linearity, 1:2 resonance has naturally been studied for the vibrations of arches and suspended cables (see e.g. Tien et al., 1994; Benedettini et al., 1995).

In the field of circular cylindrical shell vibrations, Nayfeh and Raouf (1987) performed a similar study, as they investigated the interaction between an axisymmetric mode and the two configurations of an asymmetric mode. However, they only considered the perfect case of an infinitely long cylinder. In particular they did not take into account the small detuning that necessary occur between the two preferential configurations in a real system. We will show that these imperfections have a fundamental role for explaining the experimentally observed coupling. More recently, they proposed a second-order solution (Chin and Nayfeh, 2001). Robie et al. (1999) also studied the 1:2 internal resonance, but they limited their study to free undamped vibrations, and considered one asymmetric configuration only. Alhazza (2002) analyzed the 1:2 resonance for a doubly-curved cross-ply shallow shell. Finally, a 1:1:1:2 resonance in circular cylindrical shells has been studied by Amabili et al., but the forcing was considered on one preferential configuration, thus naturally leading to coupled solutions with the first and third axisymmetric mode for any vibration amplitude (Amabili et al., 2000, Pellicano et al., 2000). Moreover, the two configurations were supposed to have exactly equal eigenfrequencies.

The present developments are aimed at filling the gap between the previous studies and sheding light on the relevance of the parameters that are specifically connected to the imperfection of the shell. More specifically, it will be shown that those parameters are crucial for understanding the nature of the coupled

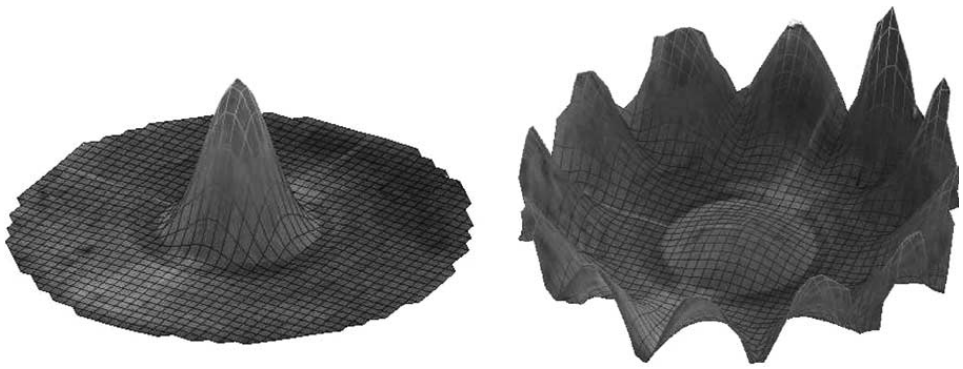

Fig. 11. Vibration pattern with (right) and without (left) coupling between the (0,1) mode and a purely asymmetric (6,0) mode, measured on a real shell with a scanning laser vibrometer. The geometry of the shell is defined by $a = 300\,\text{mm}$, $R = 1.515\,\text{m}$ and $h = 1\,\text{mm}$.

regime. It will be demonstrated that the energy transfer is specific to one of the companion asymmetric modes and that no traveling wave appear as long as the cubic terms are effectively negligible.

The spherical shell is assumed to be excited by an external sinusoidal force located at its center, whose frequency Ω is chosen close to the natural frequency (denoted here by ω_3) of an axisymmetric mode $(0,n')$ of n' nodal circles. The curvature parameter χ is chosen so that an internal resonance exist between mode $(0,n')$ and two companion asymmetric modes (k,n) of frequencies ω_1 and ω_2, so that $\omega_3 \simeq 2\omega_1 \simeq 2\omega_2$. Fig. 3 shows that these internal resonances occur for many values of χ. For example, mode $(0,1)$ can be involved in a 1:1:2 internal resonance between any of the asymmetric modes $(k,0)$ with no nodal circles. In the following, a reduced order model is deduced from the set (18) and we focus on a first-order perturbative solution. As a consequence, (i) only the modes involved in internal resonance are retained, (ii) the cubic terms are neglected with respect to the others, according to the values of the parameters ε_q and ε_c (see Table 1) and (iii) all non-resonant terms are dropped. The transverse displacement $w(r,\theta,t)$ is then written

$$w(r,\theta,t) = R_{kn}(r)(q_1(t)\cos k\theta + q_2(t)\sin k\theta) + R_{0n'}q_3(t), \tag{24}$$

where q_1 and q_2 are related to the asymmetric modes and q_3 to the axisymmetric. $R_{kn}(r)$ and $R_{0n'}(r)$ are defined in Appendix A. The $\{q_i\}_{i=1,\ldots,3}$ are solutions of the following set, deduced from (18):

$$\ddot{q}_1 + \omega_1^2 q_1 = \varepsilon_q[\alpha_1 q_1 q_3 - 2\mu_1 \dot{q}_1], \tag{25a}$$

$$\ddot{q}_2 + \omega_2^2 q_2 = \varepsilon_q[\alpha_2 q_2 q_3 - 2\mu_2 \dot{q}_2], \tag{25b}$$

$$\ddot{q}_3 + \omega_3^2 q_3 = \varepsilon_q[\alpha_3 q_1^2 + \alpha_4 q_2^2 - 2\mu_3 \dot{q}_3 + Q\cos\Omega t]. \tag{25c}$$

The forcing terms of the first two oscillators (25a) and (25b) vanish since the corresponding modes have a node at the center of the shell. The term proportional to q_3^2 in Eq. (25c) is not considered since it is non-resonant. The reduced-order model defined above is justified because the present study is focused on the loss of stability of the single degree-of-freedom (sdof) solution (defined by the directly excited axisymmetric mode only, $q_1(t) \equiv q_2(t) \equiv 0$). A first-order perturbative development is then sufficient and the formalism of non-linear normal modes need not to be used (Nayfeh and Nayfeh, 1994). This would not be the case if one was interested in predicting the hardening or softening behavior of a single mode. In this situation, it would be necessary to retain a number of additional oscillators in the model, the cubic terms as well as the non-resonant terms, as shown for example in the case of circular cylindrical shells by Amabili et al. (1999) or in a general case by Touzé et al. (2004) with the formalism of non-linear modes.

Coefficients $\{\alpha_i\}_{i=1,\ldots,4}$ can be computed from the β_{qs}^p expressed in Eq. (20). In a perfect case, one obtains $\alpha_1 = \alpha_2$, and $\alpha_3 = \alpha_4$, as shown in Table 8. However, for the sake of generality, the $\{\alpha_i\}_{i=1,\ldots,4}$ are kept variable in the following. To express the internal resonance relationships, we introduce two internal detuning parameters σ_0 and σ_1

$$\omega_2 = \omega_1 + \varepsilon_q\sigma_0, \tag{26a}$$

$$\omega_3 = 2\omega_1 + \varepsilon_q\sigma_1. \tag{26b}$$

One can notice that: $\omega_3 = 2\omega_2 + \varepsilon_q(\sigma_1 - 2\sigma_0)$. Finally an external detuning parameter σ_2 is introduced to express the nearness of the forcing frequency with the axisymmetric natural frequency

$$\Omega = \omega_3 + \varepsilon_q\sigma_2. \tag{27}$$

5.1. Multiple scale solution

System (25) is solved by the method of multiple scales. To the first-order, and for $j = 1,2,3$

$$q_j(t) = q_{j1}(T_0,T_1) + \varepsilon_q q_{j2}(T_0,T_1) + O(\varepsilon_q^2), \tag{28}$$

where $T_0 = t$ and $T_1 = \varepsilon_q t$. The first-order equations lead to express the $\{q_{j1}\}_{j=1,2,3}$ as

$$q_{j1}(T_0, T_1) = \frac{1}{2} a_j(T_1) \exp(\mathrm{i}\theta_j(T_1)) \exp(\mathrm{i}\omega_j T_0) + \text{c.c.}, \tag{29}$$

where c.c. stands for complex conjugate. Polar form is used to express the amplitude of the first-order solutions, which depends on the slow time scale T_1. Introducing (29) into the second-order equations leads to the so-called solvability condition, which can be written as a six-dimensional dynamical system by separating real and imaginary parts. Finally, the following variables allows definition of an autonomous dynamical system:

$$\gamma_1 = \sigma_1 T_1 + \theta_3 - 2\theta_1, \quad \gamma_2 = (\sigma_1 - 2\sigma_0) T_1 + \theta_3 - 2\theta_2, \quad \gamma_3 = \sigma_2 T_1 - \theta_3. \tag{30}$$

It reads

$$a_1' = -\mu_1 a_1 + \frac{\alpha_1 a_1 a_3}{4\omega_1} \sin\gamma_1, \tag{31a}$$

$$\gamma_1' = \sigma_1 - \frac{\alpha_3 a_1^2}{4\omega_3 a_3} \cos\gamma_1 - \frac{\alpha_4 a_2^2}{4\omega_3 a_3} \cos\gamma_2 - \frac{Q}{2\omega_3 a_3} \cos\gamma_3 + \frac{\alpha_1 a_3}{2\omega_1} \cos\gamma_1, \tag{31b}$$

$$a_2' = -\mu_2 a_2 + \frac{\alpha_2 a_2 a_3}{4\omega_2} \sin\gamma_2, \tag{31c}$$

$$\gamma_2' = \sigma_1 - 2\sigma_0 - \frac{\alpha_3 a_1^2}{4\omega_3 a_3} \cos\gamma_1 - \frac{\alpha_4 a_2^2}{4\omega_3 a_3} \cos\gamma_2 - \frac{Q}{2\omega_3 a_3} \cos\gamma_3 + \frac{\alpha_2 a_3}{2\omega_2} \cos\gamma_2, \tag{31d}$$

$$a_3' = -\mu_3 a_3 - \frac{\alpha_3 a_1^2}{4\omega_3} \sin\gamma_1 - \frac{\alpha_4 a_2^2}{4\omega_3} \sin\gamma_2 + \frac{Q}{2\omega_3} \sin\gamma_3, \tag{31e}$$

$$\gamma_3' = \sigma_2 + \frac{\alpha_3 a_1^2}{4\omega_3 a_3} \cos\gamma_1 + \frac{\alpha_4 a_2^2}{4\omega_3 a_3} \cos\gamma_2 + \frac{Q}{2\omega_3 a_3} \cos\gamma_3, \tag{31f}$$

where $(\cdot)'$ stands for the derivation with respect to T_1.

5.2. Fixed points

Fixed points for Eq. (31) are obtained by cancelling the left-hand side terms, which involve a derivative with respect to time. There are a priori four kinds of fixed points:

(i) *sdof solution.* It corresponds to the case where $a_1 = a_2 = 0$: no energy transfer between modes occur and the response of the system is governed by the directly excited axisymmetric mode only. Its amplitude is given by

$$a_3 = \frac{Q}{2\omega_3 \sqrt{\sigma_2^2 + \mu_3^2}}, \tag{32}$$

(ii) *C1 solution*. It corresponds to a coupling between the axisymmetric mode and the first asymmetric configuration, thus $a_1 \neq 0$, and $a_2 = 0$.

(iii) *C2 solution.* The coupling is here with the second asymmetric configuration: $a_1 = 0$, and $a_2 \neq 0$.

(iv) *C3 solution*. Coupling with both asymmetric configurations at the same time, leading to $a_1 \neq 0$ and $a_2 \neq 0$. It will be shown next that this solution exists only in the perfect case.

Analytical expressions for the *C1* and *C2* solutions are easily available with a little algebra, which is not reproduced here (see e.g. Nayfeh and Raouf, 1987; Nayfeh and Mook, 1979; Haddow et al., 1984). One then obtains:

- *C1 solution:*

$$a_3 = \frac{2\omega_1}{\alpha_1}\sqrt{4\mu_1^2 + (\sigma_1+\sigma_2)^2}, \tag{33a}$$

$$a_1 = 2\sqrt{-\Gamma_1 \pm \sqrt{\frac{Q^2}{4\alpha_3^2} - \Gamma_2^2}}, \tag{33b}$$

$$\text{with :} \quad \Gamma_1 = \frac{2\omega_1\omega_3}{\alpha_1\alpha_3}(2\mu_1\mu_3 - \sigma_2(\sigma_1+\sigma_2)), \tag{33c}$$

$$\text{and :} \quad \Gamma_2 = \frac{2\omega_1\omega_3}{\alpha_1\alpha_3}(2\sigma_2\mu_1 + \mu_3(\sigma_1+\sigma_2)). \tag{33d}$$

- *C2 solution:*

$$a_3 = \frac{2\omega_2}{\alpha_2}\sqrt{4\mu_2^2 + (\sigma_1 - 2\sigma_0 + \sigma_2)^2}, \tag{34a}$$

$$a_2 = 2\sqrt{-\Gamma_3 \pm \sqrt{\frac{Q^2}{4\alpha_4^2} - \Gamma_4^2}}, \tag{34b}$$

$$\text{with :} \quad \Gamma_3 = \frac{2\omega_2\omega_3}{\alpha_2\alpha_4}(2\mu_2\mu_3 - \sigma_2(\sigma_1 - 2\sigma_0 + \sigma_2)), \tag{34c}$$

$$\text{and :} \quad \Gamma_4 = \frac{2\omega_2\omega_3}{\alpha_2\alpha_4}(2\sigma_2\mu_2 + \mu_3(\sigma_1 - 2\sigma_0 + \sigma_2)). \tag{34d}$$

One can notice that the symmetry of the original equations (25) allows derivation of the expression for the *C2* solution from the expression found for *C1*. The symmetry of the system is of great help for the understanding and analysis of energy transfer, as shown next.

The *C3* case is considered by keeping all amplitudes different from zero. However, the operations that lead to Eqs. (33a) and (34a) are still possible. Thus, in the more general case, when the two asymmetric configurations are eventually present in the vibration, a_3 can take the two different values given by (33a) and (34a). Moreover it can be shown that if a_3 is equal to (33a) (respectively, equal to (34a)), then γ_2 (respectively, γ_1) is undefined and $a_2 = 0$ (respectively, $a_1 = 0$) is the only possible case. As a consequence, no other solutions than the ones already described (sdof, *C1* and *C2*) are available, except when Eqs. (33a) and (34a) are simultaneously fulfilled, which is true only in the perfect case (defined by: $\mu_1 = \mu_2$, $\alpha_1 = \alpha_2$, and $\omega_1 = \omega_2$, which implies $\sigma_0 = 0$). The stability analysis confirms these conclusions, as well as numerical simulations which were conducted with the software DsTool (Guckenheimer et al., 1995).

5.3. Stability analysis

A linear stability analysis is performed by computing the Jacobian matrix $\mathscr{J}$ of Eq. (31). We first investigate the stability of the sdof solution. The eigenvalues are

$$\lambda_{1,2}^{\text{sdof}} = -\mu_3 \pm \mathrm{i}\sigma_2, \tag{35a}$$

$$\lambda_1^{\text{C1}} = -\mu_1 + \frac{\alpha_1 a_3}{4\omega_1}\sin\gamma_1, \tag{35b}$$

$$\lambda_2^{\text{C1}} = -\frac{\alpha_1 a_3}{2\omega_1}\sin\gamma_1, \tag{35c}$$

$$\lambda_1^{\text{C2}} = -\mu_2 + \frac{\alpha_2 a_3}{4\omega_2}\sin\gamma_2, \tag{35d}$$

$$\lambda_2^{\text{C2}} = -\frac{\alpha_2 a_3}{2\omega_2}\sin\gamma_2. \tag{35e}$$

The superscripts indicate that each pair of eigenvalues can be easily related to: (i) the stability of the sdof solution with respect to perturbations contained within the subspace $a_1 = a_2 = 0$ (sdof case), (ii) its stability with respect to perturbations caused by the presence of the first asymmetric configuration (C1 case), (iii) its stability with respect to perturbations caused by the second asymmetric configuration (C2 case). The simple form of Eq. (35a–e) is a direct consequence of the relative decoupling and symmetry of the initial equations (25). By forming the products $\lambda_1^{\text{C1}}.\lambda_2^{\text{C1}}$ and $\lambda_1^{\text{C2}}.\lambda_2^{\text{C2}}$, and eliminating γ_1 and γ_2 in favor of the other parameters, one can exhibit two stability conditions for the sdof solutions:

$$a_3 \leqslant L_1(\sigma_2), \quad \text{where } L_1(\sigma_2) = \frac{2\omega_1}{\alpha_1}\sqrt{4\mu_1^2 + (\sigma_1+\sigma_2)^2}, \tag{36}$$

$$a_3 \leqslant L_2(\sigma_2), \quad \text{where } L_2(\sigma_2) = \frac{2\omega_2}{\alpha_2}\sqrt{4\mu_2^2 + (\sigma_1-2\sigma_0+\sigma_2)^2}, \tag{37}$$

with a_3 defined by Eq. (32). These stability conditions have been reported in Fig. 12, where the sdof solutions is unstable in the gray shaded regions.

In the perfect case—i.e., defined by the complete identity of the two configurations (i.e. $\alpha_1 = \alpha_2$, $\omega_1 = \omega_2$ and $\mu_1 = \mu_2$), the two curves $L_1(\sigma_2)$ and $L_2(\sigma_2)$ are merged. Hence both configurations are simultaneously excited when the sdof curve crosses $L_1 \equiv L_2$. It can then be shown that their amplitudes verify the following relationship:

$$a_1^2 + a_2^2 = -4\Gamma_1 + \sqrt{16\Gamma_1^2 - \left[\frac{64\omega_1^2\omega_3^2}{\alpha_1^2\alpha_3^2}(4\mu_1^2 + (\sigma_1+\sigma_2)^2)(\mu_3^2+\sigma_2^2) - \frac{4Q^2}{\alpha_3^2}\right]} \tag{38}$$

An infinity of coupled solutions are available: any solution that verify Eq. (38). This has been verified numerically. The reader interested in the perfect case is referred to Nayfeh and Raouf (1987) for a complete study.

In real situations, it is impossible to ensure perfectness, and slight perturbations are always present that break the precedent results and keep the curves $L_1(\sigma_2)$ and $L_2(\sigma_2)$ distinct, so that the situation depicted in Fig. 12 is generic. The discussion is restricted to positive values of σ_0, because the ordering of the configurations is made by their natural frequencies.

The stability of the C1 and C2 solutions is now addressed. In Fig. 12, if the sdof solution is followed from $\sigma_2 < 0$ for increasing values, it first crosses L_1 at $\sigma_2 = -1.5$, so that a C1 solution is obtained, whose

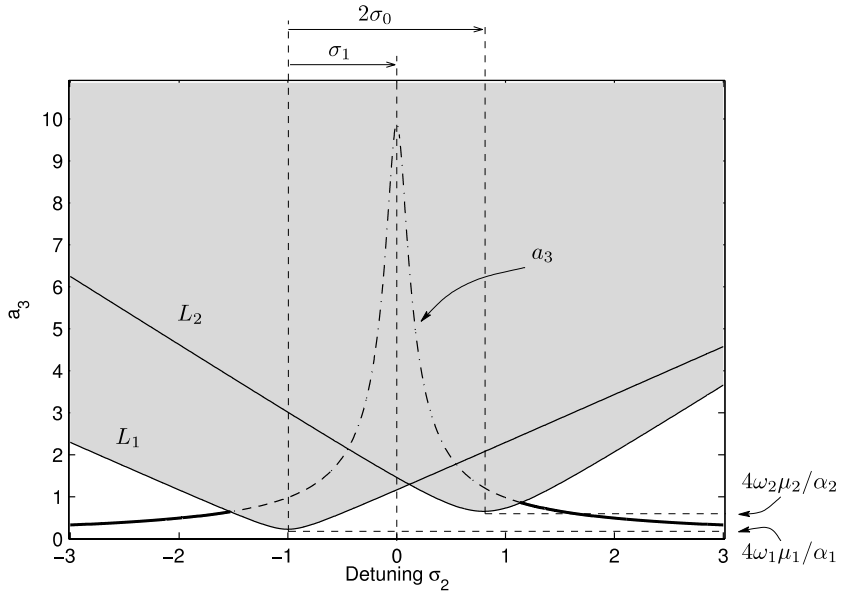

Fig. 12. Stability of the sdof solution with respect to the perturbations caused by the first configuration (L_1 curve), and by the second configuration (L_2 curve). The figure is made with $\alpha_1 = 7$, $\alpha_2 = 5$, $\mu_1 = \mu_3 = 0.1$, $\mu_2 = 0.2$, $Q = 16$, $\omega_1 = 4$, $\omega_2 = 4.09$, $\omega_3 = 8.1$.

stability is studied by substituting for Eqs. (33a) and (33b) in the Jacobian matrix $\mathscr{J}$. The eigenvalues are found to be solutions of

$$P(\lambda) = \det(\mathscr{J} - \lambda I) = \left(-\mu_2 + \frac{\alpha_2 a_3}{4\omega_2}\sin\gamma_2 - \lambda\right)\left(-\frac{\alpha_2 a_3}{2\omega_2}\sin\gamma_2 - \lambda\right)P_{C2}(\lambda), \tag{39}$$

where $P_{C2}(\lambda)$ governs the eigenvalues of the C1 solution with respect to perturbations contained within the subspace $a_2 = 0$. Hence the perturbations created by the presence of the second configuration are completely described by the first two eigenvalues, which are exactly equal to that obtained when studying the sdof solution (see Eqs. (35d) and (35e)). The C1 solution is thus stable as long as $a_3 \leqslant L_2(\sigma_2)$ with a_3 given now by Eq. (33a). For the C1 solution, a_3 (given by Eq. (33a)) takes exactly the value given by the stability condition L_1 (Eq. (36)), so that it can be read in Fig. 12 that the C1 solution is stable as long as $L1$ does not cross $L2$. In Fig. 12, the crossing occurs at $\sigma_2 = 0.30$, where a stability exchange is observed: the C1 solution loses its stability in favor of the C2 solution. Thanks to the symmetry of the system, the discussion is equivalent when following the sdof solution for decreasing values from $\sigma_2 > 0$, by replacing C1 by C2.

It has been demonstrated that the discussion on the stability can be made by simply following the values taken by the amplitude a_3 of the directly excited axisymmetric mode, and that the coupling occurs either with the first configuration, or with the second. The imperfections of the system avoid simultaneous energy transfer to the two configurations. A stability exchange occurs. Hence travelling waves are not possible.

5.4. Generalized stability curves

Fig. 13 displays the different solutions for a typical case. All branches of solutions are obtained analytically from the results of Sections 5.2 and 5.3 and have been systematically verified by numerical simulations using the software DsTool. When increasing σ_2, one observes first the sdof solution. At $\sigma_2 = -1.5$, the first coupling occurs, with the first asymmetric configuration: a_1 follows the C1 branch, as well as a_3. At $\sigma_2 = \hat{\sigma}_2 = 0.12$, the stability exchange occurs: a_1 goes down to zero while a_2 grows up to the C2 branch,

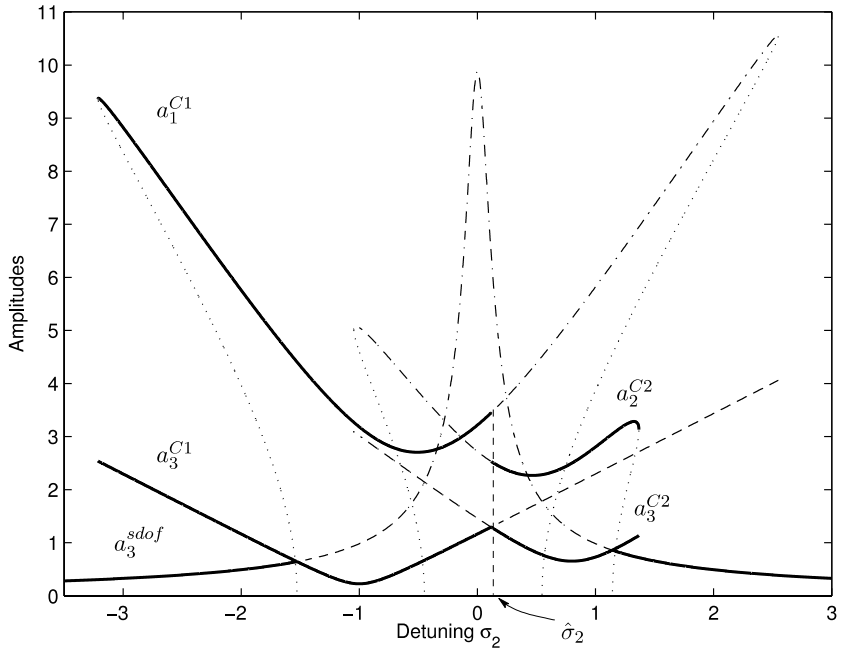

Fig. 13. Generalized stability curve for the case: $\alpha_1 = 7$, $\alpha_2 = 5$, $\alpha_3 = 3$, $\alpha_4 = 4$, $\mu_1 = \mu_3 = 0.1$, $\mu_2 = 0.2$, $Q = 16$, $\omega_1 = 4$, $\omega_2 = 4.09$, $\omega_3 = 8.1$. Stable branches are plotted with solid lines, all other branches are unstable.

and a_3 follows the C2 branch until $\sigma_2 = 1.36$. Hysteretic behaviour is present: when decreasing the excitation frequency, the second configuration is excited first for $\sigma_2 = 1.14$, the stability exchange occurs at the same value $\sigma_2 = 0.12$, from which the first configuration is excited until $\sigma_2 = -3.2$.

A complete parametric study of all possible cases is difficult to formulate because of the size of the parameter space. Nonetheless, we will give now briefly a few guidelines of the possible features by changing two important physical parameters: the internal detuning between the two configurations σ_0 and the amplitude of the forcing Q.

The stability analysis have proven that a mere glance at the relative position of the two stability curves L_1 and L_2 is sufficient to have a comprehensive idea of which coupling will occur. In particular, if e.g. configuration 1 is much more damped than the other, or if the coupling coefficient α_1 is small (see Fig. 12), the stability curve L_1 is reached for large Q values only, and thus the main observation is related to a coupling with the second configuration.

Fig. 14 shows the different behaviour exhibited when increasing the internal detuning σ_0, when all other coefficients are related to a perfect case (i.e. $\alpha_1 = \alpha_2$, $\alpha_3 = \alpha_4$, $\mu_1 = \mu_2 = \mu_3$). It is assumed in addition that $\sigma_1 = 1$.

When σ_0 is small (Fig. 14(a)–(b): $\sigma_0 = 0.1$). The second configuration is mainly observed because the L_2 curve is under L_1 in a wide instability range: $\hat{\sigma}_2 \leqslant \sigma_2 \leqslant 0.26$, where $\hat{\sigma}_2 = L_1 \cap L_2 = -1.17$ represents the intersection point. An opposite result would have been observed by setting $\sigma_1 = -1$. Increasing σ_0 leads to move the intersection point $\hat{\sigma}_2$. At $\sigma_0 = 1.1$ (Fig. 14(c)–(d)), the C2 branch becomes very short, and the coupling mainly occurs with the first configuration. As L_2 still crosses the sdof solution around $\sigma_2 = 1.1$, a short C2 branch is observed. In this specific case, an increasing sweep of the excitation frequency will then produce successively: the sdof solution ($\sigma_2 \leqslant -1.17$), the C1 solution ($-1.17 \leqslant \sigma_2 \leqslant 0.11$), the C2 solution ($0.11 \leqslant \sigma_2 \leqslant 0.31$), the sdof solution ($0.31 \leqslant \sigma_2 \leqslant 0.96$), the C2 solution ($0.96 \leqslant \sigma_2 \leqslant 1.40$) and finally the sdof solution. For higher values of σ_0 (Fig. 14(e)–(f): $\sigma_0 = 1.4$), no stable branches corresponding to C2 are present. Hence the coupling with the second configuration will not occur anymore. However, the effect of the second configuration is still present, unless the limiting value of the C1 branch defined by

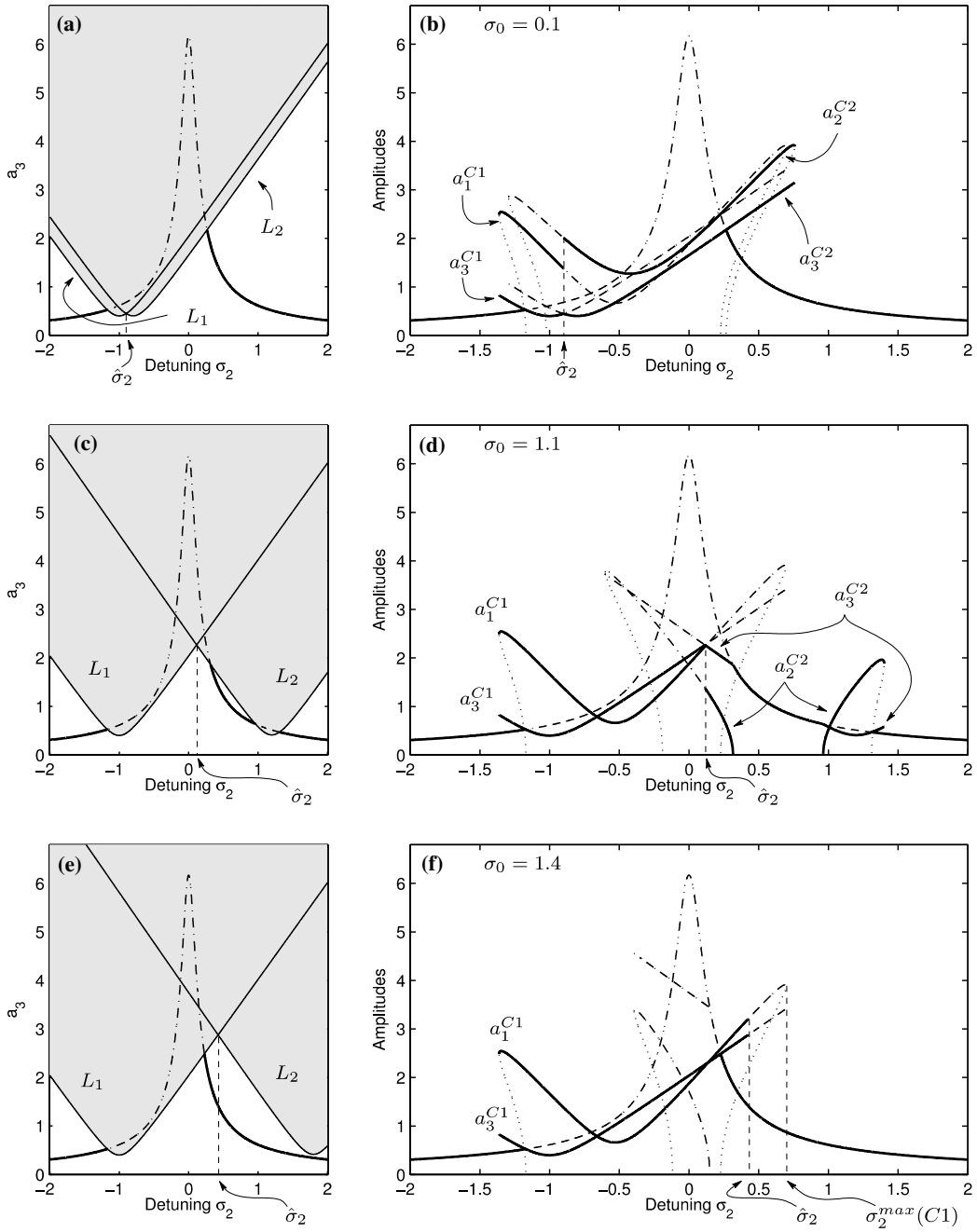

Fig. 14. Relative positions of the L_1 and L_2 stability curves (left column), and variation of the branches of solutions (right column), for increasing values of the internal detuning parameter σ_0. Other values are fixed at: $\alpha_1 = \alpha_2 = 4$, $\alpha_3 = \alpha_4 = 5$, $\mu_i = 0.1$, $Q = 10$, $\omega_1 = 4$, $\sigma_1 = 1$.

$$\sigma_2^{\max}(\mathrm{C1}) = \left(\frac{Q\alpha_1}{4\omega_1\omega_3} - \mu_3\sigma_1\right) \Big/ (2\mu_3 + \mu_1) \tag{40}$$

is lower than $\hat{\sigma}_2$. One can see in Fig. 14(f) that the stable portion of the C1 branch is shortened because of the second configuration. If one increases σ_0 further, the situation where $\hat{\sigma}_2 > \sigma_2^{\max}(\mathrm{C1})$ happens, the stable

portion of the C1 branch is not shortened and all happens as if only the first configuration was present in the dynamics.

The variations of the amplitudes of the solutions can be represented as functions of Q in order to highlight the phenomenon of saturation of the directly excited mode. Eq. (33a,b) and (34a,b) are then plotted for a given σ_2 and a variable Q. The value $\hat{\sigma}_2 = L_1 \cap L_2$ which determines the stability exchange, is independent of Q. Thus for a given external detuning, no stability exchange occurs, so that representation of this curves are the same as the already studied 1:2 resonance (see e.g. Nayfeh and Raouf, 1987; Nayfeh and Mook, 1979; Haddow et al., 1984).

5.5. Solution for the deflection

In steady state, the deflection of the shell is governed by Eq. (24), with the time functions for the three modes defined at first-order by

$$q_1(t) = a_1 \cos\left(\frac{\Omega}{2}t - \frac{\gamma_1 + \gamma_3}{2}\right), \tag{41a}$$

$$q_2(t) = a_2 \cos\left(\frac{\Omega}{2}t - \frac{\gamma_2 + \gamma_3}{2}\right), \tag{41b}$$

$$q_3(t) = a_3 \cos(\Omega t - \gamma_3), \tag{41c}$$

where a_i and γ_i take the values of a particular stable fixed point. Thus, γ_3 is the phase difference between directly excited mode q_3 and excitation, and γ_1 and γ_2 are the phase differences between modes excited through internal resonance on the one hand—respectively q_1 and q_2—and q_3 on the other hand.

6. Conclusion

In this paper, a detailed analysis of the non-linear vibrations of thin shallow spherical shells with a free edge has been proposed. The validity range of the governing equations has been quantified analytically and by comparison with a numerical solution. Then, a method of resolution via projection onto the linear modes basis has been detailed, hence presenting the general problem including asymmetric vibrations in a uniform manner.

The major set of results is the general non-linear modal interaction rules that have been established, thanks to computation of all coefficients of the non-linear quadratic and cubic terms that appear in the differential equations. Those coefficients are of major interest as their values govern the energy exchanges between mode that are likely to appear at the non-linear stage. It has been shown that an internal resonance relation between the natural frequencies of the shell is not a sufficient condition for the non-linear modal interaction to occur, since some coefficients of the non-linear terms vanish. This is a consequence of the rotational symmetry of the geometry of the structure, and coupling rules that hold on the number of nodal diameters of the involved modes have been derived. It is thus possible to predict if a particular *non-linear* energy exchange between modes is possible by considering only the *linear* modal analysis of the structure: the values of the natural frequencies determine the possible internal resonances and the number of nodal diameters of the involved modes enable to conclude on the activation of the modal interaction. Finally, an application has been treated: the specific case of a 1:1:2 internal resonance has been revisited, with emphasis on the effect of the slight imperfections of the structure on the energy transfers.

Beyond the important results derived throughout this study, the developed model framework can now be used for studying the rich variety of behaviour exhibited by non-linear shell vibrations. As the results of this

article are based on the rotational symmetry of the structure, similar results can be expected for other axisymmetric shells (cylindrical, conical or any profile). An experimental validation of the 1:1:2 internal resonance will be soon reported, showing the validity range and the precision of the model. More generally, this study can serve as a basis for analytical, or numerical-analytical solutions, computations of non-linear normal modes for prediction of the trend of non-linearity, or, in a different point of view, for analysis and synthesis of the sound produced by musical instruments such as cymbals and gongs (Chaigne et al., 2004).

Acknowledgement

The authors want to thank Éric Luminais for the scrupulous reading of the manuscript he has made.

Appendix A. Expression of the eigenmodes of the shell

This section is based on the work of Johnson and Reissner (1956), to which the interested reader can refer for further details.

A.1. General case

The eigenmodes are solutions of the linear, undamped and homogeneous problem related to Eqs. (11a) and (11b), that is written

$$\Delta\Delta w + \varepsilon_q \Delta F + \ddot{w} = 0, \tag{A.1a}$$

$$\Delta\Delta F = \frac{a^4}{Rh^3}\Delta w. \tag{A.1b}$$

The solution is separated in space and time by

$$w(r,\theta,t) = \Phi(r,\theta)q(t) \quad \text{and} \quad F(r,\theta,t) = \frac{a^4}{Rh^3}\Psi(r,\theta)q(t), \tag{A.2}$$

where w and F have the same time dependence because F is slaved to w by Eq. (A.1b). Thus, Φ and Ψ are solutions of

$$\Delta\Delta\Phi + \chi\Delta\Psi - \omega^2\Phi = 0 \quad \text{and} \quad \Delta\Delta\Psi = \Delta\Phi. \tag{A.3}$$

Eq. (A.3) writes

$$\Delta[\Delta\Delta + \chi - \omega^2]\Phi = 0, \tag{A.4}$$

where curvature parameter χ is defined by Eq. (8a). Two cases must now be considered.

- *Case I: modes written in terms of Bessel functions*

$$\omega^2 = \chi + \zeta^4, \quad \Delta[\Delta\Delta - \zeta^4]\Phi(r,\theta) = 0, \tag{A.5}$$

$$\Phi_{kn}(r,\theta) = \underbrace{\kappa_{kn}\left[A_k(\zeta_{kn})r^k + J_k(\zeta_{kn}r) + C_k(\zeta_{kn})I_k(\zeta_{kn}r)\right]}_{R_{kn}(r)} \left| \begin{matrix}\cos k\theta \\ \sin k\theta\end{matrix}\right., \tag{A.6}$$

$$\Psi_{kn}(r,\theta)=\kappa_{kn}\left[D_k(\zeta_{kn})r^k+\left(1+\frac{\zeta_{kn}^4}{\chi}\right)\frac{A_k(\zeta_{kn})}{4(k+1)}r^{k+2}-\frac{1}{\zeta_{kn}^2}(J_k(\zeta_{kn}r)-C_k(\zeta_{kn})I_k(\zeta_{kn}r))\right]\left|\begin{matrix}\cos k\theta\\ \sin k\theta\end{matrix}\right.. \tag{A.7}$$

- *Case II: modes written in terms of Kelvin functions*

$$\zeta^4<\chi,\quad \omega^2=\chi-\zeta^4,\quad \Delta\left[\Delta\Delta+\zeta^4\right]\Phi(r,\theta)=0, \tag{A.8}$$

$$\Phi_{kn}(r,\theta)=\underbrace{\kappa_{kn}[A_k(\zeta_{kn})r^k+\mathrm{ber}_k(\zeta_{kn}r)+C_k(\zeta_{kn})\mathrm{bei}_k(\zeta_{kn}r)]}_{R_{kn}(r)}\left|\begin{matrix}\cos k\theta\\ \sin k\theta\end{matrix}\right., \tag{A.9}$$

$$\Psi_{kn}(r,\theta)=\kappa_{kn}\left[D_k(\zeta_{kn})r^k+\left(1-\frac{\zeta_{kn}^4}{\chi}\right)\frac{A_k(\zeta_{kn})}{4(k+1)}r^{k+2}+\frac{1}{\zeta_{kn}^2}(\mathrm{bei}_k(\zeta_{kn}r)-C_k(\zeta_{kn})\mathrm{ber}_k(\zeta_{kn}r))\right]\left|\begin{matrix}\cos k\theta\\ \sin k\theta\end{matrix}\right.. \tag{A.10}$$

In the above equations, A_k, C_k and D_k are constants depending on boundary conditions, κ_{kn} is a normalization constant, k is the number of nodal diameters and n the number of nodal circles. J_k denotes the Bessel function of the first kind of order k and $I_k(x)=J_k(\mathrm{i}x)$ with $\mathrm{i}=\sqrt{-1}$. Kelvin functions are defined by $\mathrm{ber}_k(x)+\mathrm{i}\,\mathrm{bei}_k(x)=J_k(\mathrm{i}^{3/2}x)=(-1)^kI_k(i^{1/2}x)$. The normalization constant κ_{kn} is chosen so that Eq. (22) is fulfilled. Modes Ψ_{kn} are not normalized (κ_{kn} appears in Φ_{kn} as well as in Ψ_{kn}) as they are slaved to transverse modes Φ_{kn}.

A.2. Free-edge boundary conditions

Values of ζ, A_k, C_k and D_k are determined by introducing the boundary conditions. In the case of a free-edge, one obtains in a dimensionless form (see Eqs. (5a)–(5d)):

$$\Phi \quad\text{and}\quad \Psi \text{ are bounded at } r=0, \tag{A.11a}$$

$$\Phi_{,rr}+\nu\Phi_{,r}+\nu\Phi_{,\theta\theta}=0 \quad \text{at } r=1, \tag{A.11b}$$

$$\Phi_{,rrr}+\Phi_{,rr}-\Phi_{,r}+(2-\nu)\Phi_{,r\theta\theta}-(3-\nu)\Phi_{,\theta\theta}=0 \quad \text{at } r=1, \tag{A.11c}$$

$$\Psi_{,r}+\Psi_{,\theta\theta}=0,\quad \Psi_{,r\theta}-\Psi_{,\theta}=0 \quad \text{at } r=1. \tag{A.11d}$$

The expressions of the modes in terms of Bessel functions or Kelvin functions depends on the values of k, n and χ, results that are summarized in Table A.3.

- *Axisymmetric modes and modes with one nodal diameter* ($k\in\{0,1\}$)
  The modes express in terms of Bessel functions, so that $\zeta_{kn}=\zeta_{kn}^{(0)}$ is the nth zero of the equation

$$\mathscr{D}_k(\zeta)=0 \tag{A.12}$$

with $\mathscr{D}_k$ defined in Table A.1. This equation is independent of χ—and then of curvature—and is the equation with whom are calculated the natural frequencies (denoted by $\omega_{kn}^{(0)}=\zeta_{kn}^{(0)2}$) of the circular plate obtained with $\chi=0$. The natural frequencies of the shell are then, from Eq. (A.5), for all $k\in\{0,1\}$ and for all n

$$\omega_{kn}=\sqrt{\chi+\zeta_{kn}^4}=\sqrt{\chi+\omega_{kn}^{(0)2}}. \tag{A.13}$$

Table A.1
Coefficients for modes in terms of Bessel function

$M_{33} = \zeta(\nu-1)J'_k(\zeta) + [k^2(1-\nu) - \zeta^2]J_k(\zeta)$,
$M_{34} = \zeta(\nu-1)I'_k(\zeta) + [k^2(1-\nu) + \zeta^2]I_k(\zeta)$,
$M_{43} = \zeta[k^2(\nu-1) - \zeta^2]J'_k(\zeta) + k^2(1-\nu)J_k(\zeta)$,
$M_{44} = \zeta[k^2(\nu-1) + \zeta^2]I'_k(\zeta) + k^2(1-\nu)I_k(\zeta)$,
$\mathscr{D}_k(\zeta) = M_{33}M_{43} - M_{34}M_{44}$.
$\tilde{J}_k(\zeta) = kM_{33} + M_{43}, \tilde{I}_k(\zeta) = kM_{34} + M_{44}$,
$C_k(\zeta) = -\frac{\tilde{J}_k(\zeta)}{\tilde{I}_k(\zeta)}$,
$A_k(\zeta) = -\frac{2(1+k)\chi}{\zeta^2(\chi+\zeta^4)}\left[C_k(\zeta)(kI_k(\zeta) - \zeta I'_k(\zeta)) + (kJ_k(\zeta) - \zeta J'_k(\zeta))\right]$,
$D_k(\zeta) = \frac{1}{2\zeta^2}\left[C_k(\zeta)((k+2)I_k(\zeta) - \zeta I'_k(\zeta)) + ((k+2)J_k(\zeta) - \zeta J'_k(\zeta))\right]$,

The mode shapes are obtained by Eqs. (A.6), (A.7) and coefficients of Table A.1. One can show that $A_0 = A_1 = 0$. As a consequence, for all $k \in \{0,1\}$, both transverse and membrane mode shapes do not depend on curvature and transverse modes Φ_{kn} are identical to those of the corresponding plate (see e.g. Touzé et al., 2002). Thus, for all $k \in \{0,1\}$ and for all n

$$\Phi_{kn}(r,\theta) = \kappa_{kn}\left(J_k(\zeta_{kn}r) - \frac{\tilde{J}_k(\zeta_{kn})}{\tilde{I}_k(\zeta_{kn})}I_k(\zeta_{kn}r)\right)\begin{vmatrix}\cos k\theta\\ \sin k\theta\end{vmatrix} \tag{A.14}$$

with $\tilde{J}_k(\zeta)$ and $\tilde{I}_k(\zeta)$ defined in Table A.1.

- *Asymmetric modes with* $k \geqslant 2$
  The particular value of χ defined by

$$\chi_k^{lim} = \frac{(1-\nu)(3+\nu)k^2(k^2-1)}{1+\frac{1}{4}(1-\nu)(k-2) - \frac{k^2(k-1)(1-\nu)(4k-\nu+9)}{16(k+2)^2(k+3)}} \tag{A.15}$$

determines whether the modes writes in terms of Kelvin functions or Bessel functions.

– If $\chi < \chi_k^{lim}$, all modes are written in term of Bessel functions. ζ_{kn} is the $(n+1)$th zero of the equation

$$\frac{\zeta^4}{\chi} = \frac{\mathscr{S}_k(\zeta)}{\mathscr{R}_k(\zeta)} - 1 \quad \text{and} \quad \omega_{kn} = \sqrt{\chi + \zeta_{kn}^4}. \tag{A.16}$$

In the above equations,

$$\mathscr{S}_k(\zeta) = \frac{k}{\zeta}(\nu-1)(k-1)\left[\tilde{J}_k(\zeta)\left(\frac{k}{\zeta}I_k(\zeta) - I'_k(\zeta)\right) + \tilde{I}_k(\zeta)\left(\frac{k}{\zeta}J_k(\zeta) - J'_k(\zeta)\right)\right], \tag{A.17}$$

$$\mathscr{R}_k(\zeta) = -\frac{1}{2(1+k)}\mathscr{D}_k(\zeta), \tag{A.18}$$

with $\tilde{J}_k(\zeta)$, $\tilde{I}_k(\zeta)$ and $\mathscr{D}_k(\zeta)$ defined in Table A.1. The mode shapes are obtained by Eqs. (A.6) and (A.7) and coefficients of Table A.1.

– If $\chi > \chi_k^{lim}$, modes with no nodal circles ($n = 0$) writes in term of Kelvin functions and the others in terms of Bessel functions. Thus, ζ_{k0} is the only zero of equation:

$$\frac{\zeta^4}{\chi} = 1 - \frac{\mathscr{U}_k(\zeta)}{\mathscr{T}_k(\zeta)} \quad \text{and} \quad \omega_{k0} = \sqrt{\chi - \zeta_{k0}^4}. \tag{A.19}$$

Table A.2
Coefficients for modes in terms of Kelvin function

$M_{33} = \zeta^2 \mathrm{ber}_k''(\zeta) + \nu\zeta \mathrm{ber}_k'(\zeta) - k^2\nu \mathrm{ber}_k(\zeta)$
$M_{34} = \zeta^2 \mathrm{bei}_k''(\zeta) + \nu\zeta \mathrm{bei}_k'(\zeta) - k^2\nu \mathrm{bei}_k(\zeta)$
$M_{43} = \zeta^3 \mathrm{ber}_k'''(\zeta) + \zeta^2 \mathrm{ber}_k''(\zeta) - \zeta[1 + k^2(2-\nu)]\mathrm{ber}_k'(\zeta) + k^2(3-\nu)\mathrm{ber}_k(\zeta)$
$M_{44} = \zeta^3 \mathrm{bei}_k'''(\zeta) + \zeta^2 \mathrm{bei}_k''(\zeta) - \zeta[1 + k^2(2-\nu)]\mathrm{bei}_k'(\zeta) + k^2(3-\nu)\mathrm{bei}_k(\zeta)$
$\mathscr{D}_k(\zeta) = M_{33}M_{43} - M_{34}M_{44}$
$\tilde{J}_k(\zeta) = kM_{33} + M_{43}, \tilde{I}_k(\zeta) = kM_{34} + M_{44}$
$C_k(\zeta) = -\frac{\tilde{J}_k(\zeta)}{\tilde{I}_k(\zeta)},$
$A_k(\zeta) = \frac{2(1+k)\chi}{\zeta^2(\chi-\zeta^4)}[C_k(\zeta)(k\mathrm{ber}_k(\zeta) - \zeta\mathrm{ber}_k'(\zeta)) + (k\mathrm{bei}_k(\zeta) - \zeta\mathrm{bei}_k'(\zeta))]$
$D_k(\zeta) = -\frac{1}{2\zeta^2}[C_k(\zeta)((k+2)\mathrm{ber}_k(\zeta) - \zeta\mathrm{ber}_k'(\zeta)) + ((k+2)\mathrm{bei}_k(\zeta) - \zeta\mathrm{bei}_k'(\zeta))]$

Table A.3
Summary of calculation of modes of a spherical shell

$k \in \{0,1\}$	$\forall n \geqslant 1$	"Bessel" $\omega_{kn} = \sqrt{\chi + \omega_{kn}^{(0)2}}$ Eqs. (A.7), (A.12) and (A.14), Table A.1	
$k \geqslant 2$	$n = 0$	$\chi < \chi_k^{lim}$	$\chi > \chi_k^{lim}$
		"Bessel" $\omega_{k0} = \sqrt{\chi + \zeta_{k0}^4}$ Eqs. (A.6), (A.7) and (A.16) Table A.1	"Kelvin" $\omega_{k0} = \sqrt{\chi - \zeta_{k0}^4}$ Eqs. (A.9), (A.10), (A.19), Table A.2
$k \geqslant 2$	$n \geqslant 1$	"Bessel" $\omega_{kn} = \sqrt{\chi + \zeta_{kn}^4}$ Eqs. (A.6), (A.7) and (A.16), Table A.1	

$\omega_{kn}^{(0)}$ are the frequencies of the corresponding circular plate and χ_k^{lim} is defined by Eq. (A.15).

In the above equation

$$\mathscr{U}_k(\zeta) = -\frac{k}{\zeta}(\nu-1)(k-1)\left[\tilde{J}_k(\zeta)\left(\frac{k}{\zeta}\mathrm{ber}_k(\zeta) - \mathrm{ber}_k'(\zeta)\right) + \tilde{I}_k(\zeta)\left(\frac{k}{\zeta}\mathrm{bei}_k(\zeta) - \mathrm{bei}_k'(\zeta)\right)\right] \tag{A.20}$$

$$\mathscr{T}_k(\zeta) = -\frac{1}{2(1+k)}\mathscr{D}_k(\zeta) \tag{A.21}$$

and $\tilde{J}_k(\zeta)$, $\tilde{I}_k(\zeta)$ and $\mathscr{D}_k(\zeta)$ are defined in Table A.2. The corresponding mode shapes are obtained by Eq. (A.9) and (A.10) and coefficients of Table A.2. For modes with at least one nodal circle ($n \geqslant 1$), ζ_{kn} is the nth zero of Eq. (A.16), ω_{kn} is defined by Eq. (A.16) and the corresponding mode shapes writes with Eqs. (A.6) and (A.7) and coefficients of Table A.1.

Appendix B. Expression of functions Υ_b

Functions $\Upsilon_b(r,\theta)$ are solutions of

$$(\Delta\Delta - \xi^4)\Upsilon = 0, \tag{B.1a}$$

$$\Upsilon = 0 \quad \text{at } r = 1 \tag{B.1b}$$

$$\Upsilon_{,r} = 0 \quad \text{at } r = 1, \tag{B.1c}$$

$$\Upsilon \text{ is bounded in } r = 0. \tag{B.1d}$$

One obtains

$$\Upsilon_{lm}(r,\theta) = \lambda_{lm}\left[J_l(\xi_{lm}r) - \frac{J_l(\xi_{lm})}{I_l(\xi_{lm})}I_l(\xi_{lm}r)\right]\left|\begin{matrix}\cos l\theta \\ \sin l\theta\end{matrix}\right. \tag{B.2}$$

where the ξ_{lm} is the mth solution of the following equation:

$$J_{l-1}(\xi)I_l(\xi) - I_{l-1}(\xi)J_l(\xi) = 0. \tag{B.3}$$

Computed values of the ξ_{lm} can be found in Leissa (1993a). The normalization constant λ_{lm} is chosen so that Eq. (17) is fulfilled.

Appendix C. Calculation of coupling coefficients β^s_{pq} and Υ^s_{pqu}

The different modes that are necessary for the calculation of coefficients β^s_{pq} and Γ^s_{pqu} (Eqs. (20) and (21)) are noted separated in r and θ

$$\Phi_{0n}(r) = R_{0n}(r) \quad \text{for } k = 0; \quad \left.\begin{matrix}\Phi_{kn1}(r,\theta) \\ \Phi_{kn2}(r,\theta)\end{matrix}\right| = R_{kn}(r)\left|\begin{matrix}\cos k\theta \\ \sin k\theta\end{matrix}\right. \quad \text{for } k \geqslant 1;$$

$$\Psi_{0n}(r) = S_{0n}(r) \quad \text{for } k = 0; \quad \left.\begin{matrix}\Psi_{kn1}(r,\theta) \\ \Psi_{kn2}(r,\theta)\end{matrix}\right| = S_{kn}(r)\left|\begin{matrix}\cos k\theta \\ \sin k\theta\end{matrix}\right. \quad \text{for } k \geqslant 1;$$

$$\Upsilon_{0m}(r) = T_{0m}(r) \quad \text{for } l = 0; \quad \left.\begin{matrix}\Upsilon_{lm1}(r,\theta) \\ \Upsilon_{lm2}(r,\theta)\end{matrix}\right| = T_{lm}(r)\left|\begin{matrix}\cos l\theta \\ \sin l\theta\end{matrix}\right. \quad \text{for } l \geqslant 1.$$

In the following, subscripts γ and δ will denote the nature in cosine ($\gamma = 1$) or sine ($\gamma = 2$) of the considered mode. In order to lighten notations, subscripts p, q, s and b will sometimes replace triplets (k_p, n_p, γ_p) to identify modes Φ, Ψ and Υ. For example, Φ_p is the same than $\Phi_{k_p n_p \gamma_p}$, so that $\Phi_p(r,\theta) = R_{k_p n_p}(r)\cos k_p\theta$ if $\gamma_p = 1$ and $\Phi_p(r,\theta) = R_{k_p n_p}(r)\sin k_p\theta$ if $\gamma_p = 2$. In the same manner, $R_p(r) = R_{k_p n_p}(r)$.

C.1. Quadratic coefficients β^s_{pq}

Their expression is (Eq. (20)):

$$\beta^s_{pq} = -\underbrace{\iint_{\mathscr{S}_\perp} \Phi_s L(\Phi_p, \Psi_q)\mathrm{d}S}_{\mathscr{I}^\Psi(s,p,q)} - \frac{1}{2}\sum_{b=1}^{+\infty}\frac{1}{\xi_b^4}\underbrace{\iint_{\mathscr{S}_\perp} L(\Phi_p, \Phi_q)\Upsilon_b\,\mathrm{d}S}_{\mathscr{I}(p,q,b)}\underbrace{\iint_{\mathscr{S}_\perp}\Phi_s\Delta\Upsilon_b\mathrm{d}S}_{\mathscr{K}(s,b)}. \tag{C.1}$$

Following the definition of L (Eq. (4)) and integrating over domain $\mathscr{S}_\perp$ by separation of variables r and θ, one obtains

$$\mathscr{I}(p,q,b) = \mathbf{I}_1(p,q,b)\mathbf{\Pi}^{(1)}_{\gamma_p\gamma_q\delta}(k_p,k_q,l) - 2k_pk_q\mathbf{I}_2(p,q,b)\mathbf{\Pi}^{(2)}_{\gamma_p\gamma_q\delta}(k_p,k_q,l), \tag{C.2}$$

$$\mathscr{J}^{\Psi}(s,p,q) = \mathbf{J}_1^{\Psi}(s,p,q)\mathbf{\Pi}^{(1)}_{\gamma_s\gamma_p\gamma_q}(k_s,k_p,k_q) - 2k_pk_q\mathbf{J}_2^{\Psi}(s,p,q)\mathbf{\Pi}^{(3)}_{\gamma_s\gamma_p\gamma_q}(k_s,k_p,k_q), \tag{C.3}$$

$$\mathscr{K}(s,b) = \mathbf{K}(s,b)\mathbf{\Pi}^{(4)}_{\gamma_s\delta}(s,b), \tag{C.4}$$

where

$$\mathbf{I}_1(p,q,b) = \int_0^1 \left[R_p''\left(R_q' - k_q^2\frac{R_q}{r}\right) + R_q''\left(R_p' - k_p^2\frac{R_p}{r}\right)\right]T_b\mathrm{d}r, \tag{C.5}$$

$$\mathbf{I}_2(p,q,b) = \int_0^1 \frac{1}{r}\left[R_p' - \frac{R_p}{r}\right]\left[R_q' - \frac{R_q}{r}\right]T_b\mathrm{d}r, \tag{C.6}$$

$$\mathbf{J}_1^{\Psi}(s,p,q) = \int_0^1 R_s\left[R_p''\left(S_q' - k_q^2\frac{S_q}{r}\right) + S_q''\left(R_p' - k_p^2\frac{R_p}{r}\right)\right]\mathrm{d}r, \tag{C.7}$$

$$\mathbf{J}_2^{\Psi}(s,p,q) = \int_0^1 R_s\frac{1}{r}\left[R_p' - \frac{R_p}{r}\right]\left[S_q' - \frac{S_q}{r}\right]\mathrm{d}r, \tag{C.8}$$

$$\mathbf{K}(s,b) = \int_0^1 R_s\left(rT_b'' + T_b' - l^2\frac{T_b}{r}\right)\mathrm{d}r \tag{C.9}$$

and

$$\mathbf{\Pi}^{(1)}_{\gamma\gamma'\delta}(k,k',l) = \int_0^{2\pi}\begin{vmatrix}\cos k\theta & \cos k'\theta & \cos l\theta\\ \cdot & \cdot & \cdot\\ \sin k\theta & \sin k'\theta & \sin l\theta\end{vmatrix}\mathrm{d}\theta,$$

$$\mathbf{\Pi}^{(2)}_{\gamma\gamma'\delta}(k,k',l) = \int_0^{2\pi}\begin{vmatrix}-\sin k\theta & -\sin k'\theta & \cos l\theta\\ \cdot & \cdot & \cdot\\ \cos k\theta & \cos k'\theta & \sin l\theta\end{vmatrix}\mathrm{d}\theta,$$

$$\mathbf{\Pi}^{(3)}_{\gamma\gamma'\delta}(k,k',l) = \int_0^{2\pi}\begin{vmatrix}\cos k\theta & -\sin k'\theta & -\sin l\theta\\ \cdot & \cdot & \cdot\\ \sin k\theta & \cos k'\theta & \cos l\theta\end{vmatrix}\mathrm{d}\theta,$$

$$\mathbf{\Pi}^{(4)}_{\gamma\delta}(k,l) = \int_0^{2\pi}\begin{vmatrix}\cos k\theta & \cos l\theta\\ \cdot & \cdot\\ \sin k\theta & \sin l\theta\end{vmatrix}\mathrm{d}\theta.$$

The above notations mean that any $\mathbf{\Pi}_{\gamma\gamma'\delta}$ is obtained by making the product of three functions sine and/or cosine, each one being taken in a column of the above matrices. (γ,γ',δ) refers, respectively, to the first, the second and the third column and their values determine the line. For example, with $(\gamma,\gamma',\delta) = (2,1,2)$

$$\mathbf{\Pi}^{(3)}_{212}(k,k',l) = -\int_0^{2\pi}\sin k\theta\sin k'\theta\cos l\theta\mathrm{d}\theta.$$

Several coefficients $\mathbf{\Pi}$ equal zero for specific values of (k,k',l) (the numbers of nodal diameters) and (γ,γ',δ) (the nature in sine and/or cosine). This is the cause of the vanishing of some coefficients β^s_{pq}. The results on

Table C.1
Conditions on modes Φ_p, Φ_q, Φ_s and Υ_b that lead to non-zero $\mathscr{I}(p,q,b)$, $\mathscr{K}(s,b)$ and $\mathscr{J}^{\Psi}(s,p,q)$

$\mathscr{J}^{\Psi}(s,p,q)\neq 0$ $\Downarrow$ $k_s\in\{k_p+k_q,\lvert k_p-k_q\rvert\}$			$\mathscr{I}(p,q,b)\neq 0$ $\Downarrow$ $l\in\{k_p+k_q,\lvert k_p-k_q\rvert\}$			$\mathscr{K}(s,b)\neq 0$ $\Downarrow$ $l=k_s$	
Φ_s,γ_s	Φ_p,γ_p	$\Phi_q,\gamma_q,\Psi_q,\gamma_q$	Φ_p,γ_p	Φ_q,γ_q	Υ_b,δ	Φ_s,γ_s	Υ_b,δ
cos, 1	cos, 1	cos, 1	cos, 1	cos, 1	cos, 1	cos, 1	cos, 1
	sin, 2	sin, 2	sin, 2	sin, 2		sin, 2	sin, 2
sin, 2	cos, 1	sin, 2	sin, 2	cos, 1	sin, 2		
	sin, 2	cos, 1	cos, 1	sin, 2			

$\mathscr{I}(p,q,b)$, $\mathscr{K}(s,b)$ and $\mathscr{J}^{\Psi}(s,p,q)$ are summarized in Table C.1. To obtain a non-zero β^s_{pq}, one must have either $\mathscr{J}^{\Psi}(s,p,q)\neq 0$ or at least one mode Υ_b so that $\mathscr{I}(p,q,b)\mathscr{K}(s,b)\neq 0$. It is summarized in Table 2.

C.2. Cubic coefficients Γ^s_{pqu}

Their expression is (Eq. (20)):

$$\Gamma^s_{pqu}=\frac{1}{2}\sum_{b=1}^{+\infty}\frac{1}{\xi_b^4}\underbrace{\int\!\!\int_{\mathscr{S}}L(\Phi_p,\Phi_q)\Upsilon_b\mathrm{d}S}_{\mathscr{I}(p,q,b)}\underbrace{\int\!\!\int_{\mathscr{S}}\Phi_sL(\Phi_u,\Upsilon_b)\mathrm{d}S}_{\mathscr{J}^{\Upsilon}(s,u,b)},\tag{C.10}$$

where $\mathscr{I}(p,q,b)$ has been calculated in the above section and $\mathscr{J}^{\Upsilon}(s,u,b)$ has the same structure than $\mathscr{J}^{\Psi}(s,p,q)$ and writes

$$\mathscr{J}^{\Upsilon}(s,u,b)=\mathbf{J}_1^{\Upsilon}(s,u,b)\mathbf{\Pi}^{(1)}_{\gamma_s,\gamma_u,\delta}(k_s,k_u,l)-2k_ul\mathbf{J}_2^{\Upsilon}(s,u,b)\mathbf{\Pi}^{(3)}_{\gamma_s,\gamma_u,\delta}(k_s,k_u,l),\tag{C.11}$$

where

$$\mathbf{J}_1^{\Upsilon}(s,u,b)=\int_0^1R_s\left[R_u''\left(T_b''-l^2\frac{T_b}{r}\right)+T_b''\left(R_u'-k_u^2\frac{R_u}{r}\right)\right]\mathrm{d}r,\tag{C.12}$$

$$\mathbf{J}_2^{\Upsilon}(s,s,b)=\int_0^1R_s\frac{1}{r}\left[R_u'-\frac{R_u}{r}\right]\left[T_b'-\frac{T_b}{r}\right]\mathrm{d}r.\tag{C.13}$$

Again, non-zero Γ^s_{pqu} are obtained if $\mathscr{I}(p,q,b)\mathscr{J}^{\Upsilon}(s,u,b)\neq 0$, cases specified in Table C.2. The consequences on Γ^s_{pqu} are summarized in Table 2.

Table C.2
Conditions on modes Φ_p, Φ_q, Φ_s, Φ_u and Υ_b that lead to non-zero $\mathscr{I}(p,q,b)$ and $\mathscr{J}^{\Upsilon}(s,p,q)$

$\mathscr{I}(p,q,b)\neq 0$ $\Downarrow$ $l\in\{k_p+k_q,\lvert k_p-k_q\rvert\}$			$\mathscr{J}^{\Upsilon}(s,u,b)\neq 0$ $\Downarrow$ $l\in\{k_s+k_u,\lvert k_s-k_u\rvert\}$		
Φ_p,γ_p	Φ_q,γ_q	Υ_b,δ	Φ_s,γ_s	Φ_u,γ_u	Υ_b,δ
cos, 1	cos, 1	cos, 1	cos, 1	cos, 1	cos, 1
sin, 2	sin, 2		sin, 2	sin, 2	
sin, 2	cos, 1	sin, 2	sin, 2	cos, 1	sin, 2
cos, 1	sin, 2		cos,1	sin, 2	

References

Alhazza, K.A., 2002. Nonlinear vibrations of doubly curved cross-ply shallow shells. Ph.D. Thesis, Virginia Polytechnic Institute and State University.

Amabili, M., Païdoussis, M.P., 2003. Review of studies on geometrically nonlinear vibrations and dynamics of circular cylindrical shells and panels, with and without fluid–structure interaction. ASME Appl. Mech. Rev. 56 (4), 349–381.

Amabili, M., Pellicano, R., Païdoussis, M.P., 1998. Nonlinear vibrations of simply supported circular cylindrical shells, coupled to quiescent fluid. J. Fluids Struct. 12, 883–918.

Amabili, M., Pellicano, F., Païdoussis, M.P., 1999. Non-linear dynamics and stability of circular cylindrical shells containing flowing fluid, part II: large-amplitude vibrations without flow. J. Sound Vib. 228 (5), 1103–1124.

Amabili, M., Pellicano, F., Vakakis, A.F., 2000. Nonlinear vibrations and multiple resonances of fluid-filled, circular shells, part 1: equations of motion and numerical results. ASME J. Vib. Acoust. 122, 346–354.

Benedettini, F., Rega, G., Alaggio, R., 1995. Non-linear oscillations of a four-degree-of-freedom model of a suspended cable under multiple internal resonance conditions. J. Sound Vib. 182 (5), 775–798.

Chaigne, A., Touzé, C., Thomas, O., 2004. Mechanical models of musical instruments and sound synthesis: the case of gongs and cymbals. In: Proceedings of the International Symposium on Musical Acoustics. Nara, Japan.

Chin, C.-M., Nayfeh, A.H., 2001. A second-order approximation of multi-modal interactions in externally excited circular cylindrical shells. Nonlinear Dynam. 26, 45–66.

Chu, H.-N., Herrmann, G., 1956. Influence of large amplitudes on free flexural vibrations of rectangular elastic plates. J. Appl. Mech. 23, 532–540.

Donnell, L.H., 1934. A new theory for the buckling of thin cylinders under axial compression and bending. Trans. Am. Soc. Mech. Eng. 56, 795–806.

Efstathiades, G.J., 1971. A new approach to the large-deflction vibrations of imperfect circular disks using Galerkin's procedure. J. Sound Vib. 16 (2), 231–253.

Evensen, D.A., Fulton, R.E., oct 1965. Some studies on the nonlinear dynamic response of shell-type structures. Tech. Rep. TMX 56843, NASA Langley Research Center.

Evensen, H.A., Evan-Iwanowsky, R.M., 1967. Dynamic response and stability of shallow spherical shells subject to time-dependant loading. AIAA J. 5 (5), 969–976.

Gonçalves, P.B., 1994. Axisymmetric vibrations of imperfect shallow spherical caps under pressure loading. J. Sound Vib. 174 (2), 249–260.

Grossman, P.L., Koplik, B., Yu, Y.-Y., 1969. Nonlinear vibrations of shallow spherical shells. ASME J. Appl. Mech 39E, 451–458.

Guckenheimer, J., Holmes, P., 1983. Nonlinear Oscillations, Dynamical Systems and Bifurcations of Vector Fields. Springer-Verlag, New York.

Guckenheimer, J., Myers, M., Wicklin, F., Worfolk, P., 1995. Dstool: a dynamical system toolkit with an interactive graphical interface. Technical Report, Center for Applied Mathematics, Cornell University.

Haddow, A.G., Barr, A.D.S., Mook, D.T., 1984. Theoretical and experimental study of modal interaction in a two-degree-of-freedom structure. J. Sound Vib. 97, 451–473.

Hamdouni, A., Millet, O., 2003. Classification of thin shell models deduced from the nonlinear three-dimensional elasticity, part I: the shallow shells. Arch. Mech. 55 (2), 135–175.

Hui, D., 1983. Large-amplitude vibrations of geometrically imperfect shallow spherical shells with structural damping. AIAA J. 21 (12), 1736–1741.

Johnson, M.W., Reissner, E., 1956. On transverse vibrations of shallow spherical shells. Quart. Appl. Math. 15 (4), 367–380.

Kalnins, A., 1964. Effect of bending on vibrations of spherical shells. J. Acoust. Soc. Am. 36 (1), 74–81.

Koiter, W.T., 1965. On the nonlinear theory of thin elastic shells, part I, II and III. Proc. Kon. Neth. Akad. Wet. B69, 1–54.

Lacarbonara, W., Rega, G., Nayfeh, A.H., 2003. Resonant non-linear normal modes, part I: analytical treatment for structural one-dimensional systems. Int. J. Non-Linear Mech. 38, 851–872.

Lee, W.K., Yeo, M.H., Samoilenko, S.B., 2003. The effect of the number of nodal diameters on non-linear interactions in two asymmetric vibration modes of a circular plate. J. Sound. Vib 268 (5), 1013–1023.

Leissa, A.W., 1993a. Vibration of plates. Acoustical Society of America (original issued NASA SP-160, 1969).

Leissa, A.W., 1993b. Vibration of shells. Acoustical Society of America (original issued NASA SP-288, 1973).

Leissa, A.W., Kadi, A.S., 1971. Curvature effects on shallow shell vibrations. J. Sound. Vib. 16 (2), 173–187.

Lobitz, D.W., Nayfeh, A.H., Mook, D.T., 1977. Non-linear analysis of vibrations of irregular plates. J. Sound. Vib. 50 (2), 203–217.

Marguerre, K., 1938. Zur Theorie der Gekrümmten Platte Grosser Formänderung. In: Proceedings of the 5th International Congress on Applied Mechanics, pp. 93–101.

Miles, J.W., 1984. Resonantly forced motion of two quadratically coupled oscillators. Physica D 13, 247–260.

Morand, H.J.-P., Ohayon, R., 1995. Fluid Structure Interaction. John Wiley and Sons, New York.

Moussaoui, F., Benamar, R., 2002. Non-linear vibrations of shell-type structures: a review with bibliography. J. Sound. Vib. 255 (1), 161–184.
Mushtari, K.M., Galimov, K.Z., 1961. Non-linear theory of thin elastic shells. Israel Program for Scientific Translations (Russian ed., 1957).
Nayfeh, A.H., 2000. Nonlinear interactions: analytical, computational and experimental methods. In: Wiley Series in Nonlinear Science, New York.
Nayfeh, A.H., Balachandran, B., 1989. Modal interactions in dynamical and structural systems. ASME Appl. Mech. Rev. 42 (11), 175–201.
Nayfeh, A.H., Mook, D.T., 1979. Nonlinear Oscillations. John Wiley and Sons Inc, New York.
Nayfeh, A.H., Nayfeh, J.F., Mook, D.T., 1992. On methods for continuous systems with quadratic and cubic nonlinearities. Nonlinear Dynam. 3, 145–162.
Nayfeh, A.H., Nayfeh, S.A., 1994. On nonlinear modes of continuous systems. J. Vib. Acoust. 116, 129–136.
Nayfeh, A.H., Raouf, R.A., 1987. Non-linear oscillations of circular cylindrical shells. Int. J. Solids Struct. 23 (12), 1625–1638.
Nayfeh, A.H., Zavodney, L.D., 1988. Experimental observation of amplitude and phase-modulated responses of two internally coupled oscillators to a harmonic excitation. ASME J. Appl. Mech. 55, 706–710.
Pellicano, F., Amabili, M., Vakakis, A.F., 2000. Nonlinear vibrations and multiple resonances of fluid-filled, circular shells, part 2: perturbation analysis. ASME J. Vib. Acoust. 122, 355–364.
Qatu, M.S., 2002. Recent research advances in the dynamic behavior of shells: 1989–2000, part 2: homogeneous shells. ASME Appl. Mech. Rev. 55 (5), 415–434.
Raman, A., Mote Jr., C.D., 2001. Effects of imperfection on the non-linear oscillations of circular plates spinning near critical speed. Int. J. Non-linear Mech. 36, 261–289.
Robie, F.M., Popov, A.A., Thompson, J., 1999. Auto-parametric resonance in cylindrical shells using geometric averaging. J. Sound Vib. 227 (1), 65–84.
Soedel, W., 1981. Vibrations of Shells and Plates. Marcel-Dekker Inc., New York.
Sridhar, S., Mook, D.T., Nayfeh, A.H., 1975. Non-linear resonances in the forced responses of plates, part I: symmetric responses of circular plates. J. Sound Vib. 41 (3), 359–373.
Sridhar, S., Mook, D.T., Nayfeh, A.H., 1978. Non-linear resonances in the forced responses of plates, part II: asymmetric responses of circular plates. J. Sound Vib. 59 (2), 159–170.
Thomas, O., Touzé, C., Chaigne, A., Sep. 2001. Non-linear behavior of gongs through the dynamic of simple rods systems. In: Proceedings of the International Symposium on Musical Acoustics, Perugia, Italy, pp. 173–178.
Tien, W.M., Namachchivaya, N.S., Bajaj, A.K., 1994. Non-linear dynamics of as shallow arch under periodic excitation, I: 1:2 internal resonance. Int. J. Nonlinear Mech. 29 (3), 349–366.
Tobias, S.A., Arnold, R.N., 1957. The influence of dynamical imperfection on the vibration of rotating disks. Proc. of the Instn. of Mech. Eng. 171, 669–690.
Touzé, C., Thomas, O., 2004. Reduced-order modeling for a cantilever beam subjected to harmonic forcing. In: proc. of EUROMECH Colloquium 457: nonlinear modes of vibrating systems. Fréjus, France, pp. 165–168.
Touzé, C., Thomas, O., Chaigne, A., 2002. Asymmetric non-linear forced vibrations of free-edge circular plates, part 1: theory. J. Sound. Vib. 258 (4), 649–676.
Touzé, C., Thomas, O., Chaigne, A., 2004. Hardening/softening behaviour in nonlinear oscillations of structural systems using non-linear normal modes. J. Sound. Vib. 273 (1–2), 77–101.
Verpeaux, P., Charras, T., Millard, A., 1988. Calcul des structures et intelligence artificielle. Pluralis, ed., Paris, http://www-cast3m.cea.fr, Chapter CASTEM 2000: Une approche moderne du calcul des structures.
Yamamoto, T., Yasuda, K., 1977. On the internal resonance in a non-linear two-degree-of-freedom system. Bull. Jpn. Soc. Mech. Eng. 20, 168–175.
Yasuda, K., Kushida, G., 1984. Nonlinear forced oscillations of a shallow spherical shell. Bull. JSME 27 (232), 2233–2240.
Ye, Z.M., 1997. The non-linear vibration and dynamic instability of thin shallow shells. J. Sound Vib. 202 (3), 303–311.
Yeo, M.H., Lee, W.K., 2002. Corrected solvability conditions for non-linear asymmetric vibrations of a circular plate. J. Sound. Vib 257 (4), 653–665.

Annexe 3 : Hardening/softening behaviour in non-linear oscillations of structural systems using non-linear normal modes

Cette annexe donne le texte complet de l'article :

C. Touzé, O. Thomas et A. Chaigne : Hardening/softening behaviour in non-linear oscillations of structural systems using non-linear normal modes, Journal of Sound and Vibration, **273**(1-2), pp 77-101, 2004.

Available online at www.sciencedirect.com
SCIENCE DIRECT®
Journal of Sound and Vibration 273 (2004) 77–101
JOURNAL OF SOUND AND VIBRATION
www.elsevier.com/locate/jsvi

Hardening/softening behaviour in non-linear oscillations of structural systems using non-linear normal modes

C. Touzé*, O. Thomas, A. Chaigne

ENSTA - UME, Chemin de la Hunière, 91761 Palaiseau Cedex, France

Received 26 September 2002; accepted 14 April 2003

Abstract

The definition of a non-linear normal mode (NNM) as an invariant manifold in phase space is used. In conservative cases, it is shown that normal form theory allows one to compute all NNMs, as well as the attendant dynamics onto the manifolds, in a single operation. Then, a single-mode motion is studied. The aim of the present work is to show that too severe truncature using a single linear mode can lead to erroneous results. Using single-non-linear mode motion predicts the correct behaviour. Hence, the non-linear change of co-ordinates allowing one to pass from the linear modal variables to the normal ones, linked to the NNMs, defines a framework to properly truncate non-linear vibration PDEs. Two examples are studied: a discrete system (a mass connected to two springs) and a continuous one (a linear Euler–Bernoulli beam resting on a non-linear elastic foundation). For the latter, a comparison is given between the developed method and previously published results.

1. Introduction

One main characteristic in non-linear oscillations is the frequency dependence on vibration amplitude, which can be of hardening or softening type [1]. As a system vibrates with large amplitudes, it is a well-established fact that the mode shapes also depend on vibration amplitude (see e.g. Ref. [2]). Hence, a correct modelling has to tackle these two difficulties. Moreover, drastic reductions of the dimension of the studied phase space is a goal that is often pursued. Indeed, deriving accurate reduced order models is an appreciated methodology since it allows one to predict carefully a number of different dynamical features through simple calculations. It gives an

*Corresponding author. Tel.: +33-1-69-31-97-34; fax: +33-1-69-31-99-97.
E-mail address: touze@ensta.fr (C. Touzé).

0022-460X/$ - see front matter © 2003 Elsevier Ltd. All rights reserved.
doi:10.1016/j.jsv.2003.04.005

alternative to crude numerical computations, as well as insight into and fine comprehension of the model studied.

When considering a single-mode motion, a common—though crude—approximation, consists of projecting the non-linear partial differential equations (PDEs) governing the motion onto the considered linear eigenmode. Unfortunately, this method sometimes gives wrong qualitative results about the trend of non-linearity. More precisely, it has been frequently observed that this truncature predicts a hardening behaviour whereas experimental measures display a softening one. This problem has been encountered in circular cylindrical shells vibrations for a long time. A complete and interesting review of the literature on this problem, as well as experimental measures can be found in Refs. [3,4]. The same problematic was also met in the non-linear vibrations of buckled beams [5]. As it will be shown next, this is specific to quadratic non-linearity.

In a series of papers, Nayfeh et al. pointed out that these too severe truncatures (referred to as "the discretization method" in their papers) can lead to erroneous quantitative as well as qualitative results [6–9]. Methodologies were proposed in order to overcome these errors, by using a perturbation technique (the method of multiple scales) directly into the non-linear PDE [5,8], or by considering a spatial adjustable function in addition to the linear eigenmode [9].

An alternative, but *in fine* equivalent approach to these difficulties, is proposed by Shaw and Pierre [10,11], by constructing a mathematical framework in order to derive the definition of a *non-linear normal mode* (NNM), a concept that was proposed by Rosenberg [12] and used by several different authors, see for example Refs. [13–19]. A NNM is defined as an invariant manifold in phase space, which is tangent to its linear counterpart (the linear eigenspace) at the origin. Shaw and Pierre used centre manifold reduction theorem [10,11,19] in order to compute the geometry of these invariant manifolds. The main idea outlined is that, at the non-linear stage, one has to span the phase space with invariant manifolds rather than still using linear eigenspaces. This leads to definition of a single-mode motion with an amplitude-dependent mode shape.

The objective of this contribution is to show the equivalence of these methods, which found their theoretical foundations in Poincaré and Poincaré–Dulac's theorems [20–23]. Although these results are not new, a systematic procedure is proposed, allowing one to derive reduced order models that capture the effective trend of non-linearity without increasing the complexity, and that display amplitude-dependent mode shapes. Normal form theory defines new co-ordinates linked to the invariant manifolds, as well as the non-linear relation between these new co-ordinates and the initial (modal) ones. It results in a curved invariant-based span of the phase space. Moreover, as a result of this operation, the attendant dynamics onto the manifolds is simply given by the normal form of the problem at hand.

Normal form theory has been widely used in the past few years. To the authors' knowledge, it has first been introduced to solve non-linear vibration problems by Jezequel and Lamarque [14,15]. However, it has always been derived under its complex-diagonal form, as recommended by the mathematics. The book by Nayfeh [24] sets down normal form theory as a perturbation method amongst others and yields comparison with the multiple-scales method. Pellicano and Mastroddi used it in Ref. [25] to specify the idea of non-linear superposition, which was incorrectly proposed in Ref. [10]. Morino et al. [26] called it a "Lie transform", Amabili et al. [3] derived it in a general manner for shell vibrations problems. All these calculations used complex-diagonal form. Here, real blocks are used at the linear stage. This allows one to derive all the

calculations in a framework that is more directly readable for the mechanics community, as well as to directly compare the results with the method developed in Refs. [10,11,16,27,28].

The calculations presented are general and derived for a set of N non-linear oscillators, with N as large as required. This is to stress that the method of real normal form, as formulated here, should be systematically used in the procedure for studying non-linear vibration problems. More precisely, it is suggested to:

(i) Perform the discretization of the system through projection onto the complete linear mode basis.
(ii) Compute the non-linear change of co-ordinates, allowing one to pass from linear modal co-ordinates to *normal* co-ordinates, linked to the NNMs.

It is only when these two steps have been achieved that one could state the problem of an efficient truncature.

Simple results will be shown here for single non-linear modal motions, as a first application of this general procedure. It is shown that taking the NNMs into account can change quantitatively, as well as qualitatively, the hardening or softening behaviour of the considered mode. These theoretical results are illustrated by two examples. First, a discrete system is studied. Secondly, a linear Euler–Bernoulli beam resting on a non-linear elastic foundation is considered. This simple example has already been tackled by many authors (see e.g. Refs. [5,8,9,29–31]). A detailed comparison is provided here between the method of invariant manifold and the one proposed in Refs. [5,8], which will allow illustration of their equivalence.

2. Theory

2.1. Framework

Non-linear oscillations of structural undamped systems with geometric quadratic and cubic non-linearities are considered in the following. The motion of continuous systems is assumed to be governed by partial differential equations (e.g. Von Kármán type equations for beams, plates, archs and shells), subjected to boundary conditions. Because of the orthogonality properties of the linear eigenmodes, it is a common method to separate time and space variables, and to project the PDE onto the linear modes basis. Letting

$$w(\mathbf{x},t)=\sum_{p=1}^{+\infty} X_p(t)\Phi_p(\mathbf{x}), \tag{1}$$

where w is the displacement, $\mathbf{x}$ the spatial variables, X_p the modal co-ordinate associated to the linear eigenmode Φ_p, the problem is equivalent to

$$\forall p=1,\ldots,+\infty\colon\ \ddot{X}_p+\omega_p^2X_p+\sum_{i=1}^{+\infty}\sum_{j\geqslant i}^{+\infty}g_{ij}^pX_iX_j+\sum_{i=1}^{+\infty}\sum_{j\geqslant i}^{+\infty}\sum_{k\geqslant j}^{+\infty}h_{ijk}^pX_iX_jX_k=0. \tag{2}$$

The coefficients g_{ij}^p and h_{ijk}^p arise from the projection of the non-linear terms of the PDE onto the linear modes. Damping is omitted, mainly because only lightly damped systems are considered,

for which $\omega_p \gg \mu_p$ (where μ_p stands for the modal damping). A finite number N of linear modes is then retained in the analysis, where N is assumed to be large.

The formulation given in Eqs. (1) and (2) has been retained with the purpose of application to continuous structures. However, discrete systems can also be treated. The assumption of undamped system is central to this work since the eigenspectrum of the PDE enforced the structure of Eq. (2), as well as its normal form [21–23]. In particular, gyroscopic systems, that are conservative, can be treated with the proposed method: one has just to express the temporal problem into the form of Eq. (2), which is possible for gyroscopic systems as long as they are stable, since their eigenspectrum is composed of purely imaginary complex conjugates.

The idea of defining a non-linear normal mode is to extend the decoupling of the linear eigenspaces exhibited at the linear stage. Letting $g_{ij}^p \equiv h_{ijk}^p \equiv 0$ in Eq. (2), and initiating a motion along the pth eigendirection results in a motion which is always contained within it. This is the *invariance* property one would be able to extend to the non-linear regime.

Moreover, a *physical* definition of a NNM, as it was given for example by Rosenberg [12], is a motion of the structure such that all points pass through their static-equilibrium positions and achieve their maximum displacements at the same time. Thus, a physical NNM motion can be mathematically described by a single displacement–velocity pair governed by a single oscillator. In phase space, such motions occur on two-dimensional invariant manifolds only. The idea is then to span the phase space with the invariant manifolds, and no longer with the linear eigenspaces.

Normal form theory has been developed for a long time and relies upon ideas that are summarized in Poincaré and Poincaré-Dulac's theorems (see Refs. [21–23] and references therein). However, in vibration theory, it has generally been used as a perturbation method amongst others [24]. Here it will be used as a general tool that enables spanning the phase space with invariant manifolds, hence generalizing the approach used in the definition of the NNMs by other authors [10,11,14]. To specify the idea before entering the calculations, the situation is sketched in Fig. 1, where the phase space in the vicinity of the origin (which is the position of the structure at rest) is represented. Linear normal modes are two-dimensional orthogonal planes: they are represented here by lines for convenience, and only two of them are shown, although the number of modes is equal to N. When the system vibrates with large amplitude and enters the non-linear regime, the linear eigenspaces are not invariant anymore. Non-linear normal modes are invariant manifolds that are tangent to the linear eigenmodes at the origin. The first two modes: $\mathscr{M}_1$ and $\mathscr{M}_2$ are represented. Computing the real normal form allows one to

- Express the non-linear relationship between *modal* co-ordinates (X_p, Y_p) (where $Y_p = \dot{X}_p$ is the velocity) and the new-defined *normal* co-ordinates (R_p, S_p). These new co-ordinates are linked to the invariant manifolds, and thus the dynamics is directly expressed in a curved grid, also represented.
- Get the expression of the dynamics into the curved grid, with the normal co-ordinates.

The main results of these calculations are summarized in the next section. The complete demonstration is not given for the sake of brevity. The interested reader can find it in [32]. The case of two degree-of-freedom (d.o.f.) systems has already been treated with this formality in Ref. [33], and simple continuous structures (beams and plates) in Ref. [34].

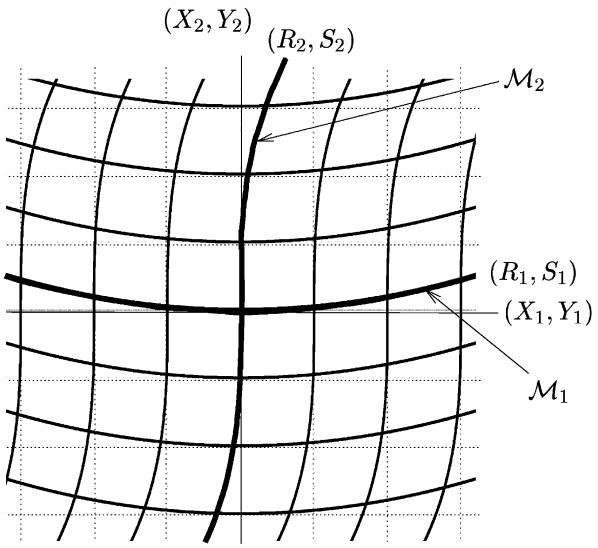

Fig. 1. Schematical representation of the phase space near the position of the system at rest, located at the origin. Orthogonal lines represent the first two linear eigenmodes, graduated by the modal co-ordinates (X_p, Y_p). The curved heavy lines, which are tangential to the axes at the origin, are the invariant manifolds (the NNMs), graduated by the normal co-ordinates (R_p, S_p). Normal form theory allows one to define the dynamics into the curved grid, in the phase space spanned by the NNMs.

2.2. Main results

Computing the normal form of a dynamical system consists of exhibiting a non-linear change of co-ordinates which cancels non-resonant terms [20,21]. Here, a third order asymptotic development is expressed. In this section, it is assumed that no internal resonance is present in the eigenspectrum $\{\pm i\omega_p\}$. The question of internal resonance is addressed in Section 2.3. The calculations, detailed in Ref. [32], are performed with the following general rules. First, Eq. (2) is set into its first order form by using the velocity $Y_p = \dot{X}_p$ as second variable. Then, at linear stage, the system is not diagonalized to keep real expressions. Oscillator-blocks, of the form

$$\begin{pmatrix} 0 & 1 \\ -\omega_p^2 & 0 \end{pmatrix} \tag{3}$$

are kept instead of diagonal, complex representation. This is the only difference with the approach used by Jezequel and Lamarque [14,15] and other authors Refs. [3,24–26]. It is however important since it allows one to keep the real oscillator form throughout the calculations: dynamical equations will always begin with $\ddot{X} + \omega^2 X + \cdots$, which is more readable for the mechanicians community. As a consequence, velocity-dependent terms arise in the expressions. The near-identity change of co-ordinates is sought by expressing its more general form, involving all the state-space variables (and thus including

the velocities), and then computing the correspondant coefficients [32]. It reads, up to order three: $\forall p = 1, \ldots, N$:

$$X_p = R_p + \sum_{i=1}^{N} \sum_{j \geqslant i}^{N} (a_{ij}^p R_i R_j + b_{ij}^p S_i S_j) + \sum_{i=1}^{N} \sum_{j \geqslant i}^{N} \sum_{k \geqslant j}^{N} r_{ijk}^p R_i R_j R_k + \sum_{i=1}^{N} \sum_{j=1}^{N} \sum_{k \geqslant j}^{N} u_{ijk}^p R_i S_j S_k, \tag{4a}$$

$$Y_p = S_p + \sum_{i=1}^{N} \sum_{j=1}^{N} \gamma_{ij}^p R_i S_j + \sum_{i=1}^{N} \sum_{j \geqslant i}^{N} \sum_{k \geqslant j}^{N} \mu_{ijk}^p S_i S_j S_k + \sum_{i=1}^{N} \sum_{j=1}^{N} \sum_{k \geqslant j}^{N} v_{ijk}^p S_i R_j R_k. \tag{4b}$$

The new-defined variables, R_p and S_p, are respectively homogeneous to a displacement and a velocity. They are called the *normal* co-ordinates. The coefficients of this non-linear change of variables (a_{ij}^p, b_{ij}^p, r_{ijk}^p, u_{ijk}^p, γ_{ij}^p, μ_{ijk}^p, v_{ijk}^p) are given in Appendix A, the complete proof leading to Eqs. (4) is given in Ref. [32].

Substituting for Eqs. (4) in Eqs. (2) gives the complete dynamics for the N oscillators, where all invariant-breaking terms have been cancelled:

$$\forall p = 1, \ldots, N: \quad \dot{R}_p = S_p, \tag{5a}$$

$$\dot{S}_p = -\omega_p^2 R_p - (A_{ppp}^p + h_{ppp}^p) R_p^3 - B_{ppp}^p R_p S_p^2 - R_p \left[\sum_{j>p}^{N} [(A_{jpj}^p + A_{pjj}^p + h_{pjj}^p) R_j^2 + B_{pjj}^p S_j^2] + \sum_{i<p} [(A_{iip}^p + A_{pii}^p + h_{iip}^p) R_i^2 + B_{pii}^p S_i^2] \right] - S_p \left[\sum_{j>p}^{N} B_{jpj}^p R_j S_j + \sum_{i<p} B_{iip}^p R_i S_i \right]. \tag{5b}$$

The coefficients (A_{ijk}^p, B_{ijk}^p) arise from the cancellation of the quadratic terms. Their expressions are

$$A_{ijk}^p = \sum_{l \geqslant i}^{N} g_{il}^p a_{jk}^l + \sum_{l \leqslant i} g_{li}^p a_{jk}^l, \tag{6a}$$

$$B_{ijk}^p = \sum_{l \geqslant i}^{N} g_{il}^p b_{jk}^l + \sum_{l \leqslant i} g_{li}^p b_{jk}^l. \tag{6b}$$

The following remarks are important here:

- In Eqs. (5), all invariant-breaking terms have been cancelled. Hence the invariance property is recovered.
- Eq. (4) is identity-tangent: the linear results are thus recovered for small amplitudes.
- Velocity-dependent terms arise in Eqs. (5) only if quadratic non-linearity is present in the initial problem given by (2). For example, for a non-linear beam problem, for which $g_{ij}^p \equiv 0$, no

velocity-dependent terms appear when considering the third order approximation of the dynamics onto invariant manifolds.

- Normal form (5) can be written with the knowledge of the linear eigenspectrum only [20,21]. Hence, *ex-nihilo* models can be written to study the dynamics onto the manifolds (see e.g. Ref. [35]). Then, one is able to recover the modal co-ordinates with Eqs. (4). The operation stated here bears a resemblance with modal decomposition usually performed at the linear stage, except that the space is now curved; and thus superposition is not straightforward.

2.3. Internal resonance

Internal resonances have been neglected in the previous section. However, considering an internal resonance in the system does not lead to tedious calculations for computing the non-linear change of co-ordinates. This is an important feature since usual methods proposed in the literature to compute the NNMs, which rely upon the centre manifold reduction theorem [10,11,36], or upon asymptotic development in the PDE [8,16,27], become very complicated in case of internal resonance.

An internal resonance appears with the failure of the calculation of one coefficient in Eq. (4). As is usual in this case, the affected coefficient has just to be set to zero, and the associated monomial stays in the normal form [20,32], as has already been done with the trivially resonant cubic terms.

2.4. Single-mode motion

In this section, the dynamical equations, that are related to the motion along a single non-linear mode, are derived. The results presented here are important because a physically observed single-mode motion occurs on an invariant manifold and, at the non-linear stage, has to be related to a non-linear normal mode motion. It is the aim of the NNMs computations to offer reduced order models, described by a limited number of variables, which hold the important properties exhibited by the non-linearity. This is achieved through invariant manifolds and will be illustrated with the hardening (or softening) behaviour of the oscillations.

To investigate the pth NNM, one has just to cancel all other variables since the bending of the phase space is contained within the non-linear change of co-ordinates:

$$\forall k \neq p\colon R_k = S_k = 0. \tag{7}$$

Substituting for Eq. (7) in Eq. (4) gives the geometry of the manifold in phase space:

$$\forall k \neq p\colon\ X_k = a^k_{pp} R_p^2 + b^k_{pp} S_p^2 + r^k_{ppp} R_p^3 + u^k_{ppp} R_p S_p^2, \tag{8a}$$

$$Y_k = \gamma^k_{pp} R_p S_p + \mu^k_{ppp} S_p^3 + \nu^k_{ppp} S_p R_p^2. \tag{8b}$$

This third order approximation of the invariant manifold has been compared with precedent calculations led by other authors [28,16], and all coefficients match.

The dynamics onto the pth manifold is found by substituting for Eq. (7) in Eq. (5):

$$\ddot{R}_p + \omega_p^2 R_p + (A^p_{ppp} + h^p_{ppp}) R_p^3 + B^p_{ppp} R_p \dot{R}_p^2 = 0. \tag{9}$$

This equation has to be compared to the usual single linear mode Galerkin approximation which is of current use for the analysis of non-linear oscillations of continuous systems. Performing a

single linear mode approximation means projecting the PDE onto the pth linear eigenspace. It is found by setting: $\forall k \neq p$: $X_k = 0$ in Eq. (2). Then the dynamics is governed by

$$\ddot{X}_p + \omega_p^2 X_p + g_{pp}^p X_p^2 + h_{ppp}^p X_p^3 = 0. \tag{10}$$

This procedure can lead to erroneous results because the linear eigenspace is not invariant. Taking the bending of the phase space into account can drastically change the behaviour. This will be underlined by deriving the amplitude-frequency relation, usually known as the backbone curve. Using any of the perturbation methods available, one can find, at first order and for Eq. (9):

$$\omega_{\mathrm{NL}} = \omega_p \left(1 + \frac{3(A_{ppp}^p + h_{ppp}^p) + \omega_p^2 B_{ppp}^p}{8\omega_p^2} a^2 \right), \tag{11}$$

where ω_{NL} is the non-linear angular frequency, which depends on the amplitude a considered.

The hardening or softening behaviour for a single non-linear mode motion is governed by the sign of the term

$$\Gamma_p = \frac{3(A_{ppp}^p + h_{ppp}^p) + \omega_p^2 B_{ppp}^p}{8\omega_p^2}. \tag{12}$$

One can see that the influences of all the linear modes are taken into account through the terms A_{ppp}^p and B_{ppp}^p. This will give a greater accuracy than considering only a single linear mode. It has to be compared to the coefficient $\tilde{\Gamma}_p$ which dictates the behaviour of the non-linear oscillations for Eq. (10), which reads

$$\tilde{\Gamma}_p = \frac{1}{8\omega_p^2} \left(3h_{ppp}^p - \frac{10 g_{pp}^{p2}}{3\omega_p^2} \right). \tag{13}$$

The remainder of this article is devoted to the processing of two examples, where the precedent theoretical results will be illustrated. A particular emphasis will be put on the erroneous results one can find when applying a single-mode Galerkin reduction.

3. Example 1: a discrete system

3.1. Equations of motion

The first example is devoted to a discrete two d.o.f. system, composed of a mass m connected to a frame by two geometrically non-linear springs (Fig. 2). The potential energy of spring i ($i \in \{1,2\}$) is assumed to be

$$\mathscr{E}_{pi} = \tfrac{1}{2} k_i l_0^2 e_i^2, \quad \text{with} \quad e_i = \tfrac{1}{2} \frac{l_i^2 - l_0^2}{l_0^2}. \tag{14}$$

k_i is the linear stiffness of spring i, and l_i is its deformed length. The tension in the springs is then

$$N_i = -\frac{\partial \mathscr{E}_{pi}}{\partial l_i} = -\tfrac{1}{2} k_i l_0 \left[\left(\frac{l_i}{l_0} \right)^3 - \frac{l_i}{l_0} \right] = -k_i \left[\Delta l_i + \tfrac{3}{2} \frac{\Delta l_i^2}{l_0} + \tfrac{1}{2} \frac{\Delta l_i^3}{l_0^2} \right], \tag{15}$$

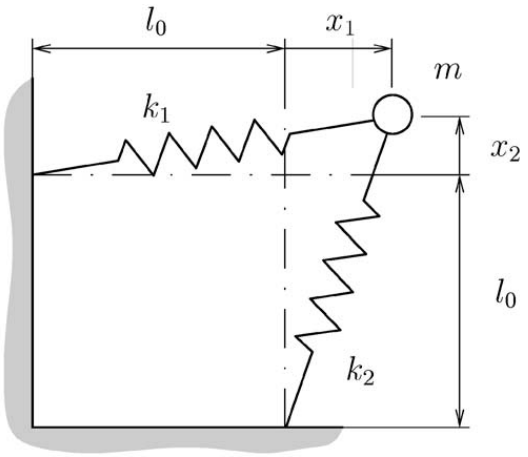

Fig. 2. The physical two d.o.f. system for example 1.

with $\Delta l_i = l_i - l_0$. One can notice that the springs have quadratic and cubic non-linearities. Applying Lagrange's equations to the mass gives the non-linear ODEs which govern the motion:

$$\mathscr{L}_i : \left(\frac{\mathrm{d}}{\mathrm{d}t}\frac{\partial}{\partial \dot{x}_i} - \frac{\partial}{\partial x_i}\right)(\mathscr{E}_k + \mathscr{E}_p) = 0 \tag{16}$$

with $\mathscr{E}_k$ denoting the kinetic energy of mass m, and $\mathscr{E}_p = \mathscr{E}_{p1} + \mathscr{E}_{p2}$ the total potential energy. It results in

$$\ddot{X}_1 + \omega_1^2 X_1 + \frac{\omega_1^2}{2}(3X_1^2 + X_2^2) + \omega_2^2 X_1 X_2 + \frac{\omega_1^2 + \omega_2^2}{2} X_1(X_1^2 + X_2^2) = 0, \tag{17a}$$

$$\ddot{X}_2 + \omega_2^2 X_2 + \frac{\omega_2^2}{2}(3X_2^2 + X_1^2) + \omega_1^2 X_1 X_2 + \frac{\omega_1^2 + \omega_2^2}{2} X_2(X_1^2 + X_2^2) = 0, \tag{17b}$$

$X_1 = x_1/l_0$ and $X_2 = x_2/l_0$ are dimensionless displacements defining the position of the mass, $\omega_1^2 = k_1/m$ and $\omega_2^2 = k_2/m$ are the natural frequencies of the system. The system is naturally linearly uncoupled, as the two linear modes of motion are X_1 and X_2. It is a consequence of the orthogonal configuration of the two springs at rest.

3.2. Regions of hardening and softening behaviour

In this subsection, a detailed comparison between the motion along the first linear mode and along the first non-linear mode is provided. It is assumed that no internal resonance exists between the two modes.

Considering the first linear mode leads to a dynamics governed by

$$\ddot{X}_1 + \omega_1^2 X_1 + \frac{3\omega_1^2}{2} X_1^2 + \frac{\omega_1^2 + \omega_2^2}{2} X_1^3 = 0. \tag{18}$$

The backbone curve in this case is given by

$$\tilde{\omega}_{\mathrm{NL}} = \omega_1\left(1 + \left(-\tfrac{3}{4} + \frac{3\omega_2^2}{16\omega_1^2}\right)a^2\right), \tag{19}$$

where $\tilde{\omega}_{\mathrm{NL}}$ stands for the non-linear angular frequency found with a linear mode approximation, and a is the amplitude of the motion considered: $X_1 = a\cos(\tilde{\omega}_{\mathrm{NL}}t + \beta_0) + \cdots$.

In the parameter plane (ω_1, ω_2), regions of hardening or softening behaviour are governed by the sign of

$$\tilde{\Gamma}_1 = -\tfrac{3}{4} + \frac{3\omega_2^2}{16\omega_1^2}. \tag{20}$$

Considering now the first non-linear mode, which is the right approximation if one is interested in a motion non-linearly vibrating along the first physical mode, indicates that the oscillations are governed by Eq. (9), with $p = 1$. Computing the coefficients and replacing in Eq. (12) shows that the hardening or softening behaviour onto the first invariant manifold is determined by the sign of

$$\Gamma_1 = -\tfrac{3}{4} + \frac{3\omega_2^2}{16\omega_1^2} + \frac{\omega_2^2(8\omega_1^2 - 3\omega_2^2)}{16\omega_1^2(\omega_2^2 - 4\omega_1^2)}. \tag{21}$$

It appears clearly that considering the bending of the phase space caused by the presence of the second oscillator gives rise to a correction on the backbone curve. More specifically, this effect can be drastic and can change the effective behaviour of the non-linear oscillations. Fig. 3 shows the hardening and softening region in the two cases (simply given by the signs of $\tilde{\Gamma}_1$ in the linear case, and Γ_1 in the non-linear case). One can notice for example the upper-left region, which is predicted to exhibit a hardening behaviour by the linear approximation, whereas the real behaviour is soft. Hence single linear mode approximation can give results that are substantially wrong. In the next subsection, numerical simulations validate these results.

3.3. Numerical simulations

Numerical simulations have been performed on system (17) in order to verify the precedent theoretical results. First, a graphical representation of the first invariant manifold is shown in Fig. 4. The third order approximation of the invariant manifold has been calculated with Eqs. (8).

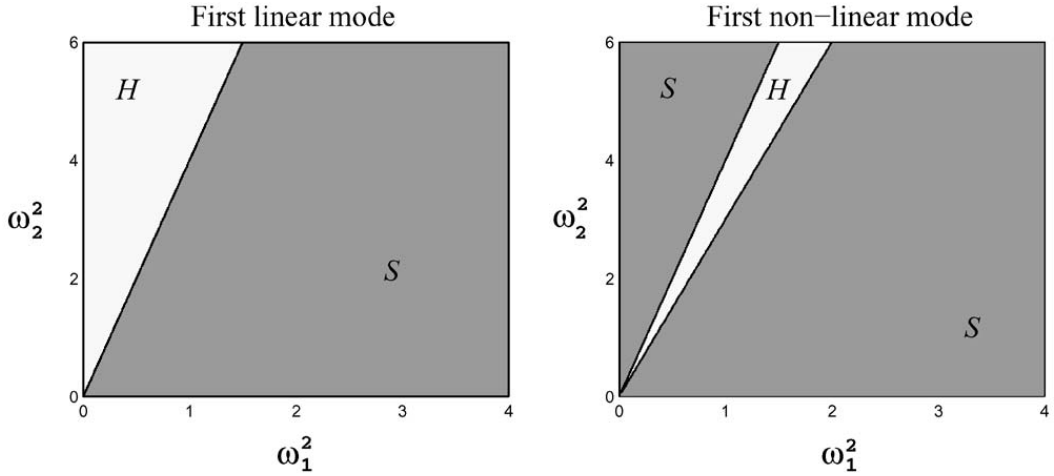

Fig. 3. Regions of hardening (H) and softening (S) behaviour for Example 1. Left: first linear mode approximation. Right: first non-linear mode.

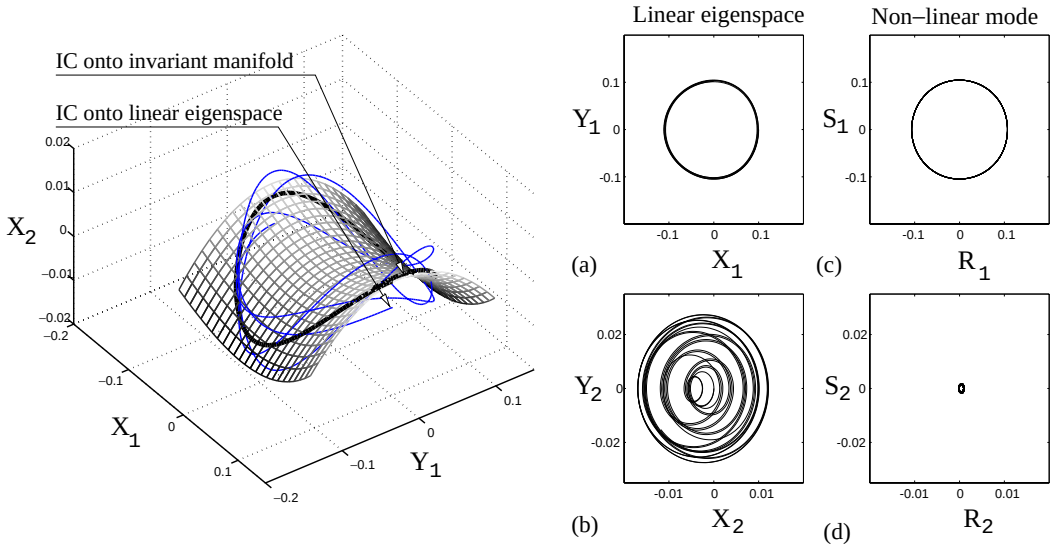

Fig. 4. Representation of the first invariant manifold with $\omega_1 = 1$ and $\omega_2 = \sqrt{3}$. Left: the surface represents the first NNM. Two trajectories have been represented with two different initial conditions (IC). Solid line: IC onto linear eigenspace. Heavy line: IC onto the first NNM. Right: projections of the two trajectories onto their respective subspaces. (a)–(b): Orbit initiated along the linear mode, projected onto the linear eigenspaces. (c)–(d): Orbit initiated along the first NNM, projected onto the two invariant manifolds.

Two orbits have been represented. The first one has for the initial condition a point which relies on the linear eigenspace. One can see that it gives rise to a whirling trajectory. The vertical displacement corresponds to the quantity that is neglected when one performs a single linear mode approximation. This is highlighted on the projections: Fig. 4(b) shows exactly the neglected quantity. For the second trajectory, the initial condition has been taken onto the invariant manifold. The real position has been found numerically by a shooting technique, which has also been utilized in Fig. 5 (second row). The neglected quantity is divided by 15. The drawback of considering only a third order approximation for the invariant manifolds can be numerically estimated on this example. Taking the initial condition onto the third order approximation of the first NNM leads to a residual contribution which is divided by seven compared to the linear case.

A second set of simulations has been conducted in order to compute numerical backbone curves, and to compare them with the analytical first order development. Fig. 5 shows the results obtained for three different cases, corresponding to the three regions highlighted in Fig. 3. For the linear-mode approximation, Eq. (18) has been used. For computing the backbone curve onto the invariant manifold, the whole system (Eqs. (17)) has been used, and the initial condition for the computed trajectory has been taken onto the first NNM, for each amplitude. The second row of Fig. 5 shows the positions of the two invariant manifolds in space (X_1, X_2). One can see that for too large amplitudes, the divergence between the third order approximation of the invariant manifolds and the real position becomes noticeable.

Through this example, it has been shown that a linear single-mode approximation can lead to wrong results when predicting hardening or softening behaviour. These errors are corrected when one considers the NNMs, which are the right approximation, at the non-linear stage, for a single-mode motion. The next section examines the same features on a continuous system.

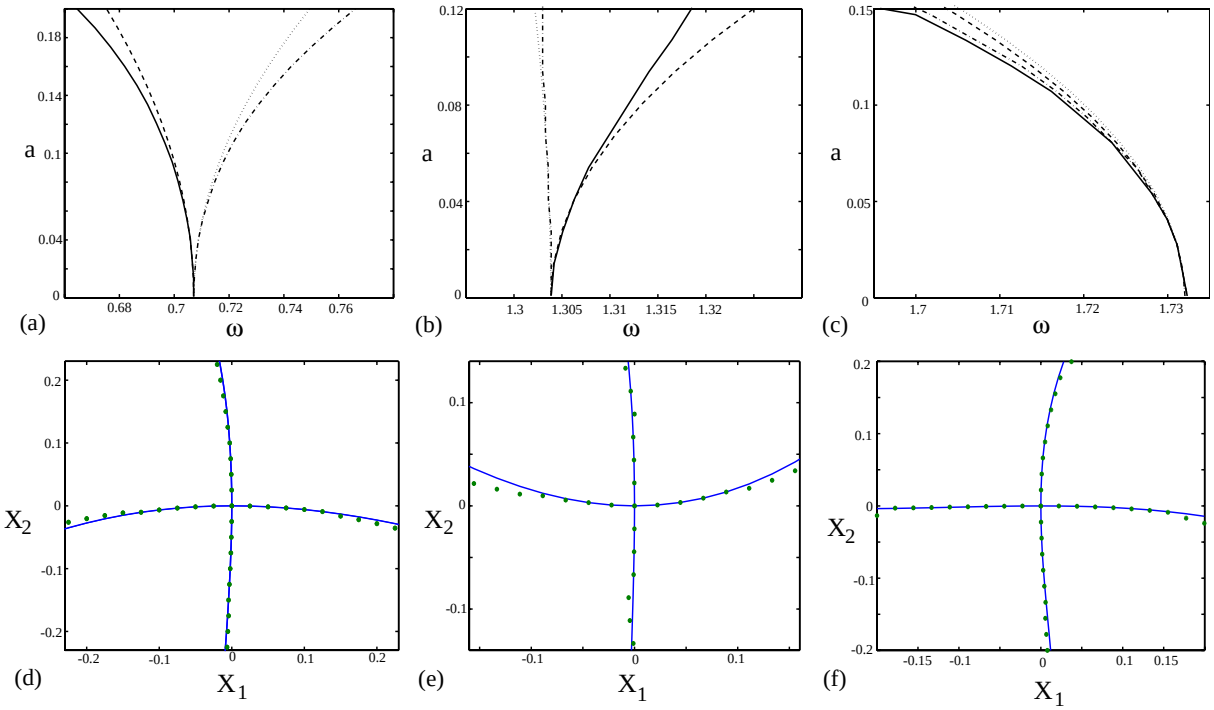

Fig. 5. First row: Comparison of analytical and backbone curves for example 1, first mode. The reference solution is given by numerically computing the amplitude/frequency relation for an initial condition onto the first invariant manifold (solid heavy line). Dashed line (- - - -): first order analytical backbone curve onto the first NNM (governed by Γ_1, cf. Eq. (11)). Dash–dotted line (- · - · -): numerical backbone curve onto the first linear eigenspace. Dotted line (.....): first order analytical backbone curve onto the first linear mode. Second row: positions of the two manifolds in space (X_1, X_2). Solid line: third order approximation; (∗): real position. (a)–(d) $\omega_1 = \sqrt{0.5}$, $\omega_2 = \sqrt{6}$; (b)–(e): $\omega_1 = \sqrt{1.7}$, $\omega_2 = \sqrt{6}$; (c)–(f): $\omega_1 = \sqrt{3}$, $\omega_2 = 1$.

4. Example 2: a continuous system

4.1. Equations of motion

A linear hinged–hinged beam resting on a non-linear elastic foundation with distributed quadratic and cubic non-linearities is considered. This example has already been studied in Refs. [5,8], and it is the aim of this section to compare their results with the methodology proposed herein, based on invariant manifolds and normal form theory.

In non-dimensional form, the undamped transverse vibrations are governed by [5,8]

$$\frac{\partial^2 w}{\partial t^2} + \frac{\partial^4 w}{\partial x^4} + \alpha_2 w^2 + \alpha_3 w^3 = 0 \tag{22}$$

with boundary conditions

$$w(x,t) = 0, \quad \frac{\partial^2 w(x,t)}{\partial x^2} = 0 \quad \text{for } x = 0, 1. \tag{23}$$

$w(x,t)$ is the transverse displacement, α_2 and α_3 are constants. The linear analysis provides the eigenmodes as well as the eigenfrequencies:

$$\Phi_n(x) = \sqrt{2}\sin(n\pi x), \tag{24}$$

$$\omega_n = n^2\pi^2. \tag{25}$$

Projection onto the linear mode basis is performed via the development:

$$w(x,t) = \sum_{p=1}^{N} X_p(t)\Phi_p(x) \tag{26}$$

which is inserted into Eq. (22). This leads to the following temporal problem: $\forall p = 1, \ldots, N$:

$$\ddot{X}_p + \omega_p^2 X_p + \sum_{i,j=1}^{N} g_{ij}^p X_i X_j + \sum_{i,j,k=1}^{N} h_{ijk}^p X_i X_j X_k = 0, \tag{27}$$

where

$$g_{ij}^p = \alpha_2 \int_0^1 \Phi_i(x)\Phi_j(x)\Phi_p(x)\,\mathrm{d}x, \quad h_{ijk}^p = \alpha_3 \int_0^1 \Phi_i(x)\Phi_j(x)\Phi_k(x)\Phi_p(x)\,\mathrm{d}x. \tag{28}$$

4.2. Internal resonances and invariance

Normal form for Eq. (27) is computed with the results presented in Section 1. As a consequence of the values of the eigenfrequencies, Eq. (25), the system exhibits many internal resonances. They are listed in Table 1, for the 10 first eigenfrequencies. Higher-dimensional invariant manifolds should be considered to study the dynamics, as strong coupling (resonant) terms arise from the internal resonance relations. But, as it is explained next, single-mode motion on two-dimensional invariant manifolds exists for the linear beam resting on a non-linear elastic foundation, because in this problem, all resonant coupling terms are not invariant-breaking.

Table 1
Internal resonance relations between the ten first eigenfrequencies

Order-two internal resonances
$\omega_5 = \omega_3 + \omega_4$
$\omega_{10} = \omega_6 + \omega_8$
Order-three internal resonances
$\omega_1 = \omega_4 + \omega_7 - \omega_8$
$\omega_1 = 2\omega_5 - \omega_7$
$\omega_2 = \omega_6 + \omega_7 - \omega_9$
$\omega_3 = \omega_1 + 2\omega_2$
$\omega_6 = \omega_2 + 2\omega_4$
$\omega_7 = \omega_2 + \omega_3 + \omega_6$
$\omega_9 = \omega_1 + \omega_8 + \omega_4$
$\omega_9 = \omega_3 + 2\omega_6$
$\omega_9 = 2\omega_4 + \omega_7$

An internal resonance of the form: $\omega_p = 2\omega_k$ (second order), or $\omega_p = 3\omega_k$ (third order) creates a monom which breaks the invariance of two-dimensional manifolds. For example, the relationship $\omega_p = 2\omega_k$ implies the presence of an unremovable monom R_k^2 in the evolution equation for R_p. Hence letting $R_p = 0$ to study the kth NNM alone is not possible because of this "source" term in the pth equation. In this particular case, a four-dimensional manifold with the NNMs p and k has to be considered.

On the other hand, internal resonance relations which strictly imply more than two eigenfrequencies do not give rise to invariant-breaking terms, since it is always possible to cancel the co-ordinates to study the dynamics onto a single two-dimensional manifold. This remark should be compared with the absence of a stable single-mode solution in a perturbative study of the dynamics of coupled oscillators with invariant-breaking terms (see e.g. Refs. [37,1]); or its presence when only resonant terms that do not break the invariance are involved in the equations (see e.g. Refs. [38,39,1]).

4.3. Hardening/softening behaviour

The dynamics onto a single NNM is now studied. Attention will be focused on the first three eigenmodes. For the pth NNM, the oscillations are governed by Eq. (9), and the hardening or softening behaviour by the sign of Γ_p (Eq. (12)). Table 2 gives the values of Γ_p for $p = 1, 2, 3$, and for an increasing value N of linear modes retained in the analysis. The coefficients α_2 and α_3 have been set, respectively, to 12 and 1 for this computation.

One can notice that taking the NNMs into account leads to a change of sign for Γ_p, for modes 2 and 3. Hence a linear-mode Galerkin approximation fails to predict the correct behaviour of the oscillations. The convergence of Γ_p for the first three modes is obtained here, with 5 significant digits of accuracy, for $N = 8$. In the following, the number of retained linear modes will thus be chosen equal to 10 to get confidence in the accuracy of the results.

Fig. 6 shows (first row) the hardening and softening regions in the parameter plane (α_2, α_3). In Fig. 6(a), for the first mode, the two regions (given, respectively, by the linear approximation and the NNM) are identical. Considering the NNM does not change the global behaviour substantially. This is not the case for modes 2 and 3. For mode 2, Fig. 6(b), the linear approximation predicts a hardening behaviour in all the plane, since the quadratic coefficient is equal to zero: $g_{22}^2 = 0$. Considering the second NNM shows that the correct result is different and that a softening region is present. The second and third rows show the backbone curves

Table 2
Convergence of the value of Γ_p, which determines the hardening or softening behaviour of the mode considered, with increasing N. The first line gives the value of $\tilde{\Gamma}_p$ (single linear mode approximation). NB.: the value of Γ_3 with two modes have been computed with modes 1 and 3. $\alpha_2 = 12$ and $\alpha_3 = 1$

N	Γ_1	Γ_2	Γ_3
1	−3.338e–3	36.091e–5	7.113e–5
2	−3.338e–3	−7.299e–5	−0.907e–5
3	−3.346e–3	−8.231e–5	−0.907e–5
5	−3.346e–3	−8.243e–5	−0.918e–5
8	−3.346e–3	−8.243e–5	−0.918e–5

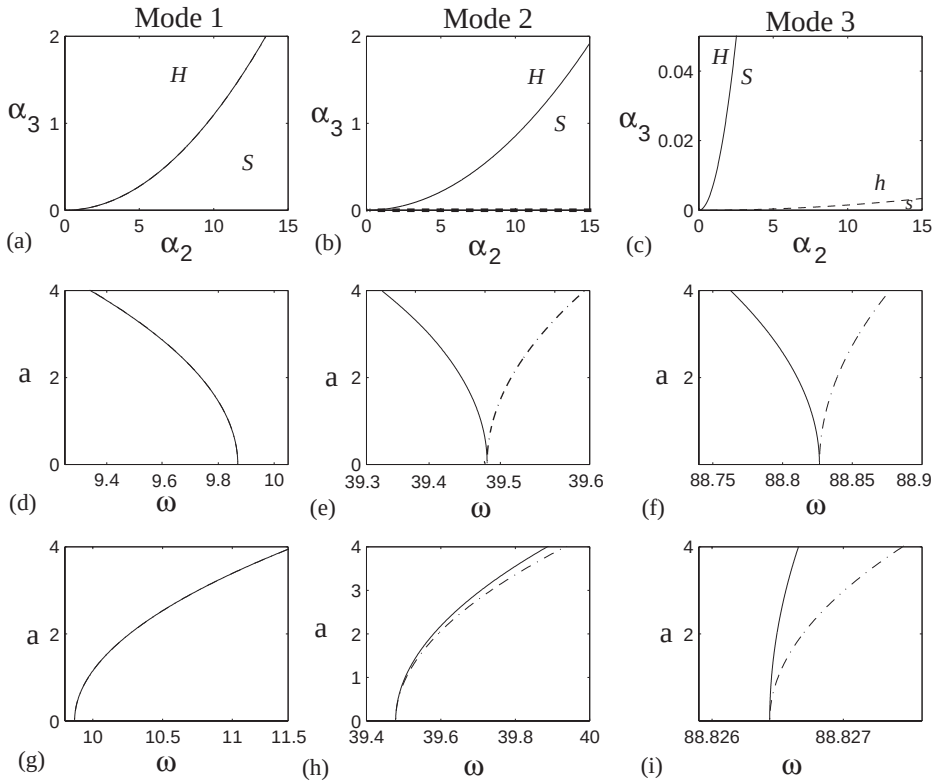

Fig. 6. First row: hardening and softening regions using the linear mode approximation (dashed lines, h/s) and the non-linear mode approximation (solid lines, H/S) for the first three modes. (d)–(i) Backbone curves in different cases, solid line:NNM, dash–dot: linear mode. (d) $\alpha_2 = 12$, $\alpha_3 = 1$. (g) $\alpha_2 = 5$, $\alpha_3 = 2$. (e) $\alpha_2 = 12$, $\alpha_3 = 0.5$. (h) $\alpha_2 = 5$, $\alpha_3 = 2$. (f) $\alpha_2 = 12$, $\alpha_3 = 0.5$. (i) $\alpha_2 = 1$, $\alpha_3 = 0.01$.

analytically obtained, respectively, onto the linear eigenspace and onto the invariant manifold, and for different values of α_2 and α_3.

These results have been compared with those derived in Refs. [5,8], where a perturbation technique (the method of multiple scales) is used directly into the PDE (22). The hardening and softening regions are exactly the same, showing that the methods are equivalent for determining the behaviour of the non-linear oscillations.

4.4. Drift and mode shapes

Using a first order perturbation technique, one can find that the solution of Eq. (9), governing the oscillations onto the manifold is given by

$$R_p = a_0 \cos(\omega_{\mathrm{NL}} t + \beta_0) + \cdots \tag{29}$$

with $\omega_{\mathrm{NL}} = \omega_p(1 + \Gamma_p a_0^2)$; for an amplitude a_0.

Substituting for Eq. (29) into the non-linear change of co-ordinates gives the solution with the modal co-ordinates. Investigating the NNM labelled p, one has to replace with

$$\forall k \neq p\colon\ X_k = a_{pp}^k R_p^2 + b_{pp}^k S_p^2 + r_{ppp}^k R_p^3 + u_{ppp}^k R_p S_p^2, \tag{30a}$$

$$k = p: \; X_p = R_p + a_{pp}^p R_p^2 + b_{pp}^p S_p^2 \tag{30b}$$

into

$$w_p(x,t) = X_p(t)\Phi_p(x) + \sum_{k \neq p} X_k(t)\Phi_k(x). \tag{31}$$

To obtain the complete solution for the displacement. $w_p(x,t)$ is written for a displacement along the pth NNM. Omitting the cubic terms in the precedent equations to get a second order solution, gives

$$w_p(x,t) = a_0 \cos(\omega_{\mathrm{NL}} t + \beta_0)\Phi_p(x) + \sum_{k=1}^{N} \left[a_{pp}^k \frac{a_0^2}{2} + b_{pp}^k \frac{a_0^2 \omega_{\mathrm{NL}}^2}{2} + \left(a_{pp}^k \frac{a_0^2}{2} - b_{pp}^k \frac{a_0^2 \omega_{\mathrm{NL}}^2}{2} \right) \cos(2\omega_{\mathrm{NL}} t + 2\beta_0) \right] \Phi_k(x). \tag{32}$$

Hence the quadratic non-linearity gives rise to a drift in the oscillations, which is written here as

$$d_p(x,t) = \sum_{k=1}^{N} \left[a_{pp}^k \frac{a_0^2}{2} + b_{pp}^k \frac{a_0^2 \omega_{\mathrm{NL}}^2}{2} \right] \Phi_k(x). \tag{33}$$

It has to be compared with the same drift predicted with a linear-mode Galerkin approximation, which reads [5,8]

$$\tilde{d}_p(x,t) = -\frac{\delta_p \alpha_2}{2\omega_p^2} a_0^2 \Phi_p(x), \tag{34}$$

where $\delta_p = (4\sqrt{2}/(3p\pi))(1 - \cos p\pi)$.

Mode shapes as well as drifts have been compared for the three methods: linear (single-mode) approximation, Non-linear single-mode motion and perturbation method directly in the PDE [5,8]. The normalized results for modes 2 and 3 are shown in Fig. 7. For the mode shapes, the

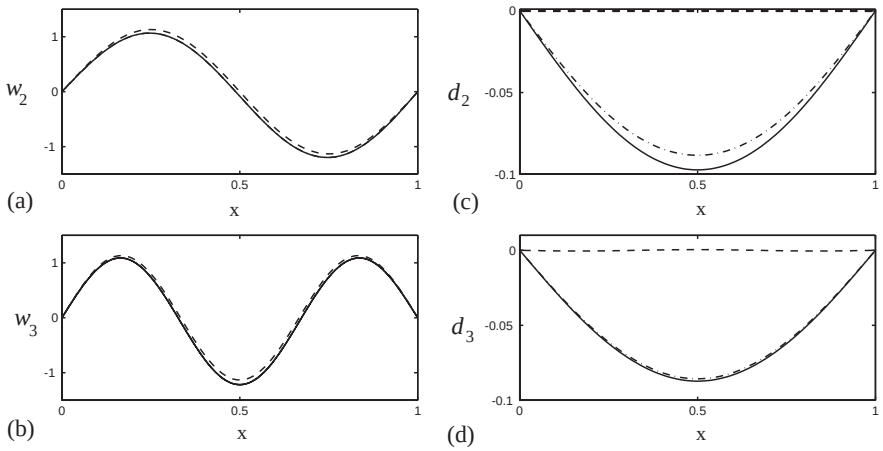

Fig. 7. Mode shapes (left column) and drifts (right) for mode 2 (first row) and 3 (second row). Solid line: NNM solution. Dash–dotted line: solution of Nayfeh and Lacarbonara, using a perturbation method directly into the PDE. Dashed line: linear solution.

method used by Nayfeh and Lacarbonara gives the same results as in this study. For the drifts, a little difference is observed for mode 2.

5. Conclusion

In this paper, normal form theory has been used in order to define non-linear normal modes. Keeping an oscillator form at linear stage (which is realized with two-dimensional real non-diagonal blocks in the linear part of the dynamics) allows one to have real equations throughout the calculations. This is contrary to the usual manner in which normal form has always been presented in vibration theory, and allows precise comparison of this method with others, already developed to define NNMs. Moreover, a clean mathematical framework to define non-linear modal analysis/synthesis is given. Indeed, the non-linear change of co-ordinates can be viewed as an extension of the linear modal method.

Analysis should be performed with the help of normal form, since it allows derivation of reduced order models that capture the essential of the dynamics, and express amplitude-dependent mode shapes. Moreover, the question of a clever truncature should be asked after the non-linear change of co-ordinates. Synthesis is simplified since the dynamics onto the invariant manifolds is simply given by the normal form of the vibratory problem, and normal form could be written with the knowledge of the linear eigenspectrum only.

Throughout the calculations, third order asymptotic developments have been used. This constitutes the main limitation of the method. However, it enables derivation of important results, which have been underlined on simple examples. Single NNM motions have been studied, showing that it allows prediction of the effective trend of the non-linearity for structural systems (hardening/softening behaviour). It has been contrasted with the single linear mode Galerkin approximation which is of current use, although it can lead to erroneous results. The role of the quadratic non-linearity has been underlined. The second example allowed comparison of the NNM results with a method proposed in Refs. [5,8] in order to overcome the problems caused by the linear truncature. It has been shown that the two methods yield the same results.

Acknowledgements

The authors would like to thank Bruno Cochelin from LMA-Marseille for suggesting the first example. Paul Manneville is also thanked for his lessons on dynamical systems theory.

Appendix A. Expressions of the coefficients for Eqs. (4)

Expressions of the coefficients (a^p_{ij}, b^p_{ij}, r^p_{ijk}, u^p_{ijk}, γ^p_{ij}, μ^p_{ijk}, v^p_{ijk}) used in Eqs. (4), which allows one to go from the modal variables (associated with the orthogonal linear grid) to the normal co-ordinates (associated to the invariant manifold and the curved grid) are given here.

A.1. Quadratic coefficients

The following expressions are obtained, $\forall p = 1, \ldots, N$:

$$\forall i = 1, \ldots, N, \ \forall j \geqslant i, \ldots, N:$$

$$a_{ij}^p = \frac{\omega_i^2 + \omega_j^2 - \omega_p^2}{D_{ijp}} g_{ij}^p, \tag{A.1a}$$

$$b_{ij}^p = \frac{2}{D_{ijp}} g_{ij}^p, \tag{A.1b}$$

$$c_{ij}^p = 0, \tag{A.1c}$$

$$\alpha_{ij}^p = 0, \tag{A.1d}$$

$$\beta_{ij}^p = 0, \tag{A.1e}$$

$$\gamma_{ii}^p = \frac{2}{4\omega_i^2 - \omega_p^2} g_{ii}^p, \tag{A.1f}$$

$$\forall i = 1, \ldots, N, \ \forall j > i, \ldots, N:$$

$$\gamma_{ij}^p = \frac{\omega_j^2 - \omega_i^2 - \omega_p^2}{D_{ijp}} g_{ij}^p, \tag{A.1g}$$

$$\gamma_{ji}^p = \frac{\omega_i^2 - \omega_j^2 - \omega_p^2}{D_{ijp}} g_{ij}^p, \tag{A.1h}$$

where $D_{ijp} = (\omega_i + \omega_j - \omega_p)(\omega_i + \omega_j + \omega_p)(-\omega_j + \omega_i + \omega_p)(\omega_i - \omega_j - \omega_p)$.

A.2. Cubic coefficients

The following coefficients, which correspond to the trivially resonant terms, are equal to zero:

$$\begin{aligned}
&\forall p = 1, \ldots, N: \quad u_{ppp}^p = r_{ppp}^p = \mu_{ppp}^p = v_{ppp}^p = 0,\\
&\forall j > p, \ldots, N: \quad r_{pjj}^p = u_{pjj}^p = u_{jpj}^p = 0,\\
&\mu_{pjj}^p = v_{pjj}^p = v_{jpj}^p = 0,\\
&\forall i < p: \quad r_{iip}^p = u_{iip}^p = u_{pii}^p = 0,\\
&\mu_{iip}^p = v_{iip}^p = v_{pii}^p = 0.
\end{aligned} \tag{A.2}$$

The non-zero coefficients are now given, $\forall p = 1, \ldots, N$:

$$\forall i = 1, \ldots, N, \ i \neq p:$$

$$r_{iii}^p = \frac{1}{D_{ip}^{(1)}} \left[(7\omega_i^2 - \omega_p^2)(h_{iii}^p + A_{iii}^p) + 2\omega_i^4 B_{iii}^p \right],$$

$$u^p_{iii} = \frac{1}{D^{(1)}_{ip}}\Big[6h^p_{iii} + 6A^p_{iii} + (3\omega_i^2 - \omega_p^2)B^p_{iii}\Big],$$

$$\mu^p_{iii} = u^p_{iii},$$

$$v^p_{iii} = \frac{1}{D^{(1)}_{ip}}\Big[(9\omega_i^2 - 3\omega_p^2)(h^p_{iii} + A^p_{iii}) + 2\omega_p^2\omega_i^2 B^p_{iii}\Big],$$

where $D^{(1)}_{ip} = (\omega_p^2 - \omega_i^2)(\omega_p^2 - 9\omega_i^2)$.

$$\forall i = 1, \ldots, N-1,\ \ i \neq p,\ \ \forall j > i, \ldots, N:$$

$$r^p_{ijj} = \frac{\omega_i^2(\omega_i^2 - 2\omega_j^2 - 2\omega_p^2) + (\omega_p^2 - 4\omega_j^2)(\omega_p^2 - 2\omega_j^2)}{(\omega_i^2 - \omega_p^2)D^{(1)}_{ijp}}\Big[A^p_{ijj} + A^p_{jij} + h^p_{ijj}\Big] - \frac{2\omega_j^4(\omega_p^2 - 4\omega_j^2 + 3\omega_i^2)}{(\omega_i^2 - \omega_p^2)D^{(1)}_{ijp}}B^p_{ijj} + \frac{2\omega_i^2\omega_j^2}{D^{(1)}_{ijp}}B^p_{jij},$$

$$u^p_{ijj} = \frac{\omega_i^2(\omega_i^2 - 2\omega_j^2 - 2\omega_p^2) + (\omega_p^2 - 4\omega_j^2)(\omega_p^2 - 2\omega_j^2)}{(\omega_i^2 - \omega_p^2)D^{(1)}_{ijp}}B^p_{ijj} + \frac{8\omega_j^2 - 6\omega_i^2 - 2\omega_p^2}{(\omega_i^2 - \omega_p^2)D^{(1)}_{ijp}}[A^p_{ijj} + A^p_{jij} + h_{ijj}] - \frac{2\omega_i^2}{D^{(1)}_{ijp}}B^p_{jij},$$

$$u^p_{jij} = \frac{1}{D^{(1)}_{ijp}}\Big[4(A^p_{jij} + A^p_{ijj} + h^p_{ijj}) - 4\omega_j^2 B^p_{ijj} + (4\omega_j^2 - \omega_p^2 + \omega_i^2)B^p_{jij}\Big],$$

$$v^p_{ijj} = \frac{6\omega_i^2\omega_j^2 + 2\omega_j^2\omega_p^2 + 2\omega_p^2\omega_i^2 - 8\omega_j^4 - \omega_p^4 - \omega_i^4}{(\omega_p^2 - \omega_i^2)D^{(1)}_{ijp}}[A^p_{ijj} + A^p_{jij} + h^p_{ijj}] + \frac{2\omega_j^4(3\omega_p^2 + \omega_i^2 - 4\omega_j^2)}{(\omega_p^2 - \omega_i^2)D^{(1)}_{ijp}}B^p_{ijj} - \frac{\omega_j^2(-\omega_p^2 + 4\omega_j^2 - \omega_i^2)}{D^{(1)}_{ijp}}B^p_{jij},$$

$$v^p_{jij} = \frac{8\omega_j^2 - 2\omega_i^2 - 2\omega_p^2}{D^{(1)}_{ijp}}[A^p_{ijj} + A^p_{jij} + h^p_{ijj}] + \frac{2\omega_j^2\omega_p^2 - 8\omega_j^4 + 2\omega_j^2\omega_i^2}{D^{(1)}_{ijp}}B^p_{ijj} + \frac{\omega_p^2\omega_i^2 + 4\omega_j^2\omega_i^2 - \omega_i^4}{D^{(1)}_{ijp}}B^p_{jij},$$

$$\mu^p_{ijj} = \frac{6\omega_i^2\omega_j^2 + 2\omega_j^2\omega_p^2 + 2\omega_p^2\omega_i^2 - 8\omega_j^4 - \omega_p^4 - \omega_i^4}{(\omega_p^2 - \omega_i^2)D^{(1)}_{ijp}}B^p_{ijj} + \frac{6\omega_p^2 + 2\omega_i^2 - 8\omega_j^2}{(\omega_p^2 - \omega_i^2)D^{(1)}_{ijp}}[A^p_{ijj} + A^p_{jij} + h^p_{ijj}] + \frac{4\omega_j^2 - \omega_i^2 - \omega_p^2}{D^{(1)}_{ijp}}B^p_{jij},$$

where $D^{(1)}_{ijp} = (\omega_p + \omega_i - 2\omega_j)(\omega_p + \omega_i + 2\omega_j)(-\omega_p + \omega_i + 2\omega_j)(-\omega_p + \omega_i - 2\omega_j)$.

$$\forall i = 1, \ldots, N-1, \ \forall j > i, \ldots, N, \ j \neq p:$$

$$r^p_{iij} = \frac{2\omega_i^2(4\omega_i^2 - 3\omega_p^2 - \omega_j^2) + (\omega_p - \omega_j)^2(\omega_p + \omega_j)^2}{(\omega_p^2 - \omega_j^2)D^{(2)}_{ijp}}\left[-A^p_{iij} - A^p_{jii} - h^p_{iij}\right] - \frac{2\omega_i^4(4\omega_i^2 - \omega_p^2 - 3\omega_j^2)}{(\omega_p^2 - \omega_j^2)D^{(2)}_{ijp}} B^p_{jii} - \frac{2\omega_i^2\omega_j^2}{D^{(2)}_{ijp}} B^p_{iij},$$

$$u^p_{jii} = -\frac{2\omega_i^2(4\omega_i^2 - 3\omega_p^2 - \omega_j^2) + (\omega_p - \omega_j)^2(\omega_p + \omega_j)^2}{(\omega_p^2 - \omega_j^2)D^{(2)}_{ijp}} B^p_{jii} + \frac{8\omega_i^2 - 2\omega_p^2 - 6\omega_j^2}{(\omega_p^2 - \omega_j^2)D^{(2)}_{ijp}}\left[-A^p_{jii} - A^p_{iij} - h^p_{iij}\right] - \frac{2\omega_j^2}{D^{(2)}_{ijp}} B^p_{iij},$$

$$u^p_{iij} = \frac{1}{D^{(2)}_{ijp}}[4(A^p_{jii} + A^p_{iij} + h^p_{iij}) - 4\omega_i^2 B^p_{jii} - (\omega_p^2 - \omega_j^2 - 4\omega_i^2)B^p_{iij}],$$

$$v^p_{jii} = \frac{8\omega_i^4 + \omega_j^4 + \omega_p^4 - 2\omega_p^2\omega_i^2 - 6\omega_i^2\omega_j^2 - 2\omega_j^2\omega_p^2}{(\omega_j^2 - \omega_p^2)D^{(2)}_{ijp}}\left[A^p_{jii} + A^p_{iij} + h^p_{iij}\right] + \frac{8\omega_i^6 - 2\omega_j^2\omega_i^4 - 6\omega_p^2\omega_i^4}{(\omega_j^2 - \omega_p^2)D^{(2)}_{ijp}} B^p_{jii} + \frac{\omega_i^2(\omega_j^2 - 4\omega_i^2 + \omega_p^2)}{D^{(2)}_{ijp}} B^p_{iij},$$

$$v^p_{iij} = \frac{8\omega_i^2 - 2\omega_p^2 - 2\omega_j^2}{D^{(2)}_{ijp}}\left[A^p_{jii} + A^p_{iij} + h^p_{iij}\right] + \frac{2\omega_i^2\omega_j^2 - 8\omega_i^4 + 2\omega_i^2\omega_p^2}{D^{(2)}_{ijp}} B^p_{jii} + \frac{-\omega_j^4 + 4\omega_i^2\omega_j^2 + \omega_j^2\omega_p^2}{D^{(2)}_{ijp}} B^p_{iij},$$

$$\mu^p_{iij} = \frac{8\omega_i^2 - 2\omega_j^2 - 6\omega_p^2}{(\omega_j^2 - \omega_p^2)D^{(2)}_{ijp}}\left[A^p_{iij} + A^p_{jii} + h^p_{iij}\right] + \frac{4\omega_i^2 - \omega_j^2 - \omega_p^2}{D^{(2)}_{ijp}} B^p_{iij} - \frac{6\omega_i^2\omega_j^2 + 2\omega_j^2\omega_p^2 + 2\omega_i^2\omega_p^2 - 8\omega_i^4 - \omega_p^4 - \omega_j^4}{(\omega_j^2 - \omega_p^2)D^{(2)}_{ijp}} B^p_{jii},$$

where $D^{(2)}_{ijp} = (\omega_p + 2\omega_i - \omega_j)(\omega_p + 2\omega_i + \omega_j)(-\omega_p + 2\omega_i + \omega_j)(-\omega_p + 2\omega_i - \omega_j)$.

$$\forall i = 1, \ldots, N-2, \ \forall j > i, \ldots, N-1, \ \forall k > j, \ldots, N:$$

$$
\begin{aligned}
u^p_{ijk} = \frac{1}{D^{(3)}_{ijkp}} [&(2\omega_j^4 - 6\omega_i^4 - 4\omega_k^2\omega_p^2 + 4\omega_i^2\omega_p^2 + 4\omega_i^2\omega_k^2 + 2\omega_k^4 \\
&+ 4\omega_i^2\omega_j^2 + 2\omega_p^4 - 4\omega_k^2\omega_j^2 - 4\omega_j^2\omega_p^2)(h^p_{ijk} + A^p_{ijk} + A^p_{kij} + A^p_{jik}) \\
&+ (-\omega_k^2\omega_j^4 - \omega_i^2\omega_k^4 - 2\omega_j^2\omega_i^2\omega_p^2 + 3\omega_j^2\omega_p^4 - \omega_k^4\omega_j^2 - 2\omega_i^2\omega_k^2\omega_p^2 \\
&+ 3\omega_i^2\omega_p^4 - \omega_j^4\omega_i^2 - \omega_i^4\omega_k^2 + 3\omega_k^2\omega_p^4 + \omega_i^6 - \omega_p^6 - 3\omega_k^4\omega_p^2 + \omega_k^6 - 3\omega_j^4\omega_p^2 \\
&+ 10\omega_i^2\omega_k^2\omega_j^2 + \omega_j^6 - 2\omega_k^2\omega_j^2\omega_p^2 - 3\omega_i^4\omega_p^2 - \omega_j^2\omega_i^4)B^p_{ijk} \\
&+ (-2\omega_j^4\omega_i^2 + 4\omega_i^4\omega_p^2 + 4\omega_j^2\omega_i^4 + 6\omega_i^2\omega_k^4 - 4\omega_i^4\omega_k^2 \\
&+ 4\omega_j^2\omega_i^2\omega_p^2 - 2\omega_i^2\omega_p^4 - 2\omega_i^6 - 4\omega_i^2\omega_k^2\omega_p^2 - 4\omega_i^2\omega_k^2\omega_j^2)B^p_{jik} \\
&+ (-2\omega_i^2\omega_p^4 + 6\omega_j^4\omega_i^2 + 4\omega_i^2\omega_k^2\omega_p^2 - 4\omega_i^2\omega_k^2\omega_j^2 - 4\omega_j^2\omega_i^2\omega_p^2 \\
&- 4\omega_j^2\omega_i^4 - 2\omega_i^2\omega_k^4 + 4\omega_i^4\omega_p^2 - 2\omega_i^6 + 4\omega_i^4\omega_k^2)B^p_{kij}],
\end{aligned}
$$

$$
\begin{aligned}
u^p_{jik} = \frac{1}{D^{(3)}_{ijkp}} [&(-2\omega_p^4 + 6\omega_j^4 - 2\omega_i^4 - 4\omega_k^2\omega_j^2 + 4\omega_k^2\omega_p^2 \\
&- 2\omega_k^4 + 4\omega_i^2\omega_k^2 - 4\omega_i^2\omega_j^2 + 4\omega_i^2\omega_p^2 - 4\omega_j^2\omega_p^2)(h^p_{ijk} + A^p_{ijk} + A^p_{kij} + A^p_{jik}) \\
&+ (2\omega_j^6 + 4\omega_k^2\omega_j^2\omega_p^2 + 4\omega_i^2\omega_k^2\omega_j^2 + 2\omega_j^2\omega_i^4 + 4\omega_k^2\omega_j^4 \\
&- 4\omega_j^2\omega_i^2\omega_p^2 + 2\omega_j^2\omega_p^4 - 4\omega_j^4\omega_i^2 - 4\omega_j^4\omega_p^2 - 6\omega_k^4\omega_j^2)B^p_{ijk} \\
&+ (3\omega_j^4\omega_p^2 + \omega_k^2\omega_j^4 - 3\omega_k^2\omega_p^4 + \omega_i^2\omega_k^4 + \omega_k^4\omega_j^2 + 3\omega_i^4\omega_p^2 \\
&+ 2\omega_i^2\omega_k^2\omega_p^2 + \omega_j^4\omega_i^2 + \omega_i^4\omega_k^2 - \omega_i^6 + 3\omega_k^4\omega_p^2 - \omega_j^6 - \omega_k^6 + 2\omega_j^2\omega_i^2\omega_p^2 + \omega_p^6 \\
&+ 2\omega_k^2\omega_j^2\omega_p^2 - 3\omega_j^2\omega_p^4 - 10\omega_i^2\omega_k^2\omega_j^2 - 3\omega_i^2\omega_p^4 + \omega_j^2\omega_i^4)B^p_{jik} \\
&+ (4\omega_i^2\omega_k^2\omega_j^2 + 4\omega_j^4\omega_i^2 + 2\omega_j^2\omega_p^4 - 6\omega_j^2\omega_i^4 + 2\omega_k^4\omega_j^2 - 4\omega_j^4\omega_p^2 \\
&+ 2\omega_j^6 - 4\omega_k^2\omega_j^4 - 4\omega_k^2\omega_j^2\omega_p^2 + 4\omega_j^2\omega_i^2\omega_p^2)B^p_{kij}],
\end{aligned}
$$

$$
\begin{aligned}
u^p_{kij} = \frac{1}{D^{(3)}_{ijkp}} [&(2\omega_p^4 + 2\omega_j^4 + 4\omega_i^2\omega_k^2 - 6\omega_k^4 + 4\omega_k^2\omega_p^2 - 4\omega_i^2\omega_p^2 \\
&+ 4\omega_k^2\omega_j^2 - 4\omega_i^2\omega_j^2 - 4\omega_j^2\omega_p^2 + 2\omega_i^4)(h^p_{ijk} + A^p_{ijk} + A^p_{kij} + A^p_{jik}) \\
&+ (-4\omega_i^2\omega_k^2\omega_j^2 - 2\omega_k^6 - 2\omega_i^4\omega_k^2 - 4\omega_k^2\omega_j^2\omega_p^2 + 4\omega_i^2\omega_k^2\omega_p^2 \\
&+ 6\omega_k^2\omega_j^4 - 2\omega_k^2\omega_p^4 + 4\omega_i^2\omega_k^4 - 4\omega_k^4\omega_j^2 + 4\omega_k^4\omega_p^2)B^p_{ijk} \\
&+ (-2\omega_k^6 - 4\omega_i^2\omega_k^4 + 4\omega_k^2\omega_j^2\omega_p^2 - 4\omega_i^2\omega_k^2\omega_p^2 - 2\omega_k^2\omega_p^4 + 6\omega_i^4\omega_k^2 \\
&- 4\omega_i^2\omega_k^2\omega_j^2 + 4\omega_k^4\omega_j^2 - 2\omega_k^2\omega_j^4 + 4\omega_k^4\omega_p^2)B^p_{jik} \\
&+ (-\omega_k^2\omega_j^4 - \omega_i^2\omega_k^4 - 2\omega_j^2\omega_i^2\omega_p^2 + 3\omega_j^2\omega_p^4 - \omega_k^4\omega_j^2 - 2\omega_i^2\omega_k^2\omega_p^2 \\
&+ 3\omega_i^2\omega_p^4 - \omega_j^4\omega_i^2 - \omega_i^4\omega_k^2 + 3\omega_k^2\omega_p^4 + \omega_i^6 - \omega_p^6 - 3\omega_k^4\omega_p^2 + \omega_k^6 \\
&- 3\omega_j^4\omega_p^2 + 10\omega_i^2\omega_k^2\omega_j^2 + \omega_j^6 - 2\omega_k^2\omega_j^2\omega_p^2 - 3\omega_i^4\omega_p^2 - \omega_j^2\omega_i^4)B^p_{kij}],
\end{aligned}
$$

$$
\begin{aligned}
r^p_{ijk} = \frac{1}{D^{(3)}_{ijkp}} [&(-\omega_k^2\omega_j^4 - \omega_i^2\omega_k^4 - 2\omega_j^2\omega_i^2\omega_p^2 + 3\omega_j^2\omega_p^4 - \omega_k^4\omega_j^2 \\
&- 2\omega_i^2\omega_k^2\omega_p^2 + 3\omega_i^2\omega_p^4 - \omega_j^4\omega_i^2 - \omega_i^4\omega_k^2 + 3\omega_k^2\omega_p^4 + \omega_i^6 - \omega_p^6 - 3\omega_k^4\omega_p^2 + \omega_k^6 \\
&- 3\omega_j^4\omega_p^2 + 10\omega_i^2\omega_k^2\omega_j^2 + \omega_j^6 - 2\omega_k^2\omega_j^2\omega_p^2 - 3\omega_i^4\omega_p^2 - \omega_j^2\omega_i^4)(h^p_{ijk} + A^p_{ijk} + A^p_{kij} + A^p_{jik}) \\
&+ (4\omega_i^2\omega_k^2\omega_j^4 - 4\omega_k^2\omega_j^4\omega_p^2 + 4\omega_i^2\omega_k^4\omega_j^2 - 4\omega_j^2\omega_k^4\omega_p^2 - 6\omega_i^4\omega_k^2\omega_j^2 + 2\omega_k^2\omega_j^2\omega_p^4 \\
&+ 4\omega_i^2\omega_k^2\omega_j^2\omega_p^2 - 4\omega_j^4\omega_k^4 + 2\omega_k^2\omega_j^6 + 2\omega_j^2\omega_k^6)B^p_{ijk} \\
&+ (4\omega_i^2\omega_k^4\omega_j^2 + 4\omega_i^2\omega_k^2\omega_j^2\omega_p^2 + 2\omega_i^2\omega_k^2\omega_p^4 + 2\omega_i^2\omega_k^6 + 2\omega_i^6\omega_k^2 - 4\omega_i^4\omega_k^4 \\
&- 6\omega_i^2\omega_k^2\omega_j^4 - 4\omega_i^2\omega_k^4\omega_p^2 - 4\omega_i^4\omega_k^2\omega_p^2 + 4\omega_i^4\omega_k^2\omega_j^2)B^p_{jik} \\
&+ (-4\omega_i^4\omega_j^4 + 2\omega_i^2\omega_j^2\omega_p^4 - 6\omega_i^2\omega_k^4\omega_j^2 + 2\omega_i^2\omega_j^6 + 2\omega_i^6\omega_j^2 - 4\omega_i^2\omega_j^4\omega_p^2 \\
&+ 4\omega_i^2\omega_k^2\omega_j^2\omega_p^2 + 4\omega_i^2\omega_k^2\omega_j^4 - 4\omega_i^4\omega_j^2\omega_p^2 + 4\omega_i^4\omega_k^2\omega_j^2)B^p_{kij}],
\end{aligned}
$$

$$
\begin{aligned}
\mu^p_{ijk} = \frac{1}{D^{(3)}_{ijkp}} [&(-4\omega_i^2\omega_j^2 + 4\omega_i^2\omega_p^2 + 12\omega_i^2\omega_k^2 - 4\omega_k^2\omega_j^2 + 4\omega_k^2\omega_p^2 + 2\omega_p^4 \\
&+ 10\omega_j^4 - 6\omega_i^4 - 6\omega_k^4 - 12\omega_j^2\omega_p^2)(h^p_{ijk} + A^p_{ijk} + A^p_{kij} + A^p_{jik}) \\
&+ (10\omega_i^2\omega_k^2\omega_j^2 - 2\omega_k^2\omega_j^2\omega_p^2 + 2\omega_i^2\omega_k^2\omega_p^2 - 6\omega_j^2\omega_i^2\omega_p^2 + 9\omega_k^2\omega_j^4 \\
&+ 3\omega_j^6 - 11\omega_k^4\omega_j^2 + \omega_k^2\omega_p^4 + 3\omega_i^2\omega_k^4 + \omega_k^4\omega_p^2 - \omega_k^6 - 3\omega_i^4\omega_p^2 \\
&+ 3\omega_i^2\omega_p^4 + \omega_i^6 - \omega_p^6 + 5\omega_j^2\omega_p^4 - 7\omega_j^4\omega_p^2 - 5\omega_j^4\omega_i^2 + \omega_j^2\omega_i^4 - 3\omega_i^4\omega_k^2)B^p_{ijk} \\
&+ (-18\omega_i^2\omega_k^2\omega_j^2 - 3\omega_j^2\omega_p^4 + 5\omega_k^4\omega_j^2 + 5\omega_j^2\omega_i^4 - \omega_k^2\omega_j^4 - \omega_j^4\omega_i^2 + 7\omega_i^4\omega_p^2 \\
&+ 3\omega_i^2\omega_k^4 + \omega_p^6 - \omega_j^6 - 3\omega_k^6 - 3\omega_i^6 + 3\omega_j^4\omega_p^2 + 7\omega_k^4\omega_p^2 + 3\omega_i^4\omega_k^2 + 6\omega_k^2\omega_j^2\omega_p^2 \\
&+ 6\omega_j^2\omega_i^2\omega_p^2 - 5\omega_k^2\omega_p^4 - 6\omega_i^2\omega_k^2\omega_p^2 - 5\omega_i^2\omega_p^4)B^p_{jik} \\
&+ (\omega_k^4\omega_j^2 + \omega_k^6 - 2\omega_j^2\omega_i^2\omega_p^2 + 10\omega_i^2\omega_k^2\omega_j^2 + 3\omega_k^2\omega_p^4 - 6\omega_k^2\omega_j^2\omega_p^2 - 3\omega_i^2\omega_k^4 \\
&+ 2\omega_i^2\omega_k^2\omega_p^2 + 5\omega_j^2\omega_p^4 + 3\omega_i^4\omega_k^2 - 11\omega_j^2\omega_i^4 - 3\omega_k^4\omega_p^2 + \omega_i^4\omega_p^2 + 3\omega_j^6 \\
&+ \omega_i^2\omega_p^4 - \omega_i^6 - \omega_p^6 + 9\omega_j^4\omega_i^2 - 7\omega_j^4\omega_p^2 - 5\omega_k^2\omega_j^4)B^p_{kij}],
\end{aligned}
$$

$$
\begin{aligned}
\nu^p_{kij} = \frac{1}{D^{(3)}_{ijkp}} [&(-2\omega_j^2\omega_i^2\omega_p^2 + \omega_j^4\omega_p^2 - \omega_j^6 + 3\omega_k^2\omega_j^4 + \omega_k^6 - 7\omega_i^4\omega_p^2 - 11\omega_j^4\omega_i^2 + 2\omega_k^2\omega_j^2\omega_p^2 \\
&+ 9\omega_j^2\omega_i^4 + 3\omega_i^6 + 5\omega_i^2\omega_p^4 + \omega_j^2\omega_p^4 - 5\omega_i^4\omega_k^2 + 10\omega_i^2\omega_k^2\omega_j^2 - 6\omega_i^2\omega_k^2\omega_p^2 + 3\omega_k^2\omega_p^4 \\
&- 3\omega_k^4\omega_p^2 - \omega_p^6 + \omega_i^2\omega_k^4 - 3\omega_k^4\omega_j^2)(h^p_{ijk} + A^p_{ijk} + A^p_{kij} + A^p_{jik}) \\
&+ (3\omega_i^4\omega_p^4 + \omega_i^8 - 6\omega_i^4\omega_k^2\omega_p^2 - 5\omega_i^4\omega_k^4 + 6\omega_i^2\omega_k^2\omega_j^2\omega_p^2 + 5\omega_i^2\omega_j^2\omega_p^4 - 7\omega_i^2\omega_j^4\omega_p^2 \\
&+ 18\omega_i^4\omega_k^2\omega_j^2 + 3\omega_i^2\omega_k^6 - 3\omega_i^2\omega_k^2\omega_j^4 - 7\omega_i^2\omega_k^4\omega_p^2 - 6\omega_i^4\omega_j^2\omega_p^2 + \omega_i^6\omega_k^2 - 3\omega_i^2\omega_k^4\omega_j^2 \\
&+ 5\omega_i^2\omega_k^2\omega_p^4 + \omega_i^6\omega_j^2 - 5\omega_i^4\omega_j^4 - 3\omega_i^6\omega_p^2 - \omega_i^2\omega_p^6 + 3\omega_i^2\omega_j^6)B^p_{jik}
\end{aligned}
$$

$$
\begin{aligned}
&+ (3\omega_k^2\omega_j^6 + 6\omega_i^2\omega_j^4\omega_p^2 + 5\omega_i^4\omega_j^4 + 7\omega_i^4\omega_j^2\omega_p^2 - 9\omega_i^4\omega_k^2\omega_j^2 - \omega_i^2\omega_j^6 + \omega_p^6\omega_j^2 - \omega_j^2\omega_k^4\omega_p^2 \\
&- 3\omega_p^4\omega_j^4 + 3\omega_j^6\omega_p^2 + 11\omega_i^2\omega_k^4\omega_j^2 - 3\omega_i^6\omega_j^2 - 5\omega_i^2\omega_j^2\omega_p^4 - 2\omega_k^2\omega_j^4\omega_p^2 - \omega_k^2\omega_j^2\omega_p^4 \\
&+ 2\omega_i^2\omega_k^2\omega_j^2\omega_p^2 + \omega_j^2\omega_k^6 - 3\omega_j^4\omega_k^4 - 10\omega_i^2\omega_k^2\omega_j^4 - \omega_j^8)B_{ijk}^p \\
&+ (-4\omega_i^4\omega_k^2\omega_j^2 - 6\omega_i^2\omega_k^4\omega_j^2 - 4\omega_i^4\omega_j^4 - 12\omega_i^4\omega_j^2\omega_p^2 + 2\omega_i^2\omega_j^2\omega_p^4 + 4\omega_i^2\omega_j^4\omega_p^2 \\
&+ 12\omega_i^2\omega_k^2\omega_j^4 + 10\omega_i^6\omega_j^2 - 6\omega_i^2\omega_j^6 + 4\omega_i^2\omega_k^2\omega_j^2\omega_p^2)B_{kij}^p],
\end{aligned}
$$

$$
\begin{aligned}
v_{jik}^p = \frac{1}{D_{ijkp}^{(3)}}[&(\omega_i^2\omega_k^4 + \omega_i^4\omega_p^2 + 3\omega_j^2\omega_i^4 + \omega_k^4\omega_p^2 - \omega_p^6 - 3\omega_j^4\omega_p^2 + 3\omega_j^2\omega_p^4 + 2\omega_j^2\omega_i^2\omega_p^2 + \omega_j^6 \\
&+ 3\omega_k^4\omega_j^2 + \omega_i^2\omega_p^4 + 2\omega_k^2\omega_j^2\omega_p^2 - \omega_k^6 + 2\omega_i^2\omega_k^2\omega_j^2 - 10\omega_i^2\omega_k^2\omega_p^2 - 3\omega_j^4\omega_i^2 \\
&+ \omega_i^4\omega_k^2 - 3\omega_k^2\omega_j^4 - \omega_i^6 + \omega_k^2\omega_p^4)(h_{ijk}^p + A_{ijk}^p + A_{kij}^p + A_{jik}^p) \\
&+ (-3\omega_i^4\omega_k^4 - \omega_i^2\omega_k^2\omega_p^4 - 2\omega_i^2\omega_k^4\omega_j^2 - 2\omega_i^2\omega_k^4\omega_p^2 - \omega_i^4\omega_k^2\omega_p^2 + \omega_i^6\omega_k^2 \\
&+ \omega_k^2\omega_j^6 - 2\omega_j^2\omega_k^4\omega_p^2 - \omega_i^4\omega_k^2\omega_j^2 + 3\omega_i^2\omega_k^6 - \omega_k^2\omega_j^2\omega_p^4 - 3\omega_p^4\omega_k^4 + 3\omega_k^6\omega_p^2 - \omega_k^2\omega_j^4\omega_p^2 \\
&- \omega_k^8 + 10\omega_i^2\omega_k^2\omega_j^2\omega_p^2 + 3\omega_j^2\omega_k^6 - 3\omega_j^4\omega_k^4 - \omega_i^2\omega_k^2\omega_j^4 + \omega_k^2\omega_p^6)B_{ijk}^p \\
&+ (-4\omega_i^2\omega_k^2\omega_j^2\omega_p^2 + 4\omega_i^2\omega_k^4\omega_j^2 + 4\omega_i^4\omega_k^2\omega_j^2 - 2\omega_i^2\omega_k^6 + 6\omega_i^2\omega_k^2\omega_p^4 - 4\omega_i^4\omega_k^2\omega_p^2 \\
&- 2\omega_i^6\omega_k^2 + 4\omega_i^4\omega_k^4 - 2\omega_i^2\omega_k^2\omega_j^4 - 4\omega_i^2\omega_k^4\omega_p^2)B_{jik}^p \\
&+ (-2\omega_i^4\omega_j^2\omega_p^2 + 3\omega_i^6\omega_k^2 - 3\omega_i^4\omega_k^4 + 3\omega_i^6\omega_p^2 - 3\omega_i^4\omega_p^4 - \omega_i^2\omega_j^2\omega_p^4 - 2\omega_i^4\omega_k^2\omega_p^2 \\
&- \omega_i^8 - \omega_i^2\omega_k^4\omega_p^2 + \omega_i^2\omega_j^6 - 2\omega_i^4\omega_k^2\omega_j^2 - \omega_i^2\omega_k^2\omega_p^4 + 3\omega_i^6\omega_j^2 + 10\omega_i^2\omega_k^2\omega_j^2\omega_p^2 \\
&+ \omega_i^2\omega_k^6 + \omega_i^2\omega_p^6 - \omega_i^2\omega_k^2\omega_j^4 - 3\omega_i^4\omega_j^4 - \omega_i^2\omega_j^4\omega_p^2 - \omega_i^2\omega_k^4\omega_j^2)B_{kij}^p],
\end{aligned}
$$

$$
\begin{aligned}
v_{ijk}^p = \frac{1}{D_{ijkp}^{(3)}}[&(-11\omega_k^2\omega_j^4 - 3\omega_i^4\omega_p^2 + 9\omega_k^4\omega_j^2 - \omega_p^6 + \omega_j^4\omega_p^2 - 7\omega_k^4\omega_p^2 - \omega_j^6 + \omega_i^4\omega_k^2 \\
&+ 2\omega_j^2\omega_i^2\omega_p^2 - 3\omega_j^2\omega_i^4 + 3\omega_k^6 - 6\omega_i^2\omega_k^2\omega_p^2 + \omega_j^2\omega_p^4 + 3\omega_i^2\omega_p^4 + 5\omega_k^2\omega_p^4 - 5\omega_i^2\omega_k^4 \\
&+ \omega_i^6 + 3\omega_j^4\omega_i^2 - 2\omega_k^2\omega_j^2\omega_p^2 + 10\omega_i^2\omega_k^2\omega_j^2)(h_{ijk}^p + A_{ijk}^p + A_{kij}^p + A_{jik}^p) \\
&+ (12\omega_i^2\omega_k^2\omega_j^4 - 6\omega_k^2\omega_j^6 - 4\omega_i^2\omega_k^4\omega_j^2 + 4\omega_i^2\omega_k^2\omega_j^2\omega_p^2 + 4\omega_k^2\omega_j^4\omega_p^2 \\
&+ 2\omega_k^2\omega_j^2\omega_p^4 - 4\omega_j^4\omega_k^4 - 12\omega_j^2\omega_k^4\omega_p^2 - 6\omega_i^4\omega_k^2\omega_j^2 + 10\omega_j^2\omega_k^6)B_{ijk}^p \\
&+ (3\omega_k^2\omega_j^6 + 6\omega_i^2\omega_k^2\omega_j^2\omega_p^2 + \omega_j^2\omega_k^6 - 3\omega_i^2\omega_k^2\omega_j^4 - \omega_k^2\omega_p^6 - 3\omega_i^4\omega_k^2\omega_j^2 \\
&+ 18\omega_i^2\omega_k^4\omega_j^2 - 6\omega_i^2\omega_k^4\omega_p^2 - 5\omega_j^4\omega_k^4 + 3\omega_i^6\omega_k^2 + \omega_i^2\omega_k^6 + 5\omega_i^2\omega_k^2\omega_p^4 - 6\omega_j^2\omega_k^4\omega_p^2 \\
&+ \omega_k^8 + 5\omega_k^2\omega_j^2\omega_p^4 - 3\omega_k^6\omega_p^2 + 3\omega_p^4\omega_k^4 - 7\omega_i^4\omega_k^2\omega_p^2 - 5\omega_i^4\omega_k^4 - 7\omega_k^2\omega_j^4\omega_p^2)B_{jik}^p \\
&+ (-\omega_i^4\omega_j^2\omega_p^2 - \omega_j^8 - 5\omega_k^2\omega_j^2\omega_p^4 + 7\omega_j^2\omega_k^4\omega_p^2 + 5\omega_j^4\omega_k^4 + 3\omega_j^6\omega_p^2 - \omega_k^2\omega_j^6 \\
&- 3\omega_p^4\omega_j^4 + \omega_i^6\omega_j^2 + 2\omega_i^2\omega_k^2\omega_j^2\omega_p^2 + 11\omega_i^4\omega_k^2\omega_j^2 + \omega_p^6\omega_j^2 - 10\omega_i^2\omega_k^2\omega_j^4 - 3\omega_j^2\omega_k^6 \\
&- 3\omega_i^4\omega_j^4 - 9\omega_i^2\omega_k^4\omega_j^2 + 3\omega_i^2\omega_j^6 + 6\omega_k^2\omega_j^4\omega_p^2 - \omega_i^2\omega_j^2\omega_p^4 - 2\omega_i^2\omega_j^4\omega_p^2)B_{kij}^p],
\end{aligned}
$$

where $D^{(3)}_{ijkp} = (\omega_k + \omega_i - \omega_p - \omega_j)(\omega_k + \omega_i - \omega_p + \omega_j)(-\omega_k + \omega_i + \omega_p + \omega_j)(-\omega_k + \omega_i + \omega_p - \omega_j)(\omega_k + \omega_i + \omega_p - \omega_j)(\omega_k + \omega_i + \omega_p + \omega_j)(-\omega_k + \omega_i - \omega_p + \omega_j)(-\omega_k + \omega_i - \omega_p - \omega_j)$.

References

[1] A.H. Nayfeh, D.T. Mook, *Non-Linear Oscillations*, Wiley, New York, 1979.

[2] R. Benamar, M.M. Bennouna, R.G. White, The effects of large vibration amplitudes on the mode shapes and natural frequencies of thin elastic structures. Part I: simply supported and clamped–clamped beams, *Journal of Sound and Vibration* 149 (2) (1991) 179–195.

[3] M. Amabili, F. Pellicano, M.P. Païdoussis, Nonlinear vibrations of simply supported, circular cylindrical shells, coupled to quiescent fluid, *Journal of Fluids and Structures* 12 (1998) 883–918.

[4] M. Amabili, Theory and experiments for large-amplitude vibrations of empty and fluid-filled circular cylindrical shells with imperfections, *Journal of Sound and Vibration* 262 (4) (2003) 921–975.

[5] W. Lacarbonara, A Theoretical and Experimental Investigation of Nonlinear Vibrations of Buckled Beams, Ph.D. Thesis, Virginia Polytechnic Institute and State University, 1997.

[6] A.H. Nayfeh, J.F. Nayfeh, D.T. Mook, On methods for continuous systems with quadratic and cubic nonlinearities, *Nonlinear Dynamics* 3 (1992) 145–162.

[7] M. Pakdemirli, S.A. Nayfeh, A.H. Nayfeh, Analysis of one-to-one autoparametric resonances in cables. Discretization vs. direct treatment, *Nonlinear Dynamics* 8 (1995) 65–83.

[8] A.H. Nayfeh, W. Lacarbonara, On the discretization of distributed-parameter systems with quadratic and cubic nonlinearities, *Nonlinear Dynamics* 13 (1997) 203–220.

[9] A.H. Nayfeh, Reduced-order models of weakly non-linear spatially continuous systems, *Nonlinear Dynamics* 16 (1998) 105–125.

[10] S.W. Shaw, C. Pierre, Normal modes for non-linear vibratory systems, *Journal of Sound and Vibration* 164 (1) (1993) 85–124.

[11] S.W. Shaw, C. Pierre, Normal modes of vibration for non-linear continuous systems, *Journal of Sound and Vibration* 169 (3) (1994) 319–347.

[12] R.M. Rosenberg, On non-linear vibrations of systems with many degrees of freedom, *Advances in Applied Mechanics* 9 (1966) 155–242.

[13] A.F. Vakakis, L.I. Mikhlin, Y.V. Philipchuck, A.A. Zevin, *Normal Modes and Localization in Nonlinear Systems*, Wiley, New York, 1996.

[14] L. Jezequel, C.H. Lamarque, Analysis of non-linear dynamical systems by the normal form theory, *Journal of Sound and Vibration* 149 (3) (1991) 429–459.

[15] L. Jezequel, C.H. Lamarque, Nonlinear modal synthesis based on normal form theory, *Proceedings of the Ninth International Modal Analysis Conference*, Florence, Italy, 1991, pp. 101–108.

[16] A.H. Nayfeh, S.A. Nayfeh, On nonlinear modes of continuous systems, *Transactions of American Society of Mechanical Engineers, Journal of Vibration and Acoustics* 116 (1994) 129–136.

[17] R.H. Rand, A direct method for non-linear normal modes, *International Journal of Non-linear Mechanics* 9 (1974) 363–368.

[18] A.F. Vakakis, Non-linear normal modes (NNMs) and their applications in vibration theory: an overview, *Mechanical Systems and Signal Processing* 11 (1) (1997) 3–22.

[19] E. Peshek, C. Pierre, S.W. Shaw, A new Galerkin-based approach for accurate non-linear normal modes through invariant manifolds, *Journal of Sound and Vibration* 249 (5) (2002) 971–993.

[20] J. Guckenheimer, P.J. Holmes, *Non-linear Oscillations, Dynamical Systems and Bifurcations of Vector Fields*, Springer, New York, 1986.

[21] V.I. Arnold, *Chapitres Supplémentaires de la Théorie des Équations Différentielles Ordinaires*, Mir/Librairie du Globe, Moscow/Paris, 1980.

[22] H. Poincaré, *Les Méthodes Nouvelles de la Mécanique Céleste*, Gauthiers-Villars, Paris, 1892.

[23] A.D. Brjuno, Analytical form of differential equations, *Transactions of Moscow Mathematical Society* 25 (1971) 131–288.

[24] A.H. Nayfeh, *Method of Normal Forms*, Wiley, New York, 1993.
[25] F. Pellicano, F. Mastroddi, Applicability conditions of a non-linear superposition technique, *Journal of Sound and Vibration* 200 (1) (1997) 3–14.
[26] L. Morino, F. Mastroddi, M. Cutroni, Lie Transformation method for dynamical systems having chaotic behaviour, *Nonlinear Dynamics* 7 (1995) 403–428.
[27] A.H. Nayfeh, C. Chin, S.A. Nayfeh, On nonlinear modes of systems with internal resonance, *Transactions of American Society of Mechanical Engineers, Journal of Vibration and Acoustics* 118 (1996) 340–345.
[28] E. Peshek, C. Pierre, A global methodology for the modal reduction of large non-linear systems containing quadratic and cubic non-linearities, *Proceedings of DETC'97*, *American Society of Mechanical Engineers Design Engineering Technology Conference*, Sacramento, CA, 1997.
[29] T.D. Burton, M.N. Hamdan, On the calculation of non-linear normal modes in continuous systems, *Journal of Sound and Vibration* 197 (1) (1996) 117–130.
[30] M.I. Qaisi, Non-linear normal modes of a continuous system, *Journal of Sound and Vibration* 209 (4) (1998) 561–569.
[31] F. Pellicano, F. Mastroddi, Nonlinear dynamics of a beam on elastic foundation, *Nonlinear Dynamics* 14 (1997) 335–355.
[32] C. Touzé, A normal form approach for non-linear normal modes, Internal Publication of the LMA, Vol. 156, Marseille.
[33] C. Touzé, O. Thomas, Determination of non-linear normal modes for conservative systems, *Proceedings of the Ninth ICSV*, Orlando, Paper N. 70, 2002.
[34] C. Touzé, O. Thomas, Modes normaux non-linéaires de systèmes continus, *Proceedings of Congrès Français de Mécanique*, Nice, 2003.
[35] P. Manneville, L.S. Tuckerman, Phenomenological modeling of the first bifurcations of a spherical Couette flow, *Journal de Physique* 48 (1987) 1461–1469.
[36] N. Boivin, C. Pierre, S.W. Shaw, Non-linear modal analysis of structural systems featuring internal resonances, *Journal of Sound and Vibration* 182 (2) (1995) 336–341.
[37] A.G. Haddow, A.D.S. Barr, D.T. Mook, Theoretical and experimental study of modal interaction in a two-degree-of-freedom structure, *Journal of Sound and Vibration* 97 (3) (1984) 451–473.
[38] S. Sridhar, D.T. Mook, A.H. Nayfeh, Nonlinear resonances in the forced responses of plates, Part I: symmetric responses of circular plates, *Journal of Sound and Vibration* 41 (3) (1975) 359–373.
[39] C. Touzé, P. Lanchantin, O. Thomas, A. Chaigne, Transferts d'énergie par couplage modal: étude d'un cas particulier, *Proceedings of Sixième Congrès Français d'Acoustique*, Lille, 2002.

Annexe 4 : Reduced-order models for non-linear vibrations of fluid-filled circular cylindrical shells : comparison of POD and asymptotic non-linear normal modes methods

Cette annexe donne le texte complet de l'article :

M. Amabili et C. Touzé : Reduced-order models for non-linear vibrations of fluid-filled circular cylindrical shells : comparison of POD and asymptotic non-linear normal modes methods, Journal of Fluids and Structures, **23**(6), pp. 885-903, 2007.

ELSEVIER

Journal of Fluids and Structures 23 (2007) 885–903

JOURNAL OF FLUIDS AND STRUCTURES

www.elsevier.com/locate/jfs

Reduced-order models for nonlinear vibrations of fluid-filled circular cylindrical shells: Comparison of POD and asymptotic nonlinear normal modes methods

M. Amabili[a,*], C. Touzé[b]

[a]*Dipartimento di Ingegneria Industriale, Università di Parma, Parco Area delle Scienze 181/A, Parma 43100, Italy*
[b]*ENSTA-UME, Unité de Recherche en Mécanique, Chemin de la Hunière, 91761 Palaiseau, Cedex, France*

Received 5 April 2006; accepted 28 December 2006
Available online 19 March 2007

Abstract

The aim of the present paper is to compare two different methods available for reducing the complicated dynamics exhibited by large amplitude, geometrically nonlinear vibrations of a thin shell. The two methods are: the proper orthogonal decomposition (POD), and an asymptotic approximation of the nonlinear normal modes (NNMs) of the system. The structure used to perform comparisons is a water-filled, simply supported circular cylindrical shell subjected to harmonic excitation in the spectral neighbourhood of the fundamental natural frequency. A reference solution is obtained by discretizing the partial differential equations (PDEs) of motion with a Galerkin expansion containing 16 eigenmodes. The POD model is built by using responses computed with the Galerkin model; the NNM model is built by using the discretized equations of motion obtained with the Galerkin method, and taking into account also the transformation of damping terms. Both the POD and NNMs allow to reduce significantly the dimension of the original Galerkin model. The computed nonlinear responses are compared in order to verify the accuracy and the limits of these two methods. For vibration amplitudes equal to 1.5 times the shell thickness, the two methods give very close results to the original Galerkin model. By increasing the excitation and vibration amplitude, significant differences are observed and discussed. The response is investigated also for a fixed excitation frequency by using the excitation amplitude as bifurcation parameter for a wide range of variation. Bifurcation diagrams of Poincaré maps obtained from direct time integration and calculation of the maximum Lyapunov exponent have been used to characterize the system.

Keywords: Proper orthogonal decomposition; Nonlinear normal modes; Cylindrical shells; Nonlinear vibration; Fluid-filled shells

1. Introduction

Reduced-order models (ROMs) are an attractive research topic in nonlinear dynamics of fluid and solid systems. By far, the two most popular methods used to build ROMs are the proper orthogonal decomposition (POD) and

*Corresponding author. Tel.: +39 0521 905896; fax: +39 0521 905705.
E-mail address: marco@me.unipr.it (M. Amabili).
URL: http://me.unipr.it/mam/amabili/amabili.html.

0889-9746/$ - see front matter © 2007 Elsevier Ltd. All rights reserved.
doi:10.1016/j.jfluidstructs.2006.12.004

the nonlinear normal modes (NNMs) methods. The first one (POD, also referred to as the Karhunen–Loève method) uses a cloud of points in phase space, obtained from simulations or from experiments, in order to build the reduced subspace that will contain most information (Zahorian and Rothenberg, 1981; Aubry et al., 1988; Sirovich, 1987; Breuer and Sirovich, 1991; Georgiou et al., 1999; Azeez and Vakakis, 2001; Sarkar and Païdoussis, 2003, 2004; Kerschen et al., 2003, 2005; Amabili et al., 2003, 2006; Georgiou, 2005). The method is, in essence, linear, as it furnishes the best orthogonal basis, which decorrelates the signal components and maximizes variance.

Amabili et al. (2003, 2006) compared Galerkin and POD models of a water-filled circular cylindrical shell from moderate to extremely large vibration amplitudes. Accurate POD models can be built by using only POD modes with significant energy. In particular, Amabili et al. (2006) found that more proper orthogonal modes (POMs) are necessary to reach energy convergence using time series extracted from more complex responses (chaotic or quasi-periodic) than from the periodic ones. Therefore, by using complex responses it is possible to build models with larger dimension, suitable to describe with accuracy large variations of the system parameters.

The second method (NNMs), constructs and defines the researched subspaces from specific properties of the dynamical systems, by adapting the reduction theorems provided by the mathematics: centre manifold theorem (Carr, 1981; Guckenheimer and Holmes, 1983) and normal form theory (Poincaré, 1892; Iooss and Adelmeyer, 1998; Elphick et al., 1987). Their application to vibratory systems led to two definitions of NNMs, which are equivalent in a conservative framework: either a family of periodic orbits in the vicinity of the equilibrium point (Rosenberg, 1966; Mikhlin, 1995; Vakakis et al., 1996), or an invariant manifold containing these periodic orbits (Shaw and Pierre, 1991). Numerous asymptotic methods have been proposed for their computation, by application of the centre manifold theorem (Shaw and Pierre, 1993), the normal form theory (Jézéquel and Lamarque, 1991; Touzé et al., 2004; Touzé and Amabili, 2006), the conservation of energy for conservative systems (King and Vakakis, 1994), or the method of multiple scales (Lacarbonara et al., 2003). Numerical procedures have also been proposed, recently by Jiang et al. (2005a, b), who extended the method proposed by Pesheck et al. (2002) for conservative cases. Bellizzi and Bouc (2005) propose a numerical resolution of an extended KBM (Krylov–Bogoliubov–Mitropolsky) method, while Slater (1996) used continuation techniques to generate the NNM.

Application of the POD and NNMs methods to reduced-order modelling enabled to show that a few degrees of freedom (dof) are generally enough to catch the nonlinear behaviour of many structures, versus the several necessary in the corresponding Galerkin models.

The aim of the present study is to provide a full comparison of the results given by the two reduction methods on a realistic example: a water-filled circular cylindrical shell. The reference solution is obtained by the Galerkin method. Its convergence has been carefully checked (Pellicano et al., 2002), and comparisons with experiments have been performed (Amabili, 2003). The construction of the POD model has been exhaustively explained in Amabili et al. (2003, 2006), whereas the asymptotic NNMs procedure used here is fully explained in Touzé and Amabili (2006). The peculiarity of the NNMs formulation is that damping is taken into account via an improvement of the real normal form calculation presented in Touzé et al. (2004). Comparisons will be drawn on two different cases. First, the ability of the methods to recover frequency–response curves will be investigated, for moderate values of the amplitude of the external force. Then, bifurcation diagrams for varying amplitude of the forcing, leading to complex dynamics, will be discussed.

2. Basic equations for nonlinear vibrations of shells

A cylindrical coordinate system $(O; x, r, \theta)$ is chosen, with the origin O placed at the centre of one end of the shell. The displacements of the middle surface of the shell are denoted by u, v and w, in the axial, circumferential and radial directions, respectively; w is taken positive inwards. By using Donnell's nonlinear shallow-shell theory, the equation of motion for finite-amplitude transverse deflection is given by (Evensen, 1967; Amabili and Païdoussis, 2003)

$$D\nabla^4 w + ch\dot{w} + \rho h\ddot{w} = f - p + \frac{1}{R}\frac{\partial^2 F}{\partial x^2} + \frac{1}{R^2}\left[\frac{\partial^2 F}{\partial \theta^2}\left(\frac{\partial^2 w}{\partial x^2}\right) - 2\frac{\partial^2 F}{\partial x \partial \theta}\left(\frac{\partial^2 w}{\partial x \partial \theta}\right) + \frac{\partial^2 F}{\partial x^2}\left(\frac{\partial^2 w}{\partial \theta^2}\right)\right], \tag{1}$$

where $D = Eh^3/[12(1-\nu^2)]$ is the flexural rigidity; E, the Young's modulus; ν, the Poisson ratio; h, the shell thickness; R, the mean shell radius; ρ, the mass density of the shell; c, the coefficient of viscous damping; p, the radial pressure applied to the surface of the shell by the contained fluid, and f is an external local excitation:

$$f = \tilde{f}\delta(R\theta - R\tilde{\theta})\delta(x - \tilde{x})\cos(\omega t), \tag{2}$$

where δ is the Dirac delta function, $\tilde{f}$ is the magnitude of the localized (point) force, and $\tilde{\theta}$ and $\tilde{x}$ give the angular and axial coordinates of the point of application of the force, respectively. The viscous damping model introduced in Eq. (1) is replaced by modal damping coefficients in the equations of motion.

In Eq. (1) the overdot denotes a time derivative, and F is the in-plane Airy stress function, which is given by the following compatibility equation (Evensen, 1967; Amabili and Païdoussis, 2003):

$$\frac{1}{Eh}\nabla^4 F = -\frac{1}{R}\frac{\partial^2 w}{\partial x^2} + \frac{1}{R^2}\left[\left(\frac{\partial^2 w}{\partial x \partial \theta}\right)^2 - \frac{\partial^2 w}{\partial x^2}\frac{\partial^2 w}{\partial \theta^2}\right]. \tag{3}$$

In Eqs. (1) and (3), the biharmonic operator is defined as $\nabla^4 = [\partial^2/\partial x^2 + \partial^2/(R^2\partial\theta^2)]^2$. Donnell's nonlinear shallow-shell equations are accurate only for modes with $n \geqslant 4$.

Attention is focused on simply supported, circumferentially closed circular cylindrical shells of length L. The following out-of-plane (shell surface) boundary conditions are imposed:

$$w = 0, \quad M_x = -D\{(\partial^2 w/\partial x^2) + \nu[\partial^2 w/(R^2\partial\theta^2)]\} = 0 \ \text{ at } x = 0, L, \tag{4a,b}$$

where M_x is the bending moment per unit length. The in-plane boundary conditions are

$$N_x = 0 \quad \text{and} \quad v = 0 \ \text{ at } x = 0, L, \tag{5a,b}$$

where N_x is the force per unit length in axial direction. In addition, u, v and w must be continuous in θ.

Excitations with frequency close to the natural frequency of the lowest modes of the shell are considered; low-frequency modes are associated with predominantly radial motion and are identified by the pair (m, n), where m is the number of axial half-waves and n is the number of circumferential waves.

2.1. Fluid–structure interaction

The contained fluid is assumed to be incompressible, inviscid and irrotational, so that potential flow theory can be used to describe fluid motion. Liquid-filled shells vibrating in the low-frequency range satisfy the incompressibility hypothesis very well. Nonlinear effects in the dynamic pressure and in the boundary conditions at the fluid–structure interface are neglected, which is a very good approximation for boundary displacements of two orders of magnitude (or more) smaller than the diameter of the fluid domain. The shell prestress due to the fluid weight is also neglected. The fluid motion is described by the velocity potential Φ, which satisfies the Laplace equation; cavitation is assumed not to occur. Both ends of the fluid volume, corresponding to the shell edges, are assumed to be open, so that a zero pressure is imposed there; this physically corresponds to a long shell periodically supported (e.g. with ring stiffeners) or it approximates a shell closed by very thin circular plates. The dynamic pressure p exerted by the contained fluid on the shell is given by Amabili (2003):

$$p = \rho_F(\dot{\Phi})_{r=R} = \sum_{m=1}^{M}\sum_{n=1}^{N} \rho_F[\ddot{A}_{m,n}(t)\cos(n\theta) + \ddot{B}_{m,n}(t)\sin(n\theta)]\frac{I_n(\lambda_m R)}{\lambda_m I_n'(\lambda_m R)}\sin(\lambda_m x), \tag{6}$$

where ρ_F is the mass density of the internal fluid, $A_{mn}(t)$ and $B_{mn}(t)$ are the generalized coordinates describing the shell oscillation (see Eq. (8) for more details), overdots indicate time derivatives, I_n is the modified Bessel function of order n, and I_n' its derivative with respect to the argument.

3. Reference solution and reduced-order models

3.1. Galerkin method

The Galerkin method, employing any set of basis functions φ_i, approximates the nonlinear partial differential equation (PDE) by transforming it into a finite set of coupled ordinary differential equations (ODEs), with the solution being expressed as

$$w(\boldsymbol{\xi}, t) = \sum_{i=1}^{K} q_i(t)\varphi_i(\boldsymbol{\xi}), \tag{7}$$

where t is time, $\boldsymbol{\xi}$ is the vector of spatial coordinate (x, θ) describing the shell middle surface Ω, $q_i(t)$ are the generalized coordinates, and K is the number of generalized coordinates (dof), i.e. the number of basis functions

assumed. The linear modal base is the best choice for discretizing the shell, as these are the eigenfunctions of the linear operator of the PDE. The orthogonality property of the eigenmodes allows decoupling the ODEs at the linear stage. Other sets of basis functions may be used, with the consequence that the ODEs are linearly coupled, and more functions are needed to attain convergence. The key question in the Galerkin method is the convergence of the solution. In order to have a reasonable number of dof, it is important to use the most significant modes. In addition to the asymmetric mode directly driven into vibration by the excitation (driven mode), it is necessary to consider (i) the orthogonal mode having the same shape and natural frequency but rotated by $\pi/(2n)$ (companion mode), (ii) additional asymmetric modes, and (iii) axisymmetric modes. In fact, it has clearly been established that, for large-amplitude shell vibrations, the deformation of the shell involves significant axisymmetric oscillations inwards. According to these considerations, the radial displacement w is expanded by using the eigenmodes of the empty shell, which are unchanged for the completely filled shell (Amabili, 2003):

$$w(x,\theta,t)=\sum_{m=1}^{3}\sum_{k=1}^{3}[A_{m,kn}(t)\cos(kn\theta)+B_{m,kn}(t)\sin(kn\theta)]\sin(\lambda_m x)+\sum_{m=1}^{4}A_{(2m-1),0}(t)\sin(\lambda_{(2m-1)}x), \tag{8}$$

where kn is the number of circumferential waves, m is the number of longitudinal half-waves (only odd values are used for symmetry), $\lambda_m=m\pi/L$, and t is the time; $A_{m,n}(t)$, $B_{m,n}(t)$ and $A_{m,0}(t)$ are the generalized coordinates that are unknown functions of t; the mode driven in resonance is $(1,n)$, i.e. the mode for $m=k=1$. The number of dof used in the present numerical calculations is 16 (Amabili, 2003).

The presence of pairs of modes having the same shape but different angular orientations, the first one described by $\cos(n\theta)$ (driven mode for the excitation given by Eq. (2)) and the other by $\sin(n\theta)$ (companion mode), in the periodic response of the shell leads to the appearance of a travelling wave around the shell in the θ direction when both these modes are active and when they have a relative time shift. This phenomenon is due to the axial symmetry of the system.

When the excitation has a frequency close to the resonance of a particular mode, say $(m=1,n)$, results for relatively low amplitude excitation (case of periodic response) show that (i) the generalized coordinates $A_{1,n}(t)$ and $B_{1,n}(t)$ have the same frequency as the excitation, (ii) the coordinates $A_{1,2n}(t)$, $B_{1,2n}(t)$, $A_{3,2n}(t)$, $B_{3,2n}(t)$ and all the coordinates associated with axisymmetric modes have twice the frequency of the excitation, and (iii) the coordinates $A_{3,n}(t)$, $B_{3,n}(t)$, $A_{1,3n}(t)$, $B_{1,3n}(t)$, $A_{3,3n}(t)$ and $B_{3,3n}(t)$ have three times the frequency of the excitation.

Expansion (8) used for the radial displacement w satisfies identically the boundary conditions given by Eqs. (4a,b); moreover, it satisfies exactly the continuity of the circumferential displacement. The boundary conditions for the in-plane displacements, Eqs. (5a,b), give very complex expressions when transformed into equations involving w. Therefore, they are modified into simpler integral expressions that satisfy Eqs. (5a,b) *on the average* (Amabili, 2003).

When the expansion of w, Eq. (8), is substituted in the right-hand side of Eq. (3), a PDE for the stress function F is obtained, composed of the homogeneous and the particular solution.

Eqs. (6) and (8) present the same spatial distribution on the shell surface. Therefore, the fluid pressure gives only an inertial effect, which is different for each mode of the expansion. Hence, the fluid is expected to change the nonlinear behaviour of the fluid-filled shell, as a consequence of the fundamental interaction among asymmetric and the axisymmetric modes. Usually the inertial effect of the fluid is larger for axisymmetric modes, thus enhancing the nonlinear softening-type behaviour of the shell.

By use of the Galerkin method, 16 second-order, ordinary, coupled nonlinear differential equations are obtained for the variables $A_{m,kn}(t)$, $B_{m,kn}(t)$ and $A_{m,0}(t)$, for $m=1,\ldots,M$ and $k=1,\ldots,3$, by successively weighting the original equation (1) with the functions that describe the shape of the modes retained in Eq. (8). These equations have very long expressions containing quadratic and cubic nonlinear terms and have been obtained by using the *Mathematica* 4 computer software (Wolfram, 1999), in order to perform analytical integrals of trigonometric functions. The generic jth Lagrange equation is divided by the modal mass associated with $\ddot{q}_j$, taking the following form:

$$\ddot{q}_j+\omega_j^2 q_j+2\zeta_j\omega_j\dot{q}_j+\sum_{i=1}^{K}\sum_{p=1}^{K}g_{ip}^{(j)}q_i q_p+\sum_{i=1}^{K}\sum_{p=1}^{K}\sum_{k=1}^{K}h_{ipk}^{(j)}q_i q_p q_k=\hat{f}_j\cos(\omega t)\quad\text{for } j=1,\ldots,K, \tag{9}$$

where $\hat{f}_j$ is projection of the nondimensionalized force, which must be set equal to zero in all the equations where $q_j=B_{m,kn}$, $g_{ip}^{(j)}$ are coefficients of quadratic terms and $h_{ipk}^{(j)}$ are coefficients of cubic terms; ζ_j is the modal damping ratio, replacing here the unrealistic viscous damping introduced in Eq. (1). In Eq. (9) each generalized coordinate q_j (and therefore the modal damping ζ_j and circular frequency ω_j) has to be referred to mode (m,n), i.e. $q_j=A_{m,n}$ or $B_{m,n}$. For computational convenience a nondimensionalization of variables is also performed: the time is divided by the period of the resonant mode and the vibration amplitudes are divided by the shell thickness h. It can be observed that nonlinear terms do not involve time derivatives of q_j. By introducing a dummy variable, the K second-order equations are

transformed into $2 \times K$ first-order nonlinear differential equations that are studied by using (i) the software AUTO 97 (Doedel et al., 1998) for continuation and bifurcation analysis of nonlinear ODEs, and (ii) direct integration of the equations of motion by using the DIVPAG routine of the Fortran library IMSL. Continuation methods allow following the solution path, with the advantage that unstable solutions can also be obtained; these are not ordinarily attainable by using direct numerical integration. The software AUTO 97 is capable of continuation of the solution, bifurcation analysis and branch switching by using pseudo-arclength continuation and collocation methods.

Direct integration of the equations of motion by using Gear's BDF method (routine DIVPAG of the Fortran library IMSL) has also been performed, when specified, to check the results and obtain the time behaviour. Gear's algorithm was used due to the relatively high dimension of the dynamical system.

The bifurcation diagram of the Poincaré maps was used in case of nonstationary response, i.e. to analyse a wide range of excitation magnitudes where the shell response changes dramatically. This bifurcation diagram has been constructed by using the time integration scheme and by varying the force amplitude.

3.2. Proper orthogonal decomposition (POD) method

The POD method optimally extracts the spatial information necessary to characterize the spatio-temporal complexity and inherent dimension of a system, from a set of temporal snapshots of the response, gathered from either numerical simulations or experimental data. In the present context, the temporal responses are obtained via the conventional Galerkin solution. The POMs obtained by the POD method will be used as a basis in conjunction with the Galerkin approach. The solution can be expressed by using the basis of the POMs $\psi_i(\xi)$,

$$w(\xi, t) = \sum_{i=1}^{\tilde{K}} a_i(t)\psi_i(\xi), \tag{10}$$

where a_i are the proper orthogonal coordinates and $\tilde{K}$ is the number of POMs (dof) used to build the POD model (in general, significantly lower than K in Eq. (7) necessary for the conventional Galerkin method).

The displacement field w is divided into its time-mean value $\bar{w}(\xi)$ and the zero-mean response $\tilde{w}(\xi, t) = (w(\xi, t) - \bar{w}(\xi))$. In the POD method, the POMs are obtained by minimizing the objective function

$$\tilde{\lambda} = \langle(\psi(\xi) - \tilde{w}(\xi, t))^2\rangle \quad \forall \xi \in \Omega, \tag{11}$$

with $\langle\ \rangle$ denoting the time-averaging operation and $\psi(\xi)$ the generic POD mode. If the temporal snapshots of $\tilde{w}$ are denoted by $\{\tilde{w}_n\}$, the time-averaging operation of a series of N snapshots is $\langle\tilde{w}(\xi, t)\rangle = (1/N)\sum_{n=1}^{N} \tilde{w}_n(\xi)$. Minimizing of the objective function (11) is obtained, after some mathematics, by solving the following eigenvalue problem:

$$\int_{\Omega} \langle\tilde{w}(\xi, t)\tilde{w}(\xi', t)\rangle\psi(\xi')\,\mathrm{d}\xi' = \lambda\psi(\xi), \tag{12}$$

where $\langle\tilde{w}(\xi, t)\tilde{w}(\xi', t)\rangle$ is the time-averaged spatial autocorrelation function.

A Galerkin projection scheme for determining POMs semi-analytically (Sarkar and Païdoussis, 2003), and in parallel to approximate the solution of the PDE, is presented next. The generic POM is projected on the eigenmodes $\varphi_i(\xi)$ of the shell as

$$\psi(\xi) = \sum_{i=1}^{K} \alpha_i\varphi_i(\xi), \tag{13}$$

where α_i are unknown coefficients. Then, the following eigenvalue problem is finally obtained:

$$\mathbf{A}\boldsymbol{\alpha} = \lambda\mathbf{B}\boldsymbol{\alpha}, \tag{14}$$

where

$$A_{ij} = \tau_i\tau_j\langle\tilde{q}_i(t)\tilde{q}_j(t)\rangle, \quad B_{ij} = \tau_i\delta_{ij}, \quad \tau_i = \int_{\Omega} \varphi_i^2(\xi)\,\mathrm{d}\xi, \tag{15–17}$$

δ_{ij} is the Kronecker delta, $\tilde{q}_i = (q_i - \bar{q}_i)$ is the zero-mean response of the ith generalized coordinate, with $\bar{q}_i$ being its mean. The norm of the basis functions τ_i in the present case is $\pi RL/2$ for asymmetric modes and πRL for axisymmetric modes; without effect on the results, they can be assumed to be 0.5 and 1, respectively. In Eq. (14), $\mathbf{A}$ and $\mathbf{B}$ are symmetric and positive definite matrices of dimension $K \times K$, and $\boldsymbol{\alpha}$ is a vector containing the K unknown coefficients of the POMs. The eigenvectors $\boldsymbol{\alpha}$ corresponding to the largest eigenvalues (known as dominant POMs) in Eq. (14) can now be inserted in Eq. (13) that gives a basis for the approximate solution of the PDE using the Galerkin approach; this

will be referred to as the POD-Galerkin scheme hereafter. The optimal number of terms $\tilde{K}$ to be retained can be estimated by $\sum_{i=1}^{\tilde{K}}\lambda_i/\sum_{i=1}^{K}\lambda_i \geqslant 0.99$ in Eq. (14); in fact, this expression gives an evaluation of the system energy associated with $\tilde{K}$ POMs with respect to the total energy of the system; for each problem this cut-off value can be different. It would be useful to check the convergence of the solution by increasing the value $\tilde{K}$; over a certain value, the results can become less accurate, because the additional terms introduced in the expansion may be highly noise-polluted. In particular, Amabili et al. (2006) found that more POMs are necessary to reach energy convergence using time series extracted from chaotic or quasiperiodic responses than from the periodic ones. Therefore, by using complex responses it is possible to build ROM with larger dimension, suitable for describing with accuracy large variations of the system parameters, even if they give a less-effective reduction of the order of the system.

In some applications, it may be better to use time responses obtained for different system parameters in order to produce better proper orthogonal modes.

By using Eqs. (7), (8) and (13), the expansion used for the POD solution is given by

$$w(\xi,t)=\sum_{i=1}^{\tilde{K}}a_i(t)\sum_{j=1}^{K}\alpha_{j,i}\varphi_j(\xi)=\sum_{i=1}^{\tilde{K}}a_i(t)\sum_{m=1}^{M}\sum_{n=0}^{N}[\alpha_{m,n,i}\cos(n\theta)+\beta_{m,n,i}\sin(n\theta)]\sin(\lambda_m x), \tag{18}$$

where on the right-hand side two different symbols, $\alpha_{m,n,i}$ and $\beta_{m,n,i}$, have been introduced to differentiate the coefficients of the POMs for cosine and sine terms in θ and are given by the corresponding $\alpha_{j,i}$. Eq. (18) is used to solve Eqs. (1) and (3) with the Galerkin method to find the equations of motion of the ROM. Moreover, Eq. (18) has still the same shape over the shell surface as Eq. (6); therefore, the fluid–structure interaction can be treated with the same approach used for the Galerkin method. This is not surprising, because the POD modes have been projected on the eigenmodes.

The POD method gives a set of equations of motion with exactly the same structure of those obtained with the conventional Galerkin method, Eq. (9), with the difference of a reduced order of dof, i.e. $\tilde{K}<K$. Table 1 gives the coefficients $\alpha_{m,n,i}$ and $\beta_{m,n,i}$ for two POD models built from time response obtained from the conventional Galerkin model (i) for $\omega/\omega_{1,n}=0.991$ and $\tilde{f}=3\,\mathrm{N}$ (quasi-periodic response), and (ii) for $\omega/\omega_{1,n}=0.92$ and $\tilde{f}=550\,\mathrm{N}$ (chaotic response); in particular, model (i) has $\tilde{K}=3$ dof and model (ii) has $\tilde{K}=5$ dof, versus the $K=16$ dof of the original Galerkin model. Both travelling waves around the shell in opposite directions have been taken into account (one obtained by direct integration and the other by changing the sign to the generalized coordinates associated to $\sin(n\theta)$ terms in Eq. (8)) to construct the POD ROM; these two time records have been equally weighted in order to construct the matrix **A** used to extract the eigenvalues in Eq. (14); this is fundamental in reproducing the axisymmetry of the shell with no preferential direction.

3.3. Asymptotic nonlinear normal modes (NNMs) method

NNMs are here defined as invariant manifolds of the state space. They are moreover chosen tangent at the origin, which corresponds to the position of the structure at rest. An asymptotic procedure, based on the normal form theory, is used to compute the NNMs of the system. The method is here briefly recalled, the interested reader is referred to Touzé and Amabili (2006) for a complete description. In particular, it allows to take modal damping into account in the derivations, hence extending previous results obtained for conservative systems (Touzé et al., 2004). A third-order asymptotic development is applied, in order to perform a nonlinear change of coordinates for the system of the damped unforced equation of motion, corresponding to Eq. (9) with the right-hand side equal to zero. A real formulation is

Table 1
Coefficients of the main proper orthogonal modes (POMs)

Time response	ith POM	$\alpha_{1,5,i}$	$\beta_{1,5,i}$	$\alpha_{1,10,i}$	$\beta_{1,10,i}$	$\alpha_{1,0,i}$	$\alpha_{3,0,i}$
$\omega/\omega_{1,n}=0.991$	1	1	0	0.000213	0	0.0000434	8.85×10^{-6}
	2	0	1	0	−0.000291	0	0
	3	0.000123	0	−0.1847	0	−0.9641	0.1855
Chaotic response, 550 N,	1	1	0	0.0006039	0	−0.009812	0.002283
$\omega/\omega_{1,n}=0.92$	2	0	1	0	−0.000273	0	0
	3	−0.02058	0	0.009702	0	−0.9914	0.1143
	4	0	−0.000873	0	0.9975	0	0
	5	−0.001390	0	−0.9965	0	−0.003704	0.009041

used, so that normal forms are expressed with oscillators. The dummy variable $y_j = \dot{q}_j$ for the nondimensional velocity permits to recast the system of equations into first order. The nonlinear change of coordinates is

$$q_j = r_j + \sum_{i=1}^{K}\sum_{p\geqslant i}^{K}(a_{ip}^{(j)} r_i r_p + b_{ip}^{(j)} s_i s_p) + \sum_{i=1}^{K}\sum_{p=1}^{K} c_{ip}^{(j)} r_i s_p + \sum_{i=1}^{K}\sum_{p\geqslant i}^{K}\sum_{k\geqslant p}^{K}(d_{ipk}^{(j)} r_i r_p r_k + e_{ipk}^{(j)} s_i s_p s_k) + \sum_{i=1}^{K}\sum_{p=1}^{K}\sum_{k\geqslant p}^{K}(t_{ipk}^{(j)} s_i r_p r_k + u_{ipk}^{(j)} r_i s_p s_k), \tag{19a}$$

$$y_j = s_j + \sum_{i=1}^{K}\sum_{p\geqslant i}^{K}(\alpha_{ip}^{(j)} r_i r_p + \beta_{ip}^{(j)} s_i s_p) + \sum_{i=1}^{K}\sum_{p=1}^{K} \gamma_{ip}^{(j)} r_i s_p + \sum_{i=1}^{K}\sum_{p\geqslant i}^{K}\sum_{k\geqslant p}^{K}(\lambda_{ipk}^{(j)} r_i r_p r_k + \mu_{ipk}^{(j)} s_i s_p s_k) + \sum_{i=1}^{K}\sum_{p=1}^{K}\sum_{k\geqslant p}^{K}(v_{ipk}^{(j)} s_i r_p r_k + \xi_{ipk}^{(j)} r_i s_p s_k), \tag{19b}$$

where r_j is the transformed nondimensional displacement and s_j is the transformed nondimensional velocity; other symbols are the transformation coefficients. After substitution of (19) into (9), the dynamics, written with the newly introduced variables (r_j, s_j), is expressed in an invariant-based span of the state space. As a result, proper truncations can now be realized, as all invariant-breaking terms between oscillators in Eq. (9), have been cancelled. The reduction can now be applied by simply selecting the most important normal coordinates for simulation (master coordinates), and cancelling all the others. In the case considered here, the minimum model must retain the NNMs corresponding to the driven mode (r_1, s_1, that are the continuations of $A_{1,5}$ and $\dot{A}_{1,5}$) and the companion mode (r_2, s_2, that are the continuations of $B_{1,5}$ and $\dot{B}_{1,5}$), as these two modes have the same eigenfrequency (1:1 internal resonance). Finally, the ROM built by selecting these two pairs of coordinates takes the form

$$\ddot{r}_1 + \omega_1^2 r_1 + 2\zeta_1\omega_1\dot{r}_1 + (A_{111}^{(1)} + h_{111}^{(1)})r_1^3 + B_{111}^{(1)} r_1\dot{r}_1^2 + (A_{212}^{(1)} + A_{122}^{(1)} + h_{122}^{(1)})r_1 r_2^2 + B_{122}^{(1)} r_1\dot{r}_2^2 + B_{212}^{(1)} r_2\dot{r}_1\dot{r}_2 + C_{111}^{(1)} r_1^2\dot{r}_1 + (C_{122}^{(1)} + C_{212}^{(1)})r_1 r_2\dot{r}_2 + C_{221}^{(1)} r_2^2\dot{r}_1 = \hat{f}\cos(\omega t), \tag{20a}$$

$$\ddot{r}_2 + \omega_2^2 r_2 + 2\zeta_2\omega_2\dot{r}_2 + (A_{222}^{(2)} + h_{222}^{(2)})r_2^3 + B_{222}^{2} r_2\dot{r}_2^2 + (A_{112}^{(2)} + A_{211}^{(2)} + h_{112}^{(2)})r_2 r_1^2 + B_{211}^{(2)} r_2\dot{r}_1^2 + B_{112}^{(2)} r_1\dot{r}_1\dot{r}_2 + C_{222}^{(2)} r_2^2\dot{r}_2 + (C_{121}^{(2)} + C_{211}^{(2)})r_1 r_2\dot{r}_1 + C_{112}^{(2)} r_1^2\dot{r}_2 = 0, \tag{20b}$$

where $h_{ipk}^{(j)}$ are the coefficients of cubic terms in Eq. (9), $A_{ipk}^{(j)}$, $B_{ipk}^{(j)}$ and $C_{ipk}^{(j)}$ arise from the cancellation of the quadratic terms, and are expressed by

$$A_{ipk}^{(j)} = \sum_{l\geqslant i}^{K} g_{il}^{(j)} a_{pk}^{(l)} + \sum_{l=1}^{l\leqslant i} g_{li}^{(j)} a_{pk}^{(l)}, \quad B_{ipk}^{(j)} = \sum_{l\geqslant i}^{K} g_{il}^{(j)} b_{pk}^{(l)} + \sum_{l=1}^{l\leqslant i} g_{li}^{(j)} b_{pk}^{(l)}, \quad C_{ipk}^{(j)} = \sum_{l\geqslant i}^{K} g_{il}^{(j)} c_{pk}^{(l)} + \sum_{l=1}^{l\leqslant i} g_{li}^{(j)} c_{pk}^{(l)}, \tag{21a,b,c}$$

where $g_{il}^{(j)}$ are the coefficients of quadratic terms in Eq. (9). A forcing term has been added at the end of the process and now appears in Eq. (20a). This is the second approximation used for building this ROM, as a time-invariant manifold is used. The most accurate solution would have consisted in constructing a periodically forced invariant manifold, see e.g. Jiang et al. (2005b). However, this results in a very complicated formulation and time-consuming numerical calculations for constructing the ROM. The proposed method has the advantage of simplicity, quickness of computation, and allows deriving a differential model that could be used easily for parametric studies. However, it is valid, strictly speaking, only for small values of $\hat{f}$.

With the NNMs method, the original 16 dof of the conventional Galerkin model have been reduced to two in Eq. (20). However, differently to the POD method, the structure of the equations of motion is changed. In fact, quadratic nonlinear terms have been cancelled, but cubic terms involve both the transformed nondimensional displacement and the transformed nondimensional velocity.

3.4. Discussion

After presentation of the two reduction methods, a first discussion on their theoretical settings is here provided in order to underline their abilities and limitations.

The POD method, which consists in finding the best orthogonal hyper-planes that contain most information, is essentially a linear method. This can be seen as an advantage since few manipulations, involving linear algebra only, are needed to construct the ROM. The key formula of the method, Eq. (14), is an eigenvalue problem. On the other hand,

the linear essence of the method may be a drawback, as curved subspaces are generally more suitable to capture clouds of points with complicated shapes. A NNM, being an invariant manifold in state space, is a curved subspace, so that the NNM reduction method is essentially nonlinear. The invariance property is the key that allows finding the lowest dimensional subspaces that contains dynamical properties, since dynamical motions do not stay within any other subspace that does not share this invariance property. This is the main advantage of the NNMs method as compared to the POD. It is expected that fewer NNMs are necessary than POD modes. This will be illustrated in Sections 4.1 and 4.2.

The POD method is global in the sense that it is able to capture any motion in state space and furnishes the adapted basis for decomposing it. This is an advantage as compared to the asymptotic NNMs method used here, which relies on a local theory. The third-order development, Eq. (19), is valid for small values of the modal amplitudes. The use of a time-invariant manifold in NNMs can give unreliable results for large values of the amplitude of the external forcing; in fact, the oscillations of the manifold will be too large, and the time-independent transformation will become too crude an approximation. When increasing the nonlinearities by feeding more energy into the system, the results provided by the asymptotic NNMs method are expected to deteriorate. This is not the case for the POD, if one has taken care to construct its POD-based ROM with clouds of points that are significant for a large range of values of the nonlinearity. In this context, it has already been argued (Kerschen et al., 2003; Amabili et al., 2006) that a chaotic response is the best candidate for building the POD.

Finally, the two methods differ radically in the way the ROM is built. For the POD, it is mandatory to have a response of the system to build the ROM. In the present context of a completely theoretical model, this is a drawback, since one must compute time responses to be in a position of reducing the system. Moreover, it has been underlined by Amabili et al. (2003, 2006) that the choice of these time responses is not an easy task that could not be done blindly. By comparison, the asymptotic NNMs method does not need any response of the system, but dynamical properties only, that are here provided by Eq. (9), i.e. after projection of the PDE with the Galerkin method. With the eigenvalues of the linear part (eigenfrequencies ω_j and damping coefficients ζ_j) in hand and the nonlinear coefficients $g_{il}^{(j)}$ and $h_{ipk}^{(j)}$, the nonlinear change of coordinates, Eq. (19), can be applied directly to obtain the ROM. As the coefficients in Eq. (19) are computed once and for all, application of the method is easy and not too demanding in terms of computation time. In the next section, all these conclusions will be illustrated with the numerical results.

4. Numerical results

The simply supported, water-filled circular cylindrical shell (without imperfections) investigated by Amabili (2003) is considered, with the following dimensions and material properties: $L = 520\,\text{mm}$, $R = 149.4\,\text{mm}$, $h = 0.519\,\text{mm}$, $E = 2.06 \times 10^{11}\,\text{Pa}$, $\rho = 7800\,\text{kg/m}^3$, $\rho_F = 1000\,\text{kg/m}^3$ and $\nu = 0.3$. Numerical calculations have been performed for the fundamental mode ($m = 1, n = 5$) of the water-filled shell. The natural frequency $\omega_{1,5}$ of this mode is 79.21 Hz, according to Donnell's theory of shells; modal damping $\zeta_{1,5} = 0.0017$ is assumed in the Galerkin model for the fundamental mode; for additional modes in the Galerkin model the following modal damping has been assumed: $\zeta_{mn} = \zeta_{15}\omega_{mn}/\omega_{15}$; the same values of modal damping have been used in all the ROMs.

The two reduction methods will be compared in two different cases. First, frequency–response curves, for a moderate value of the amplitude of the forcing, are investigated in the next section. A geometrical interpretation is then proposed, in order to visualize cuts of the subspaces where the dynamics is reduced. Finally, bifurcation diagrams at fixed frequency and for increasing amplitudes of the forcing are studied to check the ability of the methods over a large range of parameter variations with complex dynamical behaviours.

4.1. Frequency–response curves

The response of the fundamental mode of the water-filled shell to harmonic point excitation of 3 N at $\tilde{x} = L/2$ and $\tilde{\theta} = 0$ has been computed by using the conventional Galerkin model with 16 dofs; result is given in Fig. 1. The solution presents a main branch "1" corresponding to zero amplitude of the companion mode $B_{1,n}(t)$; this branch has pitchfork bifurcations (BP) at $\omega/\omega_{1,n} = 0.9714$ and at 1.0018, where branch "2" appears. This new branch corresponds to participation of both $A_{1,n}(t)$ and $B_{1,n}(t)$, giving a travelling wave response. Branch "2" undergoes two Neimark–Sacker (torus) bifurcations (TR), at $\omega/\omega_{1,n} = 0.9716$ and 0.9949. Amplitude-modulated (quasiperiodic) response is indicated in Fig. 1 for $0.9716 < \omega/\omega_{1,n} < 0.9949$, i.e. bracketed by the two Neimark–Sacker bifurcations.

The quasiperiodic time response of the shell for excitation of 3 N at frequency $\omega = 0.991\omega_{1,n}$, branch "2", is reported in Fig. 2 for the most significant generalized coordinates. This time response, which is more suitable than simple periodic

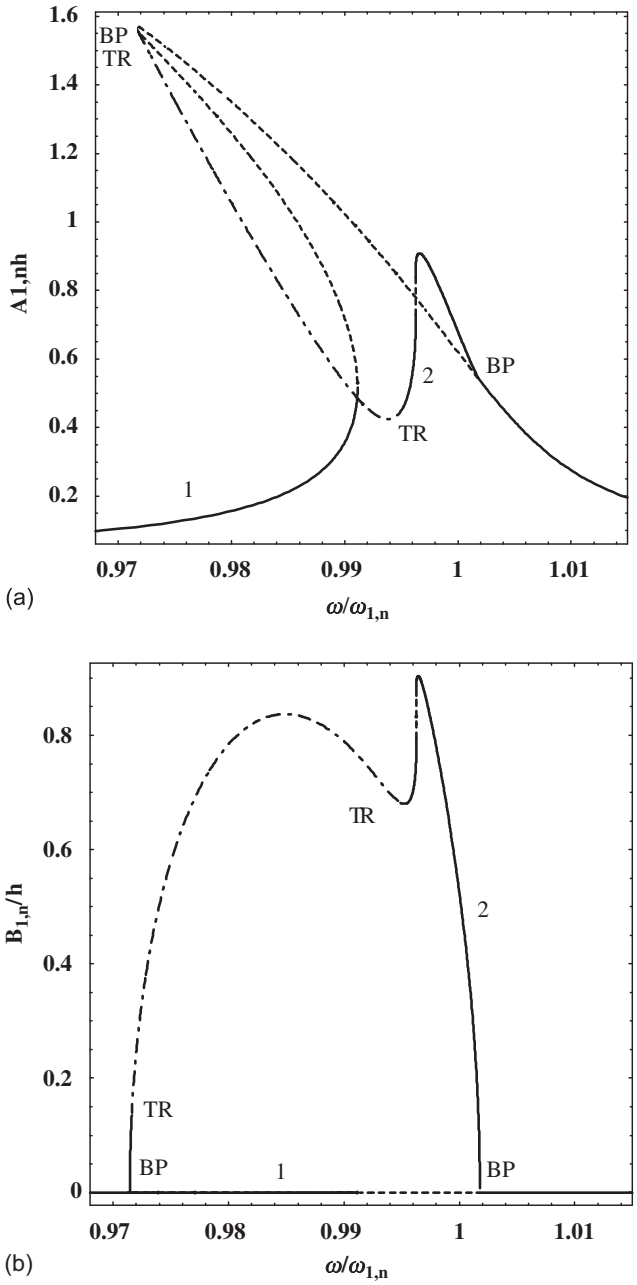

Fig. 1. Maximum amplitude of vibration versus excitation frequency, for excitation of 3 N; conventional Galerkin model, 16 dofs. (a) Maximum amplitude of $A_{1,n}(t)$, driven mode; (b) maximum amplitude of $B_{1,n}(t)$, companion mode; 1, branch "1"; 2, branch "2"; BP, pitchfork bifurcation; TR, Neimark–Sacker (torus) bifurcations. ——, stable periodic solutions; —■—, stable quasi-periodic solutions; ——, unstable periodic solutions.

responses to construct accurate POD models (Amabili et al., 2003), has been used to build a POD model. Both travelling waves around the shell in opposite directions have been taken into account (one obtained by direct integration and the other by changing the sign to the generalized coordinates associated to $\sin(n\theta)$ terms in Eq. (8)) to construct the POD ROM. The optimal number of POMs $\tilde{K}$ to be retained in the ROM can be estimated by plotting $\sum_{i=1}^{\tilde{K}}\lambda_i/\sum_{i=1}^{K}\lambda_i$ as a function of $\tilde{K}$; three POMs absorb practically all of the shell energy for the response at $\omega/\omega_{1,n}=0.991$; therefore, three POMs are used in the POD model. The coefficients of the main POMs, to be inserted in Eq. (18), are given in Table 1. The first POM is the driven mode, the second is the companion mode and the third is the axisymmetric mode.

Responses obtained by using the conventional Galerkin method (16 dofs) and by using the POD method (3 dofs) compare very well for excitation of 3 N, as shown in Fig. 3 for both driven and companion modes; the main difference is

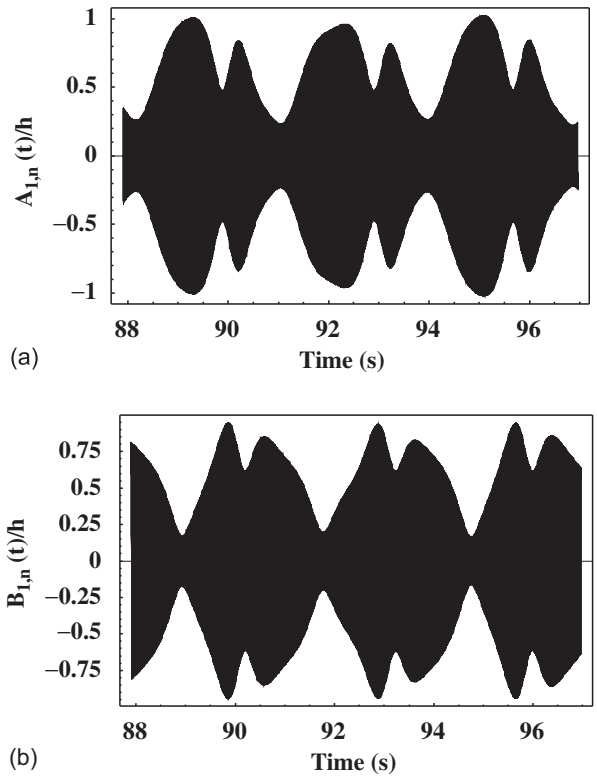

Fig. 2. Time response at excitation frequency $\omega/\omega_{1,n} = 0.991$, for excitation of 3 N; conventional Galerkin model, 16 dofs: (a) modal coordinate $A_{1,n}(t)$ associated to the driven mode; (b) modal coordinate $B_{1,n}(t)$ associated to the companion mode.

a slight shift on the right of the first bifurcation point of branch "1". It can also be observed that the natural frequency computed with the POD model is practically identical to the one computed with the Galerkin model. Fig. 3 also shows the response computed with the NNMs method with only two dof. It can be observed that also the response computed with the NNMs method compares very well with the original Galerkin model, with the curves just very slightly shifted in the left and with exact qualitative behaviour. In this case the maximum vibration amplitudes reach about $1.5h$ for the driven mode and $0.9h$ for the companion mode.

In order to compare the results also in the time domain, the quasiperiodic responses ($\omega/\omega_{1,n} = 0.991$, excitation 3 N) computed with the POD and NNMs models are reported in Figs. 4 and 5, respectively; this response is more critical to be reproduced by ROMs than simple periodic responses. Whereas the response computed with the POD is in reasonably good agreement with the one in Fig. 2 obtained with the Galerkin model, the response calculated by using the NNMs model is practically coincident with this.

Fig. 6 has been obtained with the same three models (Galerkin, NNMs and POD for which the same equations obtained with time response for excitation of 3 N has been used), but for excitation of 8 N. In this case the maximum vibration amplitudes reach about $3h$ for the driven mode and $2.5h$ for the companion mode; differences among the three models become much more significant than in the previous case. In particular, the POD model is relatively close to the original Galerkin model, the main difference being the first bifurcation point of branch "1", which is now significantly shifted on the right, giving rise to a significant difference in the qualitative behaviour of the two models. The NNMs model has qualitatively the same behaviour as the original Galerkin model, but the response is significantly shifted on the left, giving rise to the model overestimating the softening nonlinearity of the system.

It can be observed here that the POD model could be improved by using a time response computed for excitation of 8 N to find the POMs; however, it is interesting here to investigate the robustness of a ROM to changes in the system parameters, and it is therefore convenient to use the same model. On the other hand, the NNMs model is built once and for all, and may not been changed when varying the amplitude of the forcing. The observed differences with the reference solution are the consequences of the two approximations used to build it: asymptotic development and time-invariant manifold.

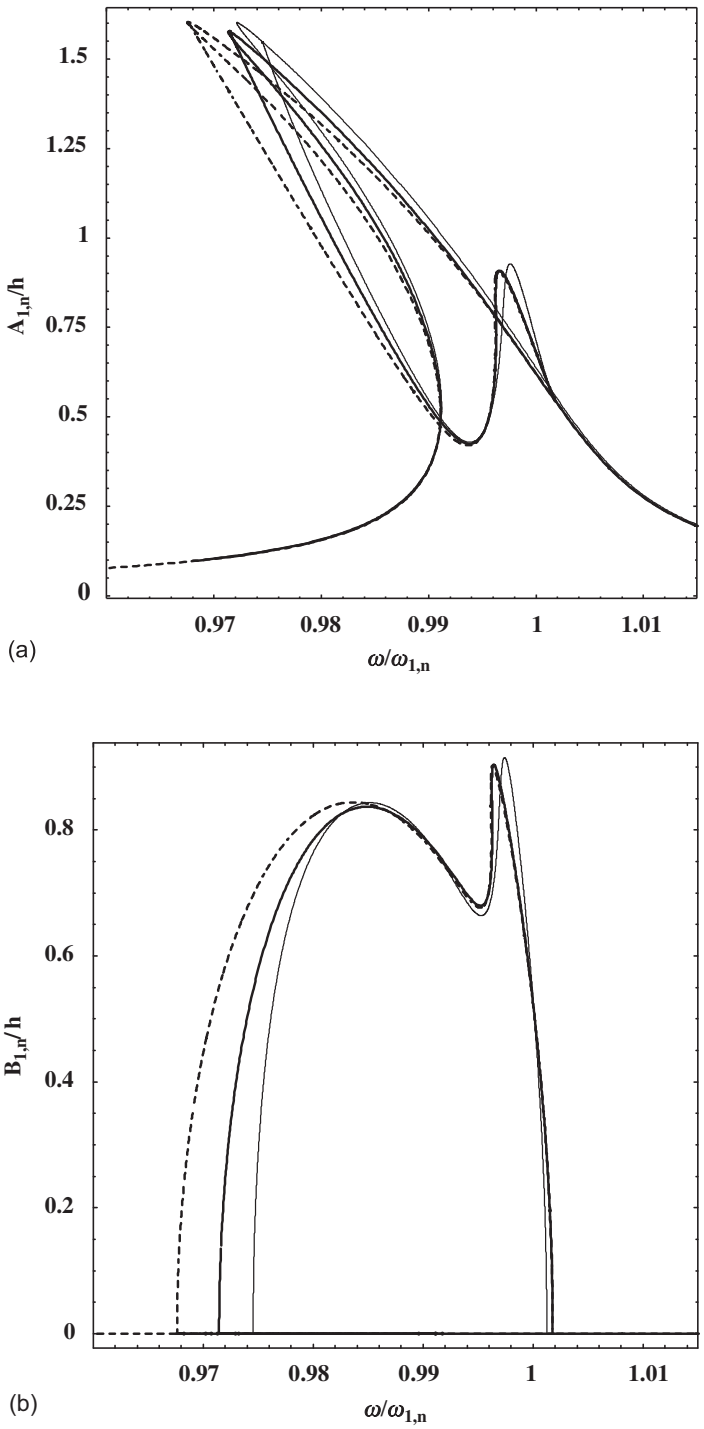

Fig. 3. Maximum amplitude of vibration versus excitation frequency, for excitation of 3 N; conventional Galerkin model, POD model with 3 modes and NNMs model with 2 modes. (a) Maximum amplitude of $A_{1,n}(t)$, driven mode; (b) maximum amplitude of $B_{1,n}(t)$, companion mode. ——, conventional Galerkin model (16 dofs); ——, POD model (3 dofs); — —, NNMs model (2 dofs).

It is well known that the contribution of axisymmetric mode, even if it is small compared to the oscillation of the fundamental mode, is fundamental to predict the correct nonlinear behaviour of the shell. It can be interesting to observe that both reduced order models do not need this knowledge *a priori*, because they act on time responses, in the case of POD, or on the equations of motion, in the case of NNMs, where this information on the system dynamics is included.

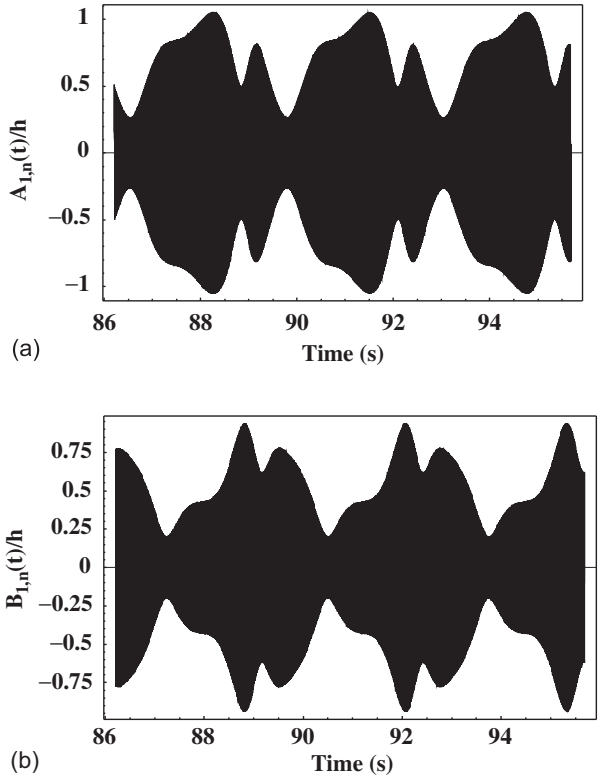

Fig. 4. Time response at excitation frequency $\omega/\omega_{1,n} = 0.991$, for excitation of 3 N; POD model, 3 dofs: (a) modal coordinate $A_{1,n}(t)$ associated to the driven mode; (b) modal coordinate $B_{1,n}(t)$ associated to the companion mode.

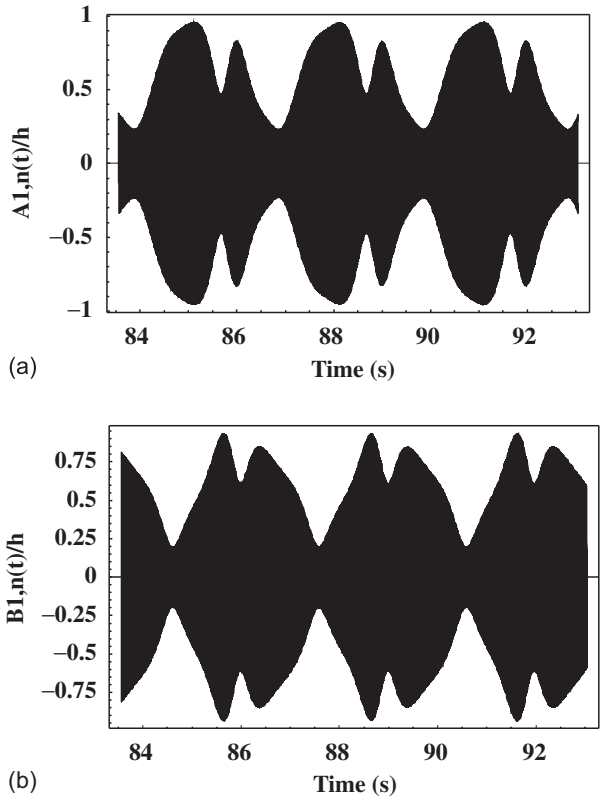

Fig. 5. Time response at excitation frequency $\omega/\omega_{1,n} = 0.991$, for excitation of 3 N; NNMs model, 2 dofs: (a) modal coordinate $A_{1,n}(t)$ associated to the driven mode; (b) modal coordinate $B_{1,n}(t)$ associated to the companion mode.

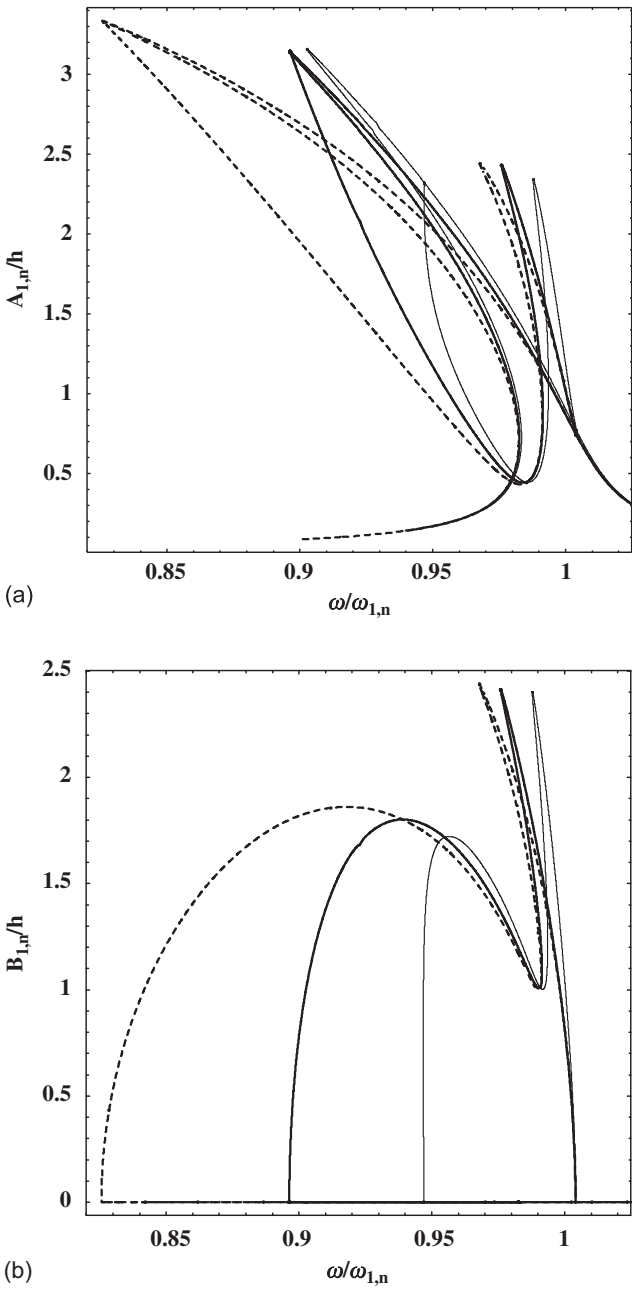

Fig. 6. Maximum amplitude of vibration versus excitation frequency, for excitation of 8 N; conventional Galerkin model, POD model with 3 modes and NNMs model with 2 modes. (a) Maximum amplitude of $A_{1,n}(t)$, driven mode; (b) maximum amplitude of $B_{1,n}(t)$, companion mode. ——, conventional Galerkin model (16 dofs); ——, POD model (3 dofs); — —, NNMs model (2 dofs).

4.2. Geometrical interpretation

In order to get a geometrical interpretation of the frequency–response curves shown in the previous section, projections and Poincaré sections of the solutions are here proposed. The state space of the reference solution, Eq. (9), is 32-dimensional (16 dofs selected with displacement and velocity as independent variables for each), plus one for the external forcing. Three different time responses are considered for excitation of 3 N: case (a), $\omega/\omega_{1,n} = 0.99$ on branch 1 with no companion mode participation; case (b), $\omega/\omega_{1,n} = 0.995$ on branch 2 with companion mode participation and harmonic response; case (c), $\omega/\omega_{1,n} = 0.991$ on branch 2 with companion mode participation and quasi-periodic response with amplitude modulations, as shown in Fig. 2.

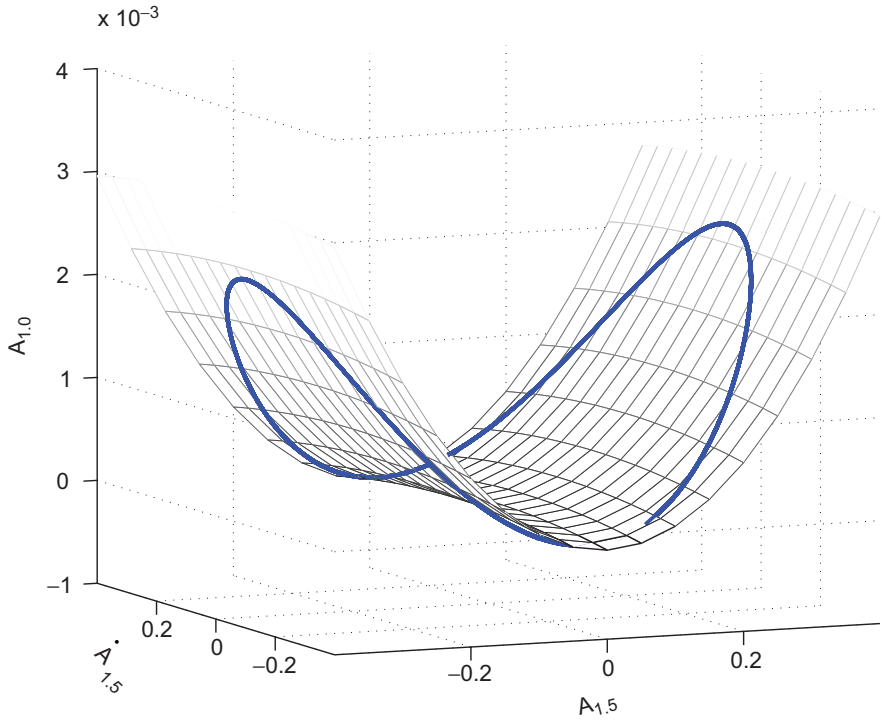

Fig. 7. Projection of the 32-dimensional state space onto the 3-dimensional subspace spanned by $(A_{1,5}, \dot{A}_{1,5}, A_{1,0})$. Closed orbit: forced motion for $\omega/\omega_{1,n} = 0.99$ and for excitation of 3 N, case (a). Curved surface: invariant manifold corresponding to the first NNM (driven mode).

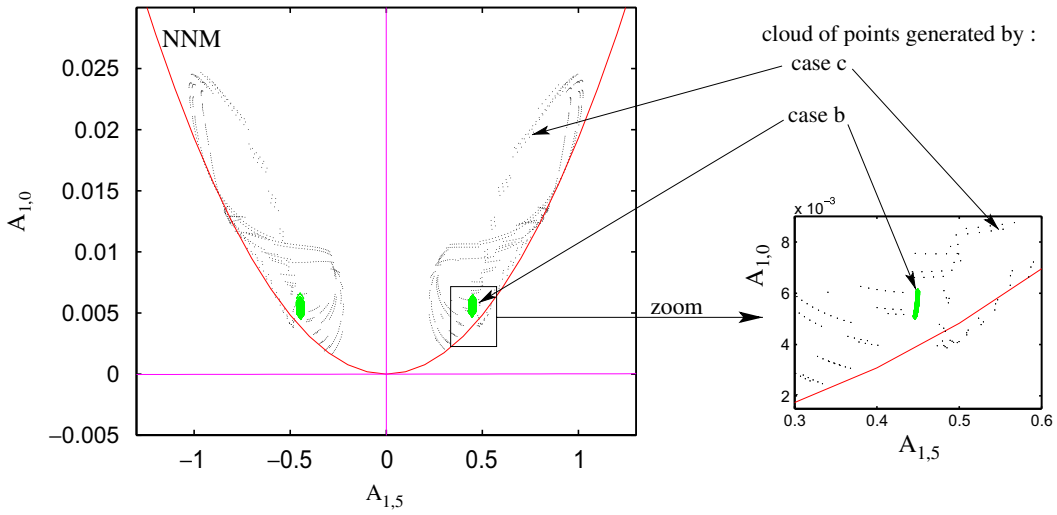

Fig. 8. Poincaré section in $(A_{1,5}, A_{1,0})$. Cloud of points: section of the orbits with the Poincaré plane, cases (b) and (c). POD differs very little from the original axis, whereas the cut of the 4-dimensional invariant manifold (curved hyperbolic line) goes right in-between the points (NNMs).

First, a two-dimensional invariant manifold, corresponding to a single NNM, is shown in Fig. 7. This NNM, defined by the coordinates (r_1, s_1) introduced in Section 3.3, corresponds to the continuation of the driven asymmetric mode: $(A_{1,5}, \dot{A}_{1,5})$. The geometry of the manifold is given by Eq. (19). Keeping N master coordinates (here $N = 1$) and cancelling the others, Eq. (19) defines a $2N$-dimensional invariant manifold in state space. The closed orbit is computed by time integration of the reference solution, and corresponds to case (a), where the companion mode is not excited, ensuring a two-dimensional motion. One can observe that the forced motion occurs in the vicinity of the time-invariant manifold, illustrating the quality of the proposed approximation. Once again, the small differences (the orbit goes

before the manifold for $A_{1,5}>0$, and behind for $A_{1,5}<0$) are due to the two approximations used for constructing the subspace.

The dynamics in the vicinity of the first eigenfrequency is essentially governed by the 1:1 internal resonance and the coupling between driven and companion mode. Hence, the dynamics is essentially four-dimensional, so that only Poincaré sections will allow illustration of the geometry of the subspaces used for reduction. Fig. 8 shows such a Poincaré map, where the selected section is the plane $(A_{1,5}, A_{1,0})$, chosen in order to show the important contribution of the first axisymmetric mode on the asymmetric motion. Two clouds of points are represented, corresponding to time series computed by the reference model at points b and c of the frequency–response curve. Point b corresponds to a coupled harmonic motion, whereas at point c the stable solution is quasiperiodic, so that the cloud of points occupies a larger part of the state space. This difference explains in particular why the POD constructed with point c is better than the one built with point b, as the problem defined by Eq. (14) is numerically better posed when the cloud of points spans a large portion of the state space. Continuous lines in Fig. 8 are the sections of the subspaces provided by POD and NNMs methods, respectively. The new POD axes are given by the α_i defined in Eq. (13), whose numerical values are recalled in Table 1. This figure clearly shows why three POD modes are necessary to recover correctly the dynamics. The new POD axes are very close to the original ones, and the cloud of point lie precisely in-between them, with a significant contribution on $A_{1,0}$. Hence, the third POD mode, which corresponds to $A_{1,0}$, must mandatorily be kept in the reduced POD model, otherwise significant dynamical information is discarded.

On the other hand, the section of the four-dimensional invariant manifold (corresponding to two NNMs) is given by the parabolic curve, which goes exactly where the computed points are. This explains why only two NNMs are necessary to recover the dynamics, as the four-dimensional manifold displays an important curvature in the direction of $A_{1,0}$. This feature is general for vibrations of shells. It allows one to use more blindly the Galerkin method in conjunction with NNMs reduction in order to recover correct qualitative behaviour, as this generic coupling between asymmetric motion and axisymmetric contraction is embedded in the NNMs. For example, this property has been used by Touzé and Thomas (2006) in order to derive the type of nonlinearity of shallow spherical shells as a function of its geometry.

Two other Poincaré sections are shown in Fig. 9, showing the contribution of the main forced motion onto $A_{3,0}$ and $A_{1,10}$. Once again, the NNMs provide a better approximation, thanks to the curvature of the reduced subspace. The corresponding POD modes could have been neglected because here the contributions are of the order of 10^{-3}.

4.3. Results for large excitations

The two ROMs are now studied on a large range of variation of the amplitude of the forcing, so as to test them in a very difficult case where numerous different dynamical behaviours have been found to coexist. Poincaré maps have been computed by direct integration of the equations of motion. The excitation frequency ω has been kept constant, $\omega = 0.92\omega_{1,n}$ (the shell displays softening-type response; therefore, for large excitation, the resonance is obtained for

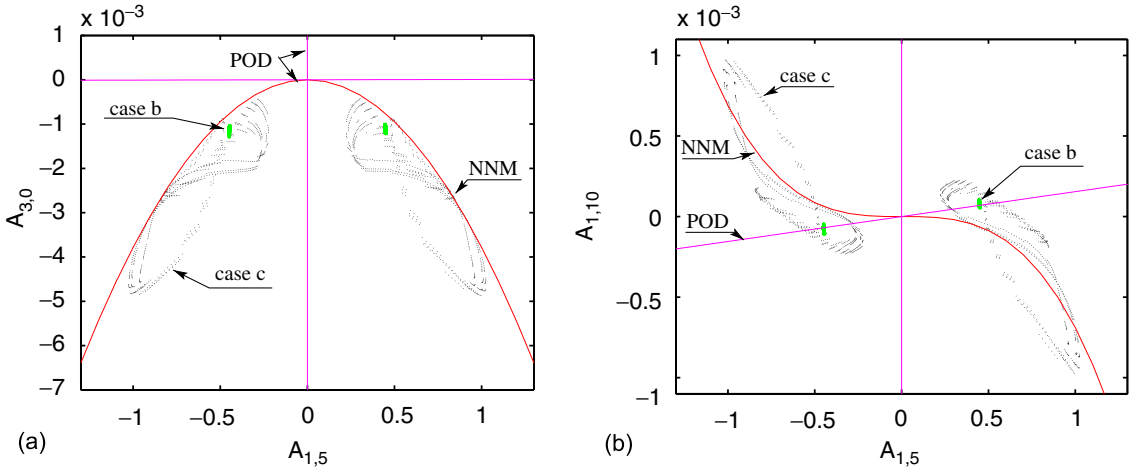

Fig. 9. Poincaré sections; cloud of points: cases (b) and (c). POD axes and NNMs sections in plain lines. (a) Poincaré section in $(A_{1,5}, A_{3,0})$; (b) Poincaré section in $(A_{1,5}, A_{1,10})$.

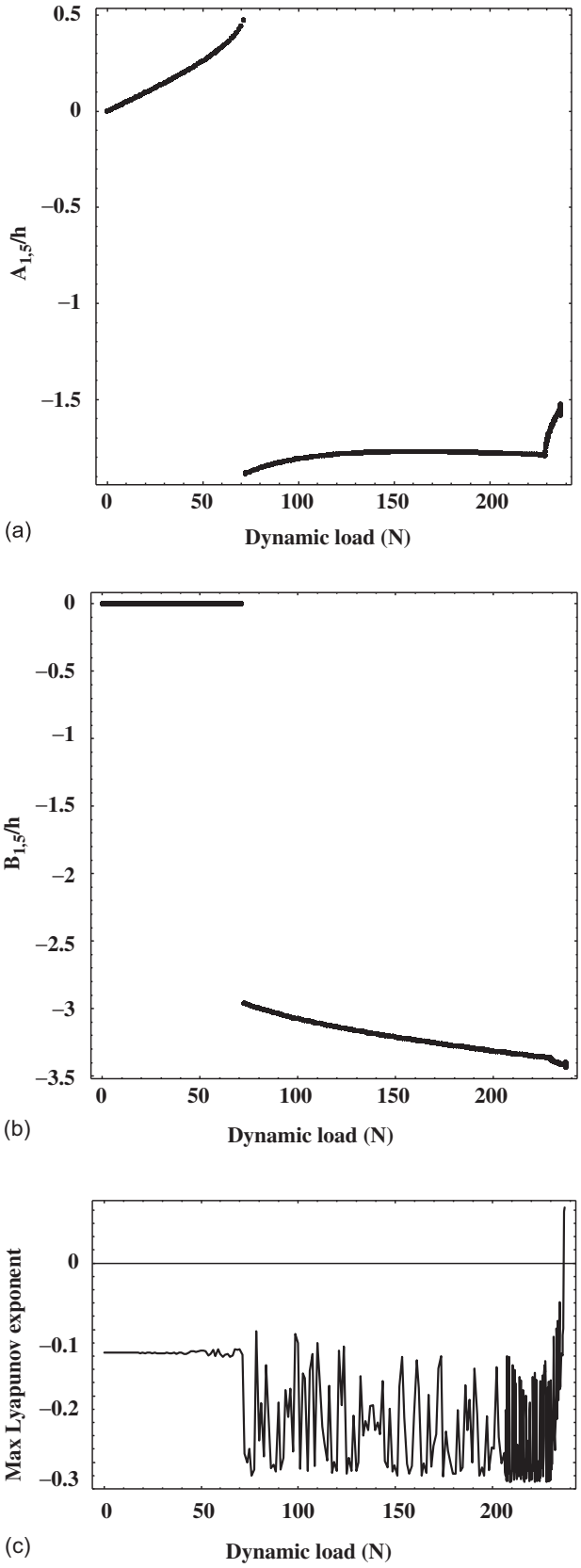

Fig. 10. Bifurcation diagram of Poincaré maps and maximum Lyapunov exponent for the shell under increasing harmonic load with frequency $\omega = 0.92\omega_{1,n}$; NNMs model, 2 dofs. (a) Generalized coordinate $A_{1,n}(t)$, driven mode; (b) generalized coordinate $B_{1,n}(t)$, companion mode; (c) maximum Lyapunov exponent.

$\omega < \omega_{1,n}$), and the excitation amplitude has been varied between 0 and 600 N. The force range has been divided into 500 steps, so that the force is varied in steps of 1.2 N. Each time the force is changed by a step, 500 periods have been allowed to elapse in order to eliminate the transient motion. The initial condition at the first step is zero displacement and velocity for all the variables. The bifurcation diagrams obtained by all these Poincaré maps by using the conventional Galerkin and the several POD models are given by Amabili et al. (2006). The POD model giving the best behaviour among those studied is the one built from chaotic time response at $\omega = 0.92\omega_{1,n}$ and excitation of 550 N; this model has 5 dofs and the coefficients of the main POMs are given in Table 1. Simple periodic motion, a period-doubling bifurcation, subharmonic response, amplitude modulations and chaotic response have been detected. This indicates the existence of complex nonlinear dynamics for the circular cylindrical shell subject to large harmonic excitation.

In the present study, this POD model (built from chaotic time response) has also been used to evaluate the frequency–response curve for excitation of 3 N. The result is not satisfactory and indicates a wrong, hardening-type nonlinearity. Therefore, a time response obtained for very different system parameters (550 N) can give an inaccurate POD model.

The bifurcation diagram for $\omega = 0.92\omega_{1,n}$, increasing excitation amplitude up to about 240 N, is given in Fig. 10(a,b) for the NNMs model with two NNMs; the corresponding maximum Lyapunov exponent is shown in Fig. 10(c). The same result has been obtained by using five nonlinear normal modes, as a consequence of the additional three modes having been found numerically to have constant null amplitude in the investigated range. The qualitative and quantitative comparison with the original Galerkin model [see Fig. 4 in Amabili et al. (2006)] is reasonably good, the main difference being that the integration of the equations obtained with the NNMs method is extremely difficult, with small perturbations stopping the integration for divergence of the solution. Moreover, it was impossible to perform the integration over the right-end point shown in Fig. 10, at about 240 N. This difficulty of integration of the NNMs model for large excitations has been related to the different structure of equations (20), where cubic terms involving velocities appear. This ill-natured behaviour of the NNMs ROM is the logical consequence of its definition. Based on a local theory and asymptotic development, the ROM is valid for small values of amplitude of forcing and modal coordinates. On the other hand, the ability of the POD to recover the essential features of the dynamics is due to its global nature. However, the numerical investigation addressed here shows that the local nature of the asymptotic NNMs allows recovering good results for an amplitude of forcing up to 240 N, and for vibration amplitudes up to $3h$, as shown in Section 4.1. As these values are not at all smaller than one, it can be concluded that the range of validity of the NNM is really greater than what could be expected. Finally, better results could be obtained by bypassing the asymptotic solution, and turning directly to a numerical resolution of the NNMs. However, the main features of the method used, which renders it particularly attractive, would be lost and replaced by an intensive numerical effort.

5. Conclusions

Both the proper orthogonal decomposition (POD) and the nonlinear normal modes (NNMs) methods have been verified to be suitable for building ROMs of a water-filled shell. In particular, a larger reduction of the model is possible by using the NNMs method. However, the asymptotic formulation used here in the NNMs method does not make it suitable for studying very large vibration amplitudes, where the POD model performs better.

These results have to be related to the properties of the two methods, discussed in Section 3.4. The nonlinear character of the invariant manifold that defines NNMs allows better reduction than the POD method, which is a linear decomposition. This property has been specifically illustrated in Section 4.2. On the other hand, the global nature of the POD provides very robust results even for complex dynamics, whereas the asymptotic NNMs has been found to fail in recovering these motions. However, it has been found that, despite being an approximation, the qualitative behaviour of the NNMs compares very well with the original solution, until the validity limits are attained. It has been found numerically that these limits are not that small: amplitude of vibration up to $3h$ and amplitude of the forcing up to 240 N.

Construction of the NNM-based ROM with the asymptotic method is direct and does not need intensive computations, as a single nonlinear change of coordinates, computed once and for all, is required. The method can thus be blindly applied, provided the Galerkin projection has been performed on a large number of modes. On the other hand, for the POD, particular care must be taken in the choice of the time responses used to build it, as already discussed in Amabili et al. (2003).

To conclude, the investigations conducted here show that for moderate vibration amplitude, the asymptotic NNMs method provides more reduced equations that always recover the qualitative behaviour. However, the method must be modified in order to bypass its main limitation, which is due to the asymptotic development. Unfortunately, only

numerical solutions are possible, thus leading to an intense numerical effort in order to build the ROM. Hence, for very large vibration amplitude and large range of parameter variations, the POD method still performs better due to its global nature.

Acknowledgements

The first author (M.A.) gratefully acknowledges fundamental cooperation on related topics with Francesco Pellicano, Michael P. Païdoussis and Abhijit Sarkar.

The second author (C.T.) gratefully acknowledges Gérard Iooss and Olivier Thomas for stimulating discussions, respectively, on the mathematical and mechanical aspects of the problems discussed herein.

References

Amabili, M., 2003. Theory and experiments for large-amplitude vibrations of empty and fluid-filled circular cylindrical shells with imperfections. Journal of Sound and Vibration 262, 921–975.

Amabili, M., Païdoussis, M.P., 2003. Review of studies on geometrically nonlinear vibrations and dynamics of circular cylindrical shells and panels, with and without fluid–structure interaction. Applied Mechanics Reviews 56 (4), 349–381.

Amabili, M., Sarkar, A., Païdoussis, M.P., 2003. Reduced-order models for nonlinear vibrations of cylindrical shells via the proper orthogonal decomposition method. Journal of Fluids and Structures 18, 227–250.

Amabili, M., Sarkar, A., Païdoussis, M.P., 2006. Chaotic vibrations of circular cylindrical shells: Galerkin versus reduced-order models via the proper orthogonal decomposition method. Journal of Sound and Vibration 290, 736–762.

Aubry, N., Holmes, P., Lumley, J.L., Stone, E., 1988. The dynamics of coherent structures in the wall region of a turbulent boundary layer. Journal of Fluid Mechanics 192, 115–173.

Azeez, M.F., Vakakis, A.F., 2001. Proper orthogonal decomposition (POD) of a class of vibroimpact oscillations. Journal of Sound and Vibration 240, 859–889.

Bellizzi, S., Bouc, R., 2005. A new formulation for the existence and calculation of nonlinear normal modes. Journal of Sound and Vibration 287, 545–569.

Breuer, K.S., Sirovich, L., 1991. The use of the Karhunen–Loève procedure for the calculation of linear eigenfunctions. Journal of Computational Physics 96, 277–296.

Carr, J., 1981. Applications of Centre Manifold Theory. Springer, New York.

Doedel, E.J., Champneys, A.R., Fairgrieve, T.F., Kuznetsov, Y.A., Sandstede, B., Wang, X., 1998. AUTO 97: Continuation and Bifurcation Software for Ordinary Differential Equations (with HomCont). Concordia University, Montreal, Canada.

Elphick, C., Tirapegui, E., Brachet, M., Coullet, P., Iooss, G., 1987. A simple global characterization for normal forms of singular vector fields. Physica D 29, 95–127.

Evensen, D.A., 1967. Nonlinear flexural vibrations of thin-walled circular cylinders. NASA TN D-4090, Washington DC, USA.

Georgiou, I.T., 2005. Advanced proper orthogonal decomposition tools: using reduced order models to identify normal modes of vibration of slow invariant manifolds in the dynamics of planar nonlinear rods. Nonlinear Dynamics 41, 69–110.

Georgiou, I.T., Schwartz, I., Emaci, E., Vakakis, A., 1999. Interaction between slow and fast oscillations in an infinite degree-of-freedom linear system coupled to nonlinear subsystem: theory and experiment. Journal of Applied Mechanics 66, 448–459.

Guckenheimer, J., Holmes, P., 1983. Non-linear Oscillations, Dynamical Systems and Bifurcations of Vector Fields. Springer, New York.

Iooss, G., Adelmeyer, M., 1998. Topics in Bifurcation Theory, second ed. World Scientific, New York, USA.

Jézéquel, L., Lamarque, C.H., 1991. Analysis of non-linear dynamical systems by the normal form theory. Journal of Sound and Vibration 149, 429–459.

Jiang, D., Pierre, C., Shaw, S., 2005a. The construction of non-linear normal modes for systems with internal resonance. International Journal of Non-Linear Mechanics 40, 729–746.

Jiang, D., Pierre, C., Shaw, S., 2005b. Nonlinear normal modes for vibratory systems under harmonic excitation. Journal of Sound and Vibration 288, 791–812.

Kerschen, G., Feeny, B.F., Golinval, J.-C., 2003. On the exploitation of chaos to build reduced-order models. Computer Methods in Applied Mechanics and Engineering 192, 1785–1795.

Kerschen, G., Golinval, J.-C., Vakakis, A.F., Bergman, L.A., 2005. The method of proper orthogonal decomposition for dynamical characterization and order reduction of mechanical systems: an overview. Nonlinear Dynamics 41, 147–169.

King, M.E., Vakakis, A.F., 1994. Energy-based formulation for computing nonlinear normal modes in undamped continuous systems. Journal of Vibration and Acoustics 116, 332–340.

Lacarbonara, W., Rega, G., Nayfeh, A.H., 2003. Resonant non-linear normal modes. Part I: analytical treatment for structural one-dimensional systems. International Journal of Non-Linear Mechanics 38, 851–872.

Mikhlin, Yu.V., 1995. Matching of local expansions in the theory of non-linear vibrations. Journal of Sound and Vibration 182, 577–588.

Pellicano, F., Amabili, M., Païdoussis, M.P., 2002. Effect of the geometry on the non-linear vibration of circular cylindrical shells. International Journal of Non-Linear Mechanics 37, 1181–1198.

Pesheck, E., Pierre, C., Shaw, S., 2002. A new Galerkin-based approach for accurate non-linear normal modes through invariant manifolds. Journal of Sound and Vibration 249, 971–993.

Poincaré, H., 1892. Les méthodes nouvelles de la mécanique céleste. Gauthiers-Villars, Paris.

Rosenberg, R.M., 1966. On non-linear vibrations of systems with many degrees of freedom. Advances in Applied Mechanics 9, 155–242.

Sarkar, A., Païdoussis, M.P., 2003. A compact limit-cycle oscillation model of a cantilever conveying fluid. Journal of Fluids and Structures 17, 525–539.

Sarkar, A., Païdoussis, M.P., 2004. A cantilever conveying fluid: coherent modes versus beam modes. International Journal of Non-Linear Mechanics 39, 467–481.

Shaw, S., Pierre, C., 1991. Non-linear normal modes and invariant manifolds. Journal of Sound and Vibration 150, 170–173.

Shaw, S.W., Pierre, C., 1993. Normal modes for non-linear vibratory systems. Journal of Sound and Vibration 164, 85–124.

Sirovich, L., 1987. Turbulence and dynamics of coherent structures, Part I: coherent structures. Quarterly Journal of Applied Mathematics 45, 561–571.

Slater, J.C., 1996. A numerical method for determining nonlinear normal modes. Nonlinear Dynamics 10, 19–30.

Touzé, C., Amabili, M., 2006. Non-linear normal modes for damped geometrically non-linear systems: application to reduced-order modeling of harmonically forced structures. Journal of Sound and Vibration 298, 958–981.

Touzé, C., Thomas, O., 2006. Non-linear behaviour of free-edge shallow spherical shells: effect of the geometry. International Journal of Non-Linear Mechanics 41, 678–692.

Touzé, C., Thomas, O., Chaigne, A., 2004. Hardening/softening behaviour in nonlinear oscillations of structural systems using non-linear normal modes. Journal of Sound and Vibration 273, 77–101.

Vakakis, A.F., Manevich, L.I., Mikhlin, Yu.V., Pilipchuk, V.N., Zevin, A.A., 1996. Normal Modes and Localization in Non-Linear Systems. Wiley, New York.

Wolfram, S., 1999. The Mathematica Book, fourth ed. Cambridge University Press, Cambridge, UK.

Zahorian, S.A., Rothenberg, M., 1981. Principal component analysis for low-redundancy encoding of speech spectra. Journal of the Acoustical Society of America 69, 519–524.

Annexe 5 : Reduced-order models for large-amplitude vibrations of shells including in-plane inertia

Cette annexe donne le texte complet de l'article :

C. Touzé, M. Amabili et O. Thomas : Reduced-order models for large-amplitude vibrations of shells including in-plane inertia, Computer Methods in Applied Mechanics and Engineering, **197**(21-24), pp. 2030-2045, 2008.

Available online at www.sciencedirect.com
ScienceDirect
Comput. Methods Appl. Mech. Engrg. 197 (2008) 2030–2045
Computer methods in applied mechanics and engineering
www.elsevier.com/locate/cma

Reduced-order models for large-amplitude vibrations of shells including in-plane inertia

C. Touzé [a,*], M. Amabili [b], O. Thomas [c]

[a] ENSTA-UME, Unité de recherche en Mécanique, Chemin de la Hunière, 91761 Palaiseau cedex, France
[b] Università di Parma, Parco Area delle scienze 181/A, Parma, Italy
[c] CNAM, Laboratoire de Mécanique des Structures et Systèmes Couplés, 2 rue Conté, 75003 Paris, France

Received 24 July 2007; received in revised form 20 December 2007; accepted 7 January 2008
Available online 24 January 2008

Abstract

Non-linear normal modes (NNMs) are used in order to derive reduced-order models for large amplitude, geometrically non-linear vibrations of thin shells. The main objective of the paper is to compare the accuracy of different truncations, using linear and non-linear modes, in order to predict the response of shells structures subjected to harmonic excitation. For an exhaustive comparison, three different shell problems have been selected: (i) a doubly curved shallow shell, simply supported on a rectangular base; (ii) a circular cylindrical panel with simply supported, in-plane free edges; and (iii) a simply supported, closed circular cylindrical shell. In each case, the models are derived by using refined shell theories for expressing the strain–displacement relationship. As a consequence, in-plane inertia is retained in the formulation. Reduction to one or two NNMs shows perfect results for vibration amplitude lower or equal to the thickness of the shell in the three cases, and this limitation is extended to two times the thickness for two of the selected models.

Keywords: Shell vibrations; Non-linear normal modes; Model reduction; Geometrical non-linearity

1. Introduction

The large amplitude, geometrically non-linear vibrations of shells leads to complicated motions with typical non-linear phenomena. As a consequence, a large number of expansion functions is generally needed for discretizing the structure in order to obtain convergence through the Galerkin method. This results in large computational times that could be prohibitive in the context of simulation or control. For this reason, there is an important need for the definition of reduced-order models (ROMs), which capture the most salient features of the non-linear dynamics with a limited number of degrees-of-freedom (dofs).

Non-linear normal modes (NNMs) are defined in order to bypass the limitations of the linear normal modes (LNMs) in the non-linear range. The idea is to "decouple" as much as possible the motions in selected sub-spaces of the phase space. This is realized by imposing the invariance of sub-spaces as the key property that must be conserved when non-linearities come into play, and leads to the definition of NNMs as invariant manifolds of the phase space [1]. As the method used for computing the NNMs is purely non-linear, it is expected to give better results than using the LNMs, or modes obtained via the proper orthogonal decomposition (POD) method [2–5].

Several methods have then been proposed to compute the NNMs. They generally rely on an asymptotic development for approximating the invariant manifold [6–11]. More recently, purely numerical methods have been proposed [12–14], but they are often restricted either by complexity (*i.e.* computational time for calculating the ROMs) or by practicality, as once the complex geometry of the manifold is computed, one has to project the equations of motion onto it. In the context of shell vibrations, reduction with asymptotic NNMs has already been applied

* Corresponding author. Tel.: +33 1 69 31 97 34; fax: +33 1 69 31 97 97.
E-mail address: cyril.touze@ensta.fr (C. Touzé).

0045-7825/$ - see front matter © 2008 Elsevier B.V. All rights reserved.
doi:10.1016/j.cma.2008.01.002

with success on a fluid-filled circular cylindrical shell described by the Donnells' shallow-shell assumptions [15], and compared with the POD method [2]. It also allows prediction of the type of non-linearity (hardening/softening behaviour) for shallow spherical shells [16].

In this study, the asymptotic NNM method is applied to shell structures, without the shallow-shell assumption. As a consequence, in-plane inertia is retained in the equations of motions, which are derived via a Lagrangian approach [17–19]. In-plane inertia must be retained for shells that cannot be considered shallow. The effect of retaining or neglecting in-plane inertia has been addressed by Amabili [17] for closed circular cylindrical shells, and by Abe et al. [20] for curved panels but only in the linear (natural frequencies) part of their study. As a consequence of taking into account these additional degrees-of-freedom, the computation of the LNMs is tedious and is thus bypassed by using as expansion functions an ad hoc basis verifying the boundary conditions. As a consequence, linear coupling terms among the discretized oscillator equations are present.

The present study is focused on the computation of frequency–response curves for harmonically forced shells vibrating at large amplitude. As a complete bifurcation diagram (with stable and unstable solution branches) in the steady-state is sought, a continuation algorithm is naturally selected. In this context, structures discretized by finite-element based methods must obviously be reduced, as the number of degrees-of-freedom involved in a classical mesh is immediately too large to be treated by standard continuation algorithm. For this reason, the LNMs and NNMs are here used for producing this reduction.

The reduction method proposed in [15] is revised in order to take into account the linear coupling terms between oscillators. In particular, these terms link together flexural and in-plane motions. The procedure is automated and thus extends earlier results presented in [21] where the in-plane motions of a plate were slaved to the flexural motions by using an invariant manifold approach. Amongst other things, the developments presented herein on the reduction process with NNMs show that the method can easily handle any set of non-linear oscillators, as well as more refined shell theories. Consequently, the method has the potential for a large class of structural problems, and could be applied to finite elements analysis of shells, where the discretization functions, as well as the underlying shell theories are distinct from those used here [22], providing that an automated step computing the projection onto the linear modes have been programmed.

Three structures are selected in order to compare the results. A doubly curved panel, and a circular cylindrical panel, with the Donnell non-linear theory without the shallow-shell assumption, are first derived. Then a closed empty shell, the kinematics of which is expressed with the Flügge-Lur'e-Byrne non-linear theory, is studied. For each case, the reference solution is compared to ROMs with an increasing number of LNMs and NNMs. The amplitude of the external forcing is also varied in order to test the validity limits of the asymptotic approach used to generate the NNMs. As side result, upper validity limits, in terms of vibration amplitude with respect to the thickness of the shells, are derived for each model.

2. Theoretical formulation

2.1. Selected cases

Three cases have been selected for studying the reduction method provided by the asymptotic NNM formulation:

(i) A hyperbolic paraboloid panel with rectangular base, referred to as the HP panel in the following.
(ii) A circular cylindrical panel, referred to as the CC panel.
(iii) A closed circular cylindrical shell, referred to as the Flügge shell.

An exhaustive presentation of the HP panel is given in [18], whereas the CC panel and the Flügge shell are respectively documented in [17,19]. These shell models have been selected in order to draw out a complete picture of the reduction process in different situations. In particular, two different kinematics are used (Donnell's non-linear shell theory is used for case (i) and (ii), while case (iii) is governed by Flügge-Lur'e-Byrne non-linear theory), and the qualitative behaviour of the closed shell (case (iii)) is appreciably different from the two panels due to the symmetry of the problem.

The three shell models will be presented in a unified manner in this section, by emphasizing the general method used to obtain the equations of motions. As a consequence, only the common features of the three models are here described. Peculiar features, such as boundary conditions or projection functions used for discretization, will be reported in Sections 4–6.

Fig. 1 shows the geometry and coordinate system for a typical shell. This geometry can handle the three cases

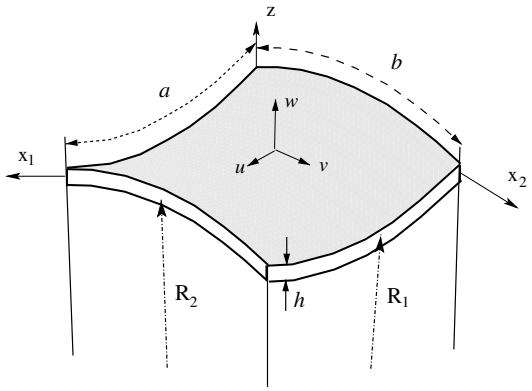

Fig. 1. Geometry and coordinate systems for the selected shells.

and is thus used here as a generic model for presenting the equations of motions. The curvilinear coordinate system is denoted by (O, x_1, x_2, z), with the origin O at one edge of the panel. R_1 and R_2 (assumed to be independent of x_1 and x_2) are the principal radii of curvature, a and b are curvilinear length, and h is the thickness. The membrane displacements are denoted by u and v, and the normal displacement is w. In the following, $\mathscr{S}$ refers to the surface of the shell, *i.e.* $\mathscr{S} = [0, a] \times [0, b]$.

2.2. Shell kinematics and external loads

The shell kinematics is described by relating the strain components ε_1, ε_2 and γ_{12} at an arbitrary point of the considered shell to the middle surface strains $\varepsilon_{1,0}$, $\varepsilon_{2,0}$ and $\gamma_{12,0}$, and to changes in the curvature and torsion of the middle surface k_1, k_2 and k_{12} by

$$\varepsilon_1 = \varepsilon_{1,0} + z k_1, \tag{1}$$

$$\varepsilon_2 = \varepsilon_{2,0} + z k_2, \tag{2}$$

$$\gamma_{12} = \gamma_{12,0} + z k_{12}, \tag{3}$$

where z is the distance of the arbitrary point from the middle surface.

For the HP and CC panels, Donnell's non-linear shell theory is used to express the strain–displacement relationship. The full expressions of the relationships between the middle surface strain–displacement and the changes in curvature and torsion can be found, for the HP panel in [18], and for the CC panel in [19]. For the Flügge shell, Flügge-Lur'e-Byrne non-linear theory is used, leading to a more complicated relationship that is not reported here for the sake of brevity. The interested reader is referred to [17,23,24] for complete expressions of the kinematics in that case.

The elastic strain energy U_S is expressed with the classical assumption of plane stress. According to the geometry shown in Fig. 1, it reads

$$U_S = \frac{1}{2}\int_{\mathscr{S}}\int_{-h/2}^{h/2}(\sigma_1\varepsilon_1 + \sigma_2\varepsilon_2 + \tau_{12}\gamma_{12})\left(1+\frac{z}{R_1}\right) \times \left(1+\frac{z}{R_2}\right)\mathrm{d}S\,\mathrm{d}z, \tag{4}$$

where the stresses σ_1, σ_2 and τ_{12} are related to the strains for an homogeneous and isotropic material by

$$\sigma_1 = \frac{E}{1-\nu^2}(\varepsilon_1 + \nu\varepsilon_2), \tag{5}$$

$$\sigma_2 = \frac{E}{1-\nu^2}(\varepsilon_2 + \nu\varepsilon_1), \tag{6}$$

$$\tau_{12} = \frac{E}{2(1+\nu)}\gamma_{12}. \tag{7}$$

The kinetic energy T_S, by neglecting rotary inertia, reads

$$T_S = \frac{1}{2}\rho h\int_{\mathscr{S}}(\dot{u}^2 + \dot{v}^2 + \dot{w}^2)\,\mathrm{d}S, \tag{8}$$

where ρ is the mass density, and overdot is used for expressing time derivation.

The virtual work W done by the external forces reads

$$W = \int_{\mathscr{S}}(q_{x_1}u + q_{x_2}v + q_z w)\,\mathrm{d}S, \tag{9}$$

where q_{x_1}, q_{x_2} and q_z are the distributed forces per unit area acting in x_1, x_2 and z directions respectively. For the three cases studied, a pointwise normal excitation due to the concentrated force $\tilde{f}$, with purely harmonic content, is considered:

$$q_{x_1} = 0, \quad q_{x_2} = 0, \quad \text{and}$$
$$q_z = \tilde{f}\,\delta(x_1 - \tilde{x}_1)\delta(x_2 - \tilde{x}_2)\cos\omega t, \tag{10}$$

where $(\tilde{x}_1, \tilde{x}_2)$ is the position of the excitation point, and ω the excitation frequency. With this expression, Eq. (9) writes

$$W(t) = \tilde{f}\cos(\omega t)w(x_1 = \tilde{x_1}, x_2 = \tilde{x_2}, t). \tag{11}$$

2.3. Lagrange equations of motions

The equations of motions are obtained via a Lagrange formulation. The displacements are expanded on a set of expansion functions $\phi_{mn}^{(u)}, \phi_{mn}^{(v)}, \phi_{mn}^{(w)}$, satisfying identically the boundary conditions

$$u(x_1, x_2, t) = \sum_{m,n=1}^{M_u,N_u} u_{mn}(t)\phi_{mn}^{(u)}(x_1, x_2), \tag{12a}$$

$$v(x_1, x_2, t) = \sum_{m,n=1}^{M_v,N_v} v_{mn}(t)\phi_{mn}^{(v)}(x_1, x_2), \tag{12b}$$

$$w(x_1, x_2, t) = \sum_{m,n=1}^{M_w,N_w} w_{mn}(t)\phi_{mn}^{(w)}(x_1, x_2). \tag{12c}$$

The explicit formulation for the selected expansion functions will be given in Section 4 for the HP panel, Section 5 for the CC panel, and Section 6 for the Flügge shell. The number of basis functions in each direction is free and governed by the integers M_u, N_u, M_v, N_v, M_w, and N_w. The damping forces are assumed to be of the viscous type. They are taken into account using Rayleigh's dissipation function

$$F = \frac{1}{2}c\int_{\mathscr{S}}(\dot{u}^2 + \dot{v}^2 + \dot{w}^2)\,\mathrm{d}S, \tag{13}$$

where c is the damping coefficient. In the remainder, modal damping is assumed, such that c will give birth to modal damping factors, that are different from one mode to another.

Let $\mathbf{q}$ be the vector of generalized coordinates, gathering together all the unknown functions of time introduced by the expansions given in Eqs. (12)

$$\mathbf{q} = [u_{m,n}, v_{m,n}, w_{m,n}]^{\mathrm{T}}, \quad m = 1, \ldots, M_u, M_v, M_w, \quad n = 1, \ldots, N_u, N_v, N_w. \tag{14}$$

In the remainder, P refers to the dimension of $\mathbf{q}$, *i.e.* the number of generalized coordinates used for discretizing the shell. The generic element of $\mathbf{q}$ is denoted by q_p.

The generalized forces Q_p are obtained by differentiation of Rayleigh's dissipation function F, provided by Eq. (13), and of the virtual work W done by external forces, Eq. (9). It reads

$$Q_p = -\frac{\partial F}{\partial \dot{q}_p} + \frac{\partial W}{\partial q_p}. \tag{15}$$

The Lagrange equations of motion can now be expressed:

$$\forall p = 1, \ldots, P: \quad \frac{\mathrm{d}}{\mathrm{d}t}\left(\frac{\partial T_S}{\partial \dot{q}_p}\right) - \frac{\partial T_S}{\partial q_p} + \frac{\partial U_S}{\partial q_p} = Q_p. \tag{16}$$

As a consequence of the kinetic energy expression, it is found that $\partial T_S/\partial \dot{q}_p = 0$. The derivation of the elastic strain energy U_S with respect to q_p shows very complicated expressions involving quadratic and cubic non-linear coupling terms among the equations. Finally, in the three considered cases, the result of the discretization gives a set of coupled non-linear oscillator equations to solve. They writes

$$\ddot{q}_p + 2\zeta_p\omega_p\dot{q}_p + \sum_{i=1}^{P} z_i^p q_i + \sum_{i,j=1}^{P} z_{i,j}^p q_i q_j + \sum_{i,j,k=1}^{P} z_{i,j,k}^p q_i q_j q_k = f_p \cos(\omega t). \tag{17}$$

Modal damping in Eq. (17) is considered in the classical form $2\zeta_p\omega_p\dot{q}_p$, and $\mathbf{f} = [f_1 \ldots f_P]^{\mathrm{T}}$ is the vector of the projected external forcing considered.

2.4. Discussion on in-plane inertia

In-plane inertia must be retained for shells that cannot be considered shallow. Moreover, for higher vibration modes of shallow shells, in-plane inertia must also be retained. A specific case is a closed circular cylindrical shells for modes with a number of circumferential waves lower than four or five. However, even for shallow curved panels and closed shells with circumferential wavenumber equal or higher than five, in-plane inertia can play a significant role, as shown by Amabili [17]. For very shallow panels, the effect of in-plane inertia can be negligible on both natural frequencies and non-linear responses.

The drawback of retaining in-plane inertia is that additional degrees-of-freedom must be taken into the expansion as a consequence that the simplified Donnell's shallow-shell formulation cannot be used. Secondly, the computation of the eigenmodes can become more difficult. Analytical eigenmodes of panels with in-plane inertia are simply obtained in case of simply supported boundary conditions. In other cases, the formulation become much more complex and it is convenient to approach the problem numerically, e.g. by using the Rayleigh–Ritz method. For these reasons, ad hoc expansion functions are here used for discretizing the problem.

3. Reduced-order modeling

3.1. Reference solution

The response of the three selected shells to concentrated harmonic force is sought. The excitation frequency ω is selected close to the first eigenfrequency of the systems. Frequency–response curves are numerically obtained with the software AUTO [25], by continuation of the solutions with the pseudo-arclength method. Bifurcation analysis, branch switching and computation of the stability is performed by AUTO. In practice, the shell response to harmonic excitation is found in two steps. Firstly, the frequency ω is set apart of the eigenfrequency, and the excitation amplitude is used as bifurcation parameter. From the stable state at rest, the excitation amplitude is raised from zero to the desired magnitude. Once this value is reached, the excitation frequency is then selected as bifurcation parameter to obtain the frequency–response curve.

The reference solution is obtained with the described method, applied to Eq. (17). The convergence of the solutions with respect to the number P of generalized coordinates retained has already been done in previous studies. It has been shown that, for the HP panel, $P = 22$ basis functions were needed for obtaining convergence [18]. For the CC panel, 19 basis functions were needed [19], whereas convergence was obtained for the Flügge shell with 16 basis functions [17]. As a consequence of these large values, computation time associated with the numerical simulations with AUTO for obtaining a single frequency–response curve are large.

The next two subsections describe two strategies for reducing the dimension P, *i.e.* the number of oscillator equations to simulate to recover the correct behaviour. These reduction strategies are crucial in order to reduce the important computational time associated to simulations with a large number of dofs, that are unavoidable when dealing with geometrically non-linear structures.

Direct integration of the equations of motion is also performed in order to obtain time responses of the selected structures. The Gear's BDF method, implemented in the DIVPAG routine of the Fortran Library IMSL, has been selected to handle the high-dimensionality of the problem associated with stiff behaviour.

3.2. Numerical computation of the linear normal modes

The first idea for reducing the size of the system is to use the linear normal modes (LNMs). Let $\mathbf{L} = [z_i^p]_{p,i}$ be the linear part of Eq. (17), and $\mathbf{P}$ the matrix of eigenvectors (numerically computed) of $\mathbf{L}$ such that: $\mathbf{P}^{-1}\mathbf{L}\mathbf{P} = \mathbf{\Lambda}$, with $\mathbf{\Lambda} = \mathrm{diag}[\omega_p^2]$, and ω_p the eigenfrequencies of the structure. A linear change of coordinates is computed, $\mathbf{q} = \mathbf{P}\mathbf{X}$, where $\mathbf{X} = [X_1 \ldots X_P]^{\mathrm{T}}$ is, by definition, the vector of modal coordinates. Application of $\mathbf{P}$ makes the linear part diagonal, so that the dynamics can now be expressed in the eigenmodes basis, and reads, $\forall p = 1, \ldots, P$:

$$\ddot{X}_p + 2\zeta_p\omega_p\dot{X}_p + \omega_p^2 X_p + \sum_{i,j=1}^{P} g_{ij}^p X_i X_j + \sum_{i,j,k=1}^{P} h_{ijk}^p X_i X_j X_k = F_p\cos(\omega t). \tag{18}$$

The application of $\mathbf{P}$ let the viscous damping unchanged, and $\mathbf{F} = \mathbf{P}^{-1}\mathbf{f} = [F_1 \dots F_P]^{\mathrm{T}}$ is the new vector of modal forces. The quadratic and cubic non-linear coupling coefficients $\{g_{ij}^p\}$ and $\{h_{ijk}^p\}$ are computed from the $\{z_{i,j}^p\}$ and $\{z_{i,j,k}^p\}$ appearing in Eq. (17) with matrix operations involving $\mathbf{P}$. The dimension of $\mathbf{X}$ is P, but truncation can now be realized by keeping any number of LNMs. Let P_{LNM} be the dimension of the truncation operated in $\mathbf{X}$. Convergence studies will be realized by increasing P_{LNM} from 1 to P. Since the LNMs possesses some interesting properties (in particular orthogonality), it is awaited to obtain convergence for $P_{\mathrm{LNM}} \leqslant P$.

3.3. Non-linear normal modes (NNMs)

Asymptotic approximation of the NNMs of the unforced structure is used to obtain further reduction of the size of the system. NNMs are defined as invariant manifold in phase space, tangent at the origin (representing the structure at rest) to the linear eigenmodes [1]. The procedure, based on normal form theory, is here briefly recalled. A complete description is provided in [15,10].

A non-linear change of coordinates is performed, in order to express the dynamics within the phase space spanned by the invariant manifolds. The invariance property is the key that allows finding reduced-order models of lower dimension than those obtained using the eigenmodes [10]. The modal velocity $Y_p = \dot{X}_p$ is used to recast the dynamical equation (18) into its first-order form. The non-linear change of coordinates, up to the third order, is computed once and for all. It reads, $\forall p = 1, \dots, P$

$$\begin{aligned} X_p = R_p &+ \sum_{i=1}^{P}\sum_{j\geqslant i}^{P}(a_{ij}^p R_i R_j + b_{ij}^p S_i S_j) + \sum_{i=1}^{P}\sum_{j=1}^{P} c_{ij}^p R_i S_j \\ &+ \sum_{i=1}^{P}\sum_{j\geqslant i}^{P}\sum_{k\geqslant j}^{P}(r_{ijk}^p R_i R_j R_k + s_{ijk}^p S_i S_j S_k) \\ &+ \sum_{i=1}^{P}\sum_{j=1}^{P}\sum_{k\geqslant j}^{P}(t_{ijk}^p S_i R_j R_k + u_{ijk}^p R_i S_j S_k), \end{aligned} \tag{19a}$$

$$\begin{aligned} Y_p = S_p &+ \sum_{i=1}^{P}\sum_{j\geqslant i}^{P}(\alpha_{ij}^p R_i R_j + \beta_{ij}^p S_i S_j) + \sum_{i=1}^{P}\sum_{j=1}^{P} \gamma_{ij}^p R_i S_j \\ &+ \sum_{i=1}^{P}\sum_{j\geqslant i}^{P}\sum_{k\geqslant j}^{P}(\lambda_{ijk}^p R_i R_j R_k + \mu_{ijk}^p S_i S_j S_k) \\ &+ \sum_{i=1}^{P}\sum_{j=1}^{P}\sum_{k\geqslant j}^{P}(\nu_{ijk}^p S_i R_j R_k + \zeta_{ijk}^p R_i S_j S_k) \end{aligned} \tag{19b}$$

The newly introduced variables, (R_p, S_p), are respectively homogeneous to a displacement and a velocity, and are called the *normal* coordinates. The introduced coefficients in Eqs. (19) are the transformation coefficients, whose analytical expressions are given in [15]. Substitution of (19) into (18) gives the dynamics expressed in the invariant-based span of the phase space. It reads, $\forall p = 1, \dots, P$

$$\begin{aligned} &\ddot{R}_p + \omega_p^2 R_p + 2\zeta_p\omega_p\dot{R}_p + \left(h_{ppp}^p + A_{ppp}^p\right)R_p^3 + B_{ppp}^p R_p\dot{R}_p^2 \\ &+ C_{ppp}^p R_p^2\dot{R}_p + R_p\left[\sum_{j>p}^{N}\left[(h_{pjj}^p + A_{pjj}^p + A_{jpj}^p)R_j^2 + B_{pjj}^p\dot{R}_j^2 \right.\right. \\ &\left.\left. +(C_{pjj}^p + C_{jpj}^p)R_j\dot{R}_j\right] \right. \\ &\left. + \sum_{i<p}\left[(h_{iip}^p + A_{iip}^p + A_{pii}^p)R_i^2 + B_{pii}^p\dot{R}_i^2 + (C_{pii}^p + C_{ipi}^p)R_i\dot{R}_i\right]\right] \\ &+ \dot{R}_p\left[\sum_{j>p}^{N}\left(B_{jpj}^p R_j\dot{R}_j + C_{jjp}^p R_j^2\right) + \sum_{i<p}(B_{iip}^p R_i\dot{R}_i + C_{iip}^p R_i^2)\right] \\ &= F_p\cos(\omega t). \end{aligned} \tag{20}$$

Eq. (20) is the normal form, up to the third order, of Eq. (18), computed without the forcing term on the right-hand side. The forcing term $\mathbf{F} = [F_1 \dots F_P]^{\mathrm{T}}$ is added after the non-linear change of coordinates on the normal oscillator equations. As a consequence of this treatment of the forcing term, the non-linear change of coordinate is time-independent. Hence two approximations have been used to build the reduced-order model based on NNMs. Firstly, the invariant manifolds are approximated via an asymptotic development up to order three. Secondly, time-independent NNMs are used to approximate time-dependent manifolds. In the mechanical context, a time-dependent formulation for computation of NNMs have been proposed by Jiang et al. [13,26], by adapting a numerical Galerkin procedure earlier developed by Pesheck et al. [12,27]. Their numerical results shows, amongst other things, that for moderate values of the forcing, the oscillations of the manifolds are small. Moreover, taking them into account requires a huge numerical effort.

Due to these two approximations, it is thus expected to obtain very good results for moderate values of the forcing and of the amplitude of the response. By increasing the amplitude of the forcing, the results are expected to deteriorate. One purpose of the present study is also to give an upper validity limit, in terms of the amplitude of the response, of these approximated NNMs, as three different cases are tested.

On the other hand, the proposed method bears a number of advantages. On the theoretical viewpoint, the main advantage of the NNM method is that it relies on the idea of invariance, ensuring proper truncations, as already shown in [10], and in [2] where a full comparison with the POD method is performed. Secondly, as compared to more numerically involved methods as the one by Jiang et al. [13], the reduction process is here quick and easy to use. Finally, the number of NNMs that one must keep in

the truncation is known beforehand by simply looking at the internal resonances in the linear spectrum. If no internal resonance is present, a single NNM is enough to catch the dynamics. This will be shown in Sections 4 and 5. If internal resonances are present, one has to keep all the NNMs involved in the internal resonance. One key point of the method presented here, relying on normal form theory, is that no extra work is needed to handle the case of internal resonance. In Section 6 concerned with the Flügge shell, as a consequence of the fact that the shell is closed, degenerate eigenvalues are present, giving birth to companion modes, linearly independent but having the same eigenfrequency. Thus 1:1 internal resonance are present, and two NNMs will be kept in order to reduce the system.

4. Hyperbolic paraboloid panel

4.1. Boundary conditions and projection functions

The HP panel is shown in Fig. 1. The curvilinear axial coordinates are specified by setting $x_1 = x$, and $x_2 = y$. The radii of curvature are such that $R_x = -R_y$.

Classical simply supported boundary conditions at the four edges are assumed, so that:

$$v = w = N_x = M_x = 0 \quad \text{at } x = 0, a, \tag{21a}$$

$$u = w = N_y = M_y = 0 \quad \text{at } y = 0, b, \tag{21b}$$

where N_x, N_y are the normal forces and M_x, M_y the bending moments per unit length.

The basis functions are respectively

$$\phi^{(u)}_{m,n}(x,y) = \cos(m\pi x/a)\sin(n\pi y/b), \tag{22a}$$

$$\phi^{(v)}_{m,n}(x,y) = \sin(m\pi x/a)\cos(n\pi y/b), \tag{22b}$$

$$\phi^{(w)}_{m,n}(x,y) = \sin(m\pi x/a)\sin(n\pi y/b). \tag{22c}$$

Two non-linear terms $\hat{u}$ and $\hat{v}$ are added to Eqs. (22a) and (22b), respectively, in order to identically satisfy the boundary conditions, as shown in [18].

4.2. Simulation results

Numerical simulations have been performed for a HP panel with $a = b = 0.1$ m, $R_x = -R_y = 1$ m, and thickness $h = 1$ mm. The material is linear elastic with Young's modulus $E = 206.10^9$ Pa, density $\rho = 7800\ \text{kg m}^{-3}$ and Poisson's ratio $\nu = 0.3$. The response of the HP panel to harmonic excitation in the vicinity of the first eigenfrequency ω_1 is numerically computed. The convergence of the solution has been carefully studied in [18] for an excitation amplitude $\tilde{f}$ of 4.37 N applied at the center of the panel. It has been shown that 22 basis functions were necessary to obtain convergence. More precisely, the generalized coordinates retained for this reference solution are $w_{1,1}$, $w_{1,3}$, $w_{3,1}$, $w_{3,3}$, $u_{1,1}$, $u_{3,1}$, $u_{1,3}$, $u_{3,3}$, $u_{1,5}$, $u_{5,1}$, $u_{3,5}$, $u_{5,3}$, $u_{5,5}$, $v_{1,1}$, $v_{3,1}$, $v_{1,3}$, $v_{3,3}$, $v_{1,5}$, $v_{5,1}$, $v_{3,5}$, $v_{5,3}$, $v_{5,5}$. The damping parameter ζ_p has been set to 0.004 for each mode: $\forall p = 1 \ldots 22, \zeta_p = 0.004$.

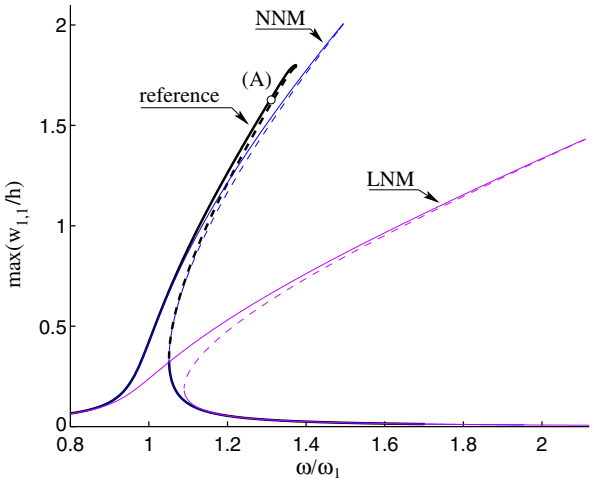

Fig. 2. Frequency–response curve for the HP panel, harmonically excited in the vicinity of the first eigenfrequency ω_1. The reference solution is compared to the solution given by keeping a single linear mode (LNM) or a single NNM. The excitation amplitude is $\tilde{f} = 4.37$ N. Point (A), with $\omega = 1.3\omega_1$, is used for time integration, see Fig. 5.

Fig. 2 shows the frequency–response curve for this reference solution, numerically obtained by a continuation method (pseudo-arclength is used) implemented within the software AUTO [25]. The reference solution with 22 basis functions is compared to two severely reduced-order models, composed of a single oscillator equation. The first one is obtained by keeping in the truncation only the first LNM ($P_{\text{LNM}} = 1$). Eq. (18) are restricted to the first one

$$\ddot{X}_1 + 2\zeta_1\omega_1\dot{X}_1 + \omega_1^2 X_1 + g^1_{11}X_1^2 + h^1_{111}X_1^3 = F_1\cos(\omega t). \tag{23}$$

Branches of solution are numerically obtained by continuation with AUTO, then the original coordinates are recovered via: $\mathbf{q} = \mathbf{PX}$, where, in $\mathbf{X}$, only the first coordinate X_1 is different from zero.

The second reduced-order model is obtained by keeping the first NNM: Eq. (20) are truncated by letting $R_p = 0$, $\forall p = 2 \ldots 22$. The dynamics onto the invariant manifold is then governed by

$$\ddot{R}_1 + 2\zeta_1\omega_1\dot{R}_1 + \omega_1^2 R_1 + (h^1_{111} + A^1_{111})R_1^3 + B^1_{111}R_1\dot{R}_1^2 + C^1_{111}R_1^2\dot{R}_1 = F_1\cos(\omega t). \tag{24}$$

Eq. (24) is solved numerically with AUTO, then one uses Eqs. (19) to come back to the modal coordinates, and finally the matrix of eigenvectors $\mathbf{P}$ allows reconstitution of the amplitudes in the basis of selected projection functions. Thanks to the non-linear nature of the change of variable (19), all the modal amplitudes are non-zero.

Fig. 2 shows the main coordinate $w_{1,1}$, having the most significant response. One can observe that the non-linearity

is of the hardening type, and that the amplitude of the response, of the order of two times the thickness, is large. The two reduced models have been selected because they share the same complexity: a single oscillator equation is used. Whereas reduction to a single linear mode gives poor result, reduction to a single NNM give a satisfactory result, with a slight overestimation of the maximum vibration amplitude.

Moreover, as shown in Fig. 3, the reduced model composed of a single NNM, thanks to the non-linear change of coordinate, allows recovering all the other coordinates that are not directly excited. Fig. 3 shows the six main coordinates, *i.e.* the first four coordinates in transverse direction, $w_{1,1}$, $w_{3,1}$, $w_{1,3}$ and $w_{3,3}$, as well as the first two longitudinal coordinates $u_{1,1}$ and $v_{1,1}$. It is observed that with the NNM ROM, energy is recovered in all the coordinates, with a good approximation of the original amplitudes. On the other hand, for the model composed of a single linear mode, non-zero amplitudes are recovered only on $w_{1,1}$, $u_{1,1}$ and $v_{1,1}$, as these three coordinates are linearly coupled to create the first eigenmode described by X_1 which is simulated. But a vanishing response is found with this LNM ROM for $w_{3,1}$, $w_{1,3}$ and $w_{3,3}$.

This first result emphasizes the main characteristic of the NNM ROM: the geometrical complexity due to the curvature of the invariant manifold, is first computed in the non-linear change of coordinates. Once the dynamics reduced to the manifold, a single oscillator equation is sufficient to recover the dynamics. Then, coming back to the original coordinates allows recovering energy onto the slave modes thanks to the non-linear projection.

Fig. 4 shows a representation of the invariant manifold (the first NNM) for the HP panel. The dimension of the phase space is 45 (22 oscillator equations with displacement and velocity as independent variables plus the external forcing), and the NNM surface is two-dimensional. A projection in the reduced space $(w_{1,1}, \dot{w}_{1,1}, w_{3,1})$ is shown. A trajectory is also represented, which has been computed by numerically integrating the original system described by Eq. (17). The closed orbit represents the true solution, as the reference equations have been used. One can observe that the closed orbit do not fully belong to the invariant manifold. This is the consequence of the two assumptions used to generate the NNM solutions: a third-order asymptotic development is used to approach the invariant manifold, and secondly, a time-invariant manifold is used. As a consequence, the trajectory do not fall completely within the NNM. However a good approximation of the local geometry is provided.

The time solutions for the four most significant coordinates is shown in Fig. 5. Once again, the reference solution is compared to the two reduced models composed of a single linear and non-linear mode. Time integrations have been performed for $\tilde{f} = 4.37$ N and $\omega = 1.3\omega_1$ (Point (A) in Fig. 2). Whereas the reduction to a single linear mode is not acceptable, the solutions provided by a single NNM are very good. Despite the fact that only one oscillator-equation is simulated, a variety of complex signals are recovered thanks to the non-linear change of coordinates.

The convergence of the solution with an increasing number of LNMs is shown in Fig. 6 for the excitation

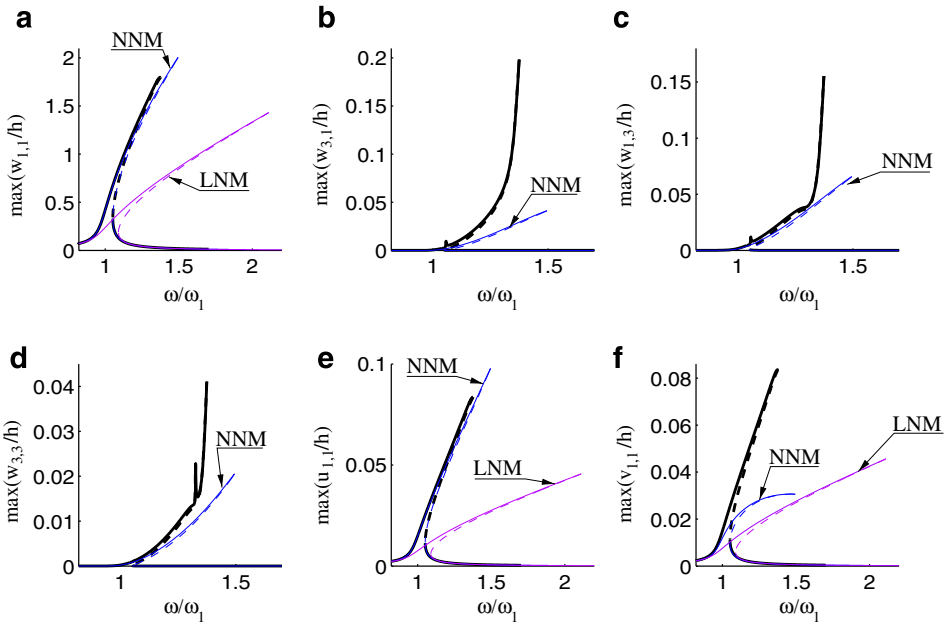

Fig. 3. Maximum amplitude of the response of six generalized coordinates versus excitation frequency, for an excitation amplitude of $\tilde{f} = 4.37$ N. Reference solution (thick line) is compared to the reduction to a single linear mode (LNM) and a single non-linear mode (NNM): (a) maximum of $w_{1,1}$, (b) maximum of $w_{3,1}$, (c) maximum of $w_{1,3}$, (d) maximum of $w_{3,3}$, (e) maximum of $u_{1,1}$ and (f) maximum of $v_{1,1}$.

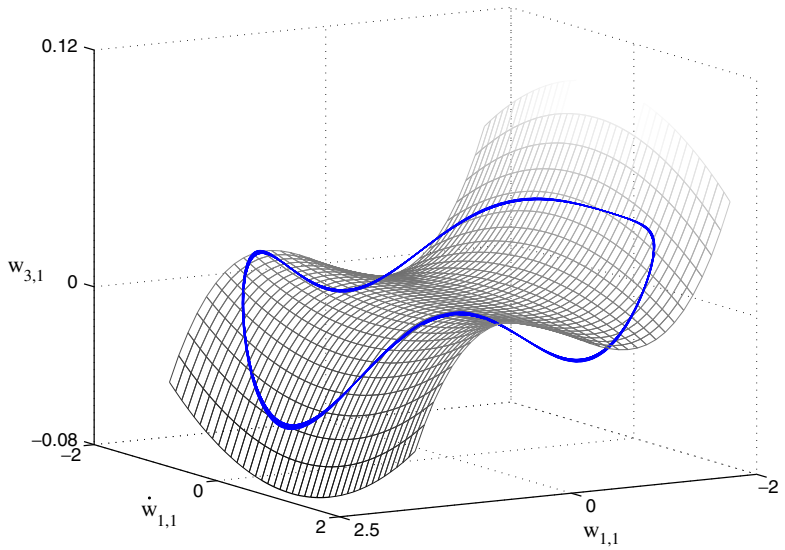

Fig. 4. The invariant manifold (first NNM) for the HP panel in the reduced phase space $(w_{1,1}, \dot{w}_{1,1}, w_{3,1})$, calculated with the third-order approximation derived from Eqs. (19). The orbit has been computed by integrating the temporal dynamics of the reference solution, with $\tilde{f} = 4.37$ N and $\omega = 1.3\omega_1$.

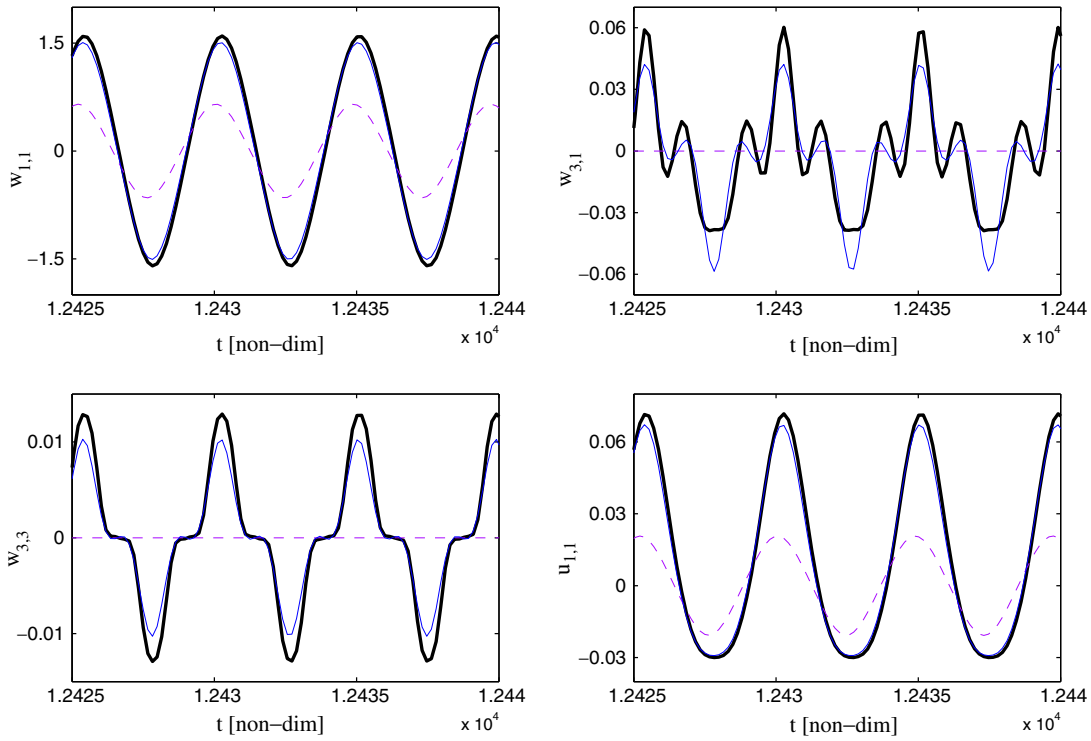

Fig. 5. Time-domain response of four generalized coordinates of the HP panel, excitation frequency $\omega = 1.3\omega_1$, amplitude $\tilde{f} = 4.37$ N. Reference solution (thick line) is compared to the NNM solution (thin line), and the LNM solution (dashed line).

amplitude of 4.37 N. It is found that the convergence is very slow: 15 LNMs are necessary to obtain an acceptable solution. The solution with 11 LNMs is qualitatively different from the converged solution with a strange loop appearing in the frequency response, and is thus not acceptable. Hence a very slow convergence with respect to increasing P_{LNM} is found, and using the linear normal modes is not very favourable as compared to the projection functions used. On the other hand, it has been found that increasing the number of NNMs kept in the truncation in Eq. (20) do not change anything in the solution: the added NNMs have been found to stay with constant neglectable

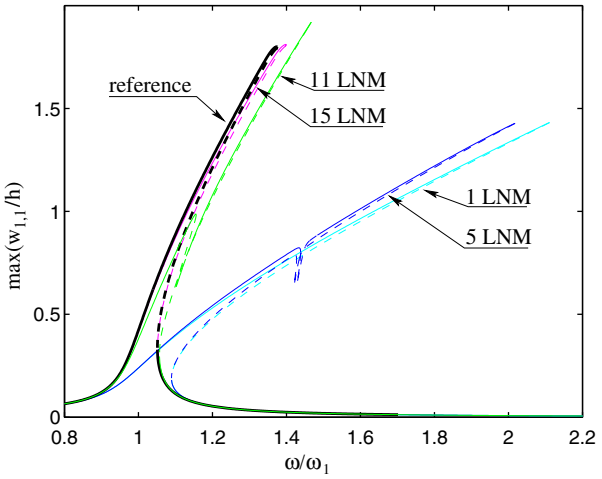

Fig. 6. Maximum amplitude response of $w_{1,1}$ versus excitation frequency for $\tilde{f} = 4.37$ N, showing the convergence of the solution when increasing P_{LNM}. Reference solution (22 basis functions) is compared to truncations with 1 linear mode, 5 LNM, 11 LNM and 15 LNM.

amplitude, and the same solution is found as the one obtained with a single NNM. This is a logical consequence of the invariance property of the NNMs. Hence the solution with a single NNM seems to be the best ROM possible. The only way to improve the results found here is not in increasing the number of NNMs, but in overshooting the two limitations of the present approximation used for generating the NNMs.

Finally, the robustness of the ROMs with respect to increasing the amplitude of the forcing, is studied. Fig. 7 shows the results obtained for a lower excitation amplitude: $\tilde{f} = 2.84$ N, and for a larger one:$\tilde{f} = 6.62$ N. For $\tilde{f} = 2.84$ N, the result given by the NNM ROM is almost perfectly coincident with the reference solution obtained with 22 basis function, whereas the model with a single linear mode give unacceptable results. For the larger amplitude, $\tilde{f} = 6.62$ N, the result deteriorates for the NNM-reduced model, which is not able to catch the saturation loop found by the reference solution at the top of the frequency–response curve. The observation of the other coordinates (not shown for the sake of brevity) shows that this loop reflects the fact that most of the energy is, at this point, absorbed by the higher modes, the amplitude of which significantly and abruptly increase. This subtil change in the dynamics of the system is not caught by the reduced model, which overpredict the maximum amplitude.

As a conclusion on the HP panel, the dynamics has been reduced from 22 dofs to a single NNM. Results shows that the reduction, computed with an asymptotic expansion to approach the invariant manifold, gives very good results for vibration amplitudes up to 1.5 times the panel thickness h. Beyond this value, the two approximations used for generating the ROM do not hold anymore. On the other hand, using truncations with LNMs did not allow substantial improvement as compared to the selected basis functions used for discretizing the problem.

5. Circular cylindrical panel

5.1. Boundary conditions and projection functions

The CC panel is shown in Fig. 8. The coordinates used to describe the geometry are $x_1 = x$ and $x_2 = \theta$, where (x, θ) are the cylindrical coordinates shown in Fig. 8. As a consequence, the radii of curvature are such that $R_1 = R_x = \infty$, and $R_2 = R$. The angular span is α, length is a and thickness h. The selected boundary conditions are:

$$w = N_x = M_x = 0, \quad N_{x,y} = 0, \quad \text{at } x = 0, a, \tag{25a}$$

$$w = N_y = M_y = 0, \quad N_{y,x} = 0, \quad \text{at } y = 0, b, \tag{25b}$$

where $y = R\theta$ and $b = R\alpha$. They modelize a restrained condition in transverse direction with fully free in-plane displacements.

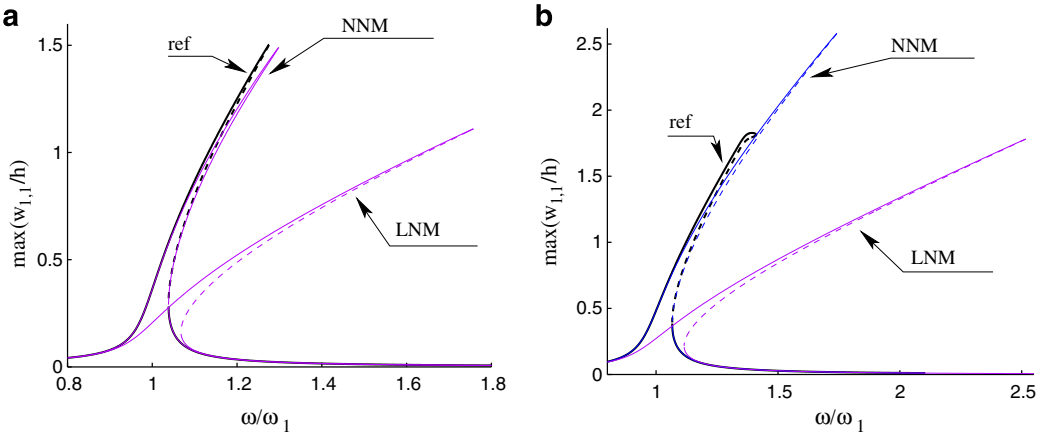

Fig. 7. Frequency–response curve for (a) $\tilde{f} = 2.84$ N, and (b) $\tilde{f} = 6.62$ N. Reference solution (ref) is compared to truncations with a single linear mode (LNM) and a single non-linear mode (NNM).

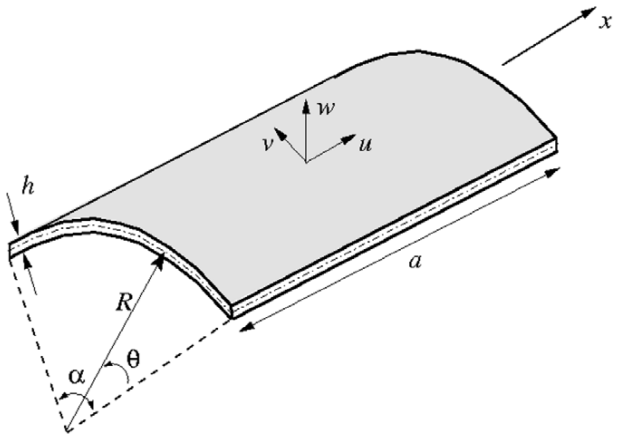

Fig. 8. Geometry and coordinates axis for the circular cylindrical panel.

The basis functions are respectively

$$\phi^{(u)}_{m,n}(x,y) = \cos(m\pi x/a)\cos(n\pi\theta/\alpha), \tag{26a}$$

$$\phi^{(v)}_{m,n}(x,y) = \cos(m\pi x/a)\cos(n\pi\theta/\alpha), \tag{26b}$$

$$\phi^{(w)}_{m,n}(x,y) = \sin(m\pi x/a)\sin(n\pi\theta/\alpha). \tag{26c}$$

Two non-linear terms $\hat{u}$ and $\hat{v}$ are added to Eqs. (26a) and (26b), respectively, in order to identically satisfy the boundary conditions, as shown in [19,28].

5.2. Simulation results

Numerical simulations have been performed for a specific panel with $a = 0.1$ m, $R = 1$ m and $h = 1$ mm. The angular span is $\alpha = 0.1$ rad, so that the panel length equals the circumferential width. Material properties are identical to that used for the HP panel so that E, ρ and ν are unchanged. The CC panel response to harmonic excitation in the vicinity of the first eigenfrequency is studied. The convergence of the reference solution has been carefully checked in [19,28], for an excitation amplitude of $\tilde{f} = 4.4$ N applied at the center of the panel. It has been found that the minimal number of basis functions should be 19. This solution will be referred to as the reference solution; the selected basis functions are: $w_{1,1}$, $w_{1,3}$, $w_{3,1}$, $w_{3,3}$, $u_{1,0}$, $u_{1,2}$, $u_{1,4}$, $u_{3,0}$, $u_{3,2}$, $u_{3,4}$, $v_{0,1}$, $v_{2,1}$, $v_{4,1}$, $v_{0,3}$, $v_{2,3}$, $v_{4,3}$, $v_{0,5}$, $v_{2,5}$, $v_{4,5}$. Damping coefficient ζ_p has been set equal to 0.004 for each generalized coordinate.

Fig. 9 shows the response of the main coordinate $w_{1,1}$ for an excitation amplitude of $\tilde{f} = 2.2$ N. The reference solution, obtained with 19 dofs, is contrasted to two ROMs composed of a single dof: a single LNM and a single NNM. The results are comparable to those obtained for the HP panel. The response of the panel is of the hardening type. The restriction to a single linear mode is a too severe truncation that leads to a huge overestimation of the hardening behaviour of the panel. On the other hand, the response provided by the NNM ROM is quasi-coincident with the reference solution.

As already mentioned for the HP panel, the NNM ROM allows recovering non-directly excited coordinates thanks to the non-linear relationship between the original (modal) coordinates and the master mode that is retained for simulation. Comparison of other coordinates are shown in Fig. 10. A particular feature of this model is the weak coupling observed between the coordinates. This is revealed here by the very small values of maximum amplitude of the non-directly excited coordinates, recovered via the changes of variables: they are an order of magnitude less compared to the HP panel. On the geometrical viewpoint, it means that the invariant manifold is rather flat. The non-linearity is here more focused on the self-exciting terms present in the normal form than in the coupling amongst eigenmodes, which are treated by the curvature of the NNM manifold. The convergence of the reduced systems have also been tested. As in the precedent case of the HP panel, a very slow convergence with increasing the number of linear modes have been found: 15 LNMs were necessary in order to recover the original results. Other more severe truncations with a number of linear modes less or equal than 8 gave unacceptable results.

Fig. 11 shows the comparison between the NNM ROM and the reference solution, for an excitation amplitude of

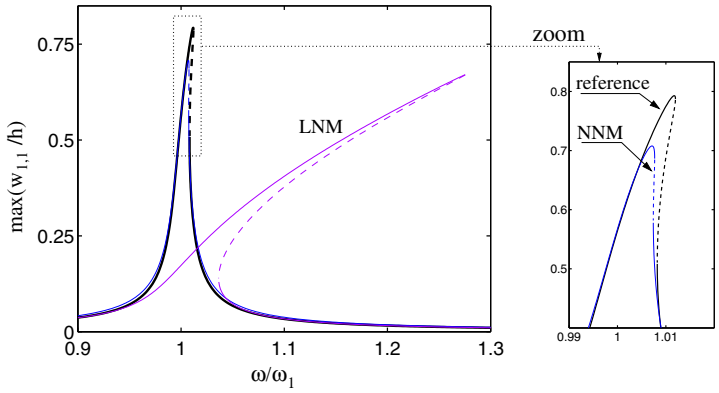

Fig. 9. Maximum amplitude of coordinate $w_{1,1}$ versus excitation frequency for the CC panel, $\tilde{f} = 2.2$ N. NNM solution is quasi-coincident with the reference solution. Truncated solution with a single linear mode (LNM) is also shown.

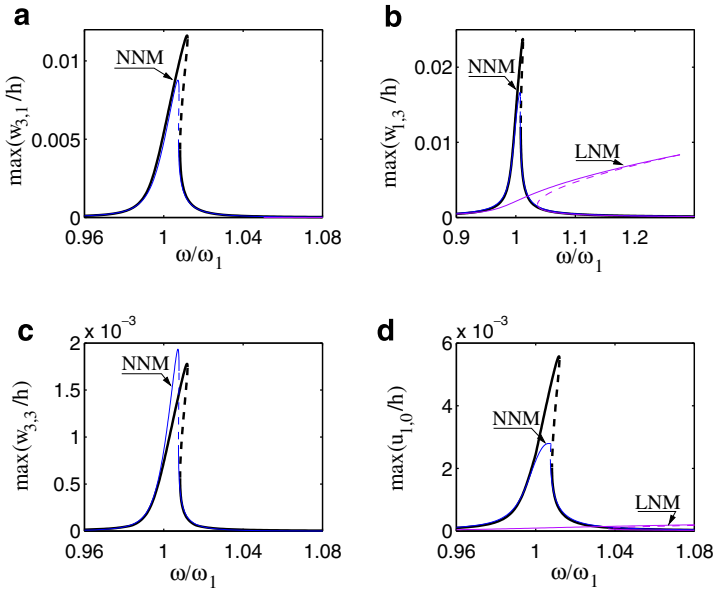

Fig. 10. Maximum amplitude versus excitation frequency, CC panel, $\tilde{f} = 2.2$ N. Reference solution (thick line) is compared to single NNM and single LNM solutions. Four non-directly excited coordinates are shown: (a) $w_{3,1}$, (b) $w_{1,3}$, (c) $w_{3,3}$ and (d) $u_{1,0}$.

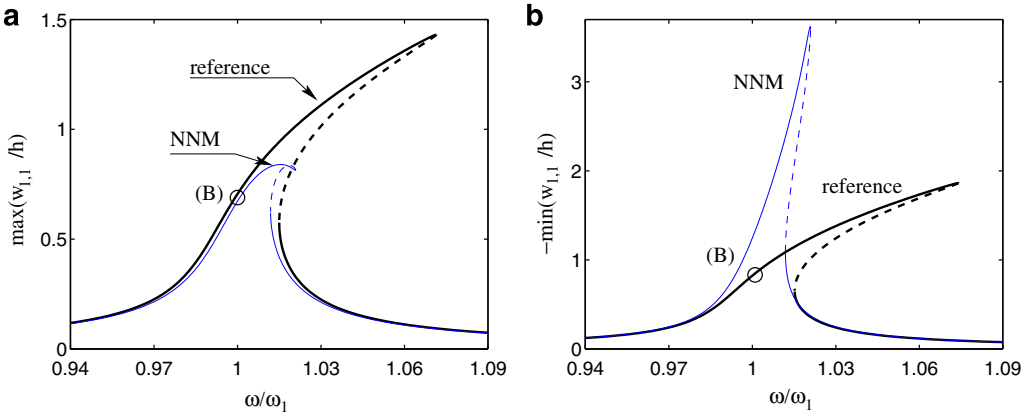

Fig. 11. Frequency–response curve for coordinate $w_{1,1}$, excitation amplitude of 4.4 N: (a) maximum amplitude response (outwards deflection) and (b) minimum amplitude response (inwards deflection). Reference solution is compared to single NNM truncation. Point (B), with $\omega = \omega_1$, is used for time integration, see Fig. 12.

4.4 N. The results provided by the single linear mode ROM has not been plotted as it was completely unacceptable. As a consequence of the weak coupling amongst generalized coordinates detected before, the NNM simulation fails in recovering the resonance curve for this level of excitation. It can be explained by the fact that the NNM ROM, in its third-order asymptotic approximation used here, has the primary ability to catch very well the coupling amongst linear modes through the non-linear change of coordinates. As these couplings are here weak, the ROM is rapidly limited by its third-order expansion, that shows some difficulties to recover the non-linearity exhibited in this case. Moreover, the reference simulation shows an important asymmetry between outwards displacements (Fig. 11a with the maximum amplitude) and inwards displacements (Fig. 11b with the minimum amplitude). This asymmetry is caught by the NNM ROM but dramatically increased. This, once again, shows that, in this case, the third-order expansion is not enough to have a good approximation of the dynamics.

Direct integration of the equations of motion for the reference model is compared to the single LNM and NNM time simulations in Fig. 12, for this large value of excitation $\tilde{f} = 4.4$ N, and $\omega = \omega_1$. As predicted by the frequency–

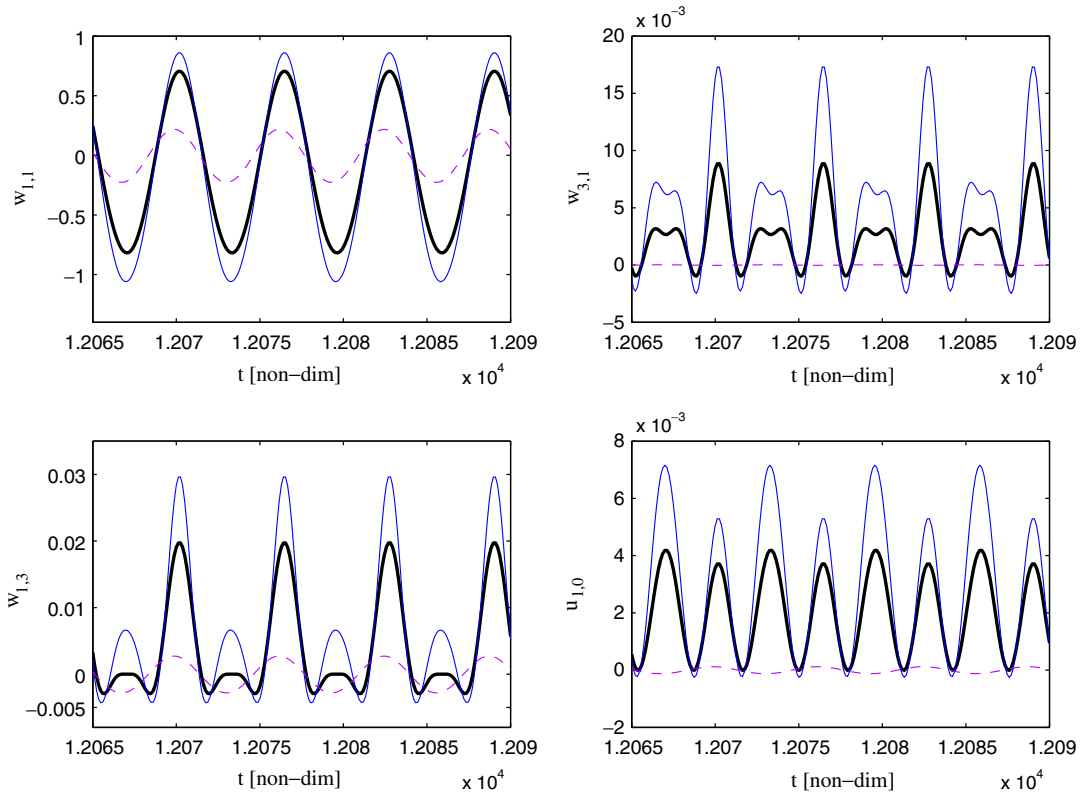

Fig. 12. Time-domain response of four generalized coordinates of the CC panel, excitation frequency $\omega = \omega_1$, amplitude $\tilde{f} = 4.4$ N. Reference solution (thick line) is compared to the NNM solution (thin line), and the LNM solution (dashed line).

response curve, the asymmetry is overestimated by the NNM ROM. However, as in the case of the HP panel, a large variety of non-linear temporal signals are well recovered, whereas a single oscillator-equation is simulated.

Finally, in the case of the CC panel, the NNM ROM gives good results for vibration amplitudes up to $0.9h$.

6. Closed circular cylindrical shell

6.1. Boundary conditions and projection functions

The third example is a closed, empty shell of length a. The geometry and coordinate system is deduced from the CC panel by selecting $\alpha = 2\pi$ for the angular span. Whereas the strain–displacement relationship for the two precedent example was given by Donnell's non-linear theory with in-plane inertia, Flügge-Lur'e-Byrne non-linear theory is used here. The reader is referred to [17,23,24] for a more thorough description of the kinematics.

The boundary conditions are simply supported at the two ends $x = 0, a$

$$w = M_x = v = N_x = 0, \quad \text{at } x = 0, a, \tag{27}$$

where M_x and N_x are respectively the bending moment and the axial force per unit length.

The response of the shell to harmonic forcing in the vicinity of mode (m, n), where m is the number of longitudinal half-waves, and n of circumferential waves, is considered. Based on past studies, where a detailed convergence study was considered for mode $(1, 5)$ (see *e.g.* [17] and references therein), the minimal expansion used for discretizing the shell has been found to be the following:

$$u(x,\theta,t) = \sum_{k=1}^{2}[u_{1,5k,c}(t)\cos(5k\theta) + u_{1,5k,s}(t)\sin(5k\theta)]\cos(\lambda_1 x) + \sum_{m=1}^{2} u_{2m-1,0}(t)\cos(\lambda_{2m-1}x) + \hat{u}, \tag{28a}$$

$$v(x,\theta,t) = \sum_{k=1}^{2}[v_{1,5k,c}(t)\sin(5k\theta) + v_{1,5k,s}(t)\cos(5k\theta)]\sin(\lambda_1 x) + [v_{3,10,c}(t)\sin(10\theta) + v_{3,10,s}(t)\cos(10\theta)]\sin(\lambda_3 x), \tag{28b}$$

$$w(x,\theta,t) = [w_{1,5,c}(t)\cos(5\theta) + w_{1,5,s}(t)\sin(5\theta)]\sin(\lambda_1 x) + \sum_{m=1}^{2} w_{2m-1,0}(t)\sin(\lambda_{2m-1}x), \tag{28c}$$

where $\lambda_m = \frac{m\pi}{a}$, and $\hat{u}$ is a non-linear term added to satisfy exactly the boundary condition $N_x = 0$. Because of the circumferential symmetry, degenerate modes appear in the structure; they are here denoted with the additional subscript c or s, indicating if the generalized coordinates is associated with a cos or sin function in the angular coordinate θ for w. This expansion gives the reference solution,

which is obtained here with 16 generalized coordinates. One can observe that the basis functions are in fact the eigenmodes of the empty shell for the transverse component.

The point excitation considered is located at a node of the mode $(1,5,s)$. Consequently, mode $(1,5,c)$ is called the driven mode, and mode $(1,5,s)$, which is not directly excited by the external load, is the companion mode. The damping coefficient ζ_p is selected such that $\zeta_p = \zeta = 0.001$ for each asymmetric modes, whereas for axisymmetric modes (present in the truncation via $w_{1,0}$, $w_{3,0}$, $u_{1,0}$ and $u_{3,0}$) we have: $\zeta_{1,0} = \frac{\omega_{1,0}}{\omega_{1,5}}\zeta$ and $\zeta_{3,0} = \frac{\omega_{3,0}}{\omega_{1,5}}\zeta$.

6.2. Simulation results

Numerical simulations have been performed for a shell whose geometric dimensions are: $a = 520$ mm, $R = 149.4$ mm, $h = 0.519$ mm. Material properties are: $E = 1.98 \times 10^{11}$ Pa, $\rho = 7800$ kg m^{-3}, $\nu = 0.3$. As a consequence of the circumferential symmetry and the appearance of degenerate modes, 1:1 internal resonances are present in the system. More particularly in the present case, the driven mode and the companion mode are 1:1 internally resonant. Hence the minimal model that could capture the dynamics should contain at least two oscillator equations. This minimal model is given by keeping the first two NNMs, corresponding respectively to the continuation of driven and companion modes, in the same way as the truncation realized on a fluid-filled cylindrical shell described by Donnell shallow-shell theory, see [15,2].

In the remainder of the study, the reference solution obtained with 16 basis functions will be compared to the solution given by the reduced model composed of 2 NNMs. The comparison with a truncation of linear modes,

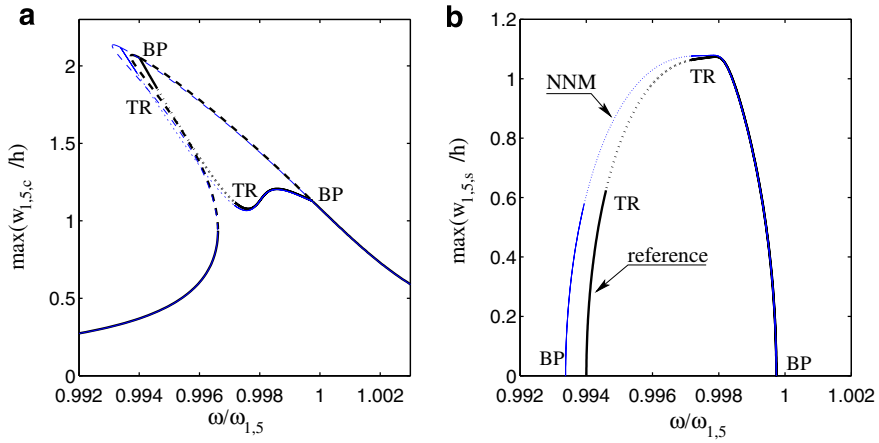

Fig. 13. Maximum amplitude of vibration versus excitation frequency for the Flugge shell, with an excitation amplitude of 2 N. Comparison of reference solution (thick line) to the ROM composed of two NNMs (NNM): (a) maximum amplitude of the driven mode $w_{(1,5,c)}$ and (b) maximum amplitude of the companion mode $w_{(1,5,s)}$. BP: branch points on the single-mode branch of solution, leading to coupled solutions (branch 2). TR: Neimarck-Sacker (Torus) bifurcation points leading to quasi-periodic solutions.

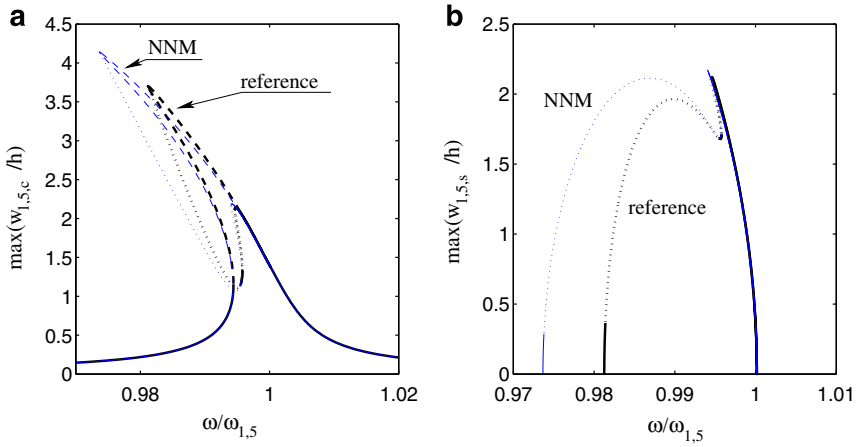

Fig. 14. Maximum amplitude of vibration versus excitation frequency for the Flugge shell, $\tilde{f} = 4$ N. Comparison of reference solution (thick line) to the ROm composed of two NNMs (NNM): (a) maximum amplitude of the driven mode $w_{(1,5,c)}$ and (b) maximum amplitude of the companion mode $w_{(1,5,s)}$.

as in the precedent cases, will not be shown for the following reason. Once again, the convergence of the solution with the number of linear modes was very slow. Moreover, all the truncations tried with an increasing number of linear modes predicted a hardening-type non-linearity, except the solution with 16 linear modes which recovers the original solution with a softening-type non-linearity for the driven mode. Hence the minimal number of linear modes is also 16, and no other truncation is acceptable.

Fig. 13 shows the comparison between the reference solution and the reduced model composed of two NNMs, for an excitation amplitude $\tilde{f} = 2$ N. The solution is composed of two branches. The first branch corresponds to the single-mode response: the companion mode has a zero amplitude. This branch displays a softening-type non-linearity, and shows two branch points (BP), from which the second branch arises. This second branch corresponds to coupled solutions where both driven and companion mode have a non-zero amplitude. Following branch 2, a bifurcation occurs via torus (Neimarck-Sacker) bifurcations (TR), leading to a quasi-periodic regime.

As shown in Fig. 13, the reduced model perfectly recovers all the details of this complicated bifurcation diagram. A slight overestimation of the softening non-linearity is detected, but all the bifurcation points, as well as their nature, are perfectly recovered. In contrast, no other solution with a truncation with the linear modes, was able to catch the softening type non-linearity. This excellent result confirms earlier investigations led on a fluid-filled cylindrical shell, see [15,2].

The robustness of the ROM is tested by increasing the external forcing amplitude up to $\tilde{f} = 4$ N. The corresponding frequency–response is shown in Fig. 14. Despite an increase in the overestimation of the maximum amplitude, all the bifurcation points are once again recovered. From these studies, it can be concluded that the ROM is reliable for vibration amplitudes up to $3h$.

7. Discussion

Reduction methods is a central question in the simulation of vibrating structures. Many different methods have been proposed in the past, one of the most popular being the Proper Orthogonal Decomposition (POD) method [3–5,29]. In this paper, the NNMs of the unforced structure are tested as basis functions for reducing the dynamics for shell models with harmonic forcing.

On the computational viewpoint, one of the main drawback of the present method is the number of coefficients that have to be computed for obtaining the reduced model. The main task consists in the computation of all the linear $\{z_i^p\}_{p,i=1\ldots P}$, quadratic $\{z_{i,j}^p\}_{p,i,j=1\ldots P}$ and cubic $\{z_{i,j,k}^p\}_{p,i,j,k=1\ldots P}$ coupling coefficients appearing in Eq. (17). This can be seen as an extra work as compared to other methods, *e.g.* discretization based on finite elements procedures, where these coefficients are generally not computed for solving out temporal response for instance. However, in the context of this study where one is interested with frequency–response curves with bifurcation points, this step is necessary. It can also be remarked that the computation of these coefficients are here realized on the basis of analytical developments, however they can easily be implemented within a finite-element based discretization. The second family of coefficients that have to be computed are those from the non-linear change of coordinates defined by Eqs. (19). However the numerical burden associated with this step is limited, so that this does not appear as a limiting factor of the method. Moreover, all these computations are made once and for all, and for the unforced structure, so that these can be seen as off-line calculations, that have not to be repeated for computing other responses. This is of course an advantage as compared to the POD method.

An assessment of the computational burden associated with the numerical results shown in previous section is given in Table 1. The computational times are only indicatory, as they strongly depend on the processor and on numerous parameters that can be tuned in a typical AUTO-run. Moreover, the computation of solution branches with AUTO depends on the complexity of the solution, thus the computational time also depends on the amplitude of the forcing. These values are here given in order to better quantify the gain in using ROMs in typical situations, which is very important. A typical AUTO-run for computing a single-dof frequency–response curve is of the order of 30 s (values given for the LNM ROM). For the NNM ROM, about 3 min are spent in order to compute the non-linear change of coordinates, that are added to the 30 s of the AUTO-run. However, as the non-linear change of coordinates is computed once and for all, the single-dof NNM ROM can be used for comput-

Table 1
Comparisons of accuracy and computational times for the three selected models

	Reference	LNM	NNM
HP Panel	22 dofs	1 dof	1 dof
Comp. time	1 h 56 min	36 s	4 min 47 s
Validity limits	/	$0.1h$	$1.5h$
CC Panel	19 dofs	1 dof	1 dof
Comp. time	1 h 28 min	35 s	3 min 43 s
Validity limits	/	$0.1h$	$0.9h$
Flügge shell	16 dofs	2 dofs	2 dofs
Comp. time	1 h 37 min	/	2 min 48 s
Validity limits	/	$0.1h$	$3h$

The computational time is defined as the time needed for computing a typical frequency–response curves. For the reference solution, this includes the time spent during an AUTO-run. For the LNM ROM, to the time spent in an AUTO-run is added the time spent in the linear change of coordinates (application of **P**). For the NNM ROM, the time spent for computing and applying the non-linear change of coordinate is also added. The amplitude of the forcing used for this table is: 4.37 N for the HP panel, 4.4 N for the CC panel, and 2 N for the Flügge shell. Computations have been realized on a standard PC with a Pentium IV processor working at 2.4 GHz. Computational time associated to the Flügge shell reduced to two LNMs is not mentioned as the model has not been able to recover to two solution branches.

ing any solution, so that the computational time indicated in the NNM column must be understood as an upper limit. From Table 1, one can see that the computation times obtained with the NNM ROMs have been reduced by a significant factor, ranging from 23 (HP panel) to 32 (Flügge shell).

The upper validity limit has also been estimated in each case by increasing the amplitude of the forcing. No validity limits is indicated for the reference solution. However, if larger values of the forcing would have been considered, the convergence study with the projection functions should have been done once again. The reduction to a single LNM generally provided poor results, and once the value of 0.1 times the thickness h is reached, the reduction to a single LNM is not acceptable. For the single NNM ROM, this value is much larger. It has been found that the NNM ROM was very accurate for amplitude up to $1.5h$ for the HP panel, $0.9h$ for the CC panel, and $3h$ for the Flügge shell. To these three cases, the case of the water-filled circular cylindrical shell studied in [2] can be added, where the accuracy has been estimated to $2.5h$.

Finally, one can also remark that the present reduction method is particularly efficient for harmonically forced responses, as the motion is confined in the vicinity of the NNMs. However, for other dynamical behaviour (*e.g.* free vibration of response to white noise), the benefit in using NNMs instead of LNMs is questionable. Due the dynamical characteristics, it is not awaited, in these cases, to obtain as good results as those presented here for forced responses.

Further research in the area of model reduction with NNMs will consist in application of the present method to structures discretized with finite elements procedures. As shown in this study, the method can handle different kinematics, and thus can be interfaced with a finite elements method. Overcoming the limitation of the asymptotic development is also the key to a reliable solution that is not amplitude-dependent.

8. Conclusion

The non-linear response to harmonic forcing in the vicinity of the first eigenfrequencies of three shell structures have been studied. Particular attention has been paid to the derivation of reduced-order models (ROMs), that could be able to describe with accuracy the non-linear frequency–response curves. Linear normal modes and non-linear normal modes computed by an asymptotic approach have been used, for three selected systems: a hyperbolic paraboloid panel, a circular cylindrical panel and a closed empty circular cylindrical shell.

For the first two cases, the reduction to a single NNM has been possible, showing very good results for moderate vibration amplitude. On the other hand, it has been observed that using the LNMs did not allow for a substantial improvement of the results, as compared to the first expansion functions used for discretizing the panels. A single LNM gives unacceptable results, and the linear convergence was very slow in the two cases. Using NNMs thus appears as the best solution for reducing the system. In the third case, a 1:1 internal resonance was present in the system, so that the minimal model was composed of two NNMs, and showed very good results in recovering every bifurcations points as well as the nature of the dynamical regimes.

However, the NNM ROMs have been computed with two approximations: a third-order asymptotic development is used to approach the invariant manifold, and time-invariant NNM is used whereas a time-dependent one should be used to recover the dependence introduced by the external forcing. Hence, for large amplitude of vibrations, the results deteriorate.

As a conclusion, one can note that the present reduction method bears a number of advantage, as it is quick and easy-to-use, and overcomes the problems of internal resonances without extra work. Its reliability can be said to be very good up to h for shell structures, and generally can give good results up to $2h$ except in the case where the coupling between the modes is weak. To overcome this limitation, the two approximations presently used for generating the NNMs must be revised.

References

[1] S.W. Shaw, C. Pierre, Non-linear normal modes and invariant manifolds, J. Sound Vib. 150 (1) (1991) 170–173.
[2] M. Amabili, C. Touzé, Reduced-order models for non-linear vibrations of fluid-filled circular cylindrical shells: comparison of POD and asymptotic non-linear normal modes methods, J. Fluids Struct. 23 (6) (2007) 885–903.
[3] G. Kerschen, J.-C. Golinval, A.F. Vakakis, L.A. Bergman, The method of proper orthogonal decomposition for dynamical characterization and order reduction of mechanical systems: an overview, Nonlinear Dynam. 41 (1–3) (2005) 147–169.
[4] R. Sampaio, C. Soize, Remarks on the efficiency of POD for model reduction in non-linear dynamics of continuous elastic systems, Int. J. Numer. Methods Engrg. 72 (1) (2007) 22–45.
[5] P. Krysl, S. Lall, J.E. Marsden, Dimensional model reduction in non-linear finite element dynamics of solids and structures, Int. J. Numer. Methods Engrg. 51 (2001) 479–504.
[6] S.W. Shaw, C. Pierre, Normal modes for non-linear vibratory systems, J. Sound Vib. 164 (1) (1993) 85–124.
[7] L. Jézéquel, C.-H. Lamarque, Analysis of non-linear dynamical systems by the normal form theory, J. Sound Vib. 149 (3) (1991) 429–459.
[8] A.F. Vakakis, L.I. Manevich, Yu.V. Mikhlin, V.N. Pilipchuk, A.A. Zevin, Normal Modes and Localization in Non-linear Systems, Wiley, New-York, 1996.
[9] W. Lacarbonara, G. Rega, A.H. Nayfeh, Resonant non-linear normal modes. Part I: Analytical treatment for structural one-dimensional systems, Int. J. Non-Linear Mech. 38 (6) (2003) 851–872.
[10] C. Touzé, O. Thomas, A. Chaigne, Hardening/softening behaviour in non-linear oscillations of structural systems using non-linear normal modes, J. Sound Vib. 273 (1–2) (2004) 77–101.
[11] I.V. Andrianov, Asymptotic construction of nonlinear normal modes for continuous systems, Non-linear Dynam. 51 (1–2) (2008) 99–109.
[12] E. Pesheck, C. Pierre, S.W. Shaw, A new Galerkin-based approach for accurate non-linear normal modes through invariant manifolds, J. Sound Vib. 249 (5) (2002) 971–993.

[13] D. Jiang, C. Pierre, S.W. Shaw, Nonlinear normal modes for vibratory systems under harmonic excitation, J. Sound Vib. 288 (4–5) (2005) 791–812.
[14] R. Arquier, S. Bellizzi, R. Bouc, B. Cochelin, Two methods for the computation of nonlinear modes of vibrating systems at large amplitudes, Comput. Struct. 84 (24–25) (2006) 1565–1576.
[15] C. Touzé, M. Amabili, Non-linear normal modes for damped geometrically non-linear systems: application to reduced-order modeling of harmonically forced structures, J. Sound Vib. 298 (4–5) (2006) 958–981.
[16] C. Touzé, O. Thomas, Non-linear behaviour of free-edge shallow spherical shells: effect of the geometry, Int. J. Non-linear Mech. 41 (5) (2006) 678–692.
[17] M. Amabili, A comparison of shell theories for large-amplitude vibrations of circular cylindrical shells: Lagrangian approach, J. Sound Vib. 264 (5) (2003) 1091–1125.
[18] M. Amabili, Non-linear vibrations of doubly-curved shallow shells, Int. J. Non-linear Mech. 40 (5) (2005) 683–710.
[19] M. Amabili, Effect of boundary conditions on non-linear vibrations of circular cylindrical panels, ASME J. Appl. Mech. 74 (4) (2007) 645–657.
[20] A. Abe, Y. Kobayashi, G. Yamada, Non-linear vibration characteristics of clamped laminated shallow shells, J. Sound Vib. 234 (2000) 405–426.
[21] I.T. Georgiou, I.B. Schwartz, Slaving the in-plane motions of a nonlinear plate to its flexural motions: an invariant manifold approach, Trans. ASME, J. Appl. Mech. 64 (1997) 175–182.
[22] D. Chapelle, K.J. Bathe, The Finite Element Analysis of Shells – Fundamentals, Springer-Verlag, Berlin, 2003.
[23] J.H. Ginsberg, Large amplitude forced vibrations of simply supported thin cylindrical shells, J. Appl. Mech. 40 (1973) 471–477.
[24] N. Yamaki, Elastic Stability of Circular Cylindrical Shells, North-Holland, Amsterdam, 1984.
[25] E.J. Doedel, R. Paffenroth, A.R. Champneys, T.F. Fairgrieve, Y.A. Kuznetsov, B.E. Oldeman, B. Sandstede, X. Wang, AUTO 2000: continuation and bifurcation software for ordinary differential equations, User's guide, Technical Report, Concordia University, 2002.
[26] D. Jiang, Nonlinear modal analysis based on invariant manifolds: application to rotating blade systems, Ph.D. thesis, University of Michigan, 2004.
[27] E. Pesheck, Reduced-order modeling of nonlinear structural systems using nonlinear normal modes and invariant manifolds, Ph.D. thesis, University of Michigan, 2000.
[28] M. Amabili, Theory and experiments for large-amplitude vibrations of circular cylindrical panels with geometric imperfections, J. Sound Vib. 298 (1–2) (2006) 43–72.
[29] A. Steindl, H. Troger, Methods for dimension reduction and their applications in nonlinear dynamics, Int. J. Solids Struct. 38 (2001) 2131–2147.

Annexe 6 : Observation of wave turbulence in vibrating plates

Cette annexe donne le texte complet de l'article :

A. Boudaoud, O. Cadot, B. Odille et C. Touzé : Observation of wave turbulence in vibrating plates, Physical Review Letters, vol. 100, 234504, 2008.

Observation of Wave Turbulence in Vibrating Plates

Arezki Boudaoud
Laboratoire de Physique Statistique, CNRS/ENS/Paris 6/Paris 7, 24 rue Lhomond, 75231 Paris Cedex 5, France

Olivier Cadot, Benoît Odille, and Cyril Touzé
ENSTA-UME, Unité de Recherche en Mécanique, Chemin de la Hunière, 91761 Palaiseau, Cedex, France
(Received 24 October 2007; published 13 June 2008)

The nonlinear interaction of waves in a driven medium may lead to wave turbulence, a state such that energy is transferred from large to small length scales. Here, wave turbulence is observed in experiments on a vibrating plate. The frequency power spectra of the normal velocity of the plate may be rescaled on a single curve, with power-law behaviors that are incompatible with the weak turbulence theory of Düring *et al.* [Phys. Rev. Lett. **97**, 025503 (2006)]. Alternative scenarios are suggested to account for this discrepancy—in particular the occurrence of wave breaking at high frequencies. Finally, the statistics of velocity increments do not display an intermittent behavior.

DOI: 10.1103/PhysRevLett.100.234504 PACS numbers: 47.27.Gs, 47.35.Jk, 62.30.+d

The statistical distribution of energy and energy fluxes are central questions concerning out-of-equilibrium dissipative systems with a large number of degrees of freedom. When waves propagate in a medium, their nonlinear interaction might generate other waves with different wave numbers, which means that energy is transferred between different length scales. If the amplitude of waves is large enough, this transfer leads to a distribution of energy on a large number of wavelengths, and the system reaches a state called wave turbulence [1], such that the energy cascades between scales and might be dissipated on a small scale. Although they share the same phenomenology, wave turbulence is much more advanced analytically [1] than hydrodynamic turbulence [2]. For waves of small amplitude, the framework of weak turbulence yields kinetic equations, the solutions of which have been derived starting from the mid-1960s and correspond to energy spectra with power-law dependence on the wave number. Wave turbulence might apply to capillary [3,4] or gravity [5,6] waves on the surface of liquids, to plasmas [7], to nonlinear optics [8], to magnetohydrodynamics [9] or even to Bose-Einstein condensates [10].

Experimental studies are much less numerous than theoretical ones; they were performed either on the oceanographic scale—waves on a stormy sea (e.g., [11]), or on the laboratory scale—capillary and gravity waves [12–18]. Besides, the domain of validity of weak turbulence theory is still a matter of debate. On the one hand, discontinuities in the slope of breaking waves result mathematically in a wide energy spectrum [19,20], as apparently observed for gravity waves [18]. On the other hand, weak turbulence theory results in Gaussian statistics for the waves, in contrast with experiments when bursts of intense motion occur [13,17], a phenomenon known as intermittency. In this context, the theoretical study in [21] is very useful as it provides a new system, vibrating plates, where wave turbulence could be observed.

Here we study experimentally a suspended plate driven at high amplitudes [22]. We show that a wide energy spectrum is generated, discuss its interpretation in terms of weak turbulence and wave breaking, and investigate whether the system is intermittent. The typical broadband spectrum observed is also of special interest for its applications, e.g., for reproducing the sound of thunder in theaters. It is also related to the bright shimmering sound of gongs and cymbals [23,24]. Transition to chaotic vibration was studied for cymbals in [23], and for panels in [25,26].

The experimental setup consists of a steel plate suspended to a rigid frame and forced with a vibration generator (shaker B&K4810, glued to the plate with beeswax) moving perpendicularly to the plate [Fig. 1(a)]. The plate comes from a reverberation unit named EMT140, that was widely used in studio recordings to add a reverberated sound effect to dry signals recorded by near-field microphones [27]. Hence, the plate was chosen for its very high modal density, obtained by large dimensions 2 m $\times$ 1 m for a thickness of $h = 0.5$ mm, as well as for the moderate values of the quality factor, in order to get a fuzzy reverberated sound. Material properties were estimated as: Young's modulus $E = 200$ GPa, Poisson's ratio $\nu = 0.3$ and mass per unit volume $\rho = 7800$ kg/m^3. The plate is fixed at its four corners, so that the boundary condition is mainly free. The forcing is sinusoidal at $f_i = 20$ Hz that is close to a resonant frequency of the plate; it was chosen in order to allow the best injection of energy in the system, so that the turbulent regime is reached more easily. A laser vibrometer gives the normal velocity $v(t)$ at a given point in the plate. The signal is acquired at the sampling frequency of 32 kHz, and the fast-Fourier-transform (FFT) is computed from 50 s of signal, averaged over time windows of 0.5 s, so that $\Delta f = 2$ Hz. A force sensor (impedance head B&K 8001) is mounted between the shaker and the plate. The simultaneous measurement of the velocity at the

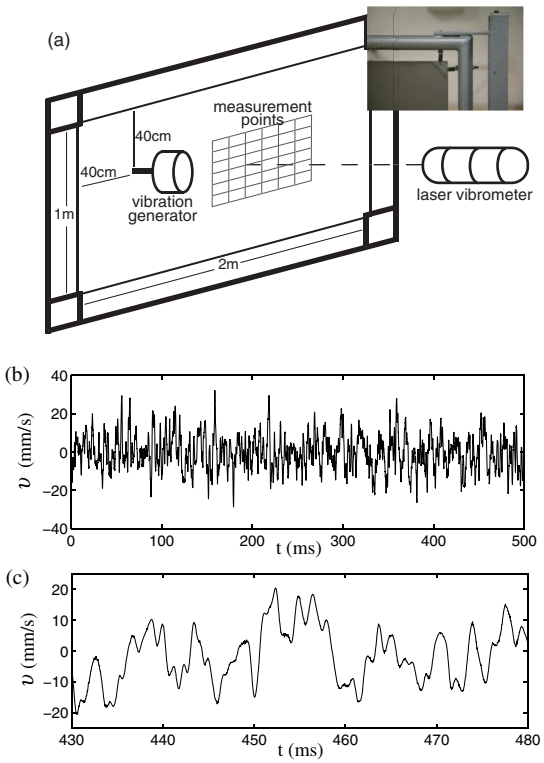

FIG. 1 (color online). The experiment. (a) Setup with a steel plate of dimensions 2 m × 1 m and thickness $h = 0.5$ mm; close-up view of the fixation. (b), (c) time series of the local transverse velocity measurements $v(t)$ for the forcing frequency $f_i = 20$ Hz; duration of 10 times (b) and 1 time (c) the forcing period.

same point gives the average power $I = \langle Fv \rangle$ injected by the generator into the system (with 1 mW of accuracy).

For a bending wave of frequency f and wave number k, the dispersion relation is

$$f = hck^2, \quad \text{with} \quad c = \sqrt{E/12\rho(1-\nu^2)}/2\pi \qquad (1)$$

proportional to the sound velocity in the bulk material. It was checked in [27] that this dispersion relation indeed holds in the present setup. It gives the space-time correspondence of the statistical properties of the velocity signal, similarly to Taylor's hypothesis for fully turbulent flows [2], when fluctuations are not too large.

For very low forcing amplitude, the velocity signal $v(t)$ recorded by the vibrometer is sinusoidal. For higher amplitude, it becomes chaotic [Figs. 1(b) and 1(c)]. In the frequency space, $v(t)$ is characterized by its power spectrum $P_v(f)$, given by the Fourier transform of the autocorrelation function, $P_v(f) = \int \langle v(t)v(t+\tau)\rangle \exp(2\pi i f\tau) d\tau$. This spectrum becomes broadband at high forcing [Fig. 2(a)], which is typical of wave turbulence; however, even with a long time averaging of the signal, P_v keeps a number of peaks corresponding to the plate eigenfrequencies. We checked homogeneity (by changing the excitation and measurement points) and independence on boundary conditions (by imposing fixed displacements at points at the edge); these changes affected very slightly the power spectra below the injection frequency.

As the forcing amplitude is increased, the spectra exhibit a wider and wider power-law dependence on frequency, $P_v(f) \sim f^{-\beta}$ with $\beta = 0.5 \pm 0.2$ (this error is an upper bound), which would correspond to the cascade regime. It is followed by a fall which could correspond to the dissipative scale. We seek the best rescaling of the spectra as a function of the injected power I. This yields the scaling form

$$P_v(f) = (I/I_0)^{1/2}\phi(f/f_c), \qquad f_c \propto f_i(I/I_0)^{\alpha}. \qquad (2)$$

Here ϕ a scaling function, I_0 a unit of power and f_c a cutoff frequency. This rescaling enables to collapse the spectra on a single curve [Fig. 2(b)]. The exponent for the dependence of f_c on I is found to be $\alpha = 0.33 \pm 0.01$ [Fig. 2(c)]. In the cascading frequency range, this implies $P_v(f) \sim I^{1/2+\alpha\beta} f^{-\beta} = I^{0.66\pm0.07} f^{-0.5\pm0.2}$.

In order to compare with previous theoretical work, we first note that the power spectrum for the transverse displacement ξ of the plate is given by $P_\xi(f) \propto P_v(f)/f^2$. When weak turbulence is attained, as investigated in [21], the spatial power spectrum of the displacement can be rewritten as $P_\xi(k) \propto c^{-1}\epsilon^{1/3}k^{-4}$, introducing energy flux ϵ per unit mass (ϵ has units of a velocity cubed and is proportional to the power input I), and omitting numerical prefactors and a logarithmic dependence on k. ϵ is proportional to the injected energy I. The $1/3$ exponents for ϵ comes from the $\xi \to -\xi$ symmetry of the plate, which involves four waves interaction. The spectrum can be translated into the frequency space $P_\xi(k)kdk \propto P_\xi(f)df$. Using the dispersion relation (1), we get $P_\xi(f) \propto h\epsilon^{1/3}f^{-2}$ and $P_v(f) \propto h\epsilon^{1/3}$ is constant. This dependence is significantly weaker than in the measurements [Figs. 2(a) and 2(b)].

In the framework of weak turbulence, nonlinearities of order p imply that $P_v(f)$ scales as $\epsilon^{1/p}$ [1]; the exponent $1/2$ obtained for $p = 2$ is the closest to the measured 0.66 ± 0.07 (2). This value of $p = 2$ means three waves interactions, a quadratic nonlinearity and no $\xi \to -\xi$ symmetry. Indeed, geometrical imperfections are unavoidable in real plates, which is known to break this symmetry and to produce quadratic nonlinearities [28]. Therefore, we assume in the following that $P_v(f) \sim \epsilon^{1/2}f^{-1/2}$, corresponding to a displacement spectrum $P_\xi(f) \sim \epsilon^{1/2}f^{-5/2}$. This assumption allows to investigate the possible role of damping in setting the cutoff frequency.

Indeed, we introduce the damping rate $\gamma(f) \sim f^\delta$. The spectrum of the energy per unit mass is $\mathcal{E}(f) \propto P_v(f) \sim \epsilon^{1/2}f^{-1/2}$. Let us consider the balance of energy over the cascade frequency range; the in-flux is ϵ while the energy dissipated till $f_c = hck_c$ is $\int^{k_c} \gamma(k)\mathcal{E}(k)dk \propto \int^{f_c} \gamma(f)\mathcal{E}(f)\sqrt{hc/f}df$. Balancing these two fluxes yields $f_c \sim \epsilon^{1/2\delta}$. For our setup, a fit to the damping coefficient

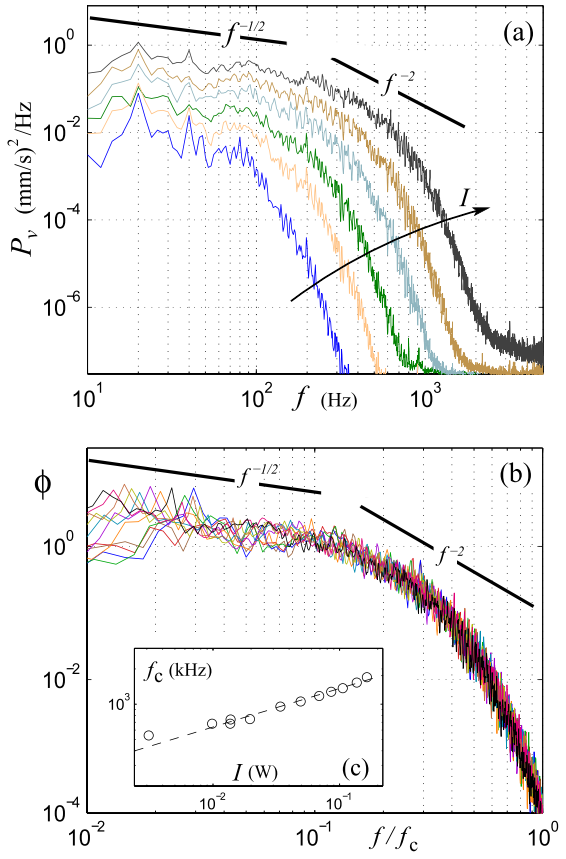

FIG. 2 (color online). Power spectra of the transverse velocity. (a) raw $P_v(f)$ as a function of frequency f, for different values of injected power I (in increasing order as displayed by the arrow: <1 mW, 2.3, 8.8, 26.4, 68.8, 136 mW); errors $\Delta f = 2$ Hz and $\Delta P_v = 10^{-7}$ (mm/s)^2/Hz. (b) Rescaled spectra $(I_0/I)P_v$ according to Eq. (2) vs f/f_c for all forcing amplitudes, where f_c is defined by $(I_0/I)^{1/2}P_v(f_c) = 10^{-5}$ mm^2/s. Inset (c) evolution of f_c with the forcing intensity. The continuous line is the best power law given in Eq. (2), yielding an exponent $\alpha = 0.33$.

measured in [27] is shown in Fig. 3 in the frequency domain of interest. It yields $\delta \simeq 1/2$, so that $f_c \sim \epsilon \sim I$, which is far from measurements (2) and so damping cannot account for the cutoff.

A last option is that the wide energy spectrum might be generated by singularities of the plate displacement as for gravity waves [19]. For plates, wave breaking would be

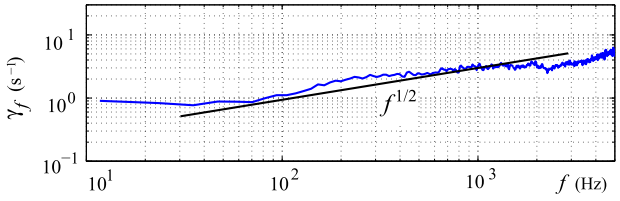

FIG. 3 (color online). Damping factor for the present plate, from [27].

replaced [21] by ridges [29,30] and d cones [31,32]. It was shown in [20] that random independent slope discontinuities result in a spectrum $P_\xi(f) \propto \nu_s \Gamma^2 f^{-4}$, ν_s being the frequency of occurrence of slope discontinuities and Γ the rms velocity impulse at each discontinuity. For the velocity $P_v(f) \propto \nu_s \Gamma^2 f^{-2}$ which compares with the second part of the spectra [Figs. 2(a) and 2(b)] over half a decade. Besides, the jump should be given by the typical rms velocity $v_{\rm rms} I^{1/2}$, so that we expect $\Gamma \sim \epsilon^{1/2}$. As a consequence, the whole spectrum could result from a three waves interaction for low frequencies, as suggested above, and singularities for higher frequencies. These two spectra match at a frequency $f = f_c$ such that $\epsilon^{1/2} f^{-1/2} \sim \epsilon f^{-2}$, yielding $f \sim \epsilon^{1/3}$, which agrees with the scaling (2) as seen in Fig. 2(c).

Finally, we consider the statistics of the velocity increments defined as $\Delta_\tau v = v(t+\tau) - v(t)$. The PDFs are displayed in Fig. 4(a) for the large forcing amplitude. An intermittent behavior of the velocity statistics would be revealed by a change in the PDFs shape as the lag τ decreases [2]. Here we can see in Fig. 4(a) that the PDF shape remains satisfactorily Gaussian whatever τ. The structure functions, $S_p(\tau) = \langle |\Delta_\tau v|^p \rangle$, are plotted in Fig. 4(b). They are generally used to determine the scaling behavior of the velocity differences statistics with the time-lag τ [2]. The structure functions start to decrease for $\tau <$ 50 ms (i.e., the forcing period). For very small $\tau < 0.3$ ms (i.e., the cutoff frequency), the velocity signal becomes smooth and a simple scaling behavior $S_p(\tau) = \tau^p$ is found. For wave turbulence, the range of interest is comprised between these two last extremes. However, within this range no clear power laws are distinguishable in Fig. 4(b). We then chose to plot the structure functions versus $S_2(\tau)$ in Fig. 4(c). This technique was used for fully developed turbulence to measure anomalous scaling exponent due to the intermittency phenomenon [33]. In our case, the scaling exponents, defined as: $S_p(\tau) \propto S_2(\tau)^{\zeta_p}$, are indicated in Fig. 4(c) for each order moment p. There is no significant deviation from $\zeta_p = p/2$, meaning that no anomalous scaling is observable. Hence, wave turbulence in plates does not exhibit any intermittency phenomenon.

To summarize, we observed a broadband spectrum in a vibrating plate and investigated the variations of the cutoff frequency. In this context, internal damping mechanisms (mainly thermoelastic and viscoelastic losses for our plate [27]) seem to be irrelevant. Losses at the edge [21] can be discarded as the plate is fixed only at the corners. The radiation of acoustic waves in air is negligible since the frequencies of interest are well below the coincident frequency, for which bending and acoustic waves have the same phase velocity. The value of this frequency has been measured as 20 kHz in our setup [27]. For thicker plates, the coincident frequency may fall in the frequency range of interest, thus leading to a huge increase of the damping factor, see, e.g., [34]. This could affect the conclusions on the cutoff. Our experimental results suggest a three-waves

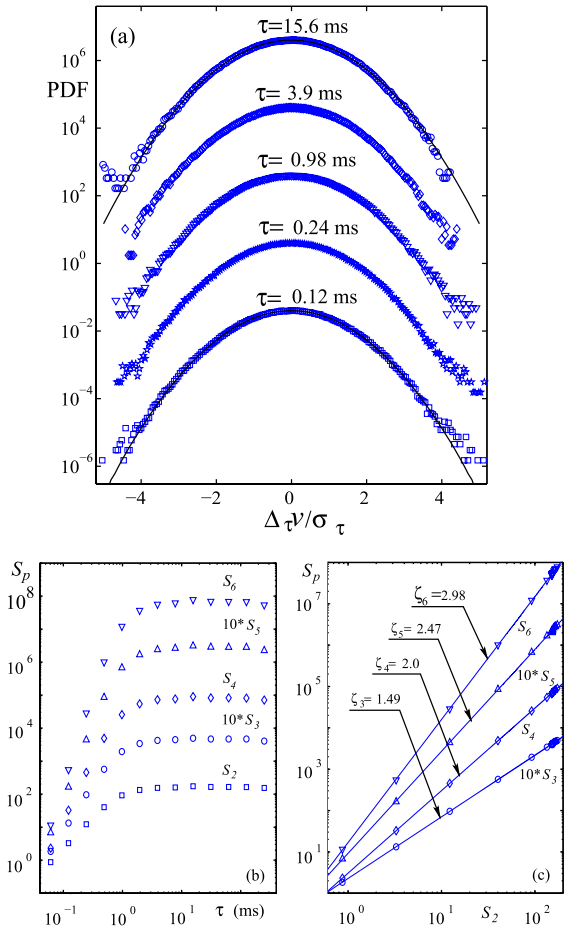

FIG. 4 (color online). Statistical properties of the velocity increments $\Delta_\tau v = v(t+\tau) - v(t)$ (injected power 136 mW). Probability density functions compared to Gaussians in (a). Structure functions of order $p = 2, 3, 4, 5, 6$, versus (b): the time lag τ, and (c): the order 2 structure function S_2. Continuous lines are best power laws fits with exponents ζ_p (see text).

spectrum matched to a spectrum of singularities where dissipation occurs. Obviously they call for more theoretical effort, in particular, concerning the weak turbulence of plates with quadratic nonlinearities or the turbulence of singularities.

We are grateful to K. Arcas, E. Hamm, F. Melo, and S. Rica for help and discussions. J.-M. Mainguy and L.-C. Trébuchet from Radio-France are also thanked for the loan of the plate reverberator. This work was partially supported by ANR Blanc OPADETO.

[1] V. E. Zakharov, V. S. Lvov, and G. Falkovisch, *Kolmogorov Spectra of Turbulence I: Wave Turbulence* (Springer-Verlag, Berlin, 1992).
[2] U. Frisch, *Turbulence* (Cambridge University Press, Cambridge, England, 1995).
[3] V. E. Zakharov and N. N. Filonenko, J. Appl. Mech. Tech. Phys. **4**, 506 (1967).
[4] A. N. Pushkarev and V. E. Zakharov, Phys. Rev. Lett. **76**, 3320 (1996).
[5] V. E. Zakharov and N. N. Filonenko, Sov. Phys. Dokl. **11**, 881 (1967).
[6] M. Onorato, A. R. Osborne, M. Serio, D. Resio, A. Pushkarev, V. E. Zakharov, and C. Brandini, Phys. Rev. Lett. **89**, 144501 (2002).
[7] S. L. Musher, A. M. Rubenchik, and V. E. Zhakarov, Phys. Rep. **252**, 177 (1995).
[8] S. Dyachenko, A. C. Newell, A. Pushkarev, and V. E. Zakharov, Physica (Amsterdam) **57D**, 96 (1992).
[9] S. V. Nazarenko, A. C. Newell, and S. Galtier, Physica (Amsterdam) **152–153D**, 646 (2001).
[10] Y. Lvov, S. V. Nazarenko, and R. West, Physica (Amsterdam) **184D**, 333 (2003).
[11] M. A. Donelan, J. Hamilton, and W. H. Hui, Phil. Trans. R. Soc. A **315**, 509 (1985).
[12] R. G. Holt and E. H. Trinh, Phys. Rev. Lett. **77**, 1274 (1996).
[13] W. B. Wright, R. Budakian, D. J. Pine, and S. J. Putterman, Science **278**, 1609 (1997).
[14] E. Henry, P. Alstrom, and M. T. Levinsen, Europhys. Lett. **52**, 27 (2000).
[15] M. Y. Brazhnikov, G. V. Kolmakov, A. A. Levchenko, and L. P. Mezhov-Deglin, Europhys. Lett. **58**, 510 (2002).
[16] E. Falcon, C. Laroche, and S. Fauve, Phys. Rev. Lett. **98**, 094503 (2007).
[17] E. Falcon, S. Fauve, and C. Laroche, Phys. Rev. Lett. **98**, 154501 (2007).
[18] P. Denissenko, S. Lukaschuk, and S. Nazarenko, Phys. Rev. Lett. **99**, 014501 (2007).
[19] O. M. Phillips, J. Fluid Mech. **156**, 505 (1985).
[20] E. A. Kuznetsov, JETP Lett. **80**, 83 (2004).
[21] G. Düring, C. Josserand, and S. Rica, Phys. Rev. Lett. **97**, 025503 (2006).
[22] A. Boudaoud, E. Hamm, and F. Melo, Phys. Rev. Lett. **99**, 254301 (2007).
[23] C. Touzé and A. Chaigne, Acta Acustica **86**, 557 (2000).
[24] A. Chaigne, C. Touzé, and O. Thomas, Acoust. Sc. Tech., Acoust. Soc. of Japan **26**, 403 (2005).
[25] T. M. K. Nagai, S. Murayama, and T. Yamaguchi, J. Sound Vib. **305**, 492 (2007).
[26] M. Amabili, Int. J. Non-Linear Mech. **40**, 683 (2005).
[27] K. Arcas, in *Proceedings of the ICA, Madrid, 2007* (Sociedad Española De Acústica, Madrid, 2007).
[28] D. Hui and A. W. Leissa, ASME J. Appl. Mech. **50**, 750 (1983).
[29] A. E. Lobkovsky, S. Gentges, H. Li, D. Morse, and T. A. Witten, Science **270**, 1482 (1995).
[30] A. E. Lobkovsky, Phys. Rev. E **53**, 3750 (1996).
[31] M. Ben Amar and Y. Pomeau, Proc. R. Soc. A **453**, 729 (1997).
[32] E. Cerda, S. Chaïeb, F. Melo, and L. Mahadevan, Nature (London) **401**, 46 (1999).
[33] R. Benzi, S. Ciliberto, R. Tripiccione, C. Baudet, F. Massaioli, and S. Succi, Phys. Rev. E **48**, R29 (1993).
[34] A. Chaigne and C. Lambourg, J. Acoust. Soc. Am. **109**, 1422 (2001).